University of Pennsylvania
ScholarlyCommons

2016

Mining Biomarkers Of Epilepsy From Large-Scale Intracranial Electroencephalography

Hoameng Ung
University of Pennsylvania, hoameng@mail.med.upenn.edu

Mining Biomarkers Of Epilepsy From Large-Scale Intracranial Electroencephalography

Abstract

Epilepsy is a chronic neurological disorder characterized by seizures. Affecting over 50 million people worldwide, the quality of life of a patient with uncontrolled epilepsy is degraded by medical, social, cognitive, and psychological dysfunction. Fortunately, two-thirds of these patients can achieve adequate seizure control through medications. Unfortunately, one-third cannot.

Improving treatment for this patient population depends upon improving our understanding of the underlying epileptic network. Clinical therapies modulate this network to some degree of success, including surgery to remove the seizure onset zone or neuromodulation to alter the brain's dynamics. High resolution intracranial EEG (iEEG) is often employed to study the dynamics of cortical networks, from interictal patterns to more complex quantitative features. These interictal patterns include epileptiform biomarkers whose detection and mapping, along with seizures and neuroimaging, form the mainstay of data for clinical decision making around drug therapy, surgery, and devices. They are also increasingly important to assess the effects of epileptic physiology on brain functions like behavior and cognition, which are not well characterized.

In this work, we investigate the significance and trends of epileptiform biomarkers in animal and human models of epilepsy. We develop reliable methods to quantify interictal patterns, applying state of the art techniques from machine learning, signal processing, and EEG analysis. We then validate these tools in three major applications: 1. We study the effect of interictal spikes on human cognition, 2. We assess trends of interictal epileptiform bursts and their relationship to seizures in prolonged recordings from canines and rats, and 3. We assess the stability of long-term iEEG spanning several years. These findings have two main impacts: (1) they inform the interpretation of interictal iEEG patterns and elucidate the timescale of post-implantation changes. These findings have important implications for research and clinical care, particularly implantable devices and evaluating patients for epilepsy surgery. (2) They provide an analytical framework to enable others to mine large-scale iEEG datasets. In this way we hope to make a lasting contribution to accelerate collaborative research not only in epilepsy, but also in the study of animal and human electrophysiology in acute and chronic conditions.

Degree Type
Dissertation

Degree Name
Doctor of Philosophy (PhD)

Graduate Group
Bioengineering

First Advisor
Brian Litt

MINING BIOMARKERS OF EPILEPSY FROM LARGE-SCALE INTRACRANIAL
ELECTROENCEPHALOGRAPHY

Hoameng Ung

A DISSERTATION

in

Bioengineering

Presented to the Faculties of the University of Pennsylvania

in

Partial Fulfillment of the Requirements for the

Degree of Doctor of Philosophy

2016

Supervisor of Dissertation   Graduate Group Chairperson

_____   _____

Brian Litt, M.D.   **Jason A. Burdick, Ph.D.**
Professor of Bioengineering and Neurology   Professor of Bioengineering

Dissertation Committee

Abba M. Krieger, Ph.D., Professor of Statistics, Operations, Information and
Decisions, and Marketing
Daniel D. Lee, Ph.D., Professor of Electrical and Systems Engineering, Computer and
Information Science, and Bioengineering
Danielle S. Bassett, Ph.D., Associate Professor of Bioengineering and Electrical and
Systems Engineering

MINING BIOMARKERS OF EPILEPSY FROM LARGE-SCALE INTRACRANIAL

ELECTROENCEPHALOGRAPHY

© COPYRIGHT

2016

Hoameng Ung

Dedicated to my parents,
for their love and sacrifice.

ACKNOWLEDGEMENTS

This dissertation is the product of years of work that would have been impossible if not for the support that I have received. As a result, there are many people I would like to express my gratitude towards.

First I'd like to thank our lab administrative staff: Carolyn Wilkinson, Ruth Krieger, John Frommeyer, Jacqueline Boccanfuso, and Heather Gatens. Carolyn, our lab manager, is my one-stop shop for answers of any kind. Ruthie, for helping me with endless requests even at the last minute and always with a cheerful smile. John, our resident programmer, who tolerates the many times I randomly show up perched on his desk for technical troubleshooting. In addition, thank you to Maggie Krall from the MD-PhD office who has managed to keep track of and support my progress with inhuman detail.

I'd also like to thank my lab mates, who made each day interesting and with whom many productive research discussions have taken place. Steve Baldassano and Ankit Khambhati have provided useful insights to various research projects and Hank Bink continues to make me double check that everything I do matters. Lohith Kini, who joined the lab shortly after me, has grown to be a close friend and will always lend a helpful ear when I needed to bounce ideas. He is also a top-notch partner for extra-curricular projects. Thank you also to Flavia Vitale for her voice of reason, Jason Moyer for his pragmatic perspectives, and Preya Shah to boost my ego. Furthermore, I'd like to thank the Melbourne crew: Dean Freestone, Pippa Karoly, and Mark Cook, for their assistance with the human NeuroVista dataset and for teaching me bits of Australian.

In addition, the clinicians in the lab have been invaluable in adding a clinical perspective to my research aims. I thank Shawniqua Williams for the hours spent annotating and teaching me the basics of EEG reading so that I am not flying (completely) blind. I must also express special gratitude to Kate Davis. She has worked and been patient with me through thick and thin to push the quantitative limits of a clinical journal and I thank her for providing both guidance and mentorship throughout this and other, more challenging situations.

Throughout my PhD I have had the privilege of working with Abba Krieger. Abba has generously dedicated many hours to one-on-one meetings, entertaining my questions about probability and statistics and reviewing my analyses. As a result of our interactions I've grown to be more comfortable and rigorous in statistics to a level I had not previously anticipated. I realize how fortunate I am to have had this chance to tap not only the wealth of his statistical knowledge but also his experiences and perspectives as a professor, which he has been more than willing to share. He has been a great mentor to me and I do not take this opportunity for granted.

Of course I'd also like to thank Brian Litt, my thesis advisor, who has proven to be much more than that. When I first met Brian he immediately struck me as a person who genuinely had my best interests in mind, and over the years I've witnessed this first hand in his advising. He has taught me how to think, how to manage a team, how to teach, and how to keep perspective on every project I embark on. He has shown me that although it is important to be a master of your work, it is as important to understand where your work fits in the greater community. Most importantly, he has trusted me with the freedom and flexibility to embark on my own self-discovery, to allow me to find out in these formative years what excites me and where I see myself in the future. He has not only given me perspective on my research, but he has also given me broader perspectives on career choices and on life. For this and much, much more, I am sincerely grateful to Brian; I would not be in this position if not for his support and guidance.

Lastly, I'd like to thank my family. My parents, who have always had faith in my education despite not understanding why I am still in school. My brother, who has served as a role model, and my sister, who has withstood the many challenges of being the youngest sibling. Finally, I'd like to thank my fiancée, Margaret Ivanov. The past 6 years have been extremely fulfilling, despite the professional responsibilities we continue to face. Her diligence and drive inspires me to be the best person I can be, and I look forward to what life has in store for us!

ABSTRACT

MINING BIOMARKERS OF EPILEPSY FROM LARGE-SCALE INTRACRANIAL
ELECTROENCEPHALOGRAPHY

Hoameng Ung

Brian Litt, M.D.

Epilepsy is a chronic neurological disorder characterized by seizures. Affecting over 65 million people worldwide, the quality of life of a patient with uncontrolled epilepsy is further degraded by medical, social, cognitive, and psychological dysfunction. Fortunately, two-thirds of these patients can achieve adequate seizure control through medications. Unfortunately, one-third cannot.

Improving treatment for this patient population depends upon improving our understanding of the underlying epileptic network. Clinical therapies modulate this network to some degree of success, including surgery to remove the seizure onset zone or neuromodulation to alter the brain's dynamics. High resolution intracranial EEG (iEEG) is often employed to study the dynamics of cortical networks, from interictal patterns to more complex quantitative features. These interictal patterns include epileptiform biomarkers whose detection and mapping, along with seizures and neuroimaging, form the mainstay of data for clinical decision making around drug therapy, surgery, and devices. They are also increasingly important to assess the effects of epileptic physiology on brain functions like behavior and cognition, which are not well characterized.

In this work, we investigate the significance and trends of epileptiform biomarkers in animal and human models of epilepsy. We develop reliable methods to quantify interictal patterns, applying state of the art techniques from machine learning, signal processing, and EEG analysis. We then validate these tools in three major applications: 1. We study the effect of interictal spikes on human cognition, 2. We assess trends of interictal epileptiform bursts and their relationship to seizures in recordings from canines and rats, and 3. We assess the stability of long-term iEEG spanning several years. These findings have two main impacts: (1) they inform the interpretation of interictal iEEG patterns and elucidate the timescale of post-implantation changes. These findings have important implications for research and clinical care, particularly implantable devices and evaluating patients for epilepsy surgery. (2) They provide an analytical framework to enable others to mine large-scale iEEG datasets. In this way we hope to make a lasting contribution to accelerate collaborative research not only in epilepsy, but also in the study of animal and human electrophysiology in acute and chronic conditions.

TABLE OF CONTENTS

LIST OF TABLES

LIST OF ILLUSTRATIONS

Chapter 1

Introduction

An estimated 50 million people in the world suffer from epilepsy, a condition characterized by chronic seizures [83]. A majority of patients with epilepsy are able to obtain adequate seizure control with anti-epileptic medications, allowing them to live relatively normal lives [70]. However, 30-40% of epilepsy patients are not well-controlled [84]. For these patients, the consequences of epilepsy are felt beyond seizures into the psychosocial, cognitive, and medical spheres that compound into a poor quality of life. Those with epilepsy are also at an increased risk of sudden unexplained death [143].

Therapies to treat this patient population are lacking. First line treatment usually involves evaluation for resective surgery, where the lesion believed to be the seizure onset zone is surgically removed. Candidacy for resective surgery considers both the localizability of the seizure onset zone (SOZ) on electroencephalography (EEG) as well as other factors including whether this region overrides functionally critical areas, known as eloquent cortex. For this evaluation, clinicians may employ non-invasive techniques such as magnetic resonance imaging (MRI) and positron emission tomography (PET) as well as invasive techniques such as intracranial EEG (iEEG), the current gold standard for localization [109]. However, not all patients are candidates and only one-fourth may find any benefit from resective surgery [91]. Certain epilepsies such as mesial temporal sclerosis with a clear focal lesion are most amenable to resection, yet even in these cases, five year seizure remission rates vary from

41-79% [136]. The prognosis for multi-focal and neocortical epilepsy is worse [145].

For patients who are not candidates for surgery or otherwise opt out, there are few available alternatives. Vagus nerve stimulation (VNS), deep brain stimulation, and responsive neurostimulation [102, 41, 58] are examples of attempts to modulate the underlying epileptic network through electrical stimulation with the goal of preventing or aborting seizures. VNS has been shown to reduce seizure frequency by approximately 20% compared to controls [58]. Deep brain stimulation of the subthalamic nucleus has shown a two-year median seizure reduction rate of 56% [41], though not currently approved in the United States. More recently, the FDA approved NeuroPace Responsive NeuroStimulator (RNS®) has reported seizure reductions of roughly 40% compared to controls [102, 10]. Recent advancements in the field have developed alternative therapies for medically refractory epilepsy, but there remains a great need for more effective therapies for these individuals.

These cases demonstrate a unique aspect of epilepsy relative to many other diseases : it is characterized by abnormal electrical signaling within the brain that can be quantitatively recorded. This results in the use of tools that can interrogate the electrical signals on the brain and digest a tremendous amount of neural activity in an attempt to localize, control, abort, or otherwise modulate seizures. EEG is the most useful diagnostic tool in an epileptologist's arsenal, and can be used to diagnose an epilepsy syndrome, determine management strategy, or localize the SOZ [110]. When patients undergo intracranial EEG monitoring in the inpatient unit, a strip or grid of electrodes consisting of 4 and 64 electrodes, respectively, may be implanted subdurally, with some centers using hundreds of electrodes. Each electrode continuously monitors the brain's neural activity, at a sampling rate often greater than 500 Hz, generating a large amount of data after which is manually reviewed by clinicians for seizures (ictal) and between seizure (inter-ictal) patterns. These patterns include interictal spikes and bursts that are rarely seen in healthy subjects and are used

by clinicians to aid in management, though the significance of spikes and bursts has yet to be fully illuminated. The NeuroPace RNS is a closed loop device that records EEG, algorithmically detects seizures, and electrically stimulates the brain in response. The exact mechanism is action unknown, but the algorithm used requires constant tuning by clinicians. The quantitative nature of EEG recordings from similar devices lends itself well to the application of automated algorithms and machine learning. With these tools, we can draw associations to inform the significance of the trends and patterns recorded in the brain and in the hopes of improving patient management and treatment.

Quantitative analysis of EEG has existed for decades ever since the advent of digital EEG in the 1950-60s. In fact, claims that EEG will be read automatically by computers emerged as early as 1967 [129], yet it has since been clear that the complexity of the neural code is not as easily deciphered as initially believed. This work is not intended to automate the reading of EEG, but instead to take an incremental step in the automated analysis of specific patterns in EEG and to help decipher the significance of said patterns. Due to relatively recent uptrend in the availability of data and high throughput computational resources, we believe the incorporation of machine learning combined with traditional analysis allows us to answers importance questions and draw novel conclusions to aid in our understanding and treatment of epilepsy.

Towards this end, this thesis is organized into eight chapters.

Chapter 2 provides relevant background into epilepsy, EEG, and quantitative EEG analysis. We introduce the main concepts used in the various projects and defer to the respective chapters for further details. We end the chapter with a general framework for biomarker detection that is employed throughout our work.

Chapter 3 investigates the significance of interictal spikes, or epileptiform discharges, on hu-

man cognition with a controlled memory task. In this chapter we automate spike detection in 67 patients with a controlled memory task.

Chapter 4 begins to look at the less well-defined interictal burst, specifically in a rat model of traumatic brain injury. In this chapter, we employ burst detection and machine learning classification in an attempt to predict epileptogenesis.

Chapters 5, 6, 7, and 8 focuses on the analysis of year-long continuous iEEG that is unique to the field. The work on bursts is extended into Chapters 5, 6 and 7 on a long-term canine model, where we study the dynamics of bursts and their relationships to seizures and seizure onset zones.

Chapter 8 begins the analysis of a long-term dataset of human epilepsy, specifically characterizing the post-implantation changes in iEEG based on EEG features currently used in neurodevices.

Lastly, Chapter 9 provides a summary of the thesis and future directions for research.

1.1   Major Contributions

The major contributions of this work are:

1. Building of a flexible framework for EEG Pattern recognition that incorporates both supervised and unsupervised learning techniques. This framework will enable the automated analysis of EEG, with the hopes of facilitating biomarker discovery to advance clinical medicine.

2. This utility of this framework has been demonstrated in human and animal datasets to inform several EEG biomarkers and trends:

    (a) Interictal Spikes affect human cognition

(b) Epileptiform bursts may predict epileptogenesis in rats

(c) Interictal bursts are similar to seizures

(d) Burst and seizure dynamics change over time in canines

(e) Intracranial EEG is unstable in the initial 100 days after implantation

Chapter 2

Background

Over 65 million people in the world and 3 million in the US suffer from epilepsy, a condition characterized by chronic seizures [107]. In 2014 the International League Against Epilepsy (ILAE) proposed a revised operational clinical definition of epilepsy as a disease of the brain defined by any of the following conditions [40]:

1. At least two unprovoked (or reflex) seizures occurring >24 h apart

2. One unprovoked (or reflex) seizure and a probability of further seizures similar to the general recurrence risk (at least 60%) after two unprovoked seizures, occurring over the next 10 years.

3. Diagnosis of an epilepsy syndrome

As a testament to the chronicity of epilepsy, the disease is only considered to be resolved for individuals who remain seizure-free for at least 10 years, with no seizure medications for the last 5 years [41]. Fortunately, patients with medically controlled epilepsy are able to live relatively normal lives [70], with the exception of side effects from medications. However, 30-40% of epilepsy patients do not respond to two or more anti-epileptics and thus have drug-resistant epilepsy [85, 84]. Uncontrolled epilepsy leads to significant medical, psychosocial, and cognitive consequences that result in a poor quality of life for many of these patients, as well as an increased risk of sudden death in epilepsy (SUDEP) [143].

2.1   Role of EEG in Epilepsy

Electroencephalography (EEG) has many clinical and research applications in humans and animals, including monitoring alertness, investigating sleep, and localizing cortical damage. In the evaluation of epilepsy, EEG is a critical tool in an epileptologists arsenal. With it, clinicians can diagnose epilepsy syndromes and determine treatment medications. A classic example of EEG's usefulness is in absence epilepsy, where a characteristic 3 Hz spike and wave absence seizure seen on noninvasive scalp EEG (Figure 1) immediately informs clinical management towards specific agents (ethosuximide, valproic acid) and away from others (carbamazepine, phenobarbital, gabapentin, and others).
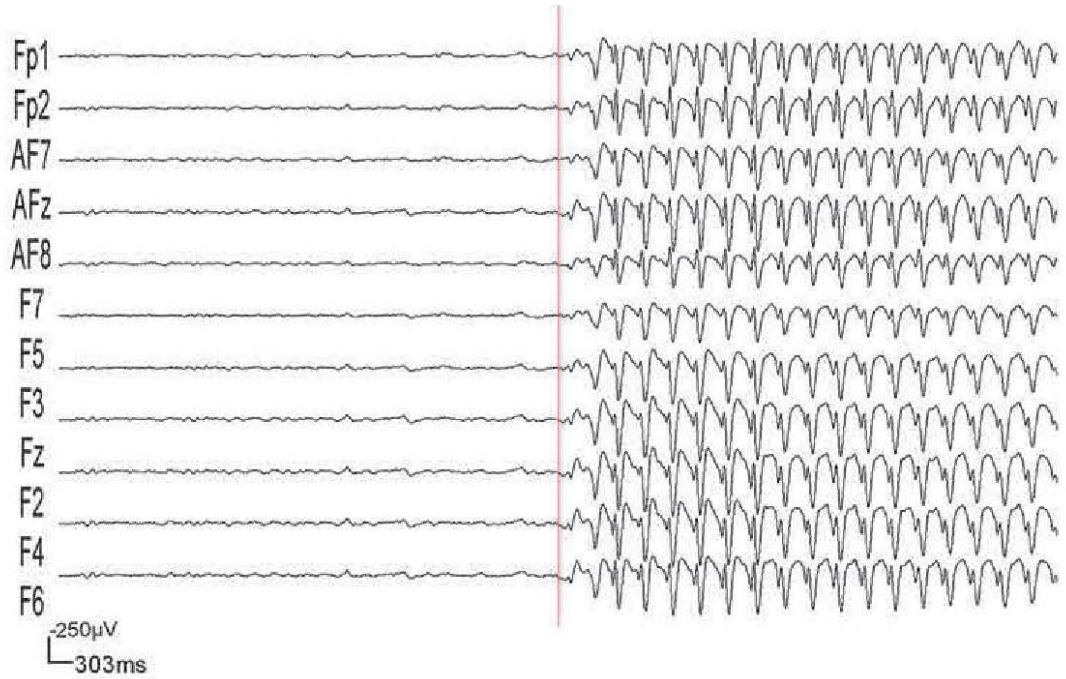
Figure 1: Absence Seizure on EEG. 3 Hz spike and wave is shown on scalp EEG, which has indications for specific medications. Ethosuximide, a T-type calcium channel blocker is known to be particularly effective against absence seizures, whereas carbamazepine, a GABA receptor agonist, is contraindicated. Figure from Amor et al.[5]

2.1.1 Invasive EEG

The majority of epilepsy patients that are referred to an epilepsy center only require non-invasive methods for surgical evaluation, particularly if there is congruency in findings between scalp EEG and imaging (MRI,PET) [110]). However, scalp electrodes may suffer in signal quality due to attenuation by the skull and are often contaminated by artifact from movement or improper electrode contact [129]. In cases where higher quality recordings are required, invasive electrodes are an option. The signal-to-noise ratio of invasive electrodes is relatively greater, allowing the detection of subtle patterns that would not otherwise manifest on surface or scalp EEG. Due to closer proximity to the brain, the spatial resolution is also finer and allows for increased specificity in defining an epileptogenic focus. For instance, one study reports that 77% of temporal lobe epilepsy patients with unclear lateralization by noninvasive methods were found to have a unilateral origination through invasive monitoring [135]. In addition to investigating uni- vs. bi-temporal onset, invasive electrodes are also useful in determining unitemporal vs. extratemporal, or extratemporal vs. bifocal/multifocal onset. However, sampling is limited to electrode placement and there is a risk of inadequate coverage. Nonetheless, due to the higher quality recordings of invasive electrodes, the analytical work presented in this thesis is based on these data.

Invasive Electrodes

It is important to consider different types of electrodes when conducting analyses, as recording characteristics (amplitudes), target tissue, and tissue reaction may vary [134]. Different types of invasive electrodes are shown in Figure 3.

1. Depth electrodes are stereotactically implanted through a small hole in the skull and guided by 3D imaging (MRI). The trajectory of implantation is intended to avoid

damaging blood vessels or important brain structures, and the final placement is usually accurate to a few millimeters. These electrodes are most commonly used in the temporal lobe to interrogate mesial structures. Onset in mesial versus lateral temporal structures has implications for spread patterns [110].

2. Subdural electrodes are implanted as strips or grids on the cortical surface (Figure 2). For this reason, EEG recorded from subdural electrodes is often referred to as electrocorticography (ECoG). Strip electrodes can be implanted through bore holes in the skull, whereas grid electrodes require a craniotomy. Grid electrodes cover a wide area of the cortex (eg. 8x8 with 1 cm spacing) and allows for accurate functional cortical mapping and seizure onset localization.
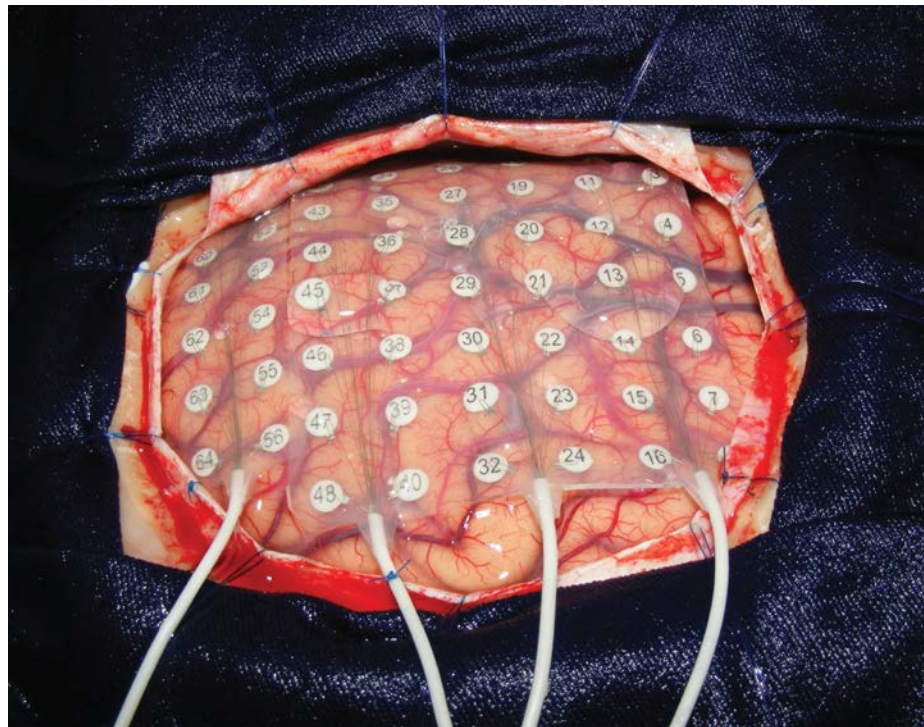
Figure 2: 64 grid subdural electrode on a patient's brain

3. Epidural electrodes are of intermediate invasiveness, and are placed on the dura

through bore holes. Their use has steadily declined due to relatively poor signal-to-noise ratio compared to subdural electrodes as well as improvements in functional and structural imaging [9].

4. Foramen ovale electrodes are essentially depth electrodes inserted inferiorly and receive their signal from the parahippocampal gyrus and surrounding areas. The trajectory avoids the brain parenchyma while still allowing the interrogation of mesial temporal structures. Similar to epidural electrodes, their use has declined due to improvements in imaging [72].

The selection of electrode type depends on the region and the question that needs to be answered by clinicians. As subdural electrodes only cover the surface of the brain, they are often combined with depth electrodes to interrogate subcortical structures. Subdural electrodes are more commonly used in the United States, and depth electrodes (stereoEEG, or SEEG) are predominant in Europe. However, more centers in the US are incorporating stereoEEG due to its ability to target subcortical structures less invasively.
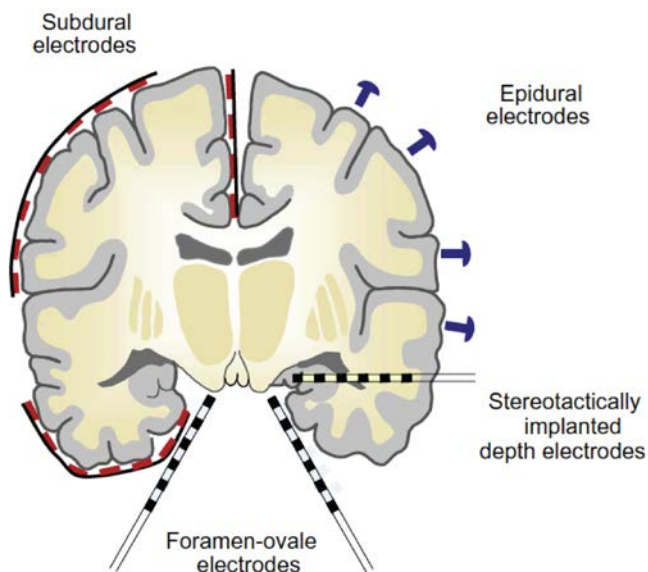
Figure 3: Schematic of different invasive electrodes and typical placement in the brain. Figure from Noachtar et al.[110]

Complications of Invasive EEG

However, invasive EEG is not without its disadvantages. The implantation of electrodes leads to acute infarction and hemorrhage in the majority of patients as soon as one day post-implantation [42]. Hallmarks of chronic inflammation and foreign body response are also seen (Figure 4). In the hospital, iEEG monitoring is collected in an artificial environment of medication withdrawal to induce observed seizures. In addition, the invasive nature of inpatient monitoring presents an infection risk that limits the monitoring period from several days to a maximum of 1-2 weeks, which offers a narrow window of time to investigate a chronic disorder. It is unclear how representative these recordings are of the baseline epileptic network, yet critical surgical and treatment decisions, such as seizure localization, are made on these recordings. In fact, repeated and extended observation periods and subsequent resection following a failed surgery have been shown to improve seizure remission

rates [51, 75]. Yet even in chronic recordings, changes in impedance as gliosis and the surrounding tissue react to the foreign body are reported [116, 134], yet it is unknown how this impacts the recorded signals.
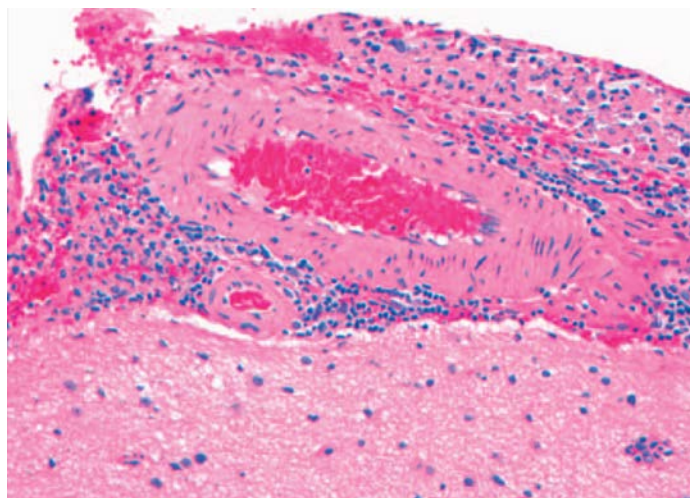
Figure 4: Perivascular leptomeningeal chronic inflammation following inpatient invasive iEEG monitoring. Hematoxylin and eosin (H & E) stain, x200, figure from Fong et al. [42]

2.1.2 Seizure localization

The primary goal of invasive monitoring for resective surgery is identification of the seizure onset zone. Surgical resection often removes a larger section of the brain than that simply outlined by clinical monitoring to ensure coverage of pathologic tissue not captured on EEG (Figure 5) [97]. Much research is focused on improving the delineation of the seizure onset zone, including the use of multimodal imaging combined with EEG. Chapter 6 is an example of work we've done investigating the utility of interictal bursts on improving localization in a canine model of epilepsy.

Table 1: Descriptions and zones of cortical lesions (adapted from Rosenow et al. [122])

Epileptogenic zone	Region of cortex that can generate epileptic seizures. By definition, total removal or disconnection of the epileptogenic zone is necessary and sufficient for seizure-freedom
Irritative zone	Region of cortex that generates interictal epileptiform discharges
Seizure onset zone	Region where the clinical seizures originate
Epileptogenic lesion	Structural lesion that is causally related to the epilepsy
Ictal symptomatogenic zone	Region of cortex that generates the initial seizure symptoms
Functional deficit zone	Region of cortex that in the interictal period is functionally abnormal, as indicated by neurological examination, neuropsychological testing, and functional imaging or non-epileptiform EEG or MEG abnormalities
Eloquent cortex	Region of cortex that is indispensable for defined cortical functions
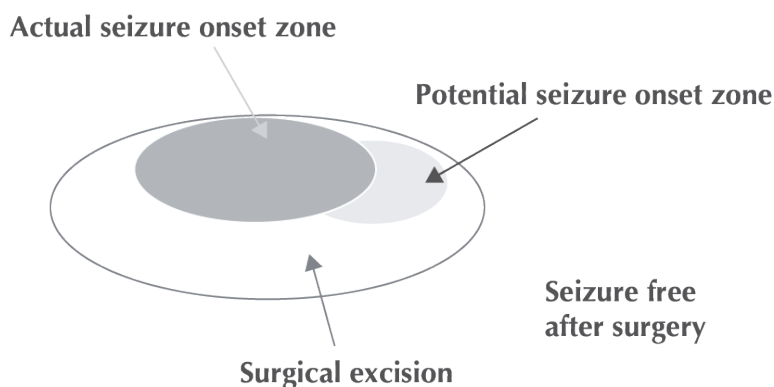
Figure 5: Seizure free resection. Ideally the resection will remove epileptogenic zone through the seizure onset zone recorded on EEG. Figure adapted from Luders et al.[97]

2.1.3   EEG Patterns

The signals recorded by ECoG and EEG is a summation of local field potentials (LFPs), which are again a summation of the unit activity of a population of inhibitory and excitatory

neurons (Figures 6 and 7). Local field potentials are commonly collected with the Utah array, whereas macro subdural and depth electrodes are reflective of neurons in the order of millions. Thus, the patterns seen on ECoG are best interpreted as a summation of underlying neuronal action potentials.
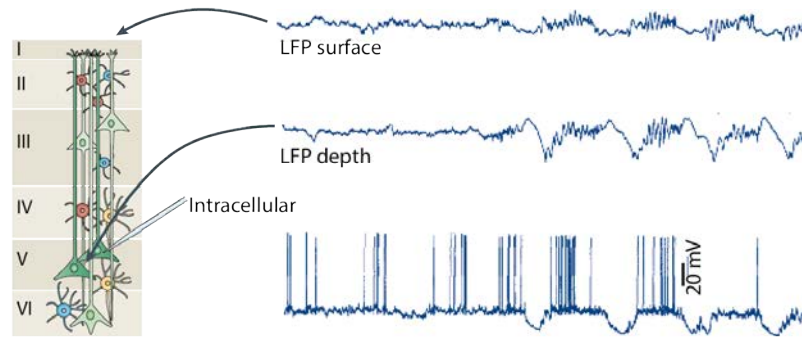
Figure 6: Representation of unit recordings on local field potentials. Figure adapted from Buzsaki et al [18].
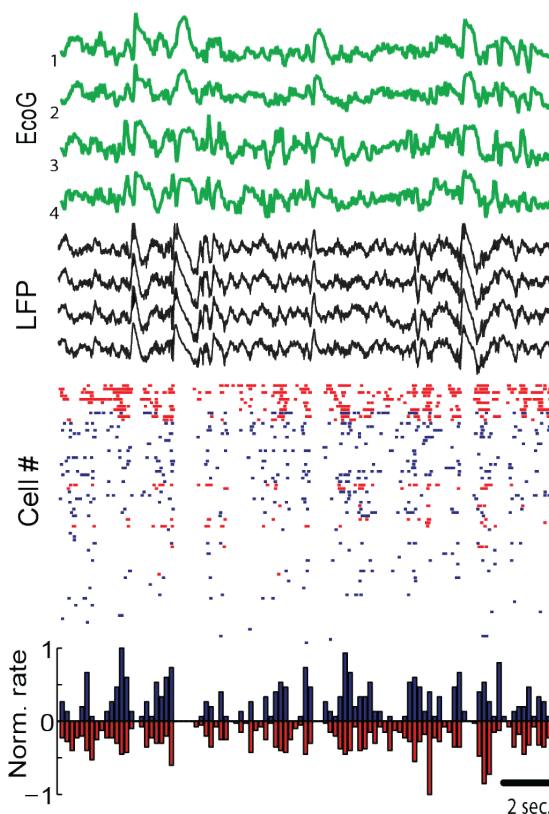
Figure 7: Representation of local field potentials on EEG. Figure adapted from Peyrache et al. [114]

Rhythms

Interestingly, neuronal firing tends to form brain rhythms that were noticed by early electrophysiologists to fall into several frequency bands. These bands have since been associated with various cortical states [129] that are used by researchers and clinicians alike to gain insight into normal and pathological states, such as the delta/alpha ratio [39]. For example, closing of eyes reliably elicits an alpha wave predominantly in the occipital lobe. For these reasons, it is often useful to characterize the power of a signal in these frequency bands. We briefly review these bands (also called Berger bands) and a few normal/abnormal states

that each fall in.

1. Delta: 0 - 4 Hz, associated with sleep, though found in lesions pathologically

2. Theta: 4 - 7 Hz, drowsiness, idling, found pathologically in focal lesions, metabolic encephalopathy, and others

3. Alpha: 8 -13 Hz, relaxed, reflexing, closing of eyes, found pathologically in comatose patients

4. Beta: 14 - 30 Hz, active thinking, alert, anxious, seen in patients on benzodiazepines

5. Gamma: 30+ Hz, cross-modal sensory processing, short-term memory, decreased gamma may indicate cognitive decline

6. Mu: 8 - 13 Hz, suppressed during motor action, found over motor cortex

Epileptiform patterns

Beyond rhythms, there are a variety of interictal epileptiform patterns seen on EEG, including spikes, sharp waves, spike-wave complexes, polyspikes, periodic lateralized epileptiform discharges (PLEDs), and bursts, to name a few. In this thesis, we choose to focus on spikes as well as bursts, which are patterns commonly seen in epilepsy patients but the significance of which remains unclear.

Interictal Spikes

Interictal spikes are brief (<200 ms) epileptiform discharges that are believed to be a result of abnormal synchronous firing of a population of neurons. Also known as interictal epileptiform discharges (IEDs)[1], they are widely accepted as a sign of epilepsy and are rarely seen

---

[1]We use spike and IEDs interchangeably in this thesis

in healthy volunteers. In a study of over 13,000 people, IEDs were observed in 0.5% [68]. In contrast, IEDs occur in up to 98% of patients with epilepsy [110]. An example of a spike recorded on intracranial electrode is shown in Figure 8 on the IEEG portal (ieeg.org).
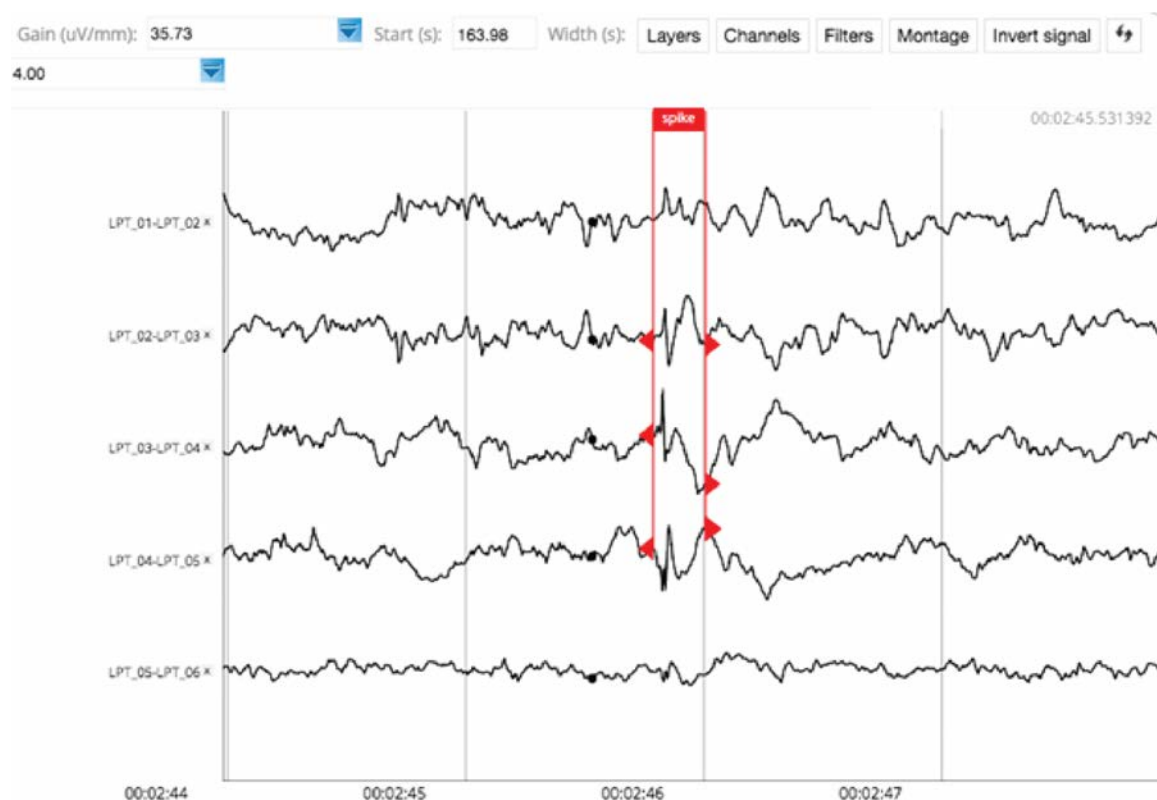
Figure 8: Example of spike spanning three bipolar channels on ECoG

The significance of IEDs is not well understood. Though they are believed to be epileptiform, interictal spikes are not limited to the epileptogenic zone and often occur in other cortical areas. The region with the most spiking does not always correlate with the lesion location. In some cases, spikes can inform prognosis: increased spiking in cases of temporal lobe epilepsy with hippocampal sclerosis leads to poor outcomes post-resection. Studies have also suggested that spikes may precede seizures, as GABA-mediated synaptic inhibition can illicit spikes experimentally [139]. Along the same lines, evidence also exists for spikes as a

sign of abnormal axonal sprouting that leads to epilepsy, a process known as epileptogenesis [139]. For these reasons, while interictal spiking is taken into account when determining resection region, it forms only an auxiliary data point [129, 98].

Quantitative marking is necessary to accurately measure IED occurrence and improve our understanding of the significance of these patterns. Automatic spike detection will allow us to generate quantitative, objective descriptions of spike density that would not be possible to do manually by human epileptologists. Being able to quantify spikes on a large scale will lead to better interpretations of the phenomena occurring in a spike and may lead to better patient diagnosis and treatment outcome.

Unfortunately, automatic spike detection is a difficult problem. The reason for this is not likely due to the lack of technical algorithms, but rather due to the lack of shared datasets, open source algorithms, and relatively poor inter-rater reliability [157]. For instance, over 80 papers have been published about a spike detection algorithm, many of which are reviewed by Moraes et al. and Wilson et al. [101, 157]. More than 22 report accuracies >90%. However, there does not exist an algorithm that performs and generalizes well to multiple datasets, and current commercial algorithms perform poorly enough that they are not used by clinicians. Many authors do not release their raw code, leaving readers to reprogram their pipeline. Yet when it fails to perform as reported, readers are unable to determine if there was a mistake in the reproduction due to small unpublished nuances, to variability in datasets, or a poorly generalizable algorithm. In the few cases where the algorithm is packaged for public use, variability between EEG recordings hinders the performance. In addition, the definition of a spike is relatively obscure, leading to disagreements between expert EEG markers. To give an example, one study investigated inter-rater reliability between five EEG readers for hand-marking 50 records of epilepsy patients. They found that the sensitivity of markings ranged from 57% to 87% [156].

Despite its shortcomings, automated spike detection is beneficial in that it remains objective and consistent. An algorithm will always return the same result given the same set of input data. Furthermore, it is necessary to uncover the significance of spikes as manual marking is unfeasible. In our experience, the parameters of each algorithm must be tuned on a patient-specific level until we have enough data to form a generalizable model. With this approach, we use machine learning to model complex variability in spike patterns guided by user provided examples. This paradigm allows for improvement in the algorithms as more data is provided. For this reason, data sharing is also a critical piece towards an automatic, generalized spike detector.

There are many different types of algorithms that have been developed, from mimetic algorithms that model each part of a spike-wave complex, to wavelet methods that model the morphology [101]. It is beyond the scope to review them all, as it is difficult to determine which is the best performing. However, the algorithms generally fall into several categories, which we can learn from to design our own spike detector and more generally a detector of any interictal pattern.

1. Mimetic - identify spikes based on duration of spike, expected amplitude, length of after-going slow wave. This may also include feature extraction and the use of classification algorithms.

2. Template based - use cross-correlation to identify spikes with high correlation with a set of template spikes. Some approaches also use the raw signal as features for a classifier.

3. Background perturbation - calculate a single feature that captures short-term perturbations due to spiking, and set a threshold based on a set of template spikes.

For the purposes of this thesis, we develop and validate our own spike detector, described

in 2, that incorporates several previous approaches as well as the use of machine learning techniques.

Bursts Furthermore, abnormal activity, such as interictal bursts (9), may provide localization or prognostic information. Interictal bursts, also referred to as brief interictal rhythmic discharges, brief rhythmic discharges, and other terms have been observed to relate to cerebral injury and epilepsy [164]. As they are observed much more frequently than seizures, any information gained from the analysis of bursts would aid in expediting inpatient monitoring. However, it is unknown whether they correlate with or localize seizures. Much of our work is focused on investigating these bursts of activity.
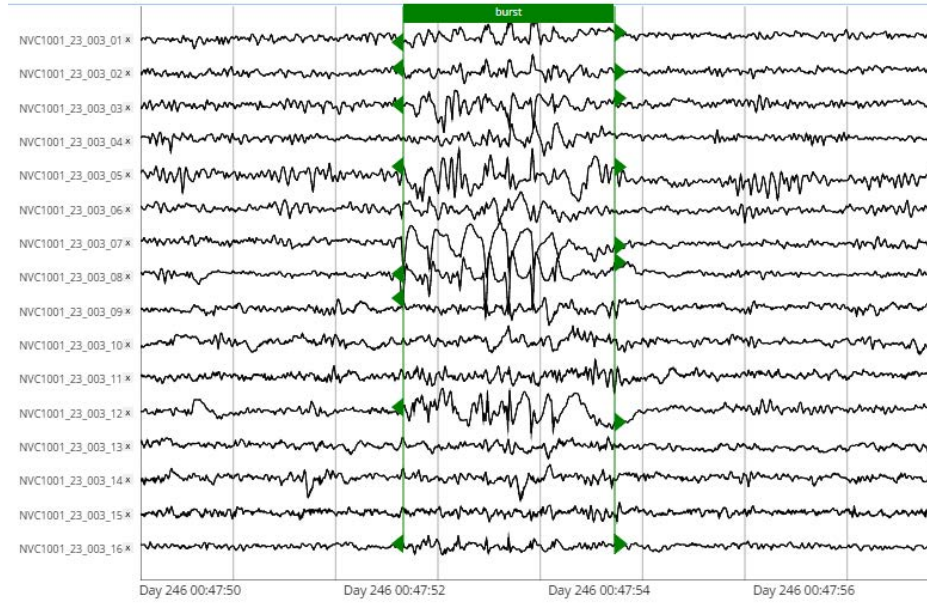
Figure 9: Example of burst in human EEG. As you can see this burst occurs in most electrodes and in some channels.

As interictal bursts are less well defined, the framework described below is meant to be flexible enough to capture well defined spikes of a fixed duration as well as bursts of variable duration and complicated morphology.

2.2 Neurodevices

For those patients who are not candidates for surgery, an alternative is an implantable device. Electrical stimulation is believed to decrease the excitability of the brain, leading to reduced occurrence of seizures. Four established therapies are listed below, though only two are currently approved for use in the United States [112].

1. Medtronic Deep Brain Stimulation - this open loop device stimulates the anterior nucleus of the thalamus. It is approved for partial onset seizures in Europe and Canada but not in the US. Studies have shown a median seizure reduction of 41% at 1 year and 69% at 5 years after implantation. [123]

2. Trigeminal Nerve Stimulation - This is an open loop noninvasive device that uses transdermal electrodes to stimulate branches of the trigeminal nerve. It is currently approved in Europe but not yet in the US. A reduction in seizure frequency of 27.4% at 6 months and 34.8% at 12 months has been observed.

3. Vagal Nerve Stimulation (VNS) - VNS is approved for use in partial onset epilepsy in the US, but also used off-label for generalized epilepsy. The device is open loop, and is set for intermittent stimulation of the left vagus nerve. VNS has been shown to result in a median seizure reduction of 35% at 1 year and 44% at 3 years [103]

4. NeuroPace Responsive NeuroStimulator (RNS ®) - The RNS is the first closed loop device for epilepsy, recently FDA approved in 2013. A stimulator is implanted within the skull and connected to a combination of up to two depth or subdural electrodes implanted over the presumed seizure focus (10). Median seizure reduction rate is 44% at 1 year and 65.7% at 6 years after implantation [10], although compared to controls the additional reduction rate is roughly 41%.
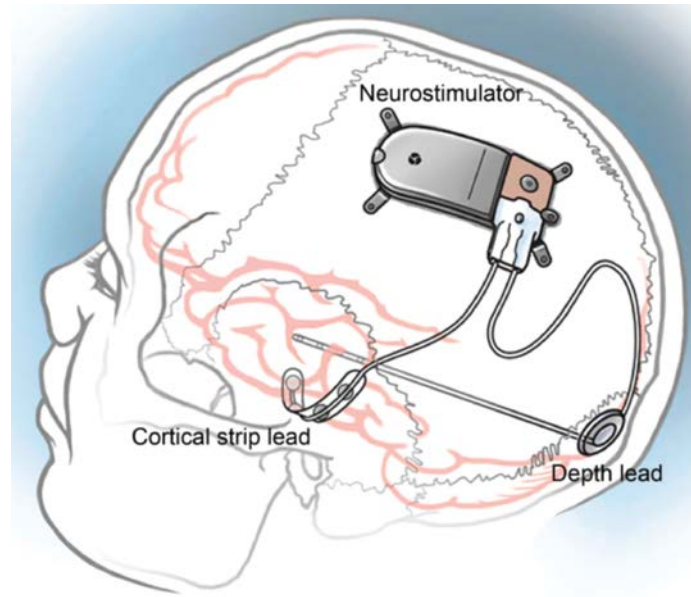
Figure 10: NeuroPace RNS®device

2.2.1   Algorithms in closed loop neurodevices

NeuroPace

The NeuroPace algorithm uses three features for seizure detection: area, line-length, and half-wave. These parameters are used in a proprietary algorithm for seizure detection. These parameters are manually set by physicians after implantation to optimize seizure detection.

NeuroVista

NeuroVista was a start-up company that developed a 16-electrode implantable device for continuous monitoring. First tested in dogs and subsequently in humans, analysis of data from this device forms a large part of this thesis, as it is the only existing long-term (years) continuously recorded EEG dataset in existence [27, 23]. In the human trial, 15 patients

with refractory epilepsy were recorded for an average of 18 months. During this trial, a seizure advisory system was in place that predicted the likelihood of seizures given the intracranial recordings. Line length, energy, and Teager-Kaiser energy were used as features into a proprietary classifier consisting of a k-nearest neighbor and decision tree hybrid.

Understanding Long Term EEG

The two devices above are the first long-term recordings in human patients with epilepsy. Thus, studying their recordings can be of much utility, particularly in the NeuroVista recordings as it is 1. continuous and 2. has a wider spatial resolution than the NeuroPace RNS. Furthermore, both devices experienced increasingly poor performance over time that requires retuning and retraining, yet the dynamics and timescale of this effect is unknown and investigated in Chapter 8.

Studying long term EEG will improve our knowledge of epilepsy dynamics and potentially improve clinical care. Recent evidence suggests that longer or repeated observation periods may improve treatment outcomes [31, 51, 75] by more accurately mapping the epileptogenic zone. Cases have been published where an initially poor surgical resection candidate achieved localization from the RNS device and subsequent seizure freedom from surgery [75]. This provides evidence that long-term EEG may provide important information in studying the underlying network of an epileptic patient.

In addition, interictal epileptiform patterns such as IEDs and bursts are routinely noted on inpatient monitoring, but the significance of these patterns is unknown. Long-term recordings will allow us to more accurately describe novel electrographic patterns by increasing our sample size. At the same time, studying the quantitative features used in neurodevices allows us to explain transient changes seen during algorithm deployment to improve performance, impacting future device development.

2.3 Animal Models

Animal models provide a useful proxy for hypothesis-driven research, and over the years range from primates, pig, and sheep to rabbits, mice and drosophila. In this thesis, we analyzed two different animal models of epilepsy: rodents and canines. Rodents have recently grown in popularity as an animal model in epilepsy due to their rapid breeding, docility, and ease of upkeep [55]. We have learned much about the dynamics of seizure generation, epileptogenesis, and kindling from rodents with chemically- or trauma- induced seizures. In Chapter 4 we analyze data from a traumatic brain injury (TBI) rat model in the hopes of identifying electrographic biomarkers of epileptogenesis, or the transition from a normal to a spontaneously epileptogenic state. Canines represent a large animal model with characteristics that are similar to humans. Anatomically they have a gyrated brain of a larger size apt for device testing. Compared to induced seizures, canines have spontaneously occurring, genetic epilepsies at a rate similar to humans with similar medication responses [150]. The seizures on iEEG show electrographic properties that are similar to human iEEG [28]. Furthermore, they are observed to have similar seizure types with a focal origin with or without secondary generalization. Interestingly, VNS was first shown to abort chemically induced seizures in canines [167], which spurred development of VNS as a neuromodulatory therapy. In Chapters 5, 6, 7, we analyze a canine dataset with long-term implanted electrodes.

2.4 Generalized Linear Mixed Models

One of the statistical models we often employ in this thesis is the Generalized Linear Mixed Model (GLMM). A brief introduction is given here and readers are referred to other sources for a more detailed description.

The motivation for this stems from the limitations of an ordinary linear model. Consider a basic linear model $Y = X\beta + \epsilon$, where $\epsilon \sim \mathcal{N}(0, \sigma^2)$. In other words, $Y \sim N(X\beta, \sigma^2)$. However, this model is not optimal if the assumptions are not met, such as if the error does not follow a normal distribution, observations are independent, or if the relationship between the response variable Y and the fixed effects $X\beta$ is not linear. The general linear model allows a link function g to "link" the predictors $X\beta$ to Y. Such a link function is often of the exponential family, such as binomial, Poisson, and other distributions, to avoid a strictly linear relationship between the variables X and the response Y. Another extension, the linear mixed model, is also widely used. This model incorporates random effects, which allows to the user to model dependencies or correlated observations, such as with repeated measurements within subjects. The GLMM incorporates both by allowing modeling of non-normal data through a link function and adding random effects to account for correlated observations. The general equation is as follows:

$$Y = h(X\beta + Z\gamma) + \epsilon$$
$$\gamma \sim \mathcal{N}(0, G)$$

where Y is our response ($N \times 1$), X is our fixed effects ($N \times P$), β are our coefficients ($P \times 1$), Z are our random effects ($N \times Q$), and γ are our random effect assignments ($Q \times 1$). Finally, $h(\cdot)$ is our link function.

2.5 Machine Learning

Throughout this thesis we incorporate various machine learning tools to achieve prediction and automatic separation of electrographic patterns. We will cover the basics of machine learning in the context of EEG signal processing, particularly of models and concepts we often employ. Note that machine learning is a vast field and beyond the scope of this background section. We only describe concepts relevant to work in this thesis.

2.5.1 Overview

The ultimate goal in machine learning is to model $Y = f(X, \theta)$ and obtain estimates of the parameters θ [2] that allows us to accurately predict the label y_i for a new example x_i. Regression or classification models are used if Y is continuous or categorical, respectively. X corresponds to the input dataset, an $N \times P$ matrix with N examples and P features describing each example. f is a function which takes as input the dataset X and a set of parameters θ. Training a model involves estimating θ, often by minimizing the error $Y - \hat{Y}$, where $\hat{Y}$ are the estimated labels [3].

There is not always a clear delineation between statistics and machine learning, also known as statistical pattern recognition. However, generally, classical statistics is based upon modeling the data generating process and evaluating model fit by using goodness-of-fit tests and residual examination. Machine learning is not as concerned about modeling the data generating process, but rather is focused on finding a function or algorithm f based on the data that has high predictive accuracy [15]. For this reason, machine learning algorithms often require larger datasets and more powerful computation resources in order to capture the variability in a dataset and achieve generalizability. Many of the algorithms involve

---

[2] Note, we use β and θ interchangeably as the parameters of a model

[3] The ˆ, or "hat", indicates that the variable of estimated. In this case, the estimates of the true labels y.

ensembles, or collections of algorithms, which each individually weigh into a prediction, which has been shown to perform better than any single algorithm. We use both classical statistical methods as well as machine learning methods depending on the goals of the experiment.

Generalization

Consider the data used to optimize a model as the training dataset, and the data used to test a model the test dataset. The best measure of how well a given model is capturing the important features in a particular problem is to test your model on out-of-sample test dataset to obtain a test error. Thus, one is able to determine whether their model is overfitting (high variance, poor generalizability) by comparing the training error with the test error. A low training error with high test error indicates overfitting. In the ideal case, one would have enough data to do a hold-out validation (removing a percentage of your dataset as the final measurement of performance). Often, cross-validation is used in cases with limited examples. In this scheme, examples are held out while a model is trained on the remaining dataset, and this process is repeated until all examples are held out. The cross-validation performance is then the average error for all examples, and has been shown to be a good proxy for generalization error [79].

2.5.2 Features

Features are also known as predictors or to statisticians as covariates. While it is possible to feed a raw signal into a model such as a neural network, the high sampling rate of EEG often makes it computationally less attractive. Instead, average features are often calculated over moving windows.

Features provide an accurate representation of a signal of interest, ideally in a reduced di-

mensional space. In the above examples for NeuroPace and NeuroVista, line length, energy, area, half-wave, and Teager-Kaiser energy are hypothesized to accurately characterize a transient and increasingly epileptic background EEG signal. The features chosen in any machine learning problem is critical, as improper representation leads to poor performance regardless of the power of a selected classifier. Often times there are many more features than examples, described as the "Curse of Dimensionality", which with certain algorithms can lead to poor generalizability. This is because as more features are included, it becomes easier to model the training dataset, yet difficult to find the subset of features that are most important. For this reason, feature selection methods are often employed prior to evaluation with an algorithm. Algorithms can also be modified, or regularized, to reduce overfitting. However, the advent of ensemble methods in machine learning, and techniques such as bootstrap aggregation (bagging), may in fact thrive on large feature sets [15].

These features are then used in an algorithm tailored with the goal in mind. In supervised learning, the true classes (labels) are known. In unsupervised learning, the algorithm is intended to separate datapoints based on natural separation in the feature matrix

2.5.3 Supervised learning

Supervised learning algorithms model a given feature matrix X according to labels y. When given a new data example x_i, the algorithm outputs a corresponding label $\hat{y}_i$. Supervised learning can be broken down into classification and regression, where the labels y are categorical or continuous, respectively. To motivate several algorithms used in this thesis, we briefly review regression and classification.

Regression - Elastic net

We start with linear regression, a familiar case.

$$y = X\beta + \epsilon \tag{2.1}$$

where y represents the true (known) labels, X is the feature matrix, and w is the estimated weights, our model. In this simple case, there is a closed form solution to optimize the weights w

$$\beta = (X'X)^{-1}X'Y \tag{2.2}$$

This optimization minimizes the sum of squares to find the optimal w, the objective function being:

$$\text{Ł}(\beta) = ||Y - \hat{Y}||_2^2 = ||Y - X\beta||_2^2 \tag{2.3}$$

$$\beta = \text{argmin}(L(\beta)) \tag{2.4}$$

Because this is a greedy optimization, efforts have been made to regularize this objective function, resulting in modifications called the least absolute shrinkage and selection operator (LASSO) [147], ridge regression [62], and more recently the elastic net [169]. In our work we make the most use of the elastic net regression (equation 2.5), where a L_1 and L_2 penalty is added to the objective function

$$\text{argmin}_\beta ||Y - X\beta||_2^2 + \lambda_1||\beta||_1 + \lambda_2||\beta||_2^2 \tag{2.5}$$

The additional penalties regularize the objective function and helps alleviate overfitting

and high variance in a given model. The L_1 penalty ($||w||_1$) minimizes the sum of absolute values (equivalent to having a Laplace prior on β) and upon minimization zeroes out many features. The L_1 penalty is integral to the LASSO. The L_2 penalty minimizes the sum of squares (equivalent to a Gaussian prior on β) is used in ridge regression, which "shrinks" the betas towards zero and helps to alleviate problems of co-linearity by preventing one feature from dominating. The resulting model fit from regularized elastic net is often more generalizable than other models.

Classification

In cases where the labels y are categorical, the problem theoretically becomes a "classification" problem. However, it is important to note that many algorithms (Support Vector Machines, Random Forests, etc.) can also give continuous predictions, making the delineation more of semantics.

Logistic Regression

Logistic regression adds a logit link function to linear regression, allowing a mapping from a line to a sigmoid between 0 and 1. This thus represents a continuous probability of a particular class outcome. Though it is a regression algorithm as it predicts a probability, the model is fit to a binary Y label. Essentially, the equation models:

$$y = \frac{1}{1 + e^{-X\beta}}, \text{where } y \in [0, 1] \tag{2.6}$$

$$\text{argmin}_\beta \sum_i^n y_i \log(X_i\beta) + (1 - y_i) \log(1 - X_i\beta) + \lambda_1 ||\beta||_1 + \lambda_2 ||\beta||_2^2 \tag{2.7}$$

This model fits the log odds of the outcome y in a linear space, while increasing bias and

selecting features. One of the advantages of logistic regression, and one of the reasons why it is popular in the medical sciences, is that the β weights are easily interpretable. An increase in 1 unit of β corresponds to an increase in 1 log odds of the outcome y. For this reason, we use logistic regression in a generalized linear mixed model (GLMM) in Chapter 3 for easier interpretation of the resulting β's. We use the elastic net penalty for multi-class feature selection before input into another classifier, as other classifiers commonly outperform logistic regression as the decision boundary is still linear in log-odds space.

Random Forest

The random forest is an ensemble classifier that takes advantage of random sampling and weak-learning decision trees to achieve high predictive accuracy [14] (Figure 11). Each random forest consists of T decision trees, where each tree is given a random sample of training datapoints and a random sample of features, or otherwise known as "bagging" on samples and on features. Given the sample of features and of data points, each tree then optimizes a split corresponding to some metric of information or entropy. This is done by iterating through a group of possible splits and selecting the split that gives the best outcome. The split we use is Gini's Diversity Index. This index is a measure of node impurity and is computed as sum of the fraction of classes at a given node.

$$GDI = 1 - \sum_i p^2(i) \hspace{3cm} (\text{i = class i at node})$$

The T decision trees then form an "ensemble" which is used to product one output, either an average for regression or a majority vote for classification.

An interesting characteristic of random forests is that as the number of trees grows $(T \to \infty)$, the performance converges to the generalization error [14]. It has been shown to produce promising results in many settings. For example, in 1992 a random forest classifier achieved

only 0.7% error when recognizing handwritten digits (MNIST dataset).

In the context of interictal pattern detection, we use random forests to separate interesting patterns from noise. The important variables in a given random forest classifier can be examined by randomly permuting each feature and calculating the difference in performance [14], as seen in the discussion on spike detection below.
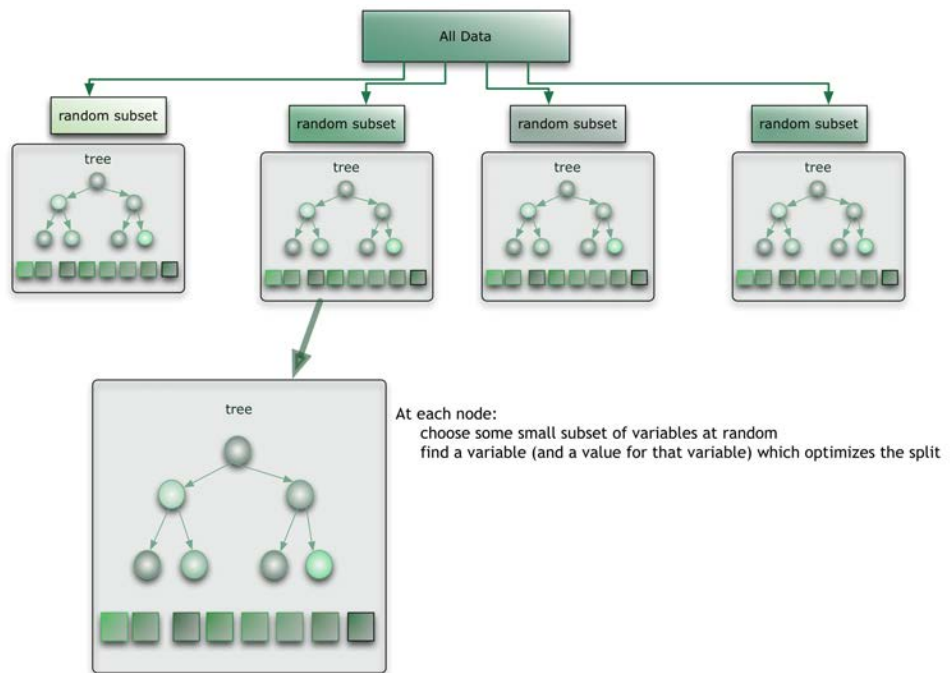
Figure 11: Random Forest Schematic. At each tree, a randomly sampled subset of features and examples are used.

2.5.4   Unsupervised learning

In unsupervised learning, we allow the algorithm to automatically determine interesting structure in the data. For the purposes of the experiments in this thesis, this entails separating EEG patterns into various groups, called clustering.

Clustering

K-means

K-means is a classic clustering algorithm that originated in the 1950-60s. Given a set of observations $(x_1, x_2, ...x_n)$ and cluster assignments $(C_1, C_2, ...C_k)$, the goal of kmeans is to find

$$\text{argmin}_s \sum_{i}^{k} \sum_{x \in S_i} ||x - \mu_i||^2, \text{ where } \mu_i \text{ is the center of points in cluster } S_i \qquad (2.8)$$

Gaussian Mixture Models

Mixture models allow separation of a dataset into distinct clusters that follow a particular distribution. Gaussian Mixture Models (GMM) is one type that is similar to K-means but is probabilistic instead of deterministic. Since K-means uses Euclidean distance as its distance metric, the covariance structure of each centroid is diagonal and shared between clusters. The GMM allows for each centroid to take a full covariance matrix, with or without sharing between clusters.

GMM can be optimized by expectation-maximation (EM) algorithm.

Likelihood

$$L(X, \theta) = \prod_i^n (\sum_c P(I_i = c) N(y_i; \mu_c, \sigma_c^2)) \quad \text{(Likelihood of observations)}$$

$$logL(X, \theta) = \sum_i^n log(\sum_c P(I_i = c) N(y_i; \mu_c, \sigma_c^2)) \qquad \text{(log likelihood)}$$

$$\frac{\partial logL}{\partial \mu_1} = \sum_i^n \frac{P(I_i = 1) N(y_i; \mu_1, \sigma_c^2)}{\sum_c P(I_i = c) N(y_i; \mu_c, \sigma_c^2)} \frac{y_i - \mu_1}{\sigma_1^2} = 0$$

$$\text{(e.g. diff w.r.t. } \mu_1)$$

Expectation

$$Let \; C_i = cluster \; assignment \; for \; example \; i$$

$$I_i(c) = 1 \; if \; obs \; i \; is \; in \; group \; c$$

$$p(C_i | y_i) = P(\hat{I}_i(c) == 1) = \frac{\prod_c P(C_i | y, \theta) N(y_i, \mu_c, \sigma_c^2))^{1(c=C_i)}}{\sum_c P(C_i = c | y, \theta) N(y_i, \mu_c, \sigma_c^2)}$$

Maximation

$$\text{(Plug in above into likelihood, solve for missing variables)}$$

$$\sum_{i=1}^n \hat{I}_i(c) \frac{y_i - \mu_c}{\sigma_c^2} = 0 \qquad \text{(subbing into likelihood)}$$

$$\mu_c = \frac{\sum_i^n \hat{I}_i(c) y_i}{\sum_i^n \hat{I}_i(c)}$$

$$\hat{\sigma}_c^2 = \frac{\sum_i^n (y_i - \mu_i)^2}{\sum_i^n \hat{I}_i(c)} \qquad \text{(Repeat steps until convergence)}$$

Gap Statistic

With both K-means and Gaussian mixture models, the choice of the number of clusters (K) must be specified. There are numerous ways for selecting this metric, though we use in

our work the gap statistic. The gap statistic essentially compares intra-cluster dispersion of the data relative to a null distribution ($E_n^* log(W_k)$) [146]. This is determined by randomly sampling within the feature space.

$$D_r \sum_{i,i' \in C_r} d_{i,i'} \qquad \text{(Distance metric between point i and centroid ii')}$$

$$W_k = \sum_{r=1}^{k} \frac{1}{2_n^r} D_r \qquad \text{(sum of all distances in cluster r to centroid)}$$

$$k = \text{argmax}_k \, Gap_n(k) = \text{argmax}_k \, E_n^* log(W_k) - log(W_k) \qquad \text{(finding k)}$$

Note that the clusters should be validated regardless of the statistic used for selection.

2.6   EEG Pattern Recognition

The tools developed to expedite the processing and detection of EEG patterns have been aggregated into a toolbox . Currently, it is integrated with the `ieeg.org` portal and requires Matlab. In theory, this toolbox is able to take marked examples of specific patterns and detect all like patterns in a given dataset, although for the purposes of this thesis it has been developed for spike, burst, and seizure detection.

The main challenges encountered during pattern detection are as follows:

1. Lack of true labels due to time required to manually mark EEG

2. Poor inter-rater reliability

3. Varying quality of datasets

4. Varying electrode placement for iEEG

5. Poorly generalizable algorithms

To overcome these shortcomings, we develop an intelligent supervised detection system that generalizes the approaches seen in literature (Figure 18). More specifically, we first adopt a hypersensitive detector based on a set of user marked true positives. This involves optimizing the distance between markings and surrounding background, selecting for the single feature as well as the threshold. Following this, all hypersensitive detections are made. These detections are expected to have many false positives. We then extract comprehensive features from all hypersensitive detections, reduce them with principal component analysis (PCA), and cluster them into an automatically selected number of clusters. Random examples are uniformly sampled from each cluster and presented to the user for marking, which maximizes the gain from marking a variety of examples. These marked examples are again, after feature extraction, placed into a classifier. Once classification is optimized and accepted by the user, all hypersensitive classifications are made.

2.6.1   Spike Detection

For spike detection, we initially segment the data to detect peaks for further classification. This can be done with various metrics, such as signal envelope [71], line length or simply amplitude post-filtering. Essentially, we attempt to detect transient perturbations in the background signal which suggests the presence of a spike, and maximize the distance between background and spikes to determine the threshold (Figure 12, Algorithm 2)[4].

---

[4]In Chapter 3 we use signal envelope as its performance had been characterized [71]. Following initial detections, we apply a spatial filter that aggregates and includes only spikes that occur in more than one channel, which increases the positive predictive value of each detected spike.
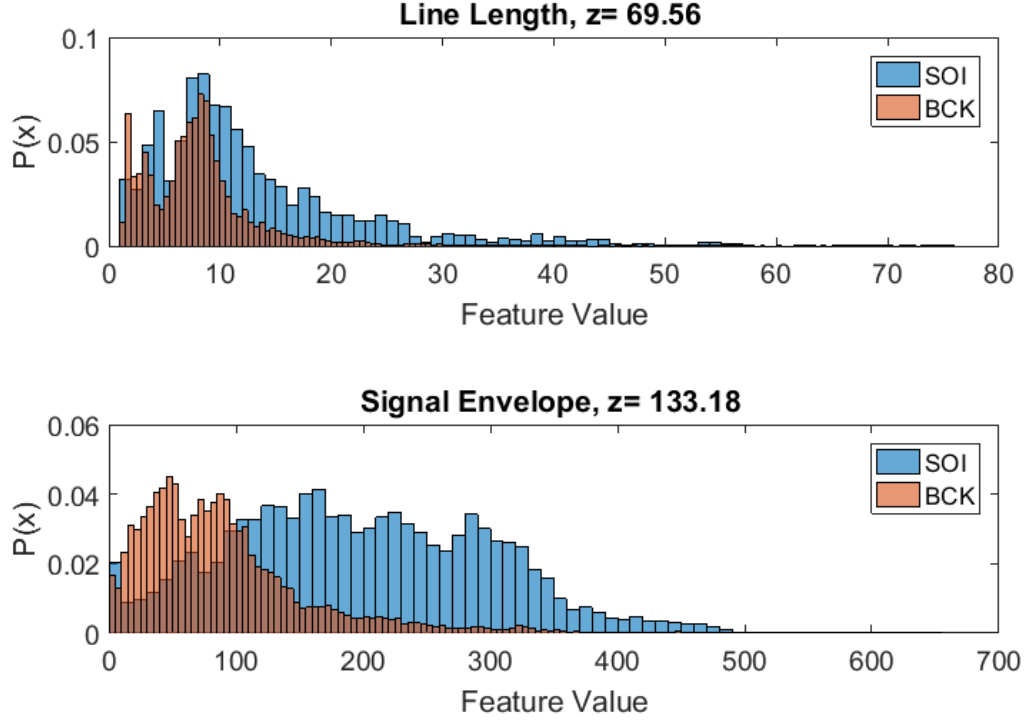
Figure 12: Selection of hypersensitive feature. Distribution of background (BCK) and signal of interest (SOI) for two features are shown. In this particular example, signal envelope better separates the two

After initial segmentation, users are prompted to mark examples of each class intelligently as detailed above. Specifically, we extract features (50 ms before and 150 ms after the peak, selected as spikes are generally <200-250 ms in total duration) from all hypersensitive detections and cluster using the GAP statistic. From this, we sample uniformly from each cluster to ensure that labels are given to samples that will provide a best representation of the class distributions. Using these layers, features are then extracted from each spike into a random forest classifier. For spike detection, we have found the normalized continuous wavelet transform (CWT) coefficients to be informative features.

Wavelet Transform

The wavelet transform is one form of time-frequency decomposition, similar to the Fourier transform, except it allows adaptive resolution in time. This means that for higher frequency signals, the time duration of a window shortens thereby allowing higher resolution. This is in contrast to the short-time Fourier transform , which has a fixed resolution due to the time-frequency duality. This advantage allows us to capture more transient signal changes as seen in spikes. In CWT, a mother wavelet is convoluted with the signal at various scales and times. Figure 13 shows the Mexican Hat wavelet at various scales, and the corresponding wavelet transform coefficients of several spikes and background are shown in Figure 14. The CWT of a function $x(t)$ for at a scale a and translation b.

$$X_w(a,b) = \frac{1}{|a|^{1/2}} \int_{-\infty}^{\infty} x(t)\bar{\phi}(\frac{t-b}{a})dt \tag{2.9}$$

Further postprocessing includes serialization of coefficients for each spike before applying principal component analysis (PCA) to capture the direction of highest variance (Figure 15). This pipeline has been shown to have 99% sensitivity and specificity and 88% positive predictive value during out of bag prediction for marked spikes in ECoG of two patients (Table 2).
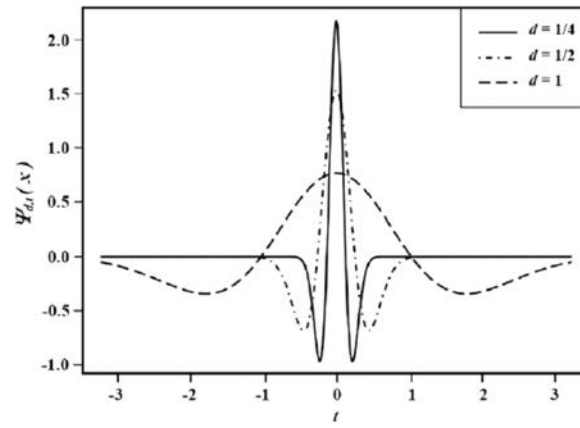
Figure 13: Mexican Hat Mother Wavelet at multiple scales

	Predicted False Spike	Predicted True Spike
False Spike	1733	22
True Spike	1	101

Table 2: Confusion matrix for CWT spike detection with random forest. Model with 2000 trees, optimizing for sensitivity by penalizing false negatives 50x more than false positives. Results of out-of-bag predictions are given. Note that this performance is on par with inter-rater reliability in spike identification [48]

(a) Continuous Wavelet Transform of two spikes

(b) Continuous Wavelet Transform of Background EEG
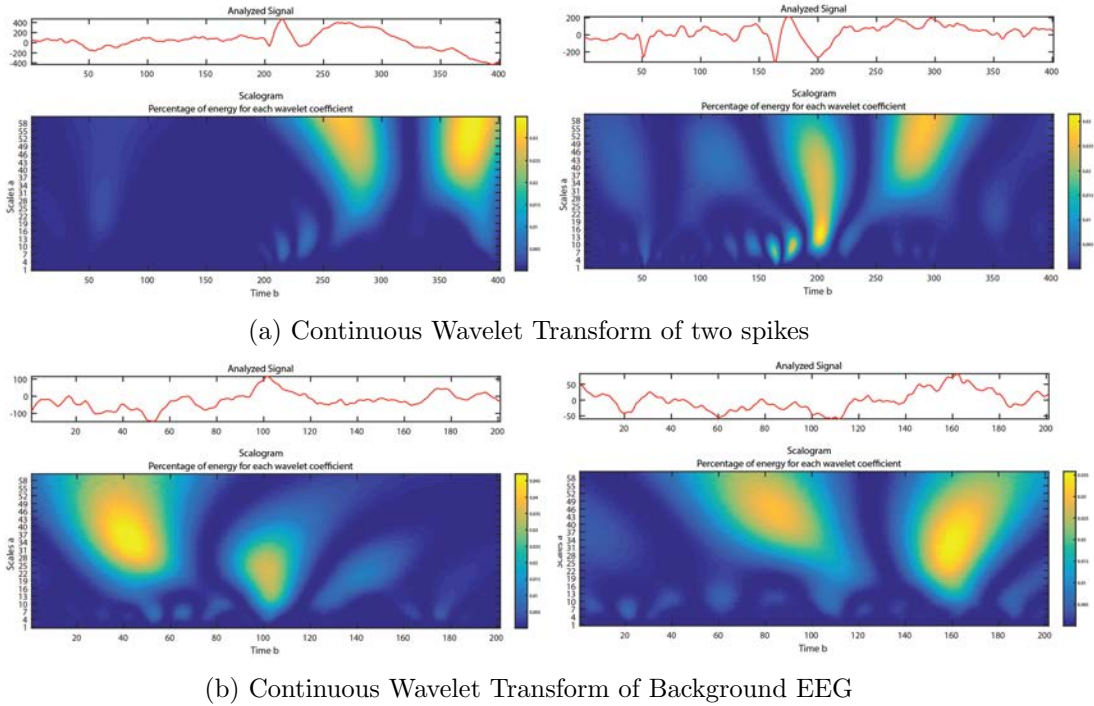
Figure 14: Continuous wavelet transform and corresponding EEG. (a) CWT of two identified spikes, centered. Notice the evolving high → low frequency evolution capturing a spike and subsequent slow wave. (b) Randomly selected interictal segments of a similar length, where the observed spike-like pattern is not seen. In each subplot, the analytical signal (top) and wavelet coefficients (bottom) are plotted. X axis is time, y axis is centered voltage (mV) for the analytical signal, scale for CWT. Higher scale indicates lower frequency components.
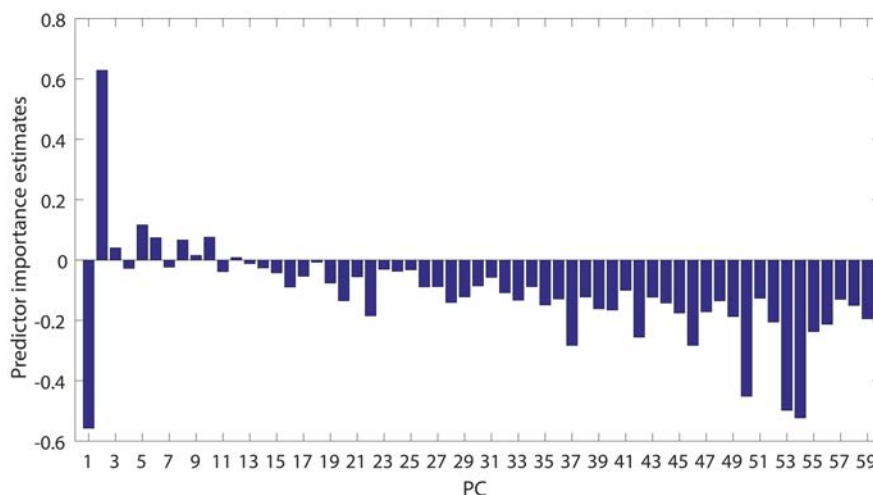
Figure 15: Variable importance. The variable importance metric for the model given in Table 2 for spike detection. Feature inputs here correspond to the principal components of the CWT coefficients. Variable importance value is calculated as the increase in prediction error if that variable's values are permuted across the out-of-bag observations. This measure is computed for every tree, averaged over the entire ensemble, and divided by the standard deviation over the entire ensemble.

In this particular case, further validation can be performed by mapping the variable importance back into the original wavelet space by multiplying the weight vector by the principal components 16.
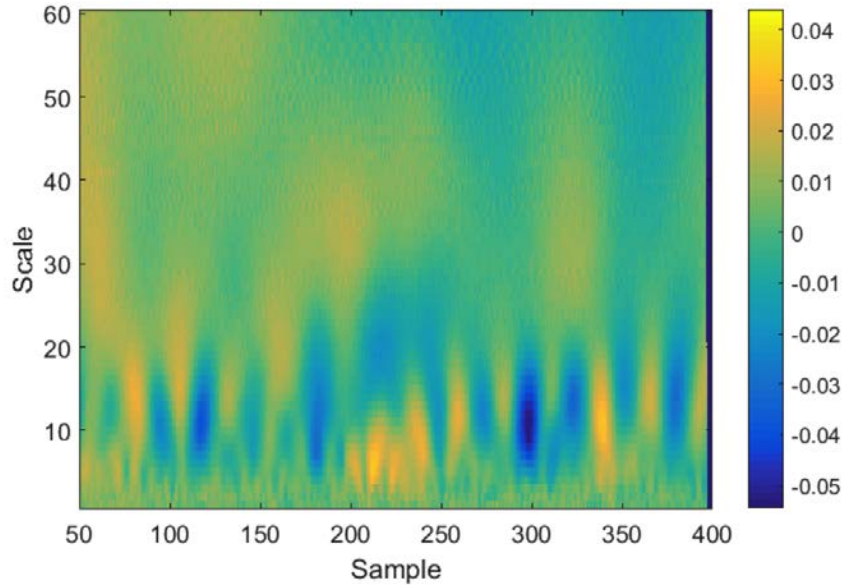
Figure 16: Variable importance In Wavelet Space. The corresponding weights are transformed back into the original space using the principal components. The colorbar indicates regions of high importance (yellow) versus low importance (blue). Notably, a sequence of importance regions at timepoint 200 indicate the high frequency component of a spike.

2.6.2   Burst Detection

Burst detection is done with the same pipeline. A hypersensitive detector is optimized based on marked patterns (Figure 15).
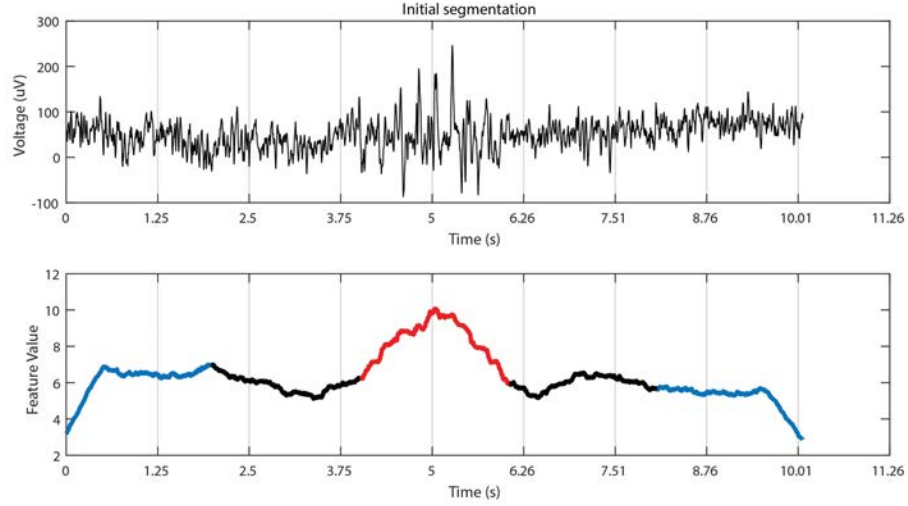
Figure 17: Example of hypersensitive detection optimization on burst. Raw signal (top) with line length feature (bottom). Red indicates pattern feature values, black indicates background. Recommended threshold is given as $mean(background) + M * sd(background)$, where M is the multiple (4 by default).

After initial segmentation, users are again prompted to mark examples of each class from the hypersensitive group or random segments will be sampled to form the negative class. The latter works well for rare events, such as seizures, where oversampling of the data will be more representative of interictal segments. Comprehensive features are extracted that include spectral characteristics (Fourier and Wavelet transforms), time domain features such as line length, as well as other features designed to pull out a particular pattern. At this stage, feature selection/reduction is performed (e.g. PCA) before clustering. Clustering allows separation of natural groups, which is useful to intelligently serve different clusters for manual marking. After manual marking, supervised algorithms can then be used.

2.6.3 Spatial Integration

One of the defining features of a real neurophysiological patterns is a field effect, meaning the activity is seen across multiple electrodes. We take advantage of this by modeling the

spatial distribution of the field and incorporating that into our feature set. This is done in two ways: 1) For the hypersensitive detections, we use channel specific thresholds and conduct a spatial integration step, which combines detections across all channels within a given window length. 2) During the classification step, the distribution of min, max, and mean voltage across all channels are included as features.

2.6.4 Algorithms
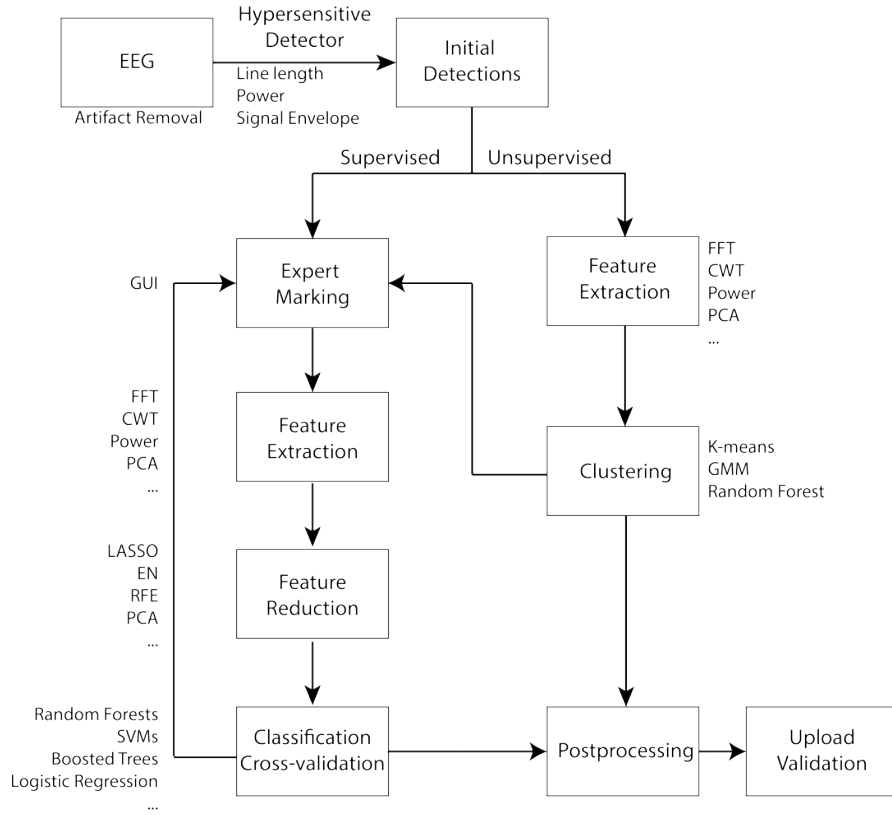
Figure 18: Pipeline overview for detection of discrete patterns in EEG. Hypersensitive detections are optimized based on an initial set of training data. After segmentation, users can choose to cluster or to mark more patterns for unsupervised detection. Marking of clusters is also available to feed as training data into a supervised classifier. Feature extraction, reduction, and classifier testing is then run for those who choose the supervised process. If it is decided more training data is necessary, additional data can be obtained from marking of initial detections.

Algorithm 1: Hypersensitive Pattern Detection Pipeline

Data: IEEGDataset from ieeg.org with examples of marked annotations

Result: All similar annotations uploaded onto ieeg.org

1 read all annotations from specified layer

2 $minChan \leftarrow$ min number of channels in training layer `// Is there a field?`

3 for *each annotation i* **do**

4 $\quad$ obtain raw EEG with padding *pad* on each side `// default `*pad*`: 2*length of min burst window`

5 $\quad$ **for** *each hypersensitive feature f* **do**

6 $\quad\quad$ compute hypersensitive feature on raw EEG

7 $\quad\quad$ extract mean surrounding background feature values $B_i f$ `// surround = same length as window for burst on each side`

8 $\quad\quad$ extract mean pattern feature values $P_i f$

9 $\quad\quad$ extract duration

10 $f \leftarrow \operatorname{argmax}_f \sum_i^n ||P_{if} - B_{if}||^2$ `// ` $f =$ `feature (e.g. LL, signal envelope, amplitude, etc. Can also use max Z from Wilcoxon Rank Sum test)`

11 $winLen \leftarrow min(duration)/2$

12 $thres \leftarrow$ min feature value above $mean(background) + mult * sd(background)$ `// default: mult=4`

13 for *each EEG block until end of dataset (parallelize here)* **do**

14 $\quad$ get data from ieeg.org

15 $\quad$ determine times where feature is above *thres*

16 $\quad$ retain times where duration $> 2 * winLen$

17 while *annotations remain* **do**

18 $\quad$ combine annotations within a specific search window `// Spatial Integration`

19 $\quad$ retain annotations that span $> minChan$ channels.

20 upload annotations to IEEGDataset

Algorithm 2: Spike Detection Pipeline

Data: IEEGDataset from ieeg.org with examples of marked spikes

Result: All similar annotations uploaded onto ieeg.org

1 read all annotations from specified layer

2 $minChan \leftarrow$ min number of channels in training layer   `// Is there a field?`

3 **for** *each hypersensitive feature f* **do**

4   **for** *each annotation* **do**

5   align peak to maximum absolute value within .5 s

6   obtain raw EEG with padding *pad* on each side   `// default `*`pad`*`:  [0.5 s`
        `before and 0.15 s after`

7   extract mean pattern feature values P_{if}

8   compute hypersensitive feature B_f on entire raw EEG in .2 s window length
    `// Process by hr blocks if too large`

9 $f \leftarrow \mathrm{argmax}_f \frac{1}{n} \sum_i^n ||P_{if} - \bar{B}_f||^2$ `//` $f =$ `feature (e.g.  LL, signal envelope,`
    `amplitude, etc), can also use Wilcoxon Rank Sum Z values for feature`
    `selection`

10 $\mathrm{mult} \leftarrow (\frac{1}{n} \sum_i^n P_{if} - \bar{B}_f)/\sigma_{B_f}$

11 $\mathrm{thres} = \bar{B}_f + mult * \sigma_{B_f}$ `// default:  mult=3.5`

12 **for** *each EEG block until end of dataset* **do**

13   get data from ieeg.org

14   calculate feature f across block using .200s windows determine times where feature is
    above thres

                             `// This block is done in parallel for speed`

15 **while** *annotations remain* **do**

16   combine annotations within a specific search window   `// Spatial Integration`

17   retain annotations that span $> minChan$ channels.

18 upload annotations to IEEGDataset

19 **for** *each spike n of N* **do**

20   extract each spike .05 s to 0.150 s around each peak

21   extract continuous wavelet transform coefficients with scales 1:60 and Mexican Hat
    wavelet

22   vectorize each set of coefficients to create data matrix $N \times p$

23 Obtain first 60 principal components

24 Optimize random forest with first 60 principal components using cross validation

25 To see top principal components, calculate variable importance and map to wavelet space

---

Algorithm 3: General Classification Pipeline

Data: IEEGDataset from ieeg.org with training and test annotations
Result: Annotated hypersensitive detections on ieeg.org

1 mark X true positives, true negatives obtain signal fingerprint from true training layer
   `// features given in appendix and dependent on signal of interest`
2 obtain signal fingerprint from false training layer
3 Feature selection   `// default: Logistic Elastic Net, optional`
4 Optimize classifier (default: Random Forest) with CV to obtain performance
5 obtain signal fingerprint from hypersensitive detections
6 Classify all hypersensitive detections
7 upload results to ieeg.org

Chapter 3

Effect of Interictal Spikes on Cognition

3.1 Abstract

Cognitive deficits are common among epilepsy patients. In these patients, interictal epileptiform discharges, also termed spikes, are seen routinely on EEG and believed to be associated with transient cognitive impairments. In this chapter, we investigate the effect of spikes on memory encoding, taking into account the spatial distribution of spikes in relation to the seizure onset zone as well as anatomical regions of the brain. Sixty-seven patients with medication refractory epilepsy undergoing intracranial EEG monitoring engaged in a delayed free recall task to test short-term memory. In this task, subjects were asked to memorize and recall lists of common nouns while intracranial electrodes recorded electrophysiological activity. We quantify the effect of each spike on the probability of successful recall using a generalized logistic mixed model. We found that in patients with left lateralized seizure onset zones, spikes outside the seizure onset zone impacted verbal word encoding, whereas those within the seizure onset zone did not. In addition, spikes in the left inferior temporal gyrus, middle temporal gyrus, and fusiform gyrus during memory encoding reduced odds of recall by as much as 19% per spike. These results suggest that interictal spikes disrupt cognitive processes in the underlying tissue, and that seizure onset regions are dysfunctional at baseline.

3.2   Background

In many epilepsy patients, cognitive and memory deficits are common complaints, some of which are not captured by traditional neuropsychological tests [13, 153]. Characteristic epileptiform patterns recorded on the electroencephalogram such as interictal spikes, rhythmic bursts, wave discharges, and focal slowing are not always accompanied by overt clinical symptoms but can still be detrimental to the patients psychosocial functioning and quality of life [64, 65]. These electrographic patterns have been associated with transitive cognitive impairment [1, 64, 76, 77], and elucidating the relationship between these electrophysiological patterns and their functional consequences is a crucial step in improving treatment and quality of life for epilepsy patients.

Parameters for functional assessment of patients with epilepsy involve neuro-psychological tests that explore cognitive, behavioral, linguistic or motor impairment. These tests provide information on a global level such as whether a person can safely live by himself, return back to work or school, or drive. Qualitative measures of patient well-being are important for treatment, but a more quantitative measure of cognitive function is required to understand the mechanism underlying the prominent memory and cognitive complaints that plague a significant portion of patients with epilepsy. Therefore, insight into the electrophysiological basis of memory encoding and decoding and its disruption due to electrographic epileptiform activity is important both clinically and neurophysiologically.

Intracranial EEG (iEEG) recordings provide higher temporal and spatial resolution of brain activity than non-invasive EEG. These data provide an opportunity to study the electro-physiological correlates of a wide range of cognitive processes with greater detail [86]. For example, IEEG has been used to study the neural basis of human cognition, using non-epileptic regions of the brain as models for normal healthy brain and as controls. Typical

electrophysiological patterns are consistently seen across various performance tasks. In studies of memory, there is evidence that electrophysiological and hemodynamic changes occur during encoding, termed the subsequent memory effect (SME) [113, 131]. High frequency oscillatory activity of neurons has been associated with specific cortical network states and has been used to quantify the electrophysiological mechanisms of memory formation and recall. Gamma oscillatory activity, for example, exhibits anatomical, temporal and functional specificity [69]. Early studies showed that increases in gamma activity in the hippocampus and the left temporal and frontal cortices is associated with successful memory formation, consistent with previous functional magnetic resonance imaging (fMRI) studies [130]. Therefore the magnitude of these oscillations during encoding indicates that synchrony in widespread networks of cortical regions can serve as a predictor for successful memory recall [131].

In this study, we focus on interictal epileptiform discharges, also termed spikes, recorded on iEEG. Interictal spikes are highly correlated with the presence of epilepsy, though their representation with respect to regions of structural and functional abnormalities, influence on patient behavior and physiology, and relationship to ictal activity has not yet been well defined [136]. EEG-fMRI studies have confirmed that interictal spikes may be separated into different populations with some resulting in modifications of metabolism well beyond the clinically identified epileptic focus [78]. This suggests that spiking activity in the epileptic foci may be deleterious for a larger section of the brain (beyond the foci) and may interrupt normal electrophysiology and functioning. Several studies have suggested that hippocampal spikes disrupt cognition [49, 76, 77], though the effect across a wider spatial distribution remains unknown. In our recent study including an independent group of 80 epilepsy patients with iEEG performed by the Restoring Active Memory collaborative research group, middle temporal inferior temporal and fusiform gyri spikes were shown to negatively impact

memory encoding [66]. We aim to validate these findings on an independent dataset and to better quantify the effect of spikes both regionally and with respect to the seizure onset zone (SOZ).

Improper memory encoding and recall in correlation with interictal spiking places emphasis on targeted therapy for cognitive dysfunction and potential improvement in the localization of epileptic foci [13]. As spikes are helpful in localization of the SOZ only in some patients [50, 98], understanding the differences between populations of spikes may better aid onset localization. We hypothesize that regional interictal spiking will have a detrimental impact on cognition by disrupting the SME, suggesting that altering epileptic networks to reduce spiking in normal brain may positively impact cognition.

The overarching hypotheses that were tested during this study are 1) interictal spikes disrupt memory encoding, 2) There is an observable functional anatomy in which these spikes lie, 3) Epileptiform activity outside of the seizure onset zone disrupt memory encoding whereas spikes within the seizure onset zone are not deleterious to verbal memory encoding . We address these hypotheses using automated spike detection in iEEG during a delayed free recall task and identify the brain regions implicated in incorrect recall.

3.3   Methods

3.3.1   Subjects

Sixty-seven patients with drug resistant epilepsy at the Hospital of the University of Pennsylvania (N=16) and Thomas Jefferson University Hospital (N=51) were included in this study. This included 45 males and 22 females, with an average age of 35.55 (Range=[15 57], SD = 12.17). Additional subject information is given in Table 7. A total of 6144 intracranial electrodes were implanted across all patients during clinical management and included

both depth and subdural electrodes. All participants provided informed consent with procedures approved by the Institutional Review Board from the University of Pennsylvania and Thomas Jefferson University Hospital.

3.3.2   Delayed Free Recall task

A delayed free recall episodic memory task was used to investigate memory encoding and recall. For each encoding period of task, subjects were asked to memorize a list of words composed of 15 common nouns, chosen at random and without replacement from a pool of high-frequency English nouns [131]. The subsequent recall period involved subjects recollecting the words presented during the encoding period in any order. Each subject received 12-60 such word lists to encode and recall in each session, the number of trials per subject as well as the number of sessions depended on the subjects interest and availability for testing.
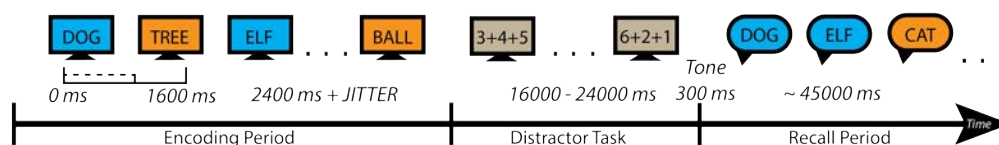
Figure 19: Delayed Free Recall Task. Blue indicates correctly recalled words and orange indicates incorrectly recalled words. Subjects were presented 15 words during the encoding period, followed by a distractor task that consisted of simple arithmetic problems. After a tone, subjects engaged in free recall, vocalizing presented words in any order. Subjects were presented 12-60 word lists in each session.

A computer program presented stimuli and recorded subject responses. Each trial began with a plus sign to alert the subject to an upcoming presentation of words. The plus sign appeared for 1600 ms followed by an 800-1200 ms blank interval. Each word was then presented for 1600 ms followed by an 800-1200 ms blank interstimulus interval. Subjects were asked to read each word aloud or to themselves to ensure attentiveness. Following the presentation of a list of words, a short distracter period was introduced between the

encoding and recall periods to reduce the recency effect often observed for free recall tasks
[104]. During this distracter period subjects were asked to solve a series of simple arithmetic
problems composed of A + B + C, where A, B, and C consisted of randomly selected one-
digit positive integers. Participants responded by typing their answer onto the keyboard,
with feedback provided through a high-pitched tone for correct answers and a low-pitched
tone for incorrect answers. Each distracter period lasted for 1600-2000 ms and was followed
by a 300 ms tone concurrent with a row of asterisks that signaled the start of the recall
period. The recall period lasted for approximately 4500 ms during which subjects were asked
to recall words in any order presented during the encoding period and their vocal responses
were recorded. Words that were presented during the encoding period and retrieved during
the recall period were considered correctly encoded and correctly recalled while those that
were not retrieved were considered incorrectly encoded. Furthermore, words from prior
encoding periods that were retrieved during a recall period were considered incorrectly
recalled.

The computer sent a pulse to an unused recording channel in order to synchronize the be-
havioral events during the memory task with the electrophysiological recordings. The time
stamps associated with these pulses were used to annotate the iEEG recordings. Annota-
tions and the iEEG recordings were converted to the Multiscale Electrophysiology Format
[16] and uploaded to IEEG.org in bipolar reference montage for analysis.

3.3.3   Preprocessing and removal of artifact channels

Sampling rates varied from 400 to 2000 Hz. Artifact channels were identified by calculating
the line length feature across each channel and those that differ by more than four times
the mean across all channels were removed [38]. This process is intended to remove grossly
artifactual channels.

3.3.4 Spike Detection

Despite complex methods in literature, automatic spike detection has proved to be a difficult task to perfect. Many detectors suffer from a high false positive rate, as some artifacts have spike-like morphology [157]. Another reason for this difficulty is reflected in the poor inter-rater reliability even among experts. Inter-rater reliability in spike marking may range from 41% to 80% [48]. However, automatic spike detection is a reasonable solution for our analysis because 1) we adopt a highly sensitive algorithm, and 2) our statistical analysis compares two groups that will be equally affected by false positives. Thus, false positive detections should be equally distributed within each individual any differences in means will be investigated.

A detector based off of an algorithm published by Janca et al. was used to automatically detect spikes for all patients [71]. This algorithm applies the signal envelope to identify spikes by modeling background activity and determining transient outliers. Briefly, signals were downsampled to 200 Hz before 10-60 Hz bandpass and 60 Hz notch filters were applied. For each channel, the signal envelope was calculated with the absolute value of the Hilbert transform. Moving windows of 5 s with 4 s overlap were used to model a log-normal statistical distribution of the signal envelope. A threshold of κ_1 * [Mode + Median] was used for the initial detection of spikes, where $\kappa_1 = 3.65$, determined empirically through cross-validation by the original authors [71]. Following initial detections and to improve our positive predictive rate, we added a spatial filter to identify spikes across multiple channels. Any spikes within 200 ms on more than one channel were combined and treated as one spike. A subset of candidate spikes was randomly selected across all patients and validated by a board certified epileptologist (KD) to ensure adequate performance, specifically positive predictive value.

The encoding phase was defined to be the period after a word stimulus prior to the subsequent word stimulus. The number of spikes during this period was extracted for all words. Any spike that involved one or more channels in the clinically determined SOZ was categorized as a seizure onset spike. Spikes were also categorized into anatomical locations determined by the Talairach coordinates of the electrodes following co-registration of post-implant CT to pre-implant T1-weighted MRI.

3.3.5   Statistical analysis

A linear model was used to test the effect of subject level variables (age and sex) versus mean recall rate and mean spike rate across all patients. Welchs t-test was used to determine differences in mean recall rates and spikes per electrode between left and right lateralized patients. To model the effect of spikes on correct versus incorrect recall on a word-by-word basis, we use a generalized linear mixed model (GLMM) with a logit link function. The GLMM was fit to predict successful recall with the serial order of word presentation, age, and the number of spikes as fixed effects (equation (3.1)). We varied the spike count according to the region of interest. In addition, we add a random effect for each subject nested by session. This allows us to model variability among subjects (with different baseline recall rates) as well as variability among different sessions within a subject. A logit link function permits us to model a binary outcome (recalled vs not recalled) and to interpret the estimated coefficients probabilistically. The fixed effects represent the mean effect across all subjects after removal of intersubject and intersession variability. To confirm the need for a mixed, nested model, a likelihood ratio test was used to test model fit before and after sequential addition of random effects and covariates (Table 3). Effect sizes (odds ratios) and confidence intervals are reported with significance by Wald statistics when testing multiple parameters. Likelihood ratios are reported when testing single parameters (regional analysis).

3.3.6 Logistic GLMM

We model recall success as a binomial distribution represented by parameter π_{ij} that represents the probability of successful recall on word i for subject j given our parameters β.

$$y|\pi_{ij} \sim Binomial(1, \pi_{ij})$$

$$\pi_{ij} = P(y_{ij} = 1|\beta)$$

Using maximum likelihood, we estimate β to maximize $P(y_{ij} = 1|\beta)$ with a logistic generalized linear mixed model of the form below. With a logit link function, we predict the log odds as a linear function of our fixed effects (age, $word\_order$, and $spike\_count$) as well as our random effects. We use a nested random effects model to account for variability in baseline recall rates for each person and, within each person, variability between sessions. This is because we expect there to be correlation between trials within each session within each subject. Below, b codes for variation in mean recall rate for subject j and $a_{k(j)}$ codes for variation in recall rates for each session k within subject j.

$$log(\frac{\pi_{ijk}}{1 - \pi_{ijk}}) = \beta_1 age_j + \beta_2 word\_order_i + \beta_3 spike\_count_{ijk} + b_j + a_{k(j)}$$

$$b_j \sim \mathcal{N}(0, \sigma^2), a_{k(j)} \sim \mathcal{N}(0, \tau_j^2)$$

(3.1)

MLE was performed using the Laplace approximation within the lme4 package in R. For better interpretation, odds (e^β) are reported with 95% confidence intervals calculated with the profile likelihood method, which makes fewer assumptions regarding the estimates. For regional analysis, $spike\_count$ was replaced with that from each region and the model refitted. Corresponding e^{β_3}'s are reported. P values are determined using the likelihood ratio test, which compares the difference between likelihood of a null model (without the corresponding

region) to an alternative model with the region, which follows a Chi-squared distribution. P values for regional analysis were corrected with the Holm-Bonferonni method.

3.3.7 Seizure onset zone

We sought to determine the effect of spikes on identified SOZs. For this analysis, 57 patients with clinically localized SOZ were included. The clinical localization process varied for each patient and was directed towards identification of the seizure etiology and onset region(s), which may include clinical semiology, imaging, electrophysiological recordings, and expert consensus. To determine the effect of spikes relative to the SOZ, channels were first divided into seizure onset and non-seizure onset channels. Since spikes may occur across multiple channels, if any channel within the SOZ was involved, the spike was categorized as a seizure onset spike. Similarly, spikes completely outside the SOZ were classified as non-seizure onset spikes. The GLMM was refitted with the addition of these two covariates as well as an interaction term for clinical SOZ lateralization.

3.3.8 Regional analysis

All 67 subjects were included for the regional analysis. Each electrode was grouped into regions corresponding to level 5 of the Talairach atlas, which includes Brodmann areas (BA) and the hippocampus [87]. Due to variability in electrode positioning across patients, independent GLMMs were fit on regions containing electrodes from 20 or more patients. For each region, a null model containing serial word position and age was fit, and an alternative model with the addition of regional spikes was fit. Significance was determined by the likelihood ratio test and adjusted for familywise error with the Holm-Bonferroni method [63].

3.4 Results

A total of 244/6144 channels were identified as artifact and removed from the analysis. Over 900 detected spikes were randomly selected from all patients and validated by a board certified epileptologist (KD). Positive predictive rate was 72.2%. False positive rate was 15.5%. Of all detected spikes, 12.3% were deemed indeterminate. An example of detected spike shown in Figure 20.
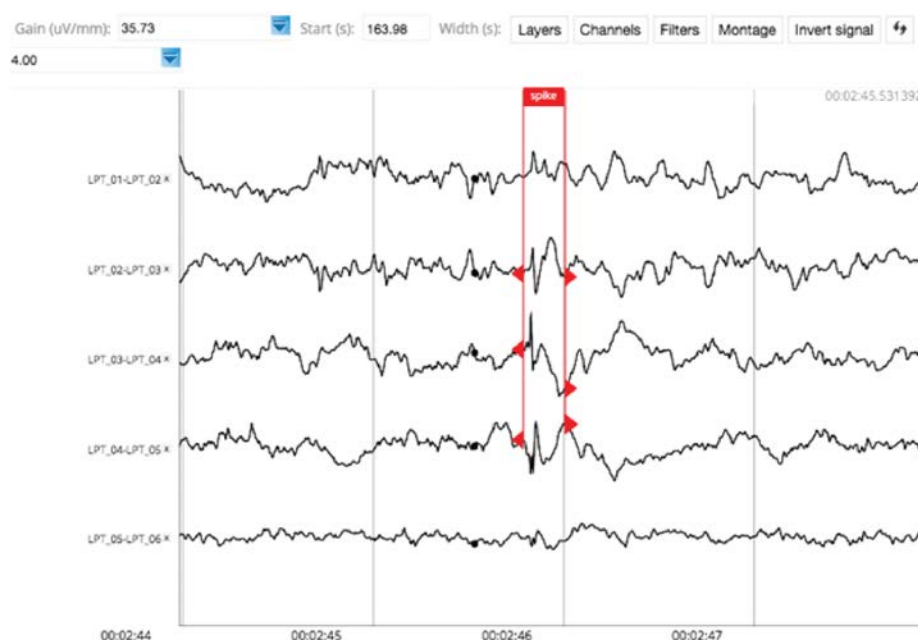
Figure 20: Example of spike spanning three bipolar channels on ECoG

Subjects on average recalled at a rate of 24% ($Range : [4 - 48\%], SD = 9\%$). Older age was significantly associated with a decrease in mean recall rates ($t(54) = -2.9, p = 0.005, R^2_{adj} = 0.1$), but not average spike rates (Figure 21A). There was no significant difference in mean recall rates or mean spike rates by sex (Figure 21B). Initial words were recalled with greater accuracy (Figure 21C). Patients with left lateralized onset regions (N=23) had lower mean recall rates than patients with right lateralized onsets (N=26)

$(t(47) = 3.1, p = 0.003, d = 0.9)$ (Figure 22). In addition, a greater percentage of spikes per electrode occurred ipsilateral to the seizure onset region (Left onset : $t(36.3) = 4.2, p < 0.001, d = 1.33$; Right onset : $t(38.1) = 4.5, p < 0.001, d = 1.34$) (Figure 22). Spike and seizure onset zone co-localization is given in 26.
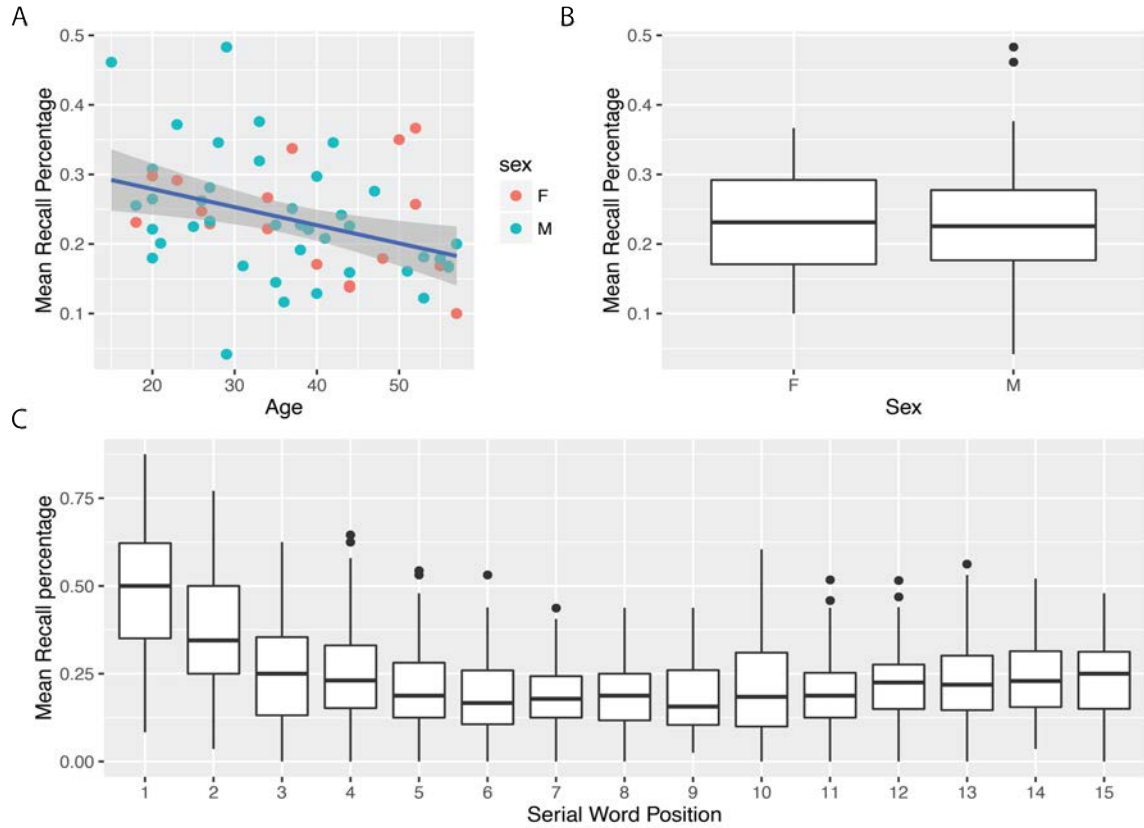
Figure 21: Mean recall percentage by (A) age, (B) sex, and (C) serial word position. Vertical axes represent the mean recall percentage across all plots. (A) Each point represents a patient with sex indicated by color. The horizontal axis indicates age. A best fit line is plotted with a standard error ribbon. (B) Mean recall by sex; boxplots indicate median, 25th, and 75th percentiles. (C) The horizontal axis indicates the serial word position, where position one is the first word presented in a given trial.
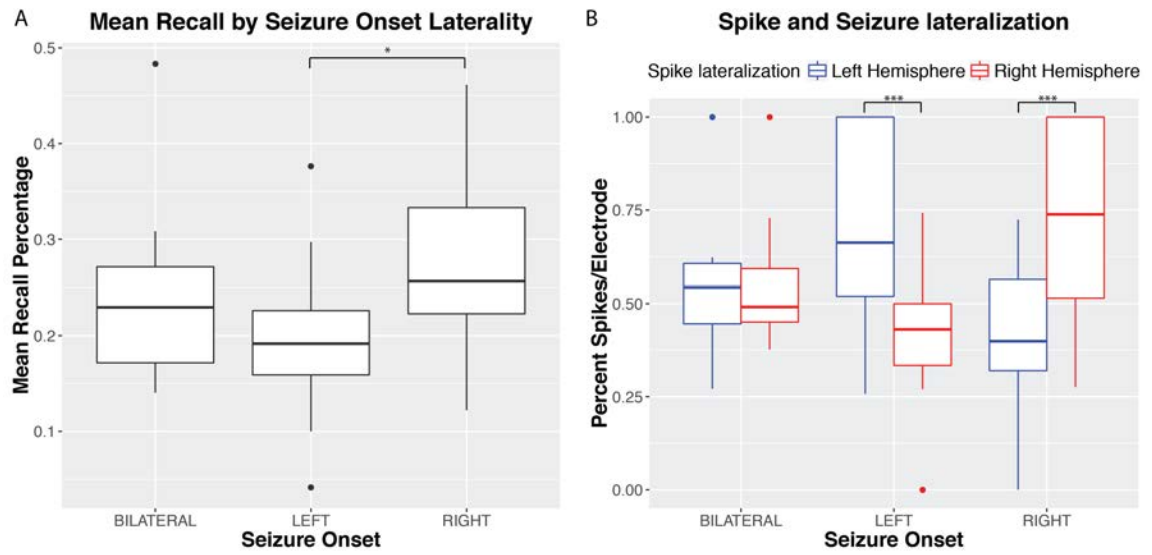
Figure 22: Mean recall (A) and spike lateralization (B) grouped by seizure onset lateralization. Boxplots indicate median, 25th, and 75th percentiles. * indicates significance at $p < 0.01$, *** indicates significance at $p < 0.001$.

Table 3: GLMM Model construction

	Fixed	Random	Testing		p
1		Patient	Word order	378.73	¡0.001
2	Word order	Patient	Age	9.93	0.0016
3	Word order + age	Patient	Sex	¡0.001	0.99
4	Word order + age	Patient	Session (Nest)	109.55	¡0.001
5	Model: recalled word_order + age + 1—patient/session				

In each iteration, a null model is compared to an alternative model to test one additional variable through the likelihood ratio test. If the alternative model fits the data better, it is retained. Spike counts are added to the final model (5) and tested in subsequent analyses.

During the encoding phase, an increased number of spikes across all electrodes was associated with decreased recall ($\chi^2(1) = 8.64, p = 0.003$). In patients with left lateralized SOZ, spikes within the SOZ did not have a significant effect on recall. However, spikes outside of the SOZ had a significant effect on recall. In patients with right lateralized onset regions, spikes were not significantly associated with recall performance, whether within or outside the SOZ (Table 4).

Table 4: Estimated odds ratios of effect of spikes relative to the seizure onset zone

	OR [95% CI]	Z	p
Right Lateralized SOZ (N=26)			
Spikes within SOZ	0.994 [0.958 1.027]	-0.331	0.7405
Spikes outside SOZ	0.991 [0.962 1.018]	-0.56	0.5752#
Left Lateralized SOZ (N=23)			
Spikes within SOZ	0.981 [0.928 1.036]	-0.679	0.497
Spikes outside SOZ	0.934 [0.900 0.969]	-3.593	0.000327*#

Estimated odds ratios of effect of spikes relative to the seizure onset zone. A logistic GLMM model was fit to a binary response variable indicating recall success (1) or failure (0). Covariates included spikes within the SOZ, outside the SOZ, and interaction of each with clinical SOZ lateralization. ORs are adjusted for age and serial word position. Patients with bilateral onsets were not included. OR = odds ratio, CI = confidence interval, significance determined by Wald statistics. *significance at $p < 0.05$; # significant difference between left and right lateralized SOZ patients (increased odds of recall for spikes outsize the SOZ if right lateralized: odds $= 1.062[1.0131.112], z = 2.513, p = 0.01$).

The top 10 regions from the regional analysis are given in Table 5. The odds ratios for all regions are shown in Figure 23. Left temporal lobe structures such as the fusiform gyrus (BA 37) and inferior temporal gyrus (BA 20) were most significant after multiple comparisons correction. The middle temporal gyrus, specifically BA 21, was also significant after correction. A plot of the percent change in epileptiform discharges during failed recall are shown in Figure 24, separated by SOZ lateralization and the significant regions from the above regional analysis. These three regions are shown along with electrode locations across all subjects in Figure 25.

Table 5: Regional effect of spikes

N	L/R	Region		Odds [95% CI]		P (adjusted)
22	L	Fusiform Gyrus	BA 37	0.810 [.753 .871]	33.7	<0.001***
45	L	Inferior Temporal Gyrus	BA 20	0.919 [.888 .951]	23.9	<0.001***
43	L	Middle Temporal Gyrus	BA 21	0.937 [.901 .974]	10.7	0.028*
21	L	Fusiform Gyrus	BA 36	0.917 [.867 .970]	9.47	0.053
24	L	Peristriate cortex	BA 19	0.848 [.755 .952]	8.1	0.106
22	L	Superior Temporal Gyrus	BA 22	0.931 [.876 .989]	5.37	0.472
28	R	Superior Temporal Gyrus	BA 22	0.955 [.911 1.000]	3.76	1
28	R	Hippocampus	Hippocampus	0.962 [.919, 1.007]	2.84	1
35	L	Sup/Mid Temporal Gyrus	BA 38	0.965 [.922 1.009]	2.47	1
47	R	Inferior Temporal Gyrus	BA 20	0.976 [.947 1.006]	2.41	1

Number of patients with electrodes in corresponding regions are also shown, along with laterality. Each region is derived from the Talairach atlas, level 5, shown with associated gyri or lobes. The effect of each spike on the odds of recall are also given. Effect size and adjusted p values from the likelihood ratio test are given after controlling for family-wise error with the Holm-Bonferroni method. BA = Brodmann area *significant at $p = 0.05$, ***significant at $p = 0.001$, CI = confidence interval
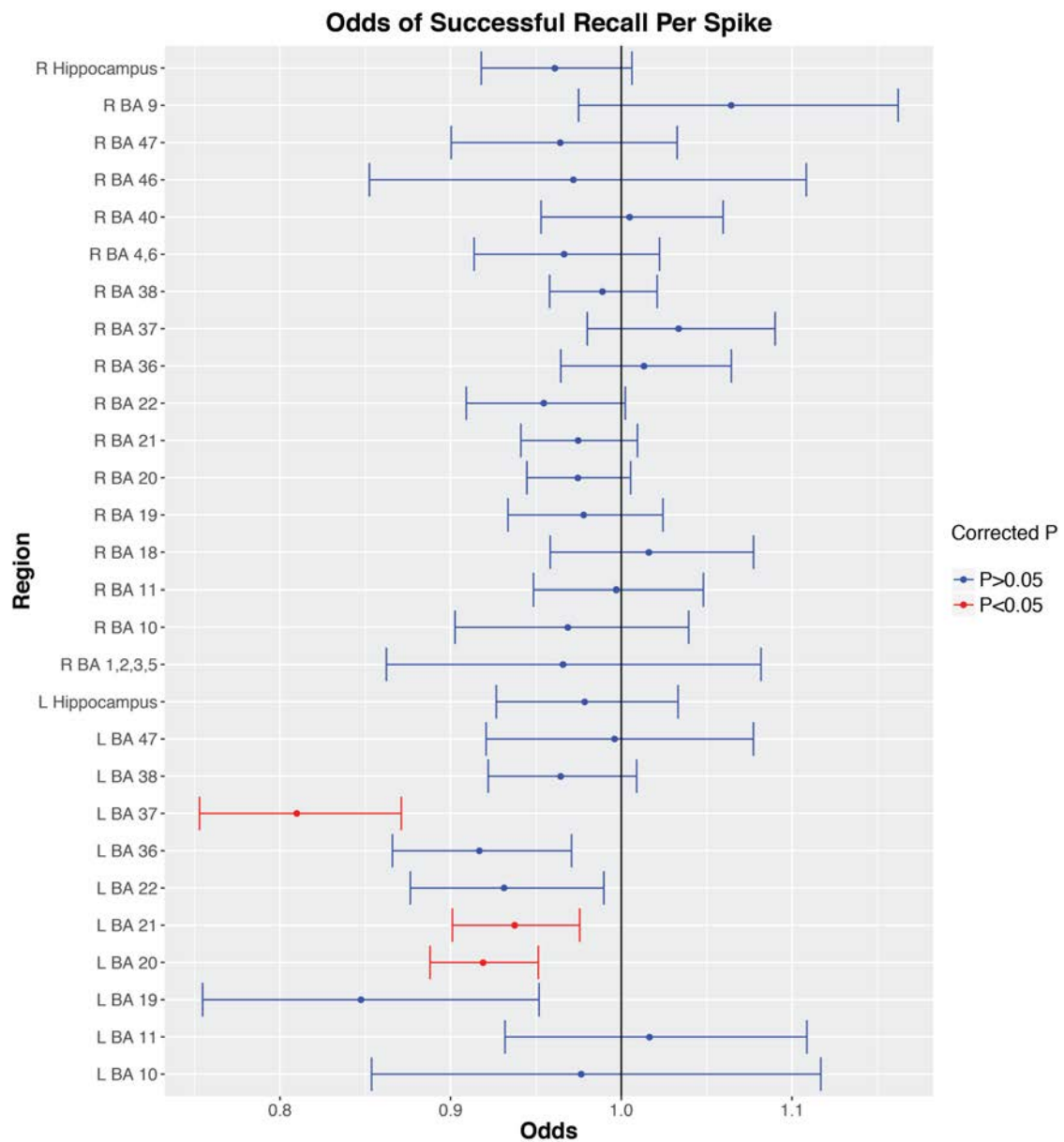
Figure 23: Estimated odds of successful recall for each region. Mean odds of successful recall per spike are shown along with 95% confidence intervals. Odds ¡1 indicate a decrease in the odds of successful recall per spike. Red indicates significant after multiple comparisons correction. BA = Brodmann Area. L/R = Left/Right hemisphere.
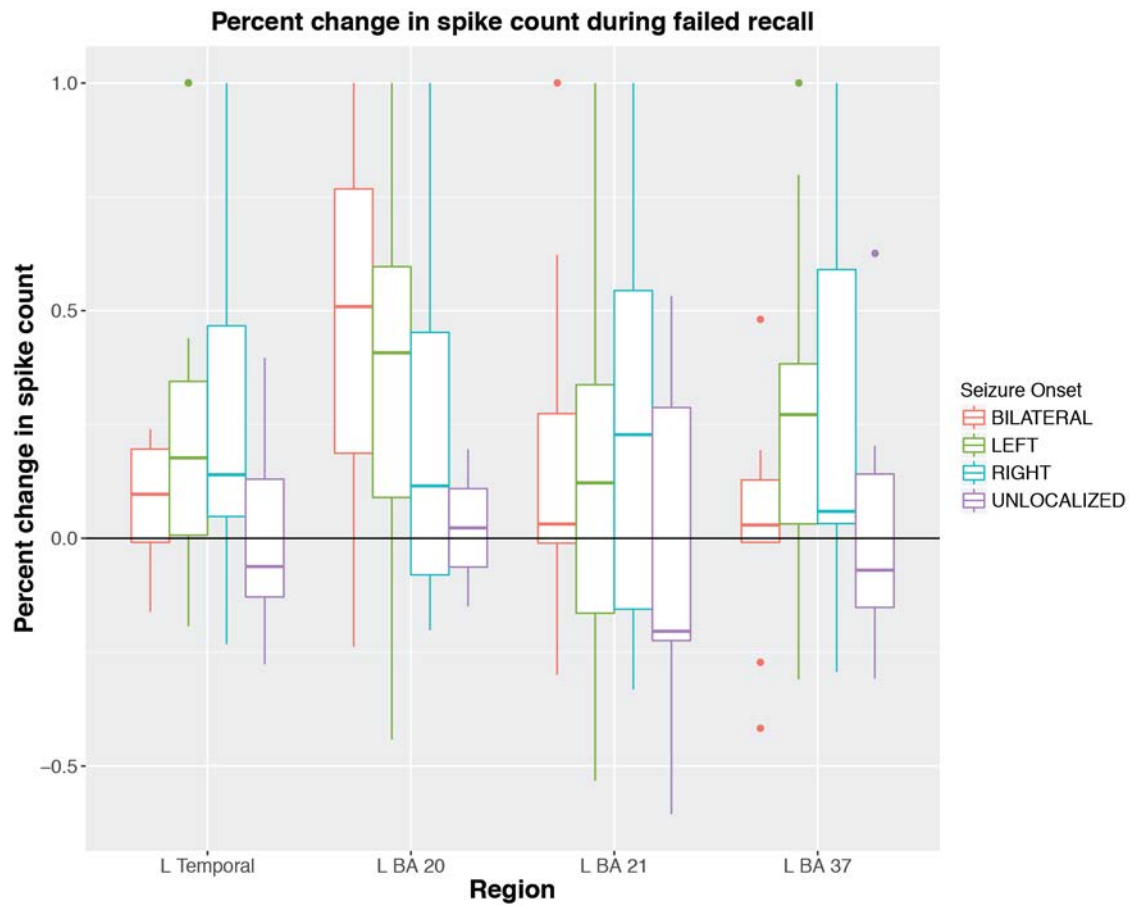
Figure 24: Percent change in spike count during failed recall for each patient. Vertical axis represents the percent change in spike count. The horizontal axis represents the left temporal lobe as well as the significant left temporal regions from our regional analysis. Boxplots represent the percent change of spikes across all patients with the given seizure onset zone lateralization. Only the recall of words in serial position greater than 5 were included to account for the primacy effect.
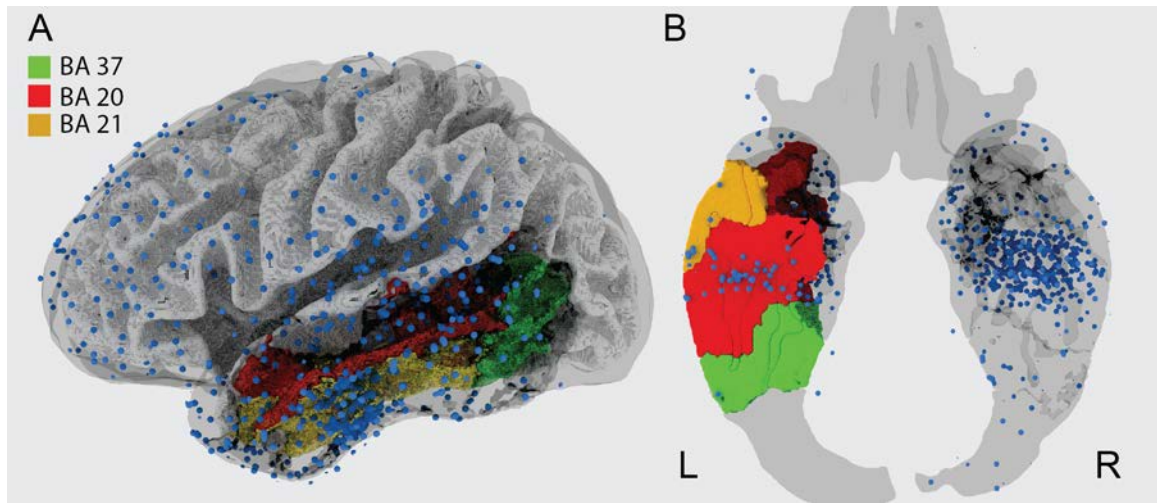
Figure 25: Electrode coverage and significant regions. 6144 electrodes (blue dots) across all patients are shown in a 3D view of the left hemisphere (A) and an axial slice (B) on a template brain in Montreal Neurological Institute (MNI) space. BA = Brodmann Area
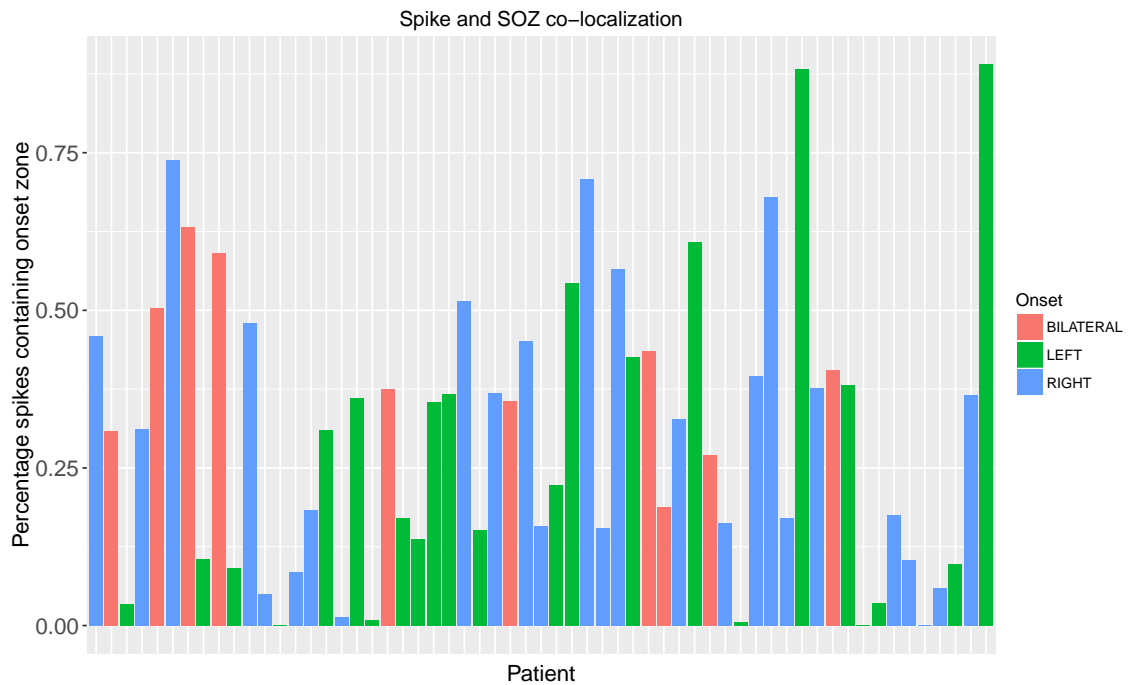
Figure 26: Percentage of spikes in the seizure onset zone. This is calculated by dividing the total number of spikes containing the seizure onset zone with the total number of spikes.

3.5 Discussion

We showed that in patients with epilepsy, interictal epileptiform spikes that occur after word presentation lead to greater likelihood of failed recall, which suggests that spikes disrupt short term verbal memory encoding. This effect is primarily seen with left lateralized spikes, which were more present in patients with left lateralized seizure onset zones. In addition, spikes outside the seizure onset zone in left lateralized patients significantly reduced recall, a finding not present in right lateralized patients. Finally, we observed that spikes in specific temporal lobe structures functionally implicated in verbal word processing and verbal memory were most impactful. Our observations support the importance of the temporal neocortex in memory encoding and extend it by elucidating the spatial distribution of spikes relative to the seizure onset zone, the lateralization of spikes, and the quantification of the effect of spikes in the verbal word recall task.

As our findings rest on the accuracy of our spike detections, we vetted a random subset of our spikes equally represented across all patients. In this group, our detections performed with a positive predictive value of 72%. Furthermore, we observed an expected association between spike and seizure onset lateralization (Figure 22).

The observation that spikes outside the SOZ affect recall greater than spikes within the SOZ suggests that epileptic regions may have some degree of dysfunction at baseline that, in a verbal word memory task, manifests most prominently in left lateralized patients (Table 4). This is supported by previous neuropathological studies showing neuronal loss in more than 90% of temporal lobe epilepsies as detailed in a review by Sutula et al. [144]. In addition, electrophysiological network studies have also shown dynamic uncoupling of the seizure onset region [17, 154]. This finding has potential implications in the clinical realm. Clinical tests are routinely used in an attempt to identify regions of eloquent cortex in order to weigh

the functional consequences versus the potential benefits of surgical resection. As new more focal surgical techniques such as laser ablation have led to improved cognitive outcomes by limiting damage to collateral structures [32], limiting the extent of resection may lead to improved cognitive outcome. Spikes have previously been shown to provide adjunctive information in the clinical mapping of the seizure onset region in certain populations [98], and our results suggest that identifying spike populations, namely those that do not impact cognition, may improve SOZ localization, surgical planning, and cognitive outcomes from surgical resection.

The regional localization of spikes may also elucidate the function of underlying tissue. Our regional analysis suggests that spikes in primarily left sided structures lead to poor recall, which agree with previous studies on cognitive impairment that lateralize functional disruption based on cortical interictal epileptiform discharges. Specifically, that the left sided and right sided spikes produce verbal and spatial task impairments, respectively [1].

Spikes in the left inferior temporal gyrus (BA 20) and nearby fusiform gyrus (BA 37) most significantly disrupted memory encoding. These regions form the ventral spatial pathway of visual memory and are involved in visual processing of words. Numerous studies have associated inferior temporal lobe function with working memory tasks in both humans and primates [80, 111, 152]. Wagner et al. demonstrated through fMRI that the ability to remember a verbal experience is predicted by the activation of regions in the left prefrontal and temporal cortices [152]. Hamame et al. recently observed increased gamma activity in the inferior temporal gyrus corresponding to increased visuo-spatial working memory load, suggesting that this region acts as a visual sketchpad during memory maintenance [57]. This, however, was a trial of only one patient, and we showed here in 67 patients that spikes in this region likely interfere with memory encoding by interrupting mental imagery of presented words.

The fusiform gyrus (BA 37) specifically has been functionally implicated in word recognition and is referred to as the Visual Word Form Area (VWFA) in a thorough review by McCandliss et al. in 2003 [99]. Literature in cognition implicates that a critical process in visual word recognition groups the letters of a word together to an integrated perceptual unit (a visual word form), a function the fusiform gyrus participates in. The VWFA within the left inferior temporal cortex has been shown to have increased activity through fMRI during visual word recognition as well as an Event Related Potential (ERP) roughly 250 ms after word presentation [22, 117]. Wagner et al. and Hamame et al., similarly found correlated activity in the fusiform gyrus during verbal memory tasks [57, 152]. Our findings support this body of literature and extend it by suggesting that spikes in the fusiform gyrus may impede successful visual recognition of a word-form and maintenance of verbal memory. We showed in Figure 23 that in words that were not recalled, there was an increased in spike rate in BA37 during the corresponding encoding period. Though we were not able to determine a causal relationship between spikes and word recall, these differences begin to appear as more words were shown in a given word list, indicating that the effect of spikes may manifest as a patient finds greater difficulty in memorizing words.

There is extensive work covering the middle temporal lobes involvement in memory processing, specifically regarding the medial structures such as the hippocampus and parahippocampal gyrus [8, 34, 121, 137, 138]. Surprisingly, we did not find these structures to be significantly affected by spikes, with the exception of Brodmann area 21. This region lies laterally in the middle temporal lobe and its relationship to memory is unclear. Several imaging studies showed that BA21 was involved with processing of auditory word-form as well as sentence generation [4, 100, 168]. In this case, it may play a role similar to the fusiform gyrus for auditory stimuli as subjects were ask to read each word aloud, but additional work is necessary to further parse out this regions function in relation to memory.

Of note, a recent study of ten patients with temporal lobe epilepsy showed that right-sided hippocampal discharges significantly reduced performance in a memory retrieval task in both humans and rats, but not encoding [77, 76]. Though we were unable to directly test retrieval, our findings agree in that there was no effect of hippocampal spikes on encoding. While the hippocampus is believed to play a role in the encoding and retrieval of unconsolidated memory [120], these results suggest that hippocampal spikes do not impede the encoding process.

Furthermore, we found that spikes did not impede recall in patients with right lateralized SOZs (Table 4). Taken into context with our previous findings showing that left sided spikes are involved in memory encoding (Table 5), this can be explained by the lack of spikes in the left hemisphere in right lateralized patients (Figure 22). However, even in right lateralized patients there is increased spiking during the encoding of words that were not recalled (Figure 24), which provides further evidence that the effect of spikes is regionally dependent. Interestingly, Kleen et al. showed that the effect of spikes is lateralized to the right hemisphere, suggesting it may be due to the laterality of epileptic foci in their cohort of patients [76]. In an attempt to shed light on this, we conducted a separate regional analysis only on right-lateralized patients, but no regions (on either hemisphere) reached significance (Table 6).

Table 6: Regional analysis of patients with right lateralized seizure onset zones.

N	L/R	Region		Odds [95% CI]		P (unadj)
21	R	Hippocampus	Hippocampus	0.943 [.879 1.011]	7.49	0.187
25	R	Superior Temporal Gyrus	BA 38	0.988 [.943 1.034]	3.67	0.596
21	R	Superior Temporal Gyrus	BA 22	0.971 [.910 1.035]	3.11	0.683
24	R	Inferior Temporal Gyrus	BA 20	0.970 [.934 1.007]	3.09	0.686
22	R	Fusiform Gyrus	BA 37	1.046 [.989 1.106]	2.68	0.748
28	R	Peristriate cortex	BA 19	0.967 [.904 1.035]	2.32	0.803
28	R	Middle Temporal Gyrus	BA 21	0.982 [.939, 1.028]	1.99	0.851

Regional analysis was performed separately for each region for only right lateralized patients. P values are unadjusted.

The question of whether spikes localize to the seizure onset zone is a topic of much debate. Marsh et al [98] showed that in some patients, spikes localized to the seizure onset zone. We find a similar result, where in 4 patients greater than 70% of spikes occurred in the SOZ. However, the majority of our patients' spikes did not localize to the SOZ ($t_6 6 = -7.8, p < 0.001$) and in fact resided outside 26.

Inferior temporal lobe involvement in memory encoding is also supported in a recent finding by the Restoring Active Memory collaborative research group [66]. Interestingly, they reported an impact of spikes in parietal lobe structures and in the SOZ, which we did not find. In fact, our analysis suggests that spikes impair recall only if outside the SOZ, and in these cases, only in left lateralized patients. Furthermore, our analysis investigated sub-lobar regions with greater specificity at the level of Brodmann areas. For example, our strongest effect was found in the left fusiform gyrus, part of the inferior temporal lobe, which has associations with verbal word formation instead of with regions traditionally thought to be involved in memory. While some of the differences between the two studies are difficult to reconcile, we believe the main complementary findings support the reproducibility of our study and are an important step to understanding the impact of spikes on cognition. Furthermore, by incorporating the ieeg.org platform into our basic laboratory organization in Penns Center for Neuroengineering and Therapeutics, data sharing and reproducibility become turnkey, and do not require any additional effort. This eliminates a huge barrier to experimental validation, where post-hoc porting of annotations, experimental details, code etc. can sometimes take longer than original experiments.

Interpretation of the model estimates show that each spike in BA37 reduces the odds of recall by 19%, where in BA20 the odds of recall are reduced by roughly 8% per spike. Figure S3 show the corresponding predicted recall percentages per spike estimated from our model. This implies that increased spiking increases the probability of failed recall and is

not necessarily an all-or-nothing mechanism. These findings show that spikes focally and additively impact function in a spatially dependent manner within a given region. Finally, it is important to note that spike occurrence across BA20, 21, and 37 are correlated ($r > 0.45$), which is expected as these regions may play similar functional roles, though further work is necessary to determine whether this contribution is additive.

3.5.1 Limitations

Although automated spike detection is a difficult challenge to perfect and validate in the field, we believe an automated algorithm that performs with acceptable true positive rate allows us to still make comparisons between groups. Furthermore, an automated algorithm allows objective detection of spikes that does not suffer from differences in inter-rater reliability.

We have shown that epileptiform discharges in various regions of the temporal lobe affect verbal word processing and memory encoding. Our ability to discern influence in other structures is limited by electrode coverage (Figure 25). Notably, our electrodes are primarily cortical, with the exception of medial temporal subcortical structures interrogated by depth electrodes.

There is rich literature supporting the notion that interictal epileptiform discharges are associated with cognitive impairments, described by Aarts et al. as transitory cognitive impairment (TCI) [1]. Though spikes may influence memory and other cognitive processes, it remains unclear whether spikes should be treated in clinical management of otherwise well controlled epilepsy [11]. In addition, while we have shown that memory encoding is affected by spikes in a spatially distributed manner, the magnitude of the effect is fairly small depending on the region (roughly a 5% decline in probability for spikes outside the seizure onset zone (Figure 27). Coupled with the observation that recall percentage is

limited to begin with, the consequence of spikes on overall patient cognition and quality of

life needs to be further studied.
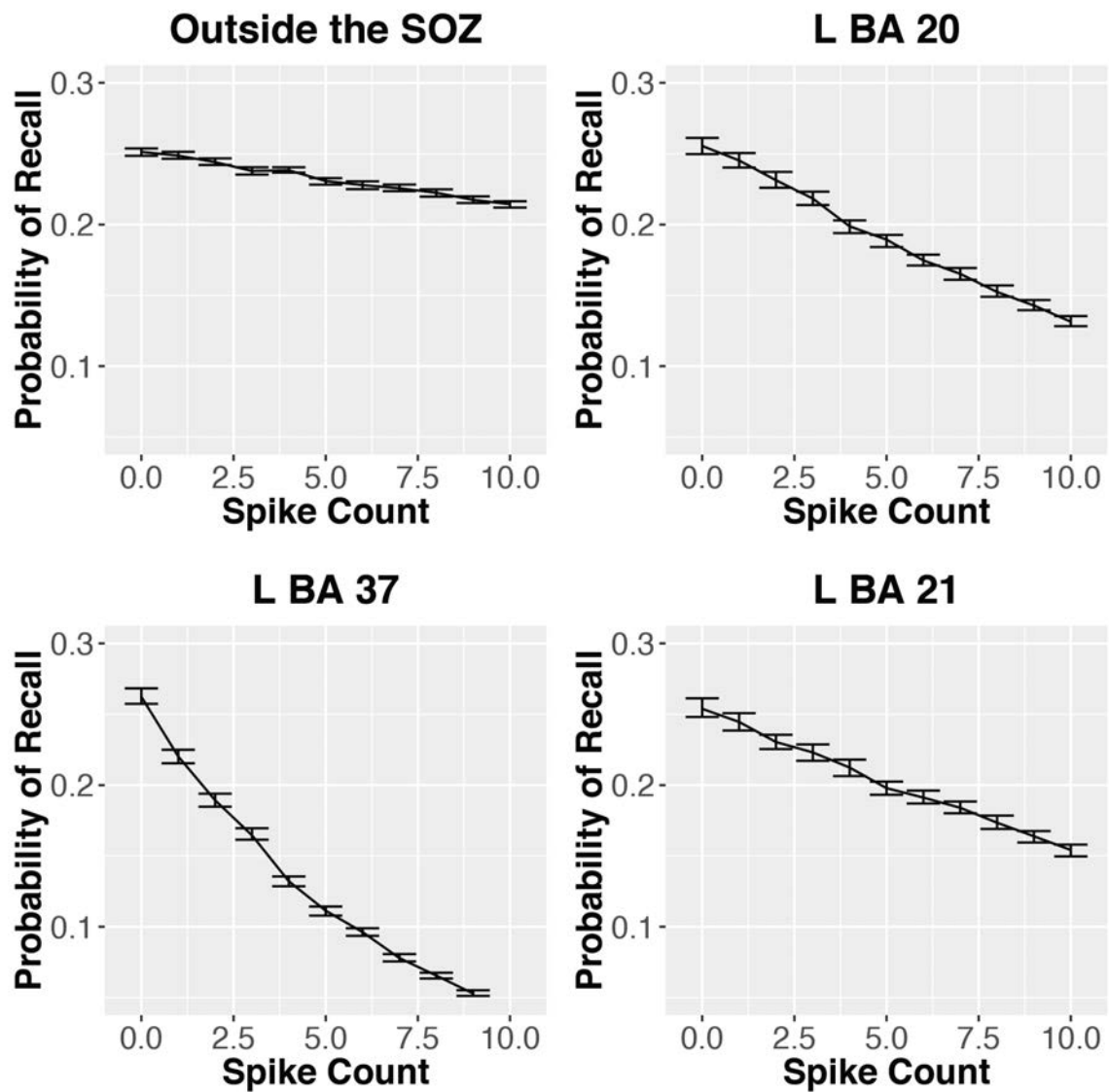
Figure 27: Posterior Predictive Probability. The vertical axis indicates the probability of recall for a given word presentation. The horizontal axis indicates the spike count in a given region for a given word presentation. The predicted probabilities and 95% confidence interval are plotted, which are derived from a predictions from 100 bootstrapped samples of 1000 word presentations.

3.5.2   Conclusion

In this study we have shown the interictal epileptiform spikes impede memory encoding when present outside the seizure onset zone and within the left temporal lobe, specifically in the inferior temporal and fusiform gyri. These results suggest that spikes are not benign and can disrupt visual word recognition as well as verbal memory processes. In addition, our findings support the use of surgical interventions that spare cortex outside of the seizure onset zone. Further study is warranted to determine the magnitude of this effect relative to known cognitive deficits in epilepsy patients.

Table 7: Cognitive Spike Patient Table

IEEGID	Patient	Hospital	Age	Sex	Lateralization	Onset	Sessions	Mean Recall Percentage
I022_P001	1	HUP	38	M	RIGHT	R Temporal	5	0.23
I022_P002	2	HUP	20	M	BILATERAL	B Temporal	2	0.18
I022_P004	3	HUP	36	M	LEFT	L Temporal	6	0.12
I022_P005	4	HUP	25	M	RIGHT	R Limbic	4	0.23
I022_P006	5	HUP	18	F	BILATERAL	B Limbic, R Temporal	3	0.23
I022_P007	6	HUP	27	F	RIGHT	R Limbic, R Temporal	2	0.23
I022_P008	7	HUP	55	F	BILATERAL	B Limbic	2	0.17
I022_P009	8	HUP	18	M	UNLOCALIZED		3	0.35
I022_P010	9	HUP	38	F	UNLOCALIZED		1	0.2
I022_P011	10	HUP	40	M	LEFT	L Temporal, L Occipital	4	0.3
I022_P012	11	HUP	27	M	BILATERAL	B Temporal	2	0.28
I022_P013	12	HUP	20	M	LEFT	L Frontal	4	0.22
I022_P014	13	HUP	37	M	RIGHT	R Temporal	3	0.25
I022_P015	14	HUP	42	M	RIGHT	R Occipital	2	0.35
I022_P016	15	HUP	30	F	LEFT	L Frontal	3	0.21
I022_P017	16	HUP	40	M	RIGHT	R Frontal	1	0.13
I027_P001	17	TJUH	25	M	UNLOCALIZED		3	0.32
I027_P002	18	TJUH	40	F	RIGHT	R Temporal, R Limbic	4	0.17
I027_P003	19	TJUH	39	M	LEFT	L Limbic	1	0.22
I027_P004	20	TJUH	34	F	RIGHT	R Temporal	10	0.22
I027_P006	21	TJUH	44	M	LEFT	L Temporal	1	0.16
I027_P007	22	TJUH	29	M	LEFT	L Central	1	0.04
I027_P008	23	TJUH	43	M	BILATERAL	B Temporal	4	0.24
I027_P009	24	TJUH	21	M	LEFT	L Frontal	3	0.2
I027_P010	25	TJUH	56	M	LEFT	L Temporal	3	0.17
I027_P011	26	TJUH	57	F	LEFT	L Temporal, L Limbic	3	0.1
I027_P012	27	TJUH	20	M	LEFT	L Frontal	3	0.27
I027_P013	28	TJUH	41	M	RIGHT	R Temporal	2	0.21
I027_P014	29	TJUH	34	F	LEFT	L Temporal	4	0.27
I027_P015	30	TJUH	52	F	RIGHT	R Temporal	1	0.37
I027_P016	31	TJUH	44	M	UNLOCALIZED		3	0.45
I027_P017	32	TJUH	44	F	BILATERAL	B Temporal	4	0.14
I027_P018	33	TJUH	33	M	RIGHT	R Frontal	4	0.32
I027_P019	34	TJUH	23	F	RIGHT	R Temporal	5	0.29
I027_P020	35	TJUH	50	F	UNLOCALIZED		2	0.35
I027_P021	36	TJUH	33	M	LEFT	L Temporal	3	0.38
I027_P022	37	TJUH	44	M	LEFT	L Temporal	4	0.23
I027_P023	38	TJUH	15	M	RIGHT	R Occipital, R Temporal	4	0.46
I027_P024	39	TJUH	23	M	RIGHT	R Temporal, R Frontal	4	0.37
I027_P025	40	TJUH	53	M	RIGHT	R Temporal, R Limbic	2	0.12
I027_P026	41	TJUH	53	M	LEFT	L Temporal	2	0.18
I027_P028	42	TJUH	29	M	BILATERAL	B Temporal	2	0.48
I027_P029	43	TJUH	35	M	BILATERAL	B Temporal	3	0.23
I027_P030	44	TJUH	48	F	RIGHT	R Frontal, R Temporal	8	0.18
I027_P031	45	TJUH	20	F	UNLOCALIZED		15	0.44
I027_P032	46	TJUH	35	M	LEFT	L Temporal, L Frontal	3	0.15
I027_P033	47	TJUH	20	M	BILATERAL	L frontal, R Temporal	9	0.31
I027_P034	48	TJUH	52	F	RIGHT	R Temporal	3	0.26
I027_P035	49	TJUH	26	F	LEFT	L Frontal	3	0.25
I027_P036	50	TJUH	20	F	RIGHT	R Temporal, R Frontal	2	0.3
I027_P037	51	TJUH	31	M	RIGHT	R Temporal, R Frontal	2	0.17
I027_P038	52	TJUH	50	M	UNLOCALIZED		3	0.21
I027_P039	53	TJUH	18	M	RIGHT	R Temporal	3	0.26
I027_P040	54	TJUH	44	F	LEFT	L Temporal	2	0.14
I027_P041	55	TJUH	28	M	RIGHT	R Temporal	3	0.35
I027_P042	56	TJUH	51	M	BILATERAL	B Temporal	5	0.16
I027_P043	57	TJUH	38	M	LEFT	L Temporal	1	0.19
I027_P044	58	TJUH	26	F	LEFT	L Frontal	3	0.12
I027_P045	59	TJUH	56	M	LEFT	L Temporal	2	0.17
I027_P046	60	TJUH	47	M	RIGHT	R Temporal	1	0.28
I027_P047	61	TJUH	26	M	RIGHT	R Frontal	3	0.26
I027_P048	62	TJUH	25	M	RIGHT	R Frontal	1	0.21
I027_P049	63	TJUH	27	M	RIGHT	R Frontal	1	0.23
I027_P050	64	TJUH	20	F	UNLOCALIZED		3	0.42
I027_P051	65	TJUH	55	M	LEFT	L Frontal	1	0.18
I027_P053	66	TJUH	37	F	RIGHT	R Frontal	3	0.34
I027_P054	67	TJUH	57	M	LEFT	L Temporal	2	0.2

Patient demographics and experimental information. Pt = Patient, Hosp = Hospital, Ons = onset lateralization, Sess = total number of sessions.

Chapter 4

Bursts as a biomarker of epileptogenesis

4.1 Abstract

Up to 53% of patients with severe traumatic brain injury (TBI) develop spontaneous recurrent epileptic seizures. The ability to predict epileptogenesis in these patients may reduce the burden of post-traumatic epilepsy by enabling earlier interventions in the disease process as well as personalized therapy according to the likelihood of developing epilepsy. Here, we use a two-stage machine learning detection algorithm and analyze the utility of postulated epileptiform spikes and bursts as potential electrographic biomarkers of epileptogenesis in a rat model of TBI.

Hippocampal depth recordings from 23 rats monitored continuously for a one-week period three months following a fluid-percussion-induced traumatic brain injury (17) or sham surgery (6) were analyzed. All recordings were obtained prior to first seizure. Eight of the 17 rats with injury developed spontaneous seizures after the initial recording period. Candidate bursts were detected and automatically classified into rhythmic bursts, epileptiform bursts, and artifact. Permutation tests across rats were used to assess statistical significance in burst rate and duration across three groups (sham, no-seizure, and seizure).

Epileptiform bursts were detected in all groups that received surgery and electrode implantation. Three subtypes of bursts were detected and subsequently classified into rhythmic

bursts, epileptiform bursts, and electrode artifact. Among the 17 rats that received injury, a subgroup of those that developed seizures displayed significantly greater epileptiform burst rate than controls.

Our results show that in this sample of 17 rats, there is a trend that epileptiform bursts are more prevalent in rats that develop seizures versus rats that do not. There was no difference in interictal spikes between groups. However, there was a significant effect between a week 8 and a week 10 recording, thus limiting the impact of our findings. Furthermore, the observation of bursts in sham animals suggests that these patterns may represent hippocampal theta bursts seen in previous studies, although the spectral characteristics do not match exactly. This work encourages further investigation of bursts as a potential biomarker of epileptogenesis, but requiring simultaneous EMG and video recording to determine the cause of the observed bursts.

4.2   Background

In patients with severe traumatic brain injury, 17-53% will develop spontaneous seizures and subsequently post-traumatic epilepsy (PTE) [6, 46]. These patients constitute up to 20% of all symptomatic epilepsies, and often suffer from significant disability [3]. The time to first unprovoked seizure is variable among patients who develop PTE and the risk is present more than 10 years after injury, which enables possibilities for intervention [20]. Identification of biomarkers of epileptogenesis would facilitate the development of interventions necessary to reduce the burden of disease by identifying pathogenic regions, tracking disease progression, providing markers of drug efficacy for animal trials, and enriching clinical trials [35, 37].

In this study, we use a validated rodent model of PTE induced by fluid percussion to evaluate electrographic epileptiform bursts as biomarkers of epileptogenesis [73]. Lateral fluid percussion injury (LFPI), a widely used preclinical model for closed head injury, results

in approximately 50% development of PTE. As each injury is applied in a controlled fashion, the EEG recording post-injury but before seizure development may reflect a pathogenic process towards spontaneous seizures that can be differentiated between rats that do not develop PTE and rats that do.

We focus our analysis around epileptiform bursts captured on EEG. Epileptiform bursts of activity have been previously described in literature but have not been well characterized [47, 105, 126, 132, 164]. Though bursts have previously been shown to be associated with cerebral injury and neonatal epilepsy [132, 164], their exact significance is still unknown. In fact, it is uncertain whether these patterns represent ictal or interictal events, reflective of a term recently used to describe them - brief potentially ictal rhythmic discharges (B(I)RDs) [164]. Electrographically they have characteristics similar to seizures, and in particular to seizure onsets [28], but are shorter in duration. In this study, we define bursts as less than 10 seconds after historic clinical conventions for subclinical seizures [165]. Epileptiform bursts in the rodent theta band (7 Hz) have also been noted previously in a rat model of FPI at the site of injury and associated with increased glial activity on histological examination [25], though these bursts were recorded from epidural electrodes around the lesion versus the hippocampal depth electrodes in our dataset. Further quantitative analysis would be worthwhile to determine significance and trends in the context of epileptogenesis.

Continuous datasets of this length would require quantitative analyses to determine significant patterns in relevant EEG waveforms. In this domain, automated machine learning algorithms are suitable due to the vast quantities of data that need to be analyzed as well as the quantitative nature of EEG. Interfacing with the International Epilepsy Electrophysiology Portal (ieeg.org), algorithms can be quickly and transparently executed on the relevant datasets. For burst detections, we employ a supervised two stage algorithm, where the first stage focuses on a hypersensitive detection screen and the second stage is focused on
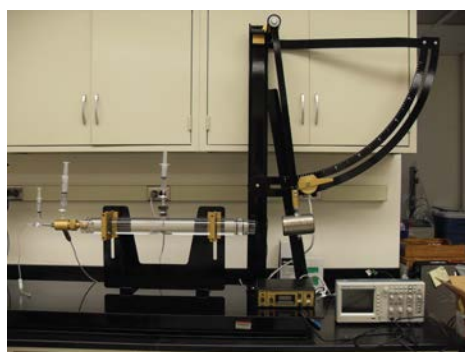
(a) Picture of fluid percussion injury (FPI) apparatus
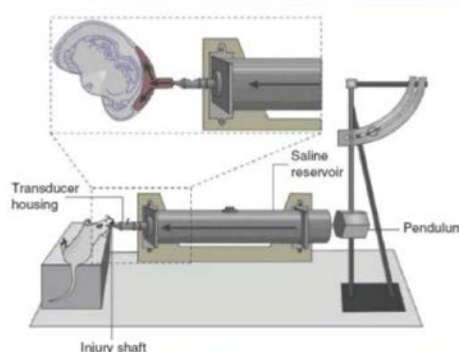
(b) Image of fluid percussion injury (FPI) apparatus

Figure 28: Picture and schematic of fluid percussion setup. A pendulum induced roughly 2.6 - 3.3 atm of pressure through the saline transducer to inflict severe lateral fluid percussion brain injury

classification aided by expert markings by a board certified epileptologist (DM).

4.3 Methods

4.3.1 Dataset

The data collection is described in detail by Kharatishvilli in 2006 and are briefly summarized [73]. Twenty-three Harlan Sprague-Dawley rats received severe TBI induced by lateral fluid percussion based injury (LFPI) (N=17) or sham surgery without LFPI (N=6). The fluid percussion aparatus (28a) and schematic (28b) are shown in Figure 28 .

One to two weeks post-injury, a depth electrode ($\oslash$ 0.127 mm) was implanted ipsilaterally to the trauma (6 mm caudal to the bregma, 4.6 mm lateral from the midline, and 7.0 mm ventral to the surface of the skull according). Activity was monitored using the Nervus EEG Recording system with a Nervus magnus 32/8 amplified and filtered (high-pass with 0.3 Hz cutoff, low-pass with 100 Hz cutoff). Analyses are based on one week of continuous recordings 8 and 10 weeks post-injury 29.
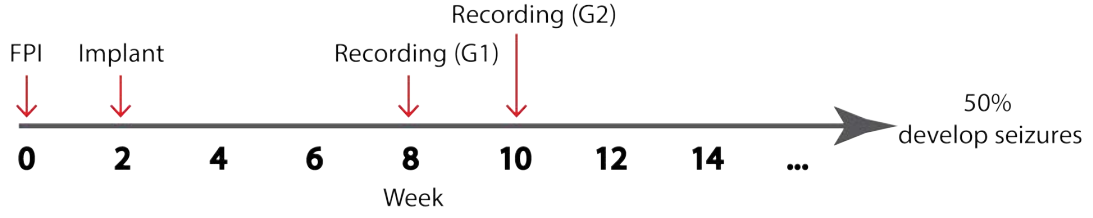
Figure 29: Experimental overview. Fluid percussion injury (FPI) administetered on day 0, followed by implant and two recording periods.

After this recording period, eight rats developed spontaneous seizures and were categorized into the seizure (SZ) group. Nine rats did not develop spontaneous seizures and were categorized into the non-seizure (Non-SZ) group. None of the six rats that underwent sham surgery developed seizures. Readers are referred to the original publication by Karastishvili for further experimental details [73].

4.3.2 IEEG Portal

The datasets were uploaded to the International Epilepsy Electrophysiology Portal (www.ieeg.org). Analysis was conducted using in-house Matlab algorithms described below interfacing with the IEEG Matlab toolbox (v1.13).

4.3.3 Burst detection

The burst detection and classification scheme is given in Figure 30. A hypersensitive burst detector was developed based on the line-length feature [38]. Line-length is a calculated feature that provides a measure of amplitude as well as frequency and has been shown to be effective in detecting seizures and other transient changes in the baseline EEG. Continuous line-length passing a threshold 2 times the standard deviation of a surrounding background window was selected as burst candidates 31. Detections with durations greater than 0.5 seconds were retained. These parameters were optimized to capture a group of manually

marked patterns and is intended to be highly sensitive. Upon viewing, these candidates included different types of bursts as well as electrode artifacts, prompting a need for further refinement.
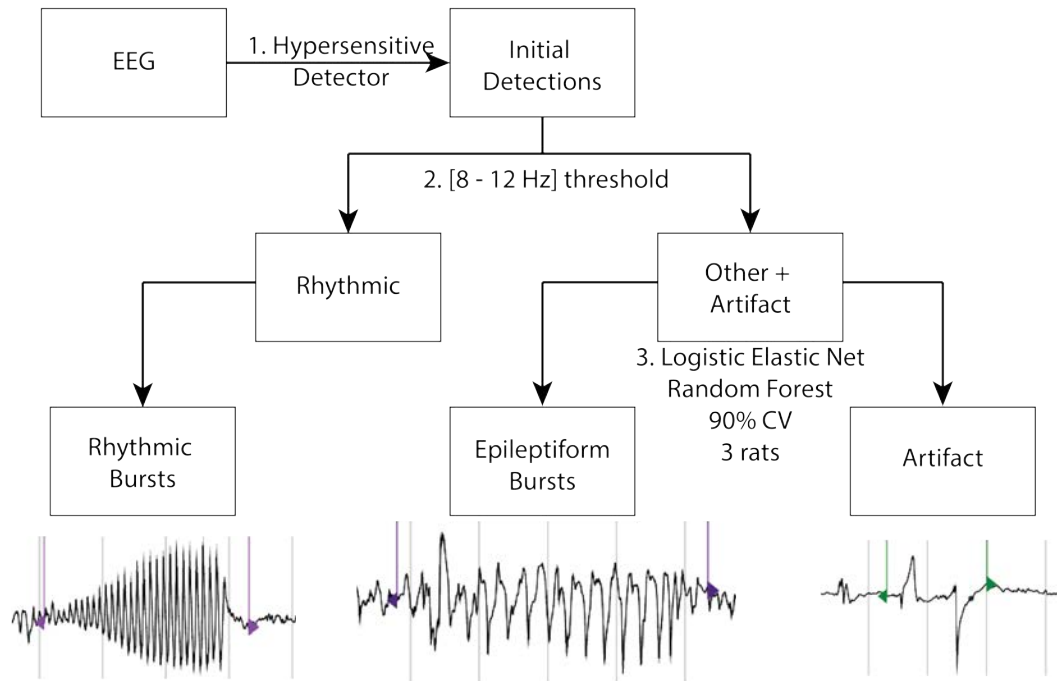
Figure 30: Schematic of burst detection. 1. A hypersensitive detector is used to segment the EEG before a 2. 8-12 Hz power threshold is used to extract rhythmic bursts. The group with more complex frequency activity is then separated using a random forest classifier trained on 3 rats that performed with 90% cross-validation accuracy.
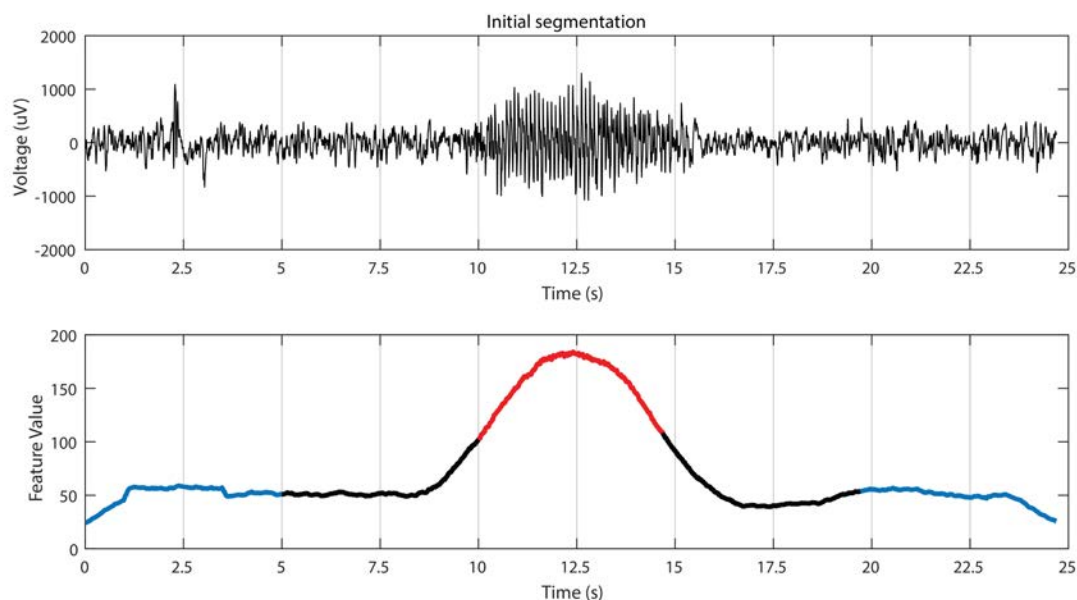
Figure 31: Example of hypersensitive detection. Epileptiform burst (top) and corresponding feature value (bottom) intended for hypersensitive detection. The red line indicates the feature values of the pattern of interest, and the black lines indicate background.

4.3.4   Burst classification

Bursts were then classified into three groups (Rhythmic bursts, epileptiform bursts, and artifact) in two steps.

Rhythmic bursts were observed to have a clear single dominant frequency with no modulation. To separate rhythmic bursts, candidate bursts from all rats were combined and bursts with greater than 60% of power in the 8-10 Hz or 10-12 Hz bands were classified as rhythmic. This threshold extracted bursts with one dominant frequency range.

The remaining candidate bursts were observed to be epileptiform or artifact, both with more complex frequency distributions and waveforms. To separate epileptiform bursts from artifacts, a training set was created, where a board certified epileptologist (DM) classified

100 bursts from three rats each. Spectral and time-domain features were extracted from each burst, which were selected by manual observation of the frequency and time domain signals belonging to epileptiform bursts and artifacts. These features included power (1-4, 4-8, 8-10, 12-14, 14-30, 30-60 and 60-90 Hz bands), area, zero crossings, line length, as well as autoregressive (AR) coefficients from a 5th order AR model. Since many of these features were expected to be uninformative and reduce the performance of the algorithm, feature selection was performed on the first three rats using a penalized logistic regression model using 10-fold cross-validation. The final set of features corresponding to optimal cross-validation was selected.

A random forest classifier with 300 trees was then trained to separate artifacts from epileptiform bursts using this reduced feature set. To assess algorithm performance, the model was trained on 30% and tested on 70% of the training set, resulting in 89% accuracy (0% false positive rate, 13% false negative rate) in classifying epileptiform bursts (positives) from artifacts (negatives). A final model was trained on the entire training set and was subsequently used to remove artifacts from all 23 rats.

4.3.5 Statistical analysis

The rate of epileptiform and rhythmic bursting per day was extracted from all rats. Furthermore, the duration of each burst was extracted. One-sided T tests were conducted to determine the difference in the rate and duration of each type of burst between the sham, non-seizure, and seizure rats. Significance was determined using a non-parametric permutation test iterated 10000 times, where in each permutation, the group of each rat was randomly permuted.

4.3.6   Results

Two distinct types of candidate bursts were identified. Representative examples of each and the correspond frequency spectrum is shown in Figure 32. The clustering step separated over 15,492 initial bursts for roughly 2432 epileptiform bursts and 6399 rhythmic bursts and removed 6661 artifacts across 332 hours of recordings. No differences were found in the number of rhythmic bursts between the sham, non-seizure, and seizure groups.
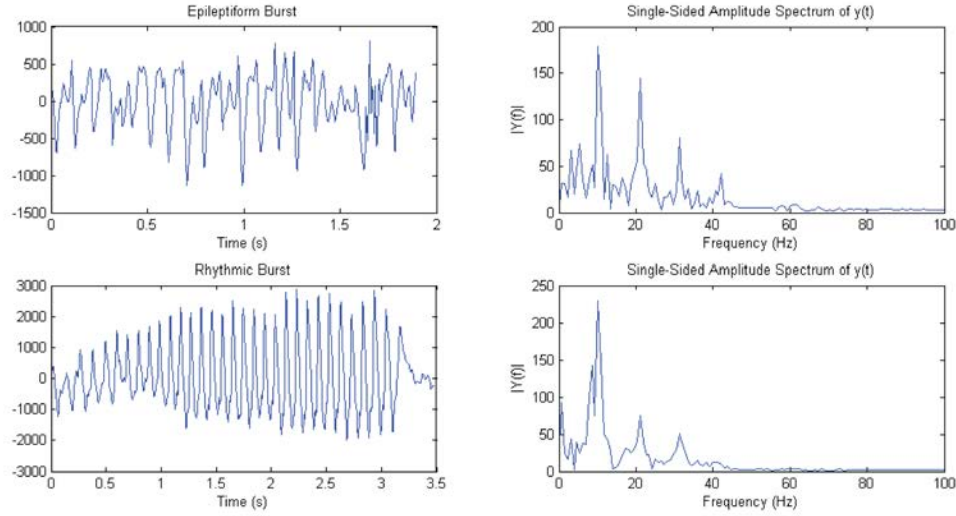
Figure 32: Example of epileptiform and rhythmic burst with corresponding FFTs. Note that each contains a primary peak between 8-12 Hz, though the epileptiform burst contains more complex frequencies. The additional frequencies appear to be harmonics at first, but upon closer inspection, these higher frequencies are visible on the time domain signal.

Similarly, no significant difference was seen in the number of epileptiform bursts ($p = 0.8$, Wilcoxin rank sum), though variability existed between rats (Figure 33). This difference is noted to exist between the two recording periods (Week 8 vs Week 10) (Figure 34,36). There was also no difference in epileptiform burst duration (37). The number of rhythmic bursts as well as artifacts are shown in Figures 38 and 39.
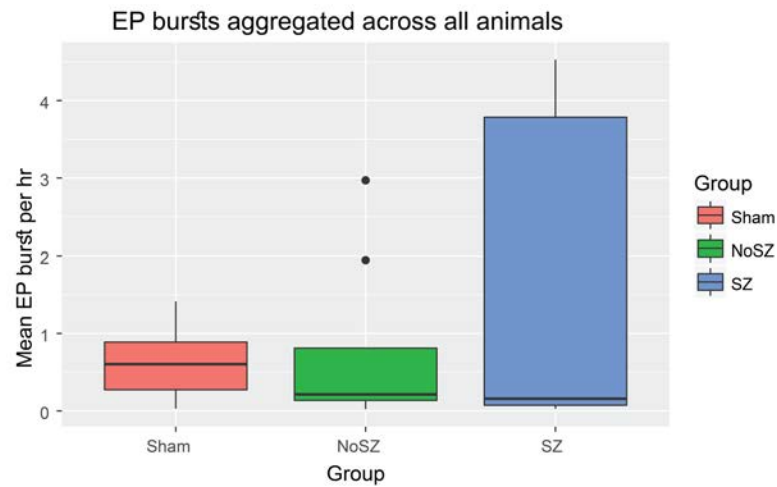
Figure 33: Epileptiform bursts for all groups. Note skewed boxplot for the SZ group. There was no significant differences between groups by Kruskal-Wallis test.
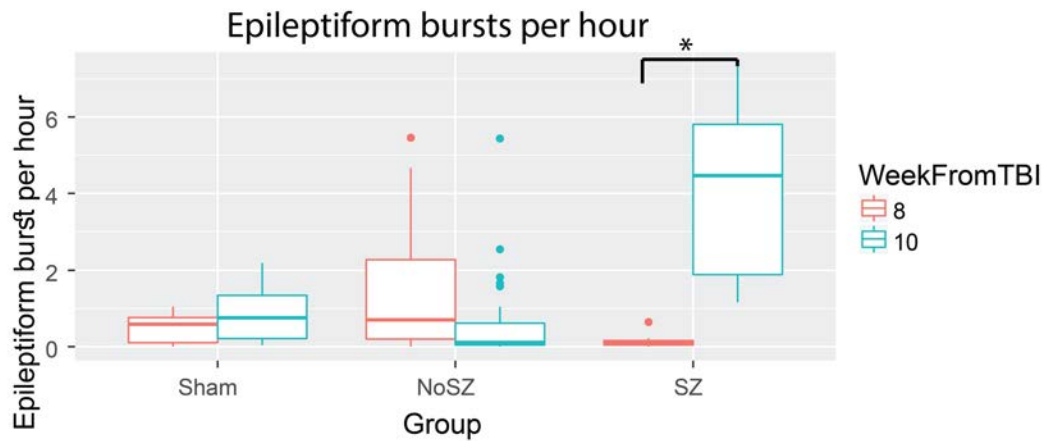
Figure 34: Epileptiform bursts per hour per group, separated by Week. It is noted that there is a significant difference between Week 8 and Week 10 rats.
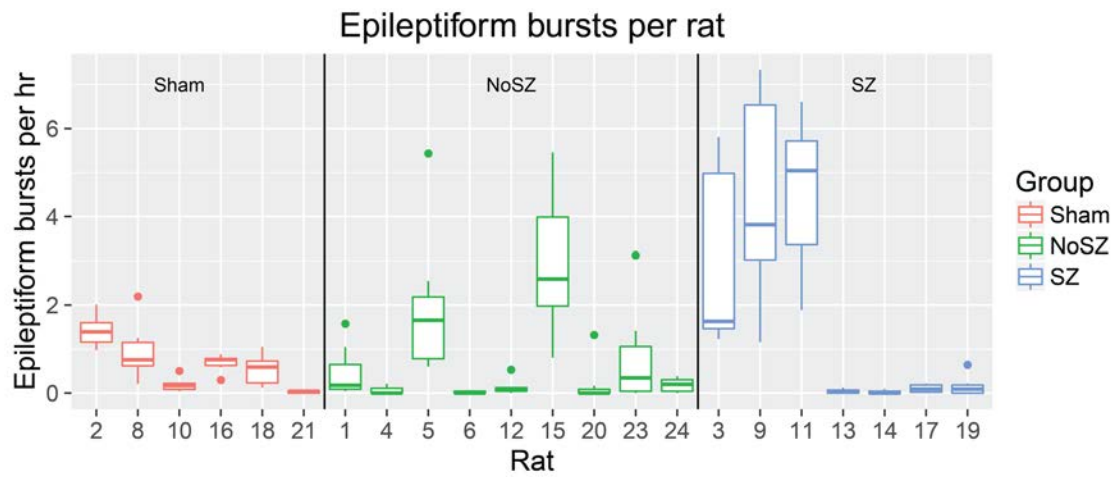
Figure 35: Note that three of seven rats in the SZ group had elevated epileptiform bursts per hour.
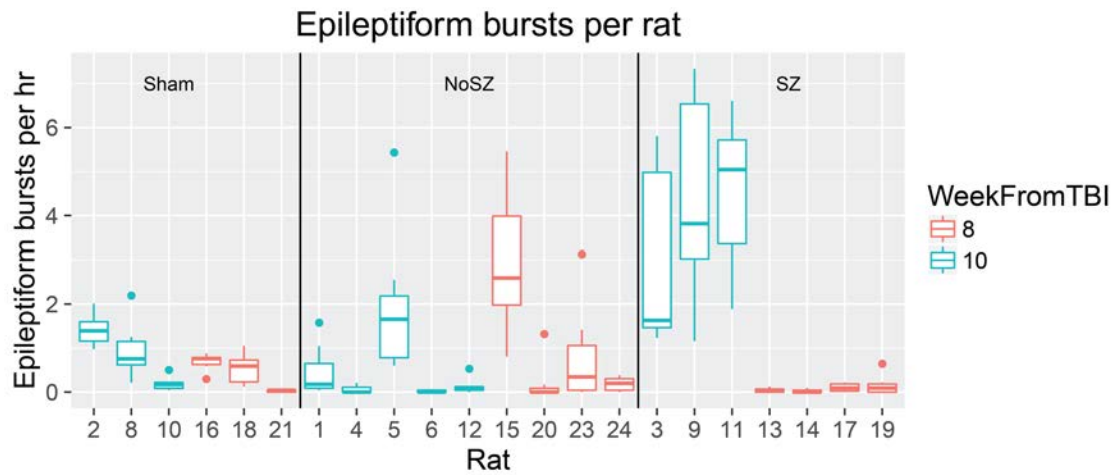
Figure 36: Epileptiform bursts per rat by week from TBI. There is a significant difference between the epileptiform bursts for rats from Week 8 vs Week 10 (Wilcoxon Rank Sum, p¡0.001)
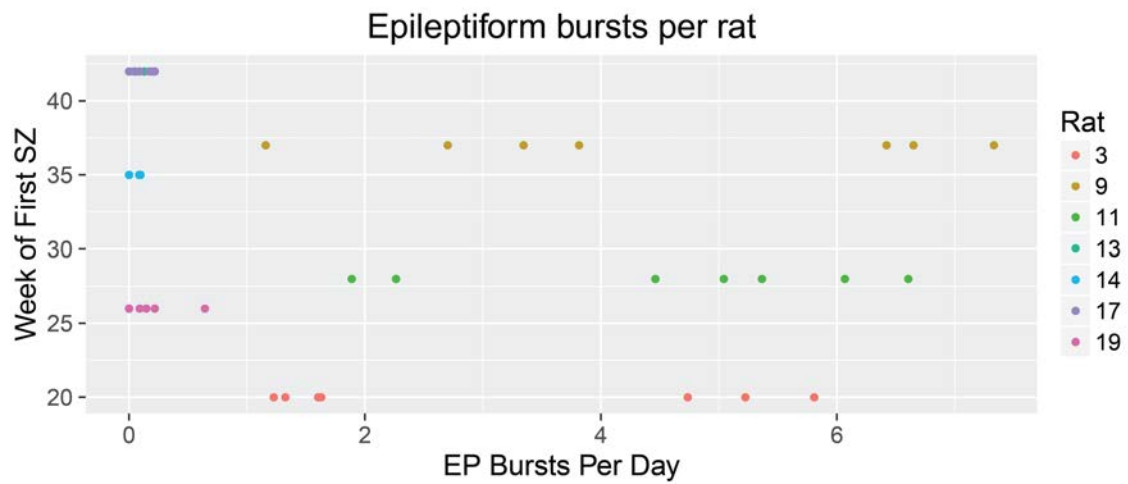
Figure 37: Duration of Epileptiform bursts per rat. There is no relationship between the week of first seizure and the number of bursts per day.
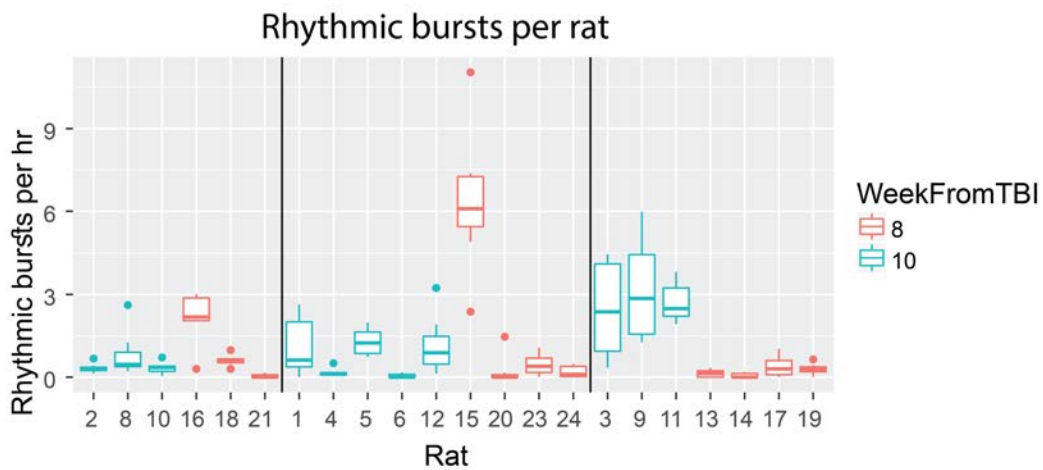
Figure 38: Rhythmic Bursts per rat, grouped by Week from TBI. Note that the number of detections mirror epileptiform bursts
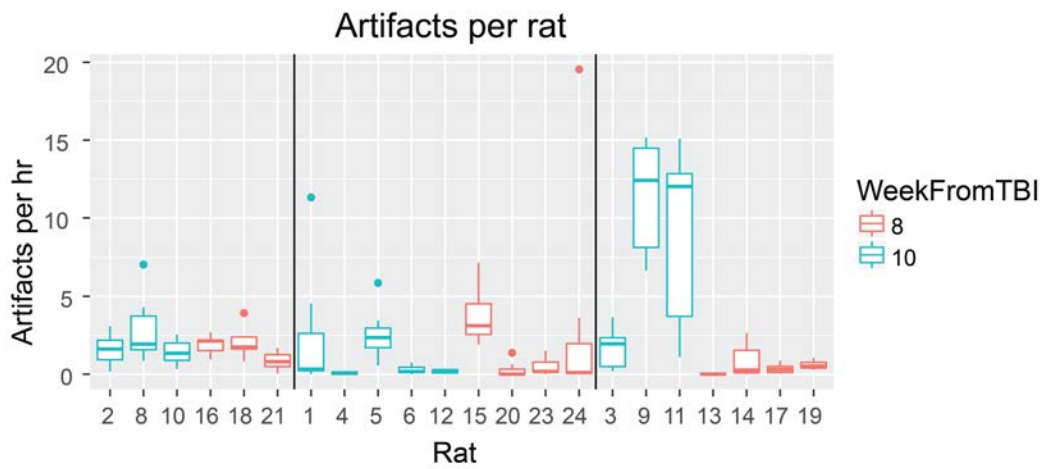
Figure 39: Artifacts Per Rat
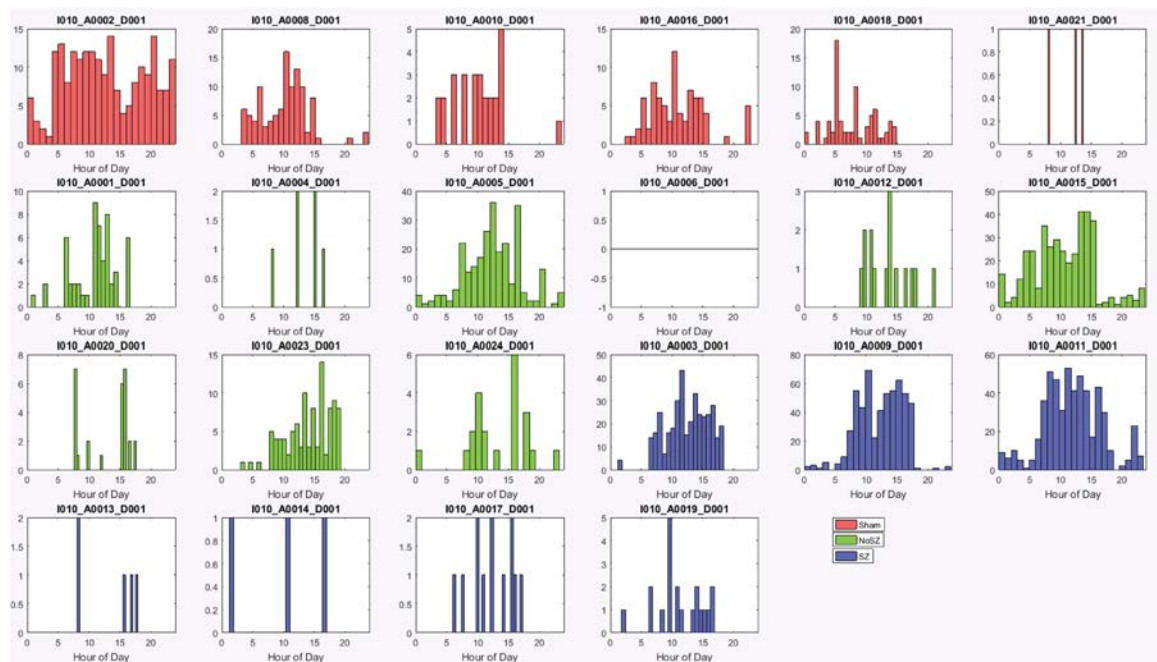
Figure 40: Circadian pattern of epileptiform bursts. Note that the x axis does not represent real time.
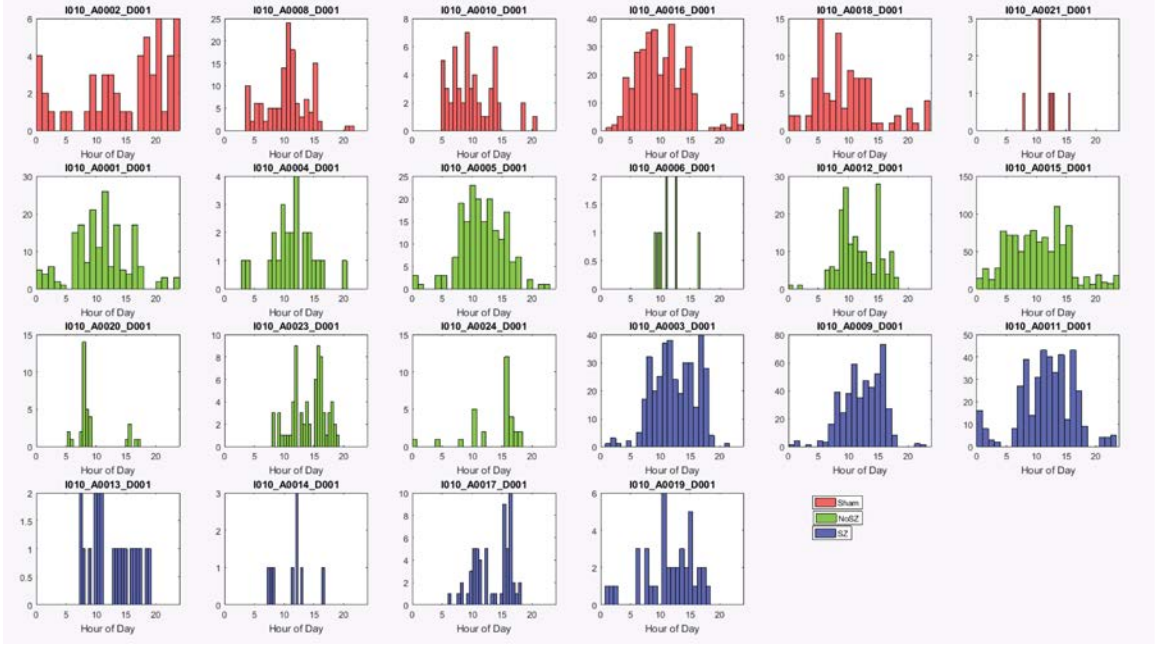
Figure 41: Circadian pattern of rhythmic bursts. Note that the x axis does not represent real time.

4.4   Discussion

In this study, we investigated interictal epileptiform bursts in hippocampal depth recordings in rats that received lateral FPI as well as a sham surgery group. Approximately half of the rats that received lateral FPI developed seizures over the course of the year, and we found that in this group, the number of epileptiform bursts were significantly greater in both count and duration.

4.4.1   Rhythmic Bursts

The bursts described here as rhythmic bursts have one dominant frequency in the 10 Hz range but with significantly smaller frequency components in the 20 and 30 hz range (Fig2). There was no difference in the frequency of rhythmic bursts between the sham, non-seizure,

and seizure groups. This may be explained by the origin of these oscillations. These bursts may correspond to movement artifacts, such as grooming or chewing (Winson, 1974), as well as representative of nonspecific activity associated with aging in this particular strain (citation). Due to this, it was important to separate them in the analyses.

4.4.2   Epileptiform Bursts

The epileptiform bursts detected in this analysis have a dominant frequency in the 10 Hz range, similar to rhythmic bursts, but have a much more prominent higher frequency component in the 20 Hz and 30Hz (Fig 2). The lower amplitude 20Hz and 30Hz components at first appear to be harmonics, but from manual observation there were clear higher frequency components to each of these bursts. The complexity of the signal is similar to that described by DAmbrosio [25], though the specific frequencies do not completely align. In DAmbrosios experiments, the epileptiform patterns had peaks in the 7Hz, 15Hz, and 21Hz range. The reason for these differences is unclear, and may reflect differences in hardware or software or a different underlying physiologic process altogether. These bursts may be a consequence of abnormal firing associated with increased mossy fiber sprouting originally seen on histology in animals with PTE [73].

Furthermore, as interictal bursts have not been well characterized before, this study attempts to quantify and describe different kinds of bursts seen in this dataset. While many bursts are observed that are rhythmic with one dominant frequency, and many bursts are clearly epileptiform, the delineation may be less clear and difficult to classify even to a trained eye. We see here a separation of bursts into rhythmic and epileptiform. Further study of these patterns may address the significance of signal complexity in the context of epileptogenesis.

We also found that the bursts in the epileptic group were on average of greater duration

than the sham group and non-seizure group (Fig 5). This trend is an interesting finding that may indicate that both the count and length of a burst contain information. We speculate that longer bursts may indicate greater severity of injury and a reduced ability of control mechanisms to inhibit bursting. It is plausible that if bursting activity continues longer than a threshold, propagation leads to clinical seizures.

It is difficult to reconcile the observation that epileptiform bursts occurred in all groups, including the sham group. Previous human studies have attributed epileptiform discharges to cerebral injury, and presence of these bursts in the sham group may reflect surgical or electrode implantation injury. It is also plausible that the increased frequency of bursts may correlate with an underlying epileptogenic process. Thus, more severe trauma (e.g. through FPI) may lead to higher frequency, longer duration bursts that reflect cerebral injury and leads to a higher incidence of epilepsy [3]. It is important to note that the rats were follow-up for roughly one year before sacrifice, and thus it cannot be excluded that many of the rats would have developed epilepsy given a longer follow-up. However, there was no correlation between the number of bursts of any kind and the time to first seizure.

4.4.3 Spikes

The exact significance of interictal spikes in the context of epilepsy is a topic of debate. Interictal spikes are often used to aid in the diagnosis of epilepsy, and many papers have suggested that they may help localize epileptogenic tissue and possibly the prediction of seizures [19, 67, 115, 155]. In this particular analysis, we do not see any differences in the frequency of spikes between the sham, non-seizure, and seizure group.

4.4.4 Limitations

There are several limitations to this study. First, this analysis is based on recordings captured during a relatively brief window of time into a presumably longer epileptogenic

process. Although we did not see any trends in burst counts or duration over the one-week recording, the time scale may be too small to draw a significant conclusion. Further analysis should be performed on numerous recordings with longer durations to identify longitudinal trends. In addition, having more animals for longer durations will allow us to assess relationships between these patterns of EEG and time to first seizure, which may have a better defined relationship irrespective of time of monitoring.

Second, there was variability between rats in each group. Some rats in the seizure group had very few epileptiform bursts during their recordings, while several rats in the non-seizure group had more epileptiform bursts than expected. The bursts in these rats were manually reviewed and determined to be correctly classified. There are several possible explanations for this variability. Rats that developed seizures but were observed to have relatively few interictal bursts may have a slower, more chronic epileptogenic process, and bursts would be seen if recorded closer to first seizure. Alternatively, this may suggest that bursts are only part of the picture, and some epileptogenic processes may be captured by different biomarkers than what was studied. Thus, we believe that bursts may only be a proxy or endophenotype of epileptogenesis and a final prediction model will need to be informed by other features as well.

Finally, we make the assumption during our statistical analysis that burst counts per day are independent and identically distributed. However, we did not see a significant linear trend when viewing burst counts over times, and believe it is a valid assumption given the relatively short time window in the process of epileptogenesis.

4.4.5 Conclusions

In this study we have analyzed spikes and bursts in a rat fluid percussion model of traumatic brain injury, and found that the group that developed seizures had a greater number of

epileptiform bursts that were also longer in duration relative to rats that did not receive injury. These differences were not seen with more rhythmic bursts or spikes. We believe that the epileptiform bursts may be a marker of cerebral injury or epileptogenesis that deserves further study as a potential biomarker of the epileptogenic process post-injury.

Chapter 5

Bursts related to seizure onset

5.1 Abstract

Brain regions are localized for resection during epilepsy surgery based upon rare seizures observed during a short time period of intracranial EEG (iEEG) monitoring. Interictal epileptiform bursts, which are more prevalent than seizures, may provide complementary information to aid in epilepsy evaluation. In this study, we leverage a long-term iEEG dataset from canines with naturally occurring epilepsy to investigate interictal bursts and their electrographic relationship to seizures. Four dogs were included in this study, each previously monitored with continuous iEEG for periods of 475.7, 329.9, 45.8, and 451.8 days respectively for a total of over 11,000 hours. Seizures and bursts were detected and validated by two board-certified epileptologists. A published Bayesian model was applied to analyze the dynamics of interictal epileptic bursts on EEG and compare them to seizures. In three dogs, bursts were stereotyped and found to be statistically similar to periods before or near seizure onsets. Seizures from one dog during status epilepticus were markedly different than other seizures in terms of burst similarity. Shorter epileptic bursts explored in this work have the potential to yield significant information about the distribution of epileptic events. In our data, bursts are at least an order of magnitude more prevalent than seizures and occur much more regularly. Our finding that bursts often display pronounced similarity to seizure onsets suggests that they contain relevant information about the epileptic networks

from which they arise and may aide in the clinical evaluation of epilepsy in patients.

5.2   Background

Prior to surgical resection, patients with neocortical epilepsy typically undergo intracranial EEG (iEEG) monitoring to localize the seizure onset zone. Unfortunately, after undergoing extensive pre-surgical evaluation often lasting several weeks, only ∼50% of patients with neocortical epilepsy will become seizure-free or have a significant reduction in their seizure burden following surgery [88]. A long-standing goal of the epilepsy research community is to identify electrophysiological biomarkers of epileptic networks and their dynamics to better target anti-seizure therapies, particularly surgery and implantable devices. The identification and validation of these biomarkers necessitates long-term iEEG recordings through which many repeated observations can be detected and analyzed.

In prior work from our lab, we presented recordings from a novel implantable device that continuously records iEEG for prolonged periods [27]. Six dogs with naturally occurring cryptogenic localization related epilepsy were monitored for over 11,000 hours with 16 intracranial electrodes, eight implanted over each hemisphere. Over 200 ictal events which showed remarkable similarity to human seizures were recorded across these canines. Background EEG and interictal bursts of epileptiform discharges in these animals were also indistinguishable from human iEEG recordings. This work validated canines with spontaneous seizures as a promising model of human epilepsy and provides a rich dataset of unprecedented length for biomarker detection and analysis.

One potential biomarker of interest is interictal bursts observed on human iEEG as well as on our canine recordings. These bursts have been described in various studies as brief rhythmic discharges (BRDs) and brief potentially ictal rhythmic discharges (B(I)RDs) [2, 27, 47, 105, 126, 164] and have been associated with epilepsy and cerebral trauma. These

patterns exhibit similarities to electrographic seizures in that they are paroxysmal, stereo-typed, and can evolve temporally and spatially. However, it is currently not known how these epileptiform bursts relate to epileptic networks, their dynamics, or if they quanti-tatively resemble epileptic seizures. Some investigators differentiate between bursts and seizure by an arbitrary duration set at 10 seconds, which we investigate and address in the discussion below. Furthermore, since interictal bursts occur much more regularly than seizures, they may aid in the localization of epileptic networks for surgical resection or serve as an important feature in seizure prediction.

The primary goal of this study is to investigate interictal bursts and to determine their relationship to clinical seizures on continuous iEEG from canines with naturally occurring epilepsy. Specifically, we aim to characterize interictal bursts and determine their dynamic similarity to seizures. Assessing the relationship between bursts to well-established seizures will allow us to determine the importance of these epileptiform discharges and to justify future in-depth studies of these interictal patterns. Furthermore, we can improve our un-derstanding of how these bursts relate to seizures and potentially shed light on mechanisms of seizure onset and propagation. A secondary goal of this study is to focus on the chal-lenges presented by new devices that continuously monitor and process human data over long periods - "big neural data". This work has evolved and improved steadily over recent years, embodied in devices to detect, predict and respond to seizures in several new im-plantable devices [27, 41, 102]. Traditionally, iEEG is interpreted by human readers and marked by hand. The large archive of continuous data analyzed for this project required rigorous, automated methods for detecting and processing bursts of activity. In this study we leverage automated, machine learning approaches to data reduction to study interictal bursts in data streams too long and complex to be marked manually by human readers. These methods offer more flexibility and the ability to learn patterns from data, a substan-

tial improvement from rule-based methods employed in epilepsy monitoring equipment and implantable anti-seizure devices currently being deployed.

5.3 Methods

5.3.1 Dataset

Four dogs originally described by Davis [27] were included in this study each monitored with continuous iEEG for periods of 475.7, 329.9, 45.8, and 451.8 days [27] (Figure 42). All dogs were observed to have spontaneous focal epilepsy of unknown etiology with secondary generalization. All dogs exhibited focal onset seizures with and without generalization. The dogs were normal on physical and neurological exam with no history of trauma. The dogs were housed at BioAssist Inc., a USDA Class R research facility located in Vacaville, CA. None of the dogs were on antiepileptic medication at the start of the study. One of the four dogs included in the present study died from status epilepticus during the monitoring period, after which phenobarbital (PHB) therapy was initiated in all remaining dogs. The results from this dog are discussed separately.
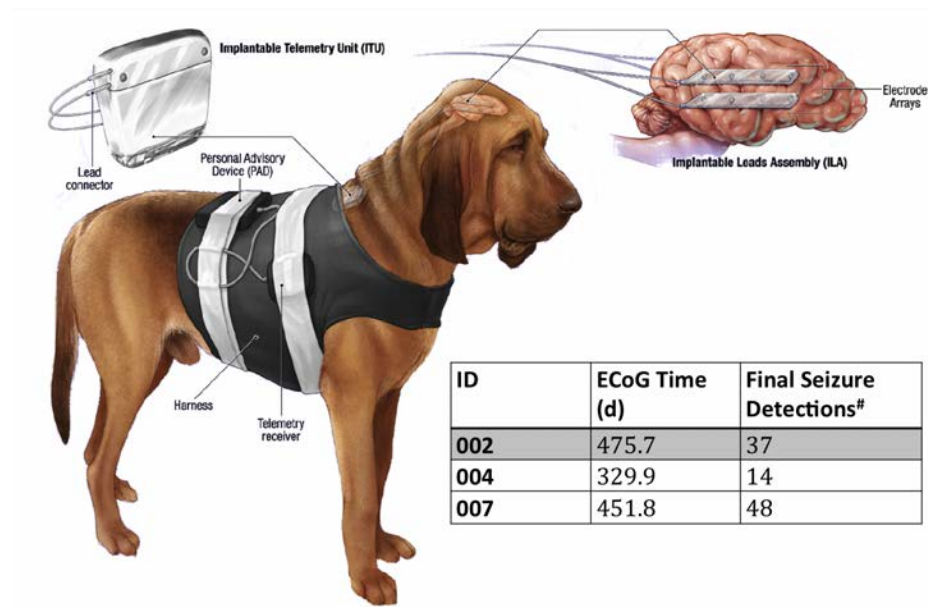
Figure 42: Schematic of canine implant with recorded timepoints durations for Dogs 002, 004, and 007.

Each dog exhibited similar seizure symptomatology. Typically, these are focal seizures with secondary generalization proceeded in four phases. The first phase lasted 5-12 seconds and started with vigorous side-to-side shaking of the head, or jerking of the head followed by shaking, with altered awareness. The second tonic phase lasted 2-15 seconds with extensor rigidity of the jaw and opisthotonus of the head, neck, and limbs. These tonic movements were followed by rhythmic clonic jerking of the limbs, which were initially rapid (25-30 seconds) but slowed to resembled post-ictal running movements (10-50 seconds). In the recovery phase, the dogs lay quietly in lateral recumbency, with occasional jerks and hyperventilation.

5.3.2   Event Detection

Both seizures as well as interictal bursts were initially detected with a sensitive line-length detector and subsequently validated manually. Line-length is a feature that incorporates both the amplitude and frequency components of a signal and has been shown to be robust for detection of epileptiform events [38]. Detections that were interrupted by data dropout from device dysfunction or repair were eliminated from analysis. Three channels with significant electrode artifacts in dog 4 were also omitted from analysis. To detect seizures, the average line-length feature was calculated across all 16 channels with a 2-second moving window, and candidate event EEG clips with line-length above a specified threshold were saved. Thresholds for each dog were individually set to be of high sensitivity and low specificity in order to capture all events. Clinical seizure candidates were validated with simultaneously video by a consensus of two board-certified epileptologists (B.L. and G.W.). To detect interictal bursts, a similar line-length detector was used and candidate bursts were further refined by both quantitative and qualitative criteria. We excluded candidate events with maximum average line length feature values two times above the maximum value observed during known ictal events, since artifacts often displayed large-amplitude, high-frequency noise simultaneously on all channels. We eliminated candidate non-seizure events with above-threshold activity shorter than 500 ms and longer than 30 seconds. Longer events were manually reviewed to insure that real clinical events were not eliminated. Burst detections were validated by a consensus of two board-certified epileptologists (B.L. and K.D.). After interictal epileptiform burst and seizure detections were finalized, each iEEG event was low-pass filtered at 100 Hz and downsampled from 400 Hz to 200 Hz, preserving event features relevant to clinical practice while reducing computational burden. iEEG voltages in each event were rescaled to [-10, 10] based on data that lies within a 99% confidence interval. This scaling prevents the extreme outliers from compressing the majority of the

data and is necessary for numerical stability of statistical inference, but no data in any event was discarded. Once the events (bursts and seizures) were identified, we then aimed to parse the dynamic activity of each event into states and determined the relationship between bursts and seizures.

5.3.3 Modeling

In order to assign a state to each timepoint during the bursts as well as seizures, we looked directly at the evolution of raw EEG voltages across time. This approach is similar to that which an epileptologist would use to analyze EEG, and captures evolving trends within time-traces. Here, we use an autoregressive hidden Markov model (AR-HMM) to parse the voltage signal into interpretable states that switch. Specifically, we model a single channel's activity as switching between a set of autoregressive (AR) processes, which are each locally stationary to account for the non-stationary properties of EEG. From a particular configuration of channel states, we can then assign global event states at any point in time[163]. This global event state, capturing the activity of all channels, is the focus of our analysis and the basis for determining similarity between two events. Notably, two extensions make this model suitable for this analysis. We mimic focal changes in the iEEG by allowing channels to share AR states and allowing asynchronous state switching. Finally, a spatial constraint is added due to the physical electrode configuration, allowing for spatial propagation of activity and more tractable statistical inference. Readers are referred to published literature by Drausin Wulsin for further details and technical implementation [163, 162].

5.3.4 Event comparisons

For each dog, all bursts and seizure events, regardless of focality were modeled together. This allows sharing of event states between both bursts and seizures as well as comparing dynamic similarity between events. We then ask the question: what parts of a seizure are

most similar to bursts? This can be answered by determining the similarity of the timepoints in a seizure to all bursts. Specifically, we first calculate the probability that a given timepoint in a seizure is assigned to the same state as a given timepoint in a burst. This probability is derived from the Bayesian estimation of the ARHMM model, and readers are referred to the supplementary materials and references for further details [44, 45, 163]. Secondly, we take the maximum probability across all time points in the given burst to find the similarity between the seizure timepoint and the given burst. Finally, we average this probability across all bursts to obtain the similarity between a given timepoint in a seizure and all bursts. Intuitively, this represents the average probability that a given time point in a seizure clusters with a burst. The model inference and analysis were run primarily on a cluster of ten 8-core Amazon EC2 machines `http://aws.amazon.com/documentation/`, linked together into a cluster with the third-party StarCluster `http://star.mit.edu/cluster/`. Matlab code for this model is available online `www.seas.upenn.edu/~wulsin`.

5.4   Results

Table 8 summarizes resulting data segments containing event detections analyzed for each of the four subject dogs. Bursts were on average 3.97 seconds long with a standard deviation of 2.48 seconds. The 95% interval is between 1.2 seconds and 11.08 seconds. Qualitative analysis of bursts indicates that they are very similar to the bursts described in human EEG. Figure 43 shows examples of 4 bursts from one dog in this study, which is representative of all animals monitored for this experiment. Figure 43A shows a burst of sharply contoured rhythmic alpha activity present over both hemispheres, most prominent at channels L5, L6, R3, and R4. In Figure 43B, a burst of diffuse rhythmic gamma activity most marked at channels L4, L5, R3 and R4 is present. The sharply contoured burst of rhythmic gamma activity is more focal in Figure 43C in the left hemisphere channels 4 and 5. Figure 43D also shows a burst of more focal sharply contoured beta activity also in the left hemisphere

channels 4 and 5.

Table 8: Data summary from four dogs with recorded iEEG

D	ECoG Time (days)	Initial Burst Detections	Final Burst Detections	Final Seizure Detections#
002	475.7	1,846	740	37
004	329.9	16,026	758	14
005*	45.8	6,437	811	91
007	451.8	11,149	1001	48

Initial and final detections are noted. Dog 005 died from status epilepticus during this study. # clinically validated.
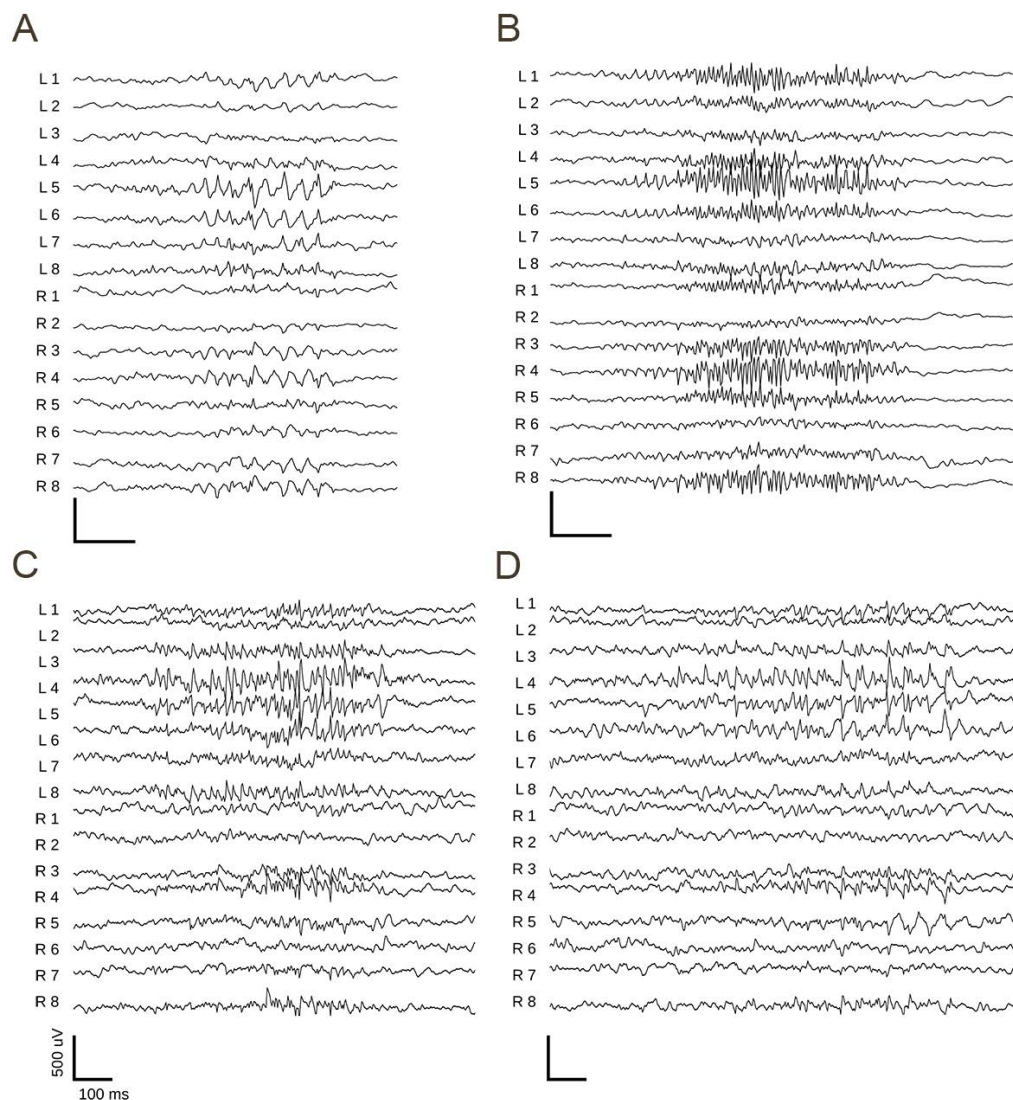
Figure 43: Examples of bursts detected on the canine iEEG data. There are 8 electrodes on each hemisphere, two parallel strips of four electrodes each. L1-8 are over the left hemisphere and R1-8 are over the right hemisphere. An average referential montage is displayed. (A) Burst of sharply contoured rhythmic alpha activity seen bilaterally most prominent at channels L5, L6, R3, R4. (B) Burst of diffuse rhythmic gamma activity most marked at channels L4, L5, R3, R4. (C) Focal burst of rhythmic gamma activity most prominent in L4, L5. (D) Burst of focal sharply contoured beta activity most prominent at L4, L5.
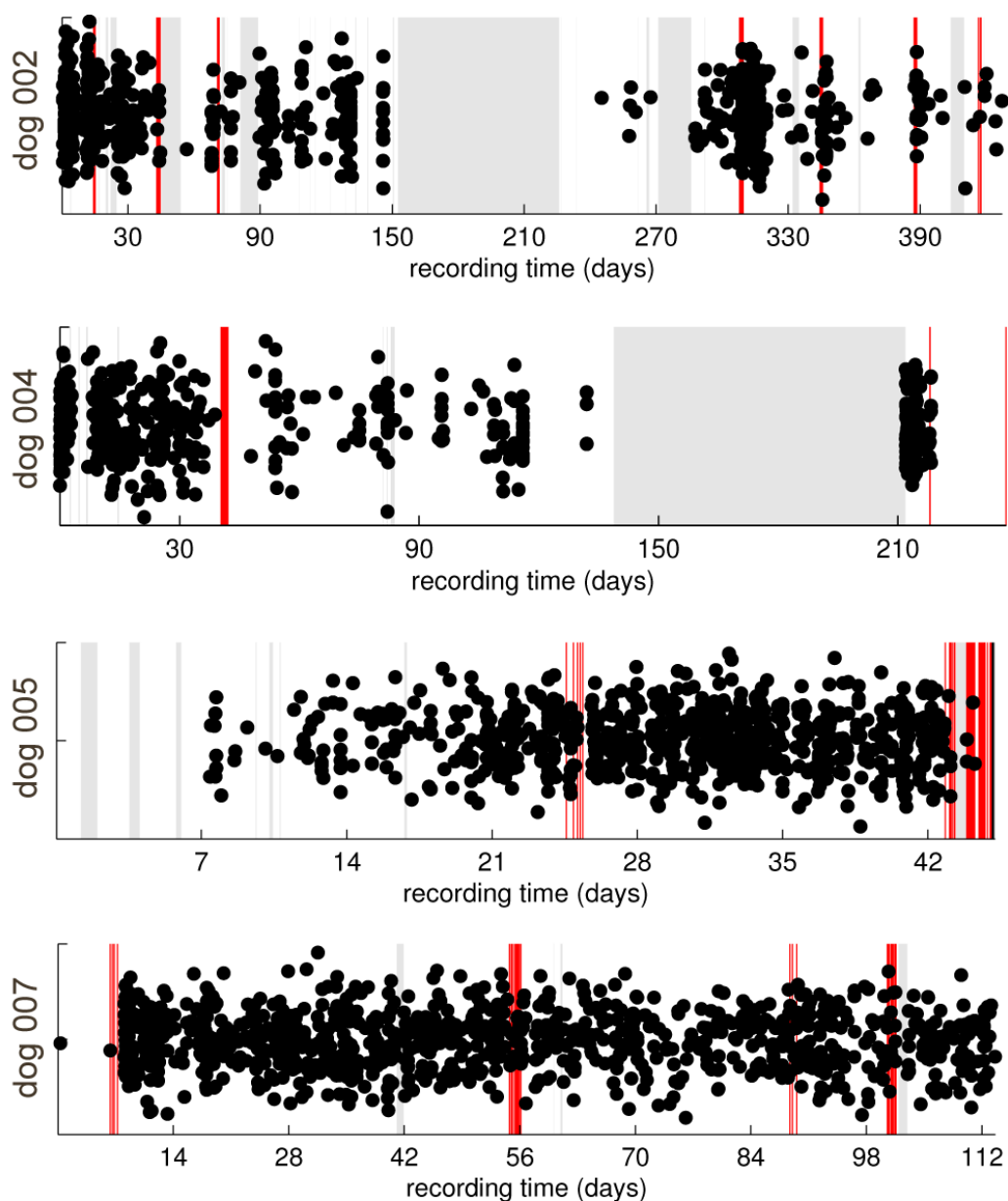
Figure 44: Timelines of the seizures (red vertical bars) and sub-clinical bursts (dots jittered vertically for display) for each dog over the span of the continuous recording. Gray periods in the recording denote times of no available data. The majority of the seizures occur in groups spaced a few hours from each other. The last 73 days of dog 004's record are omitted because only bursts excluded during the culling (and no seizures) occurred during that time frame. Figure modified from [161].

5.4.1   Do Bursts Correlate with Seizures?

A time line of the seizures (red vertical bars) and sub-clinical bursts (dots scattered vertically for display) is shown in Figure 44 for each dog over the span of the dogs entire continuous recording. Note that most seizures occur in clusters spaced a few hours from each other. A correlation analysis of burst distribution with seizure distribution indicated that bursts tended to cluster around seizures in dog 2, though not tightly ($r = 0.31, p = 0.006$). This pattern was not evident in the other dogs and bursts did not statistically predict seizures in any of the 4 subjects.

5.4.2   Bursts Characteristics and Similarity to Seizures

An example of event state assignments over EEG is shown in Figure 45. In panel A, the full seizure and 5 seconds of the seizure onset are shown. The colors beneath each EEG represent the state assignment at each timepoint. In panel B, the state assignments are shown for two bursts with transient decrease in activity in the center. Panel C shows the state assignments for the onset of a burst.
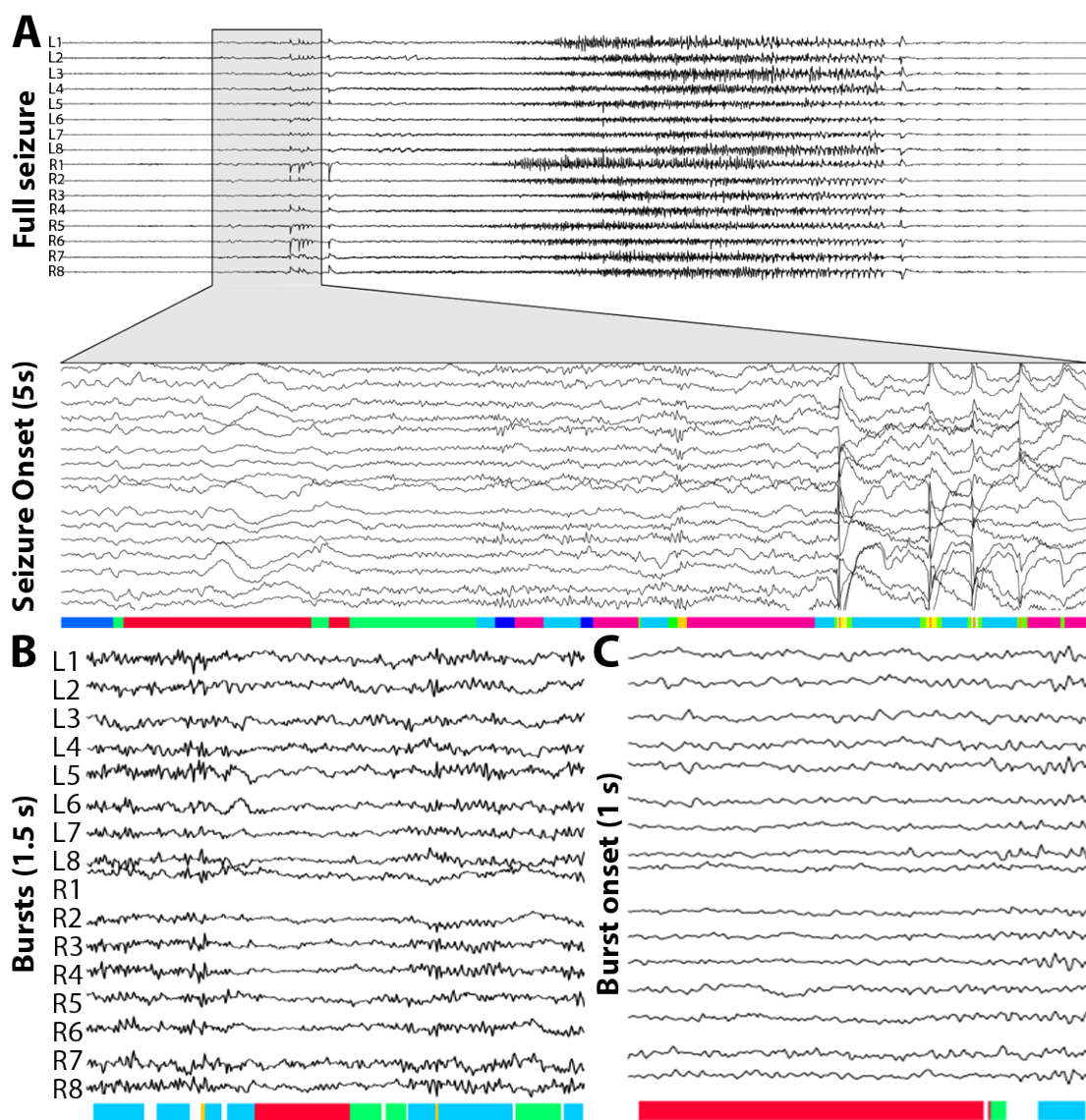
Figure 45: Multichannel examples of seizure onset and interictal bursts with corresponding event states. Colors below EEG represent state assignment. (A) Full seizure with event state assignments for the seizure onset (5 s). (B) Interictal bursts and corresponding state assignments (1 s). (C) Interictal EEG showing burst onset (1 s). Figure modified from [161].

Figure 46 shows the average burst similarity for one representative seizure from each dog. In

three dogs (excluding dog 5, who died from status epilepticus) bursts were stereotyped and found to be statistically similar to periods before or near seizure onsets. Higher amplitude activity following seizure onset had relatively little similarity with interictal bursts.
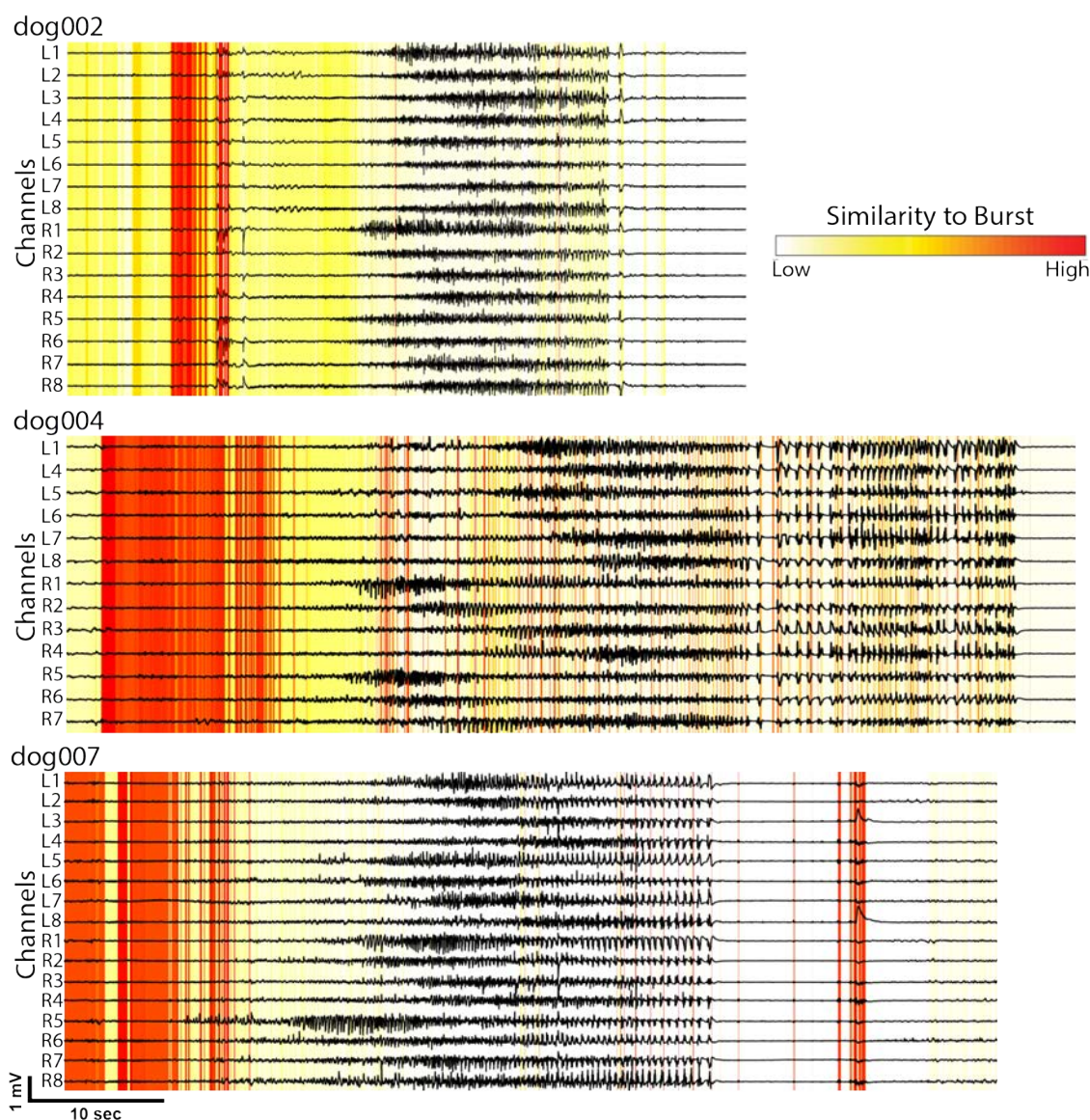
Figure 46: Burst similarities for a representative seizure in each dog. Each horizontal line is a channel. Vertical lines indicate averaged similarity of given timepoint with all bursts. Red denotes timepoints with high similarity to all bursts. Bursts were stereotyped and found to be statistically similar to periods before or near seizure onsets. Figure modified from [161].

Figure 47 shows the averaged burst similarity across all the seizures for each dog 10 seconds prior to marked unequivocal electrographic onset (UEO) 12, where each row contains the same information in the EEG shown in Figure 3. This displays how the burst similarities change across seizures and over each subjects monitoring period. Of particular interest, note how each cluster of seizures (denoted by the horizontal black lines) tends to display similar organization. There were few seizures during phenobarbital administration, but the relationship of bursts to non-status epilepticus seizures was unchanged.
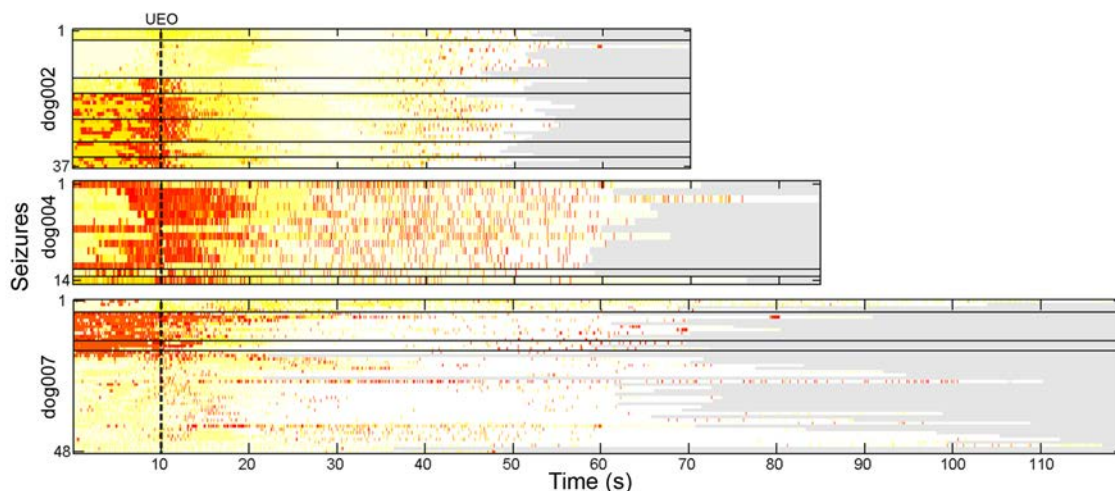
Figure 47: Burst similarities across all the bursts for each seizure in each dog. Horizontal axis denotes the time series of each seizure. The vertical axis stacks seizures in time over the course of the monitoring period. Horizontal black lines separate clusters of seizures, defined as >24 hours apart. Vertical dashes line defines the unequivocal electrographic onset (UEO). Red denotes timepoints with high similarity to all bursts. Figure modified from [161].

In dog 2, the first two clusters of seizures have little onset similarity with interictal bursts, though the later groups all display strong onset similarities. The high-amplitude seizure activity is in general not very similar to the bursts, though very discrete periods of the offsets tend to display strong similarities. The less marked similarity present at the end of the seizures occur at discrete, low-amplitude post-ictal discharges. In dog 4, 12 of the 14

seizures recorded occurred within the period of just a few days. These all display strong onset similarities with a subset of interictal bursts on iEEG, generally those bursts that occur before the large data gap shown in Figure 2. The two seizures occurring much later in the record contain similarities across more of the bursts. As in dog 2, all of the seizures in dog 4 contain patterns of very brief but very strong similarity at seizure offset. In dog 7, an early cluster of four seizures, as well as a late cluster of 32 seizures which occurred within two days also showed onset similarities with the bursts. However, the strongest similarity occurs with two clusters totaling 12 seizures. Bursts are similar to seizure onsets in the first three groups of seizures. Dog 5 is a particularly interesting case in that it contained two main groups of seizures, the second of which occurred while the dog was in status epilepticus. The five seizures in the first group all contain very strong onset similarities and a few brief periods of offset similarity across almost all the bursts, as in dogs 2, 4, and 7. The second group of seizures display physiologic changes associated with status epilepticus that manifest in changes in iEEG seizure dynamics (Figure 48, see discussion below). During status epilepticus the bursts no longer are similar to the seizure onset or offset as seen in prior seizures.
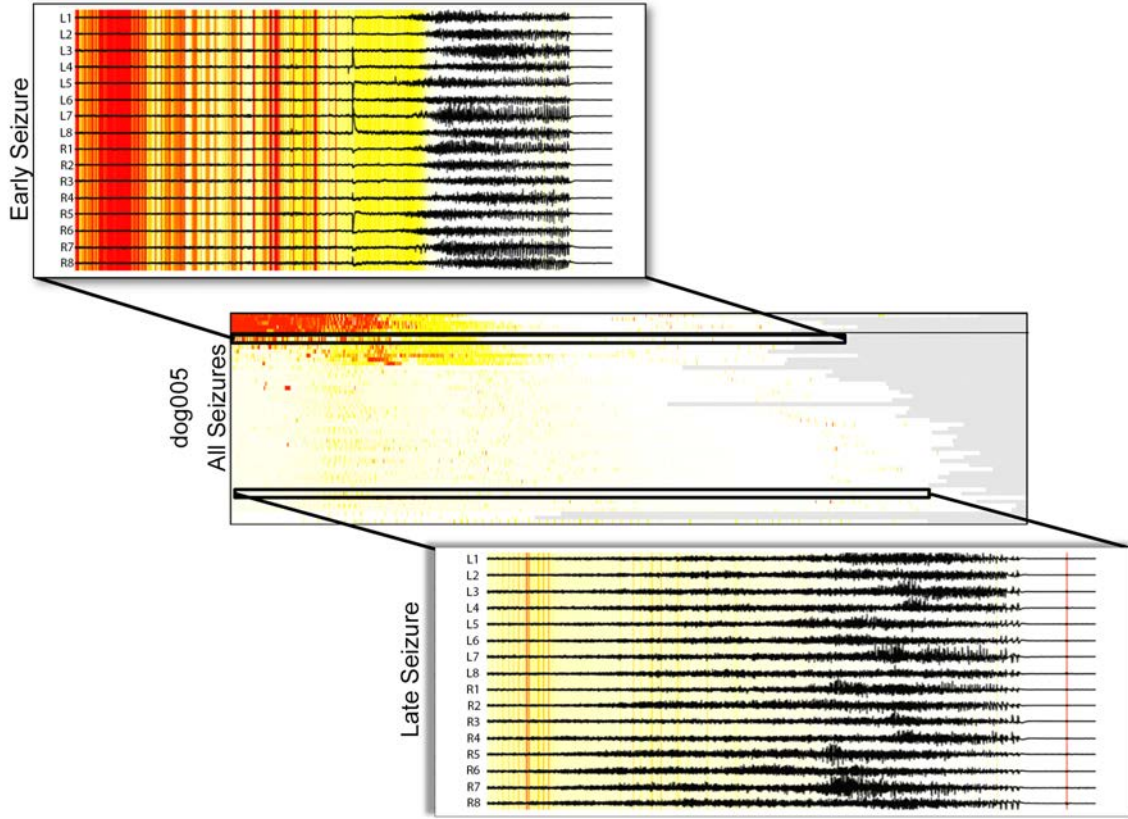
Figure 48: Burst similarities for the seizures of dog 005 (middle), similar to those shown for the other three dogs in Figure 47. An early (top) and late seizure (bottom) in dog005s status epilepticus, where the time points of each seizure are colored based on their similarities to the other bursts. Red denotes timepoints with high similarity to all bursts.

5.5 Discussion

EEG representations of seizures can be thought of as observations from a complex physiologic network. We have every reason to believe that this network can change, especially after acute injury like traumatic brain injury or electrode implantation. We can think about these networks as creating a probability distribution of epileptic events, where each epileptic event is a sample from this distribution. Perturbations increase the probability of certain epileptic events, including seizures. Ideally, clinicians would have a reasonably high degree

of confidence about the distribution of epileptic events, and thus confidence in the proba-bility of future seizures, before making a dramatic clinical decision. However, this requires many observations of epileptic events, and often only a few seizures are recorded over weeks of intracranial monitoring. Furthermore, the network can generate a multimodal seizure distribution, meaning that a patient may have more than one type of seizure which could be missed during observations in the Epilepsy Monitoring Unit. Furthermore, the network can change, meaning that a seizure observed at one point in time may not be representative of events in the future. Can we really be confident in the conclusions we draw about the underlying epileptic networks when we have so few observations generated by it?

We believe that the interictal bursts explored in this work have the potential to yield significant information about the distribution of epileptic events. Our data show that bursts are at least an order of magnitude more prevalent than seizures and occur much more regularly. Interestingly, although our algorithm detected all bursts less than 30 seconds, 95% of the finalized bursts were between 1.2 seconds and 11.8 seconds. This aligns with the 10 second cutoff that originated from the Young Criteria for subclinical seizures which is often extrapolated to the intracranial EEG setting by clinicians [165]. However, since bursts longer than 11.8 seconds were rare, it is plausible that bursts represent a continuous spectrum of subclinical seizures and that a longer duration interictal burst may reach a physiological threshold for propagation, manifesting as clinical seizures.

We also showed that bursts display pronounced similarity to seizure onsets, suggesting that they contain relevant information about the epileptic networks from which they arise. In Figure 45, the state assignments of two interictal segments provide insight into the particular burst patterns and their similarity to seizure onset. Panel B shows two bursts with state assignments similar to high voltage activity at the earliest electrographic onset (EEC). The transient decrease in voltage, assigned a red state, likely corresponds to a quieting phase

as seen in Panel C before burst onset. Because these event states are switching between AR processes, similar state assignments can be interpreted on a high level as having similar evolving frequency compositions. Physiologically, this similarity of bursts to the onset of a seizure may represent aborted seizure onsets, and comparing them to seizures may yield important mechanistic information on how clinical events are generated and guide surgical decision making.

In addition to being similar to seizure onset, we noted that burst similarities were statistically similar to seizure offset as well, but not the middle of seizures. Similar findings have been noted by other investigators who have shown dynamic iEEG network synchronization and desynchronization as a seizure progresses [82, 127], which is thought to reflect changes in network topology. It is, however, not well understood why the middle of seizures shows decreased network synchronization. Some have postulated that there exists a relationship between network topology and bursting dynamics, which is also supported by in vitro studies [81, 106]. It is plausible that bursting activity characterizes a transition between various brain states, which would explain the similarity to seizure onsets and offsets, but not the middle of seizures.

Dog 5, who unfortunately died from status epilepticus, is a case that allows us to explore differences between isolated seizures and status epilepticus. The onsets of the initial isolated seizures were similar to interictal bursts. However, seizures that occurred during status epilepticus were not similar to the bursts. Although not well established in the literature, clinicians often note a substantial change in seizure characteristics during status epilepticus, in comparison with isolated spontaneous seizures in the same individual. The lack of burst similarity in dog 5 during status epilepticus is consistent with this finding. The transition of burst dynamics as this animal entered status epilepticus is also of great interest. The change in structure appears to change abruptly within the first several clinical events, suggesting

that status epilepticus may represent an acute transition in epileptic networks, not a gradual transition into a stable, pathological state. However, these anecdotal observations are of only one dog, and further study in a larger dataset is needed for confirmation.

5.5.1 Limitations

The observations in this study suffer from several potential short-comings. First, the number of animals is quite small, as this was a pilot study meant to gather preliminary data for a larger, more detailed study. Though there is variability between dogs in this study, recording periods were very prolonged, much longer than previous work in the literature, and our conclusions regarding bursts, their relationship to seizures and their clustering behavior are supported by a large number of observed events and strong statistical significance. Secondly, the question of seizure typing and classification in the dogs used in this study is one that affects the extension of our findings to human epilepsy. While there is significant literature qualitatively describing canine epilepsy [96], there is little published on iEEG in these animals, and their epilepsy syndromes are poorly characterized. We have described the seizure disorders and EEG in our subject animals previously [27] and found both well localized partial onset epilepsy in these animals, as well as poorly localized, regional onset frontal lobe seizures, though these were partial in onset. However, the range of patterns observed compares well to humans with medically refractory epilepsy undergoing iEEG presurgical evaluation. None of the animals monitored in this study appeared to have syndromes suggestive of disorders analogous to human primary generalized epilepsy, though these entities are less well described in these animals. Certainly relating our findings to those in human epilepsy will require similar extended recordings in patients, in order to determine whether our findings hold in the human condition.

Finally, the interictal bursts detected in this study likely encapsulated different subtypes. Here, the bursts we studied involved the majority of EEG channels because we were in-

terested in the electrographic characteristics of each burst and not the spatial patterns. However, there was clear focality in many of these bursts. Furthermore, in the current analysis we did not stratify our analyses by the variability in the frequency composition (such as those shown in Figure 46). It is possible that a certain subtype of burst with certain frequency composition or focality is most similar to seizure onsets, and this is current topic of investigation in our lab.

5.5.2 Future directions

We believe we can use burst-burst similarity to determine when the epileptic network has stabilized and thus when the seizure observations from that network are truly representative of the future events. Based upon the known immunologic reaction to chronic intracranial implants and the resulting anatomical changes, [59, 116, 119, 141, 151, 166] some investigators postulate that the implantation process itself may introduce epileptiform activity that can confound localization of epileptiform activity. Current work in our lab is focused on analysis of burst dynamics to determine if these patterns can be used as a proxy for network stabilization.

Future research will help determine whether these bursts also contain localization information similar to that found in seizures. Since we have established that interictal bursts occur with greater frequency than seizures, this information might be harnessed to reduce or perhaps eliminate the requirement to record ictal events to map patients for epilepsy surgery or device placement. This study was not designed to test this hypothesis, but suggests that further investigation in this area could be fruitful. This issue that has not been assessable until now, with the appearance of prolonged intermittent recordings and more detailed, continuous recordings from devices like the one used in this study [102]. Finally, an underlying theme of this research is using unsupervised methods to analyze massive streams of continuous iEEG, raising the significance of big neural data in clinical care. Our ability to

analyze and categorize continuous iEEG recordings spanning up to a year in duration on Amazons Elastic Computing Cloud, suggests a possible paradigm shift in epilepsy research and potential clinical care. We now possess tools that make continuous access to extremely dense, prolonged and detailed brain recordings possible, with the ability to share them world wide on The Cloud. These advances have tremendous potential to accelerate collaborative research and facilitate rigorous validation of studies like this one. In this light, we are posting all of the data from this study on the International Epilepsy Electrophysiology Portal (`http://ieeg.org`) after publication of this study.

5.5.3   Conclusion

We believe that the findings in this study expand our current knowledge about the prevalent interictal bursts observed on iEEG and warrant further investigation into the predictive and localizing ability of these patterns. We show that these interictal bursts are very similar to both the onsets and offsets of seizures, potentially indicating that the bursts represent aborted seizures or changes in brain state. Whether this belief is correct will depend upon further human studies, now in progress, on a richer, larger continuous iEEG dataset. We also believe that the power of faster digital computers, machine learning, cloud computing and big neural data are poised to have dramatic impact on epilepsy research and clinical care.

Chapter 6

Burst Localization

6.1 Abstract

In the localization of seizure onset for resective surgery, confidence increases with the number of observed seizures. Invasive intracranial monitoring may thus last for several days if seizure frequency is low. In addition, inflammation from implantation may affect characteristics of the EEG immediately afterward. Studying relatively frequent interictal epileptiform bursts over an extended period of time may provide improved localizing information to aid in surgical resection.

Three dogs with spontaneously occurring epilepsy were implanted with 16 electrodes, 8 in each hemisphere, and continuously recorded for 476, 330, and 452 days respectively. Seizures were automatically detected, clinically validated, and onset channels identified. A high sensitivity in-house burst detector was used to identify focal bursts, followed by a culling procedure and an unsupervised Gaussian mixture model to remove false positives and separate bursts subtypes from noise. Channels of maximum average power and power in theta, alpha, beta, and gamma were calculated for each subtype and compared to clinically validated seizure onset channels.

Each dog had multiple seizure types, with onset channels in multiple foci. The power characteristics of each burst also evolved over time. The channels with high power in specific

frequency bands (alpha, gamma) correlated with the seizure onset channels determined by a board-certified epileptologist. However, there was variability between dogs. For dog 002, burst power in the delta and theta band was maximum in the onset channels. For dog 004, the theta band peaked in seizure onset channels, though they were less distinct from other channels. For dog 007, peaks in gamma bands localize to onsets of a subset of seizures.

The extended intracranial recording of dogs with spontaneous epilepsy shows an evolution of interictal burst characteristics. Power analysis of detected interictal bursts show that power in certain frequency bands are more prominent in channels that were predetermined to be located in the seizure onset area, though significant variability is present. These results suggest that the analysis of more frequent interictal bursts in humans may improve localization for the surgical treatment of epilepsy.

6.2 Background

Seizure localization is an integral part of the treatment of refractory epilepsy. During inpatient evaluation of a patient's candidacy for surgery, non-invasive methods (scalp EEG, imaging) are employed and if necessary, invasive methods (intracranial EEG, iEEG) are also employed. During iEEG monitoring in the inpatient unit, video and iEEG recordings of each patient is collected to correlate observed behavioral symptoms with seizure semiology on iEEG [110]. Though necessary for localization, the process is not benign, and associated with hemorrhage, ischemia, and infection risk [42, 31]. The risks of monitoring are balanced with the need to observe the patient's seizure semiology, and any possibility of shortening the duration of monitoring is important for the patient's health.

We showed previously in chapter 5 that bursts are dynamically similar to seizures [28]. This suggests that the underlying seizure generating network may also be activated in interictal bursts. Interestingly, the inverse relationship between the frequency of bursting

and frequency of seizures [95] may indicate a release of energy by bursting that reduces the frequency of seizures. This, coupled with the finding that bursts are dynamically similar to seizure onset [28], suggests that bursts may localize to seizure onset. Since bursts occur with higher frequency, this would expedite the invasive inpatient intracranial monitoring.

One of the hallmarks used for seizure localization is a sudden change in frequency, such as a gamma buzz. For this reason, we examine the spectral characteristics of each burst to determine if a particular frequency necessarily localizes to the onset zone or not.

6.3   Methods

6.3.1   Dataset

Three dogs originally described by Davis [27] were included in this study each monitored with continuous iEEG for periods of 475.7, 329.9, and 451.8 days.

6.3.2   Event Detection

In contrast to detecting global bursts in chapters 5, in this experiment we focus on detecting focal bursts. This is determined by pattern detection in each individual channel without spatial integration. Using the detection pipeline above, we detect focal bursts from marked datasets using line length as the initial segmentation feature. To account to transient changes in the signal, this feature was normalized within every 1 hour block of data. A window length of 2 seconds with a 3 second padding was used. A total of 113 features were extracted:

1. Duration (1)

2. Line Length in each channel (16)

3. Energy in each channel (16)

4. Zero crossings in each channel (16)

5. Power in 4 frequency bands (4×16): 4-8, 8-13, 13-30, 30-100 hz

6.3.3 Modeling

As we expect these detections to be hypersensitive and contain many different types of bursts, it may be the case that a subset of bursts are more important for localization. The above features were each normalized before a gaussian mixture model with full covariance structure was used to automatically separate all bursts into groups. The optimal number of groups was selected based on the gap statistic [146]. The gap statistic is a metric that compares the distribution of points with a. After clustering, random patterns from each cluster were visualized for confirmation.

6.3.4 Localization

After separating the bursts into distinct clusters, we then determine which channels had significantly more power in each frequency band. These channels thus represent a higher frequency of the bursts detected and may serve to localize seizure onset. As seizure onset is often characterized by changes in frequencies from background activity (e.g. gamma activity or higher frequency oscillations), relative power in four bands were extracted from each channel in each burst in each cluster. Channels with higher relative power to the distribution of power for all channels were identified. Statistical testing was performed for each band using a Z-test on any outliers to determine the burst foci.

Table 9: Canine Seizure Onset Channels and Spread.

Dog	Seizure type	Onset Channels
002	1	$9/10 \rightarrow 13/14$
	2	$5/6 \rightarrow 9/10$
	3	$13/14 \rightarrow 9/10$
004	1	$1/5 \rightarrow 6/7$
	2	$7/8$
	2	$9/13$
007	1	$13/14 \rightarrow 5$
	2	$5 \rightarrow 13$
	3	$5/6$
	4	$13/14 \rightarrow 9/10$

$\rightarrow$ details spread. All seizures were
noted to secondarily generalize.

Table 10: Proportion of bursts overlapping with SOZ. Each column corresponds to the frequency band component extracted from bursts

	[0-4]	[4-8]	[8-13]	[13-30]	[30-100]
Dog 002	0.97	0.58	0.31	0.22	0.12
Dog 004	0.09	0.56	0.44	0.39	0.45
Dog 007	0.00	0.36	0.46	0.45	0.68

6.4   Results

The power characteristics of each burst evolved over time, with certain clusters appearing initially after implantation and others emerging later. Several power frequencies corresponded with burst onset, though there is significant variability across power frequencies as well as dogs. Delta and theta bands were useful in localizing seizure onset in dog 2, theta in dog 4, and gamma in dog 7 (Table 10). Seizure onset channels noted for all dogs are shown in Table 9. Seizure foci, burst foci, and any overlap are shown in Figure 53.
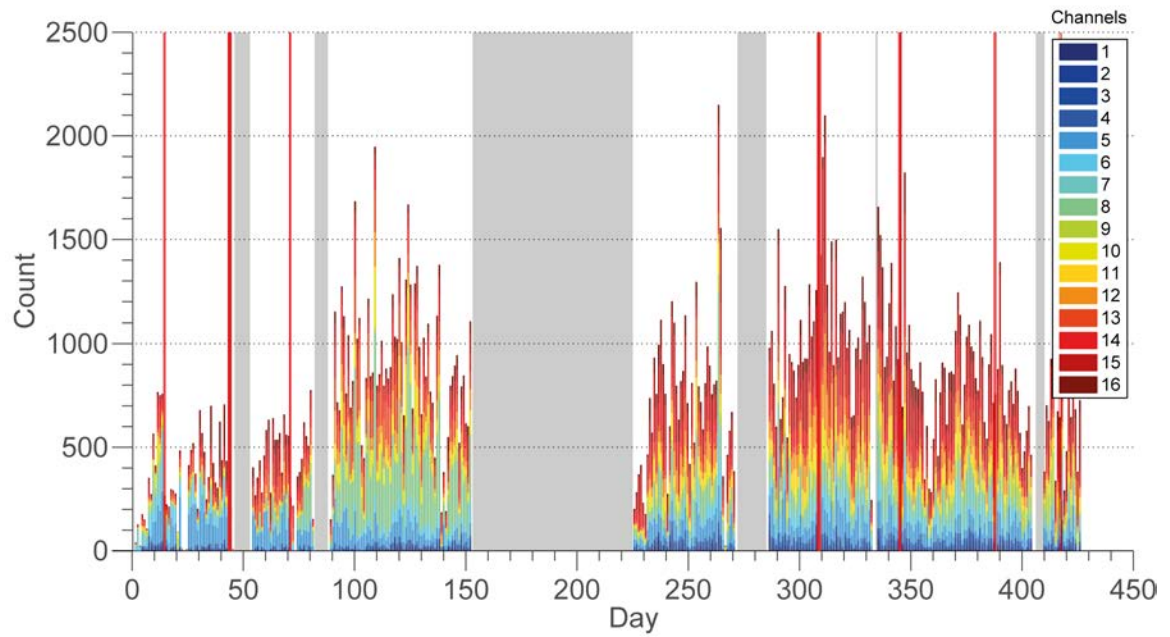
Figure 49: Histogram of interictal bursts for dog 002 over time, colored by channel of maximum power. Vertical red lines indicate seizure occurrence (37 total). Grey regions indicate periods where no data was collected.
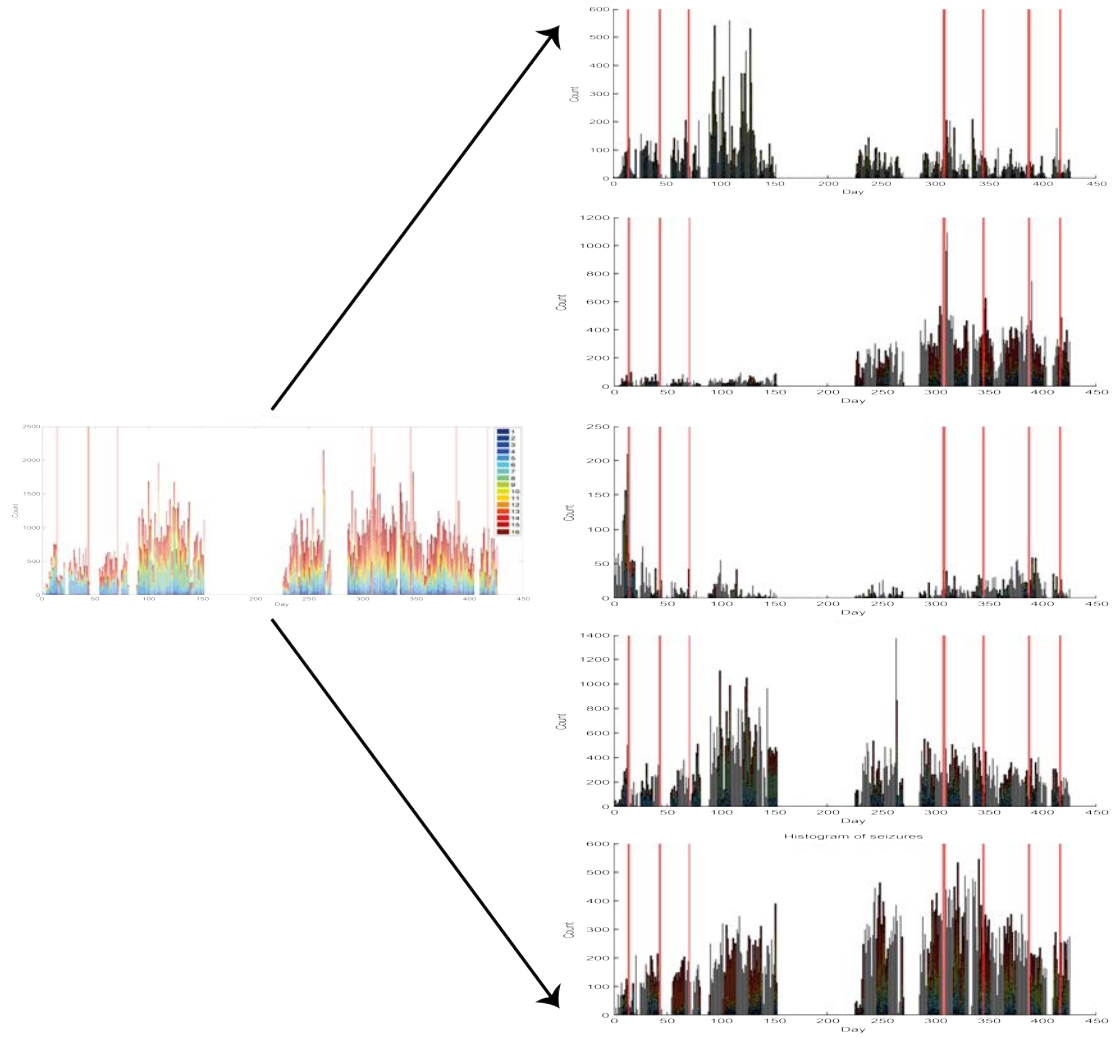
Figure 50: Interictal burst clustering. Original bursts (left) clustered into 5 clusters based on the gap statistic.
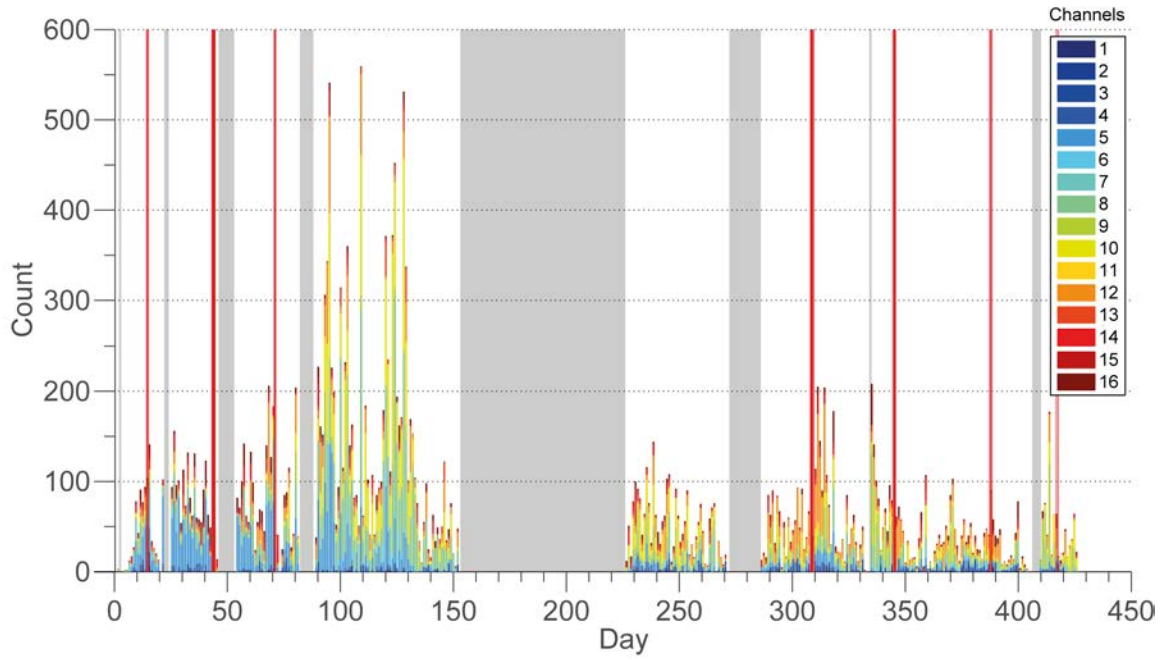
(a) Cluster 1
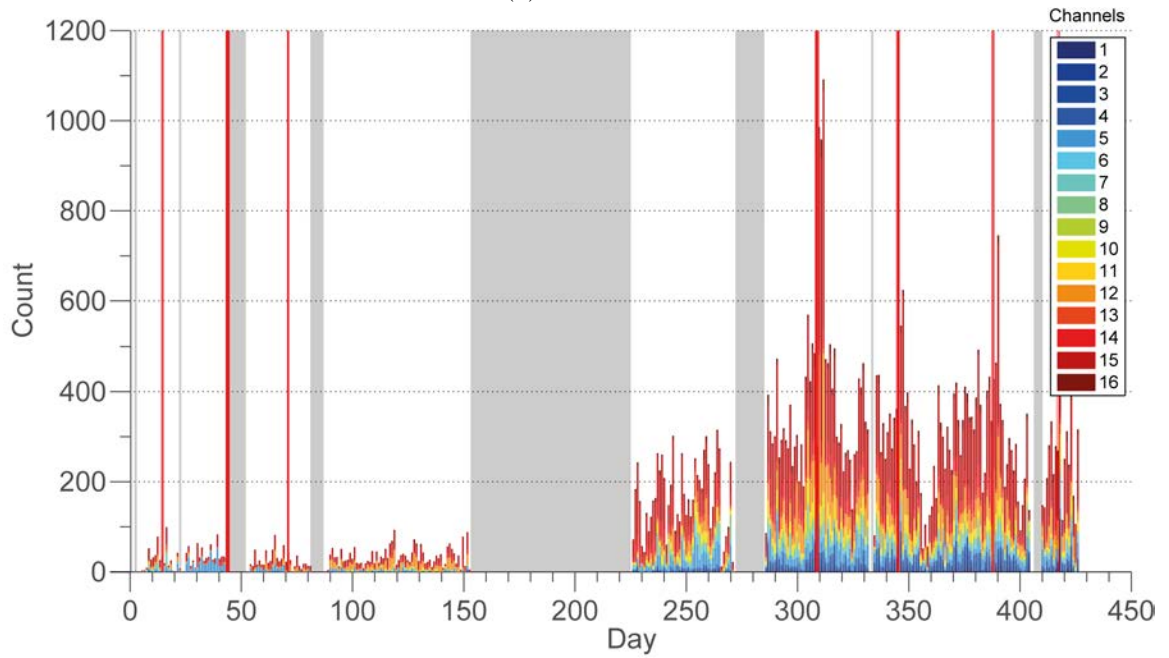
(b) Cluster 2

Figure 51: Histograms of two of the five clusters of bursts, similar to Fig 49 above. These two clusters were chosen to represent two distinct groups of bursts with differential power spectrums as indicated by the channels of maximum power.

(a) Cluster 1 (b) Cluster 2
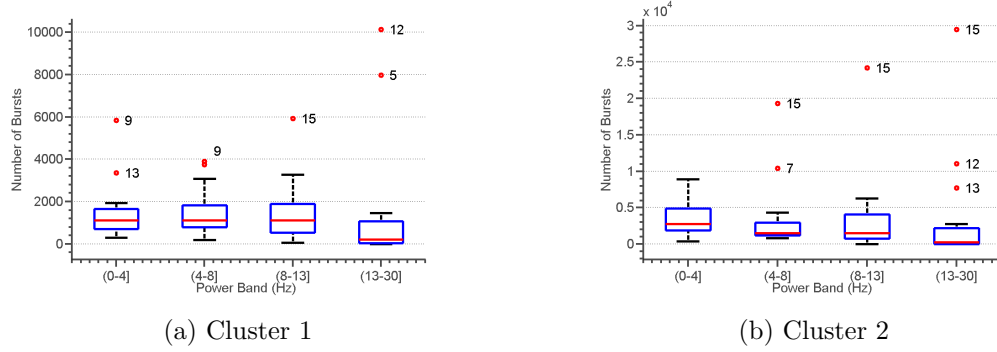
Figure 52: Number of bursts in each channel with maximal power in given frequency bands. Only the first two clusters are shown out of a total of five clusters. The outliers are indicated and labeled with channel number.
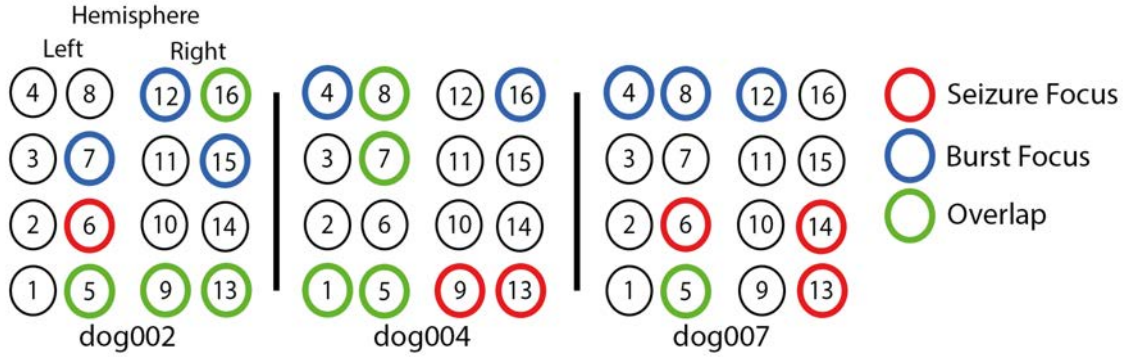
Figure 53: Foci for each dog delineated by focus type, collapsed over each clinical band. Red outlined circles indicate seizure foci. Blue outlined circles indicate common burst foci aggregated across first four non-noise clusters. Green outlined circles indicate overlap between seizure and burst foci.

6.5 Discussion

The extended intracranial recording of dogs with spontaneous epilepsy show an evolution of interictal bursts, both in time and in spectral characteristics. Power in specific certain frequency bands are more prominent in channels that were predetermined to be located in the seizure onset area, though significant variability is present. These results suggest that

the analysis of more frequent interictal bursts may be promising, though variability between dogs and also in seizure localization may be barriers that will need to be investigated in future datasets (See future directions). In dog 002, we see that burst onsets co-localize with 4 of 5 seizure onsets. However, bursts suggested seizure foci in 3 additional channels that are neighboring to manually identified seizure onset zone are evident. As seen in Chapter 7, it may be the case that specific clusters of bursts localize to certain seizure types, especially given the temporal separation of burst characteristics seen in Figure 51. Though onset in all three seizure types are represented (electrodes 5, 9, 13), cluster 2, which occurs later in the recording, coincides with seizure type 3 for dog 002 and seems to suggest an onset in electrode 15 from a power analysis (Figure 52b). In dog 004, all left hemispheric onset electrodes were localized by bursts, although none of the right hemisphere electrodes were. In dog 007, only one of the four seizure foci were localized. These findings are limited by several factors, which have implications for future directions. First is the small number of dogs. The variability present between dogs, with one of two showing decent localization and a third dog with poor localization, limits the interpretation of our findings. Furthermore, the multi-focal epilepsy present in dogs as well as the limited spatial resolution casts doubt on the localizability of the seizures to begin with. It is possible that bursts may identify the extent of an epileptogenic region, yet the variability between animals and the complexity of their epilepsy make it difficult to draw such a conclusion. Further work is required to determine the relationship of bursts to nearby seizures as well as to incorporate other features into the filtering and clustering of the detected bursts. Ideally, this analysis would be carried out on data primarily of unifocal patients where surgical outcome, and thus ground truth, is available.

Chapter 7

Temporal Trends of bursts

7.1 Abstract

Epilepsy is a chronic disorder, but seizure recordings are usually obtained in the acute setting. The chronic behavior of seizures and the interictal bursts that sometimes initiate them is unknown. Localization of bursts in Chapter 6 suggests that seizures may follow similar patterns. We investigate the variability of these electrographic patterns over an extended period of time using chronic intracranial recordings in canine epilepsy.

Continuous, year-long intracranial EEG recordings from four dogs with naturally occurring epilepsy were analyzed for seizures and interictal bursts. Following automated detection and clinician verification of interictal bursts and seizures, temporal trends of seizures, burst count, and burst-burst similarities were determined. One dog developed status epilepticus, the recordings of which were also investigated.

Multiple seizure types, determined by onset channels, were observed in each dog, with significant temporal variation between types. The first 14 days of invasive recording, analogous to the average duration of clinical invasive recordings in humans, did not capture the entirety of seizure types. Seizures typically occurred in clusters, and isolated seizures were rare. The count and dynamics of interictal bursts form distinct groups and do not stabilize until several weeks after implantation.

There is significant temporal variability in seizures and interictal bursts after electrode implantation that requires several weeks to reach steady state. These findings, comparable to those reported in humans implanted with the NeuroPace RNS device [31, 75], suggest that transient network changes following electrode implantation may need to be taken into account when interpreting or analyzing intracranial EEG during evaluation for epilepsy surgery. Chronic, ambulatory intracranial EEG may be better suited to accurately map epileptic networks in appropriate individuals.

7.2   Introduction

In the absence of obvious causal lesions, candidates for surgery and neurodevice implants are determined based on intracranial EEG (iEEG) and to an increasing extent, neuroimaging (PET, SPECT). The purpose is to localize the seizure onset zone prior to surgical resection or to identify network locations that may be amenable to neuromodulation. Unfortunately, these therapies have less than ideal efficacy: only approximately 50% of patients with neocortical epilepsy will achieve a clinically meaningful improvement in seizure frequency following surgery [88]. Similarly, median seizure reduction rates are 53% in a recent study of responsive neurostimulation [10]. Therefore, there is great interest in the research community in increasing the rate of seizure freedom in this challenging patient population.

New biomarkers in epilepsy are poised to impact patient care, from tracking epileptogenesis, to steering development of new pharmacologic agents, to enriching clinical trials [37]. Recently, our group has shown that interictal bursts are dynamically similar to seizure onsets, but occur with much greater frequency [28]. These bursts, described in adults as brief potentially ictal rhythmic discharges (B(I)RDs) [164], have been associated with increased propensity for seizures in the critically ill but their exact significance is still unknown. Studying these patterns in chronic ambulatory recordings will better allow scientists to

understand the natural temporal dynamics of epileptic brain.

Canine epilepsy is similar to human epilepsy in its epidemiology, spontaneity, and its response and resistance to therapy [118]. The similarities make canine models a promising animal model for testing new therapies, particularly neurodevices. In fact, vagal nerve stimulation was first shown to interrupt chemically induced seizures in a canine model [167]. We previously presented recordings from a novel implantable device that continuously monitors iEEG deployed in six dogs with naturally occurring epilepsy [27]. This work further validated canine epilepsy as a promising model of human epilepsy and generated a set of continuous iEEG data of unprecedented length for analysis. These data are the first of its kind to be publicly available on the International Epilepsy Electrophysiology Portal (`http://ieeg.org`). The recordings, which contained over 200 observed seizures, exhibit remarkable electrographic similarity to human recordings both in seizure onset patterns as well as features of background EEG.

Importantly, this dataset provides epileptic iEEG recordings of an unparalleled length, an average of 14 months across the three main dogs in this study. These recordings are significantly longer than the typical human inpatient iEEG recordings of days to a few weeks in duration [110] and provides 1) a greater number observations in time which allow us to describe temporal changes of observed bursts and seizures with greater statistical confidence, and 2) an opportunity to characterize transient post-implantation changes in epileptiform patterns. It is known that chronic iEEG implants and the surgery to implant them for invasive monitoring alters the underlying healthy cortex. The changes they induce, including hemorrhage, ischemia, and inflammation affects overall signal quality, electrode impedance, and possibly the representation of the epileptic network [151]. It is unknown how changes in this acute setting influence localization of the epileptic network, as current literature is primarily based on electrographic recordings during this period of inflammation.

It is also unclear whether interictal and ictal intracranial electrographic biomarkers currently used for surgical localization are stable within the typical recording period. One recent study analyzing 82 patients implanted chronically with a responsive neurostimulator demonstrates that an accurate representation of the spatial and temporal variability of seizures in these patients require at least 30 days of continuous monitoring [75]. Another study demonstrates that this prolonged monitoring may reveal patients who have well localized seizures and be good surgical candidates, though this was not apparent during acute monitoring [31].

In this study, we investigate temporal changes of both seizures and interictal bursts over extended iEEG recordings. This dataset provides an unprecedented opportunity to track temporal changes in epileptiform patterns over long periods of time after implantation, and to assess how well acute monitoring represents epileptic networks at steady state. Furthermore, in contrast to existing long-term iEEG findings in literature derived from two recording electrodes recording several minutes per day, our extended dataset contains continuous recordings from a total of 16 contacts. We pay particular attention comparing the initial one to three weeks after intracranial implant to the steady state in these recordings. Lastly, we study quantitative dynamics of interictal bursts, specifically identifying how bursts fluctuate throughout the recordings.

7.3   Methods

7.3.1   Dataset

The canine dataset described in Chapter 5 is used here. To recap, six dogs with naturally occurring focal epilepsy were originally implanted with four bilateral 4-contact subdural strip electrodes, a total of 8-contacts over each hemisphere, for chronic iEEG recording from a wireless system. Four of these dogs were selected for analysis due to the occurrence of seizures. Dogs 2, 4, 5, and 7 were recorded for 475.7, 329.9, 45.8, and 451.8 days,

respectively (Table 8). Dogs were withdrawn from any medications at enrollment. Dog 5 died from status epilepticus, after which all dogs received intermittent (2 mg/kg, twice a day) phenobarbital (PHB) administration (detailed in Figure 54) during monitoring. In all dogs this occurred well after the acute implantation period.

7.3.2   Event Detection

Both seizures and bursts were detected as described in prior work [28] (Chapter 5). Those steps are summarized below.

7.3.3   Seizures

Seizures were identified with an automatic detector based on the line-length feature, which captures both amplitude and time components of the signal and is shown to be robust for seizure detection [38]. Of these initial detections, valid electrographic seizures were verified with simultaneous video and the consensus of two board certified epileptologists (BL and GW). They were further subtyped according to localization of the seizure onset zone by a board-certified epileptologist (KD). All dogs were observed to have focal epilepsy of unknown etiology with secondary generalization and exhibited similar seizure symptomatology. Typically, seizures that began focally and secondarily generalized proceeded in four phases. The first phase of typical seizures lasted 5-12 seconds and started with vigorous side-to-side shaking of the head, or jerking of the head followed by shaking, with altered awareness. The second tonic phase lasted 2-15 seconds with extensor rigidity of the jaw and opisthotonus of the head, neck, and limbs. These tonic movements were followed by rhythmic clonic jerking of the limbs, which were rapid for 25-30 seconds, then slowed to resembled post-ictal running movements for 10-50 seconds. In the recovery phase, the dogs lay quietly in lateral recumbency, with occasional jerking movements and hyperventilation.

7.3.4   Interictal bursts

Interictal bursts lasting greater than 500 milliseconds and less than 30 seconds were extracted by using a threshold on the average line-length feature across all the channels. Candidate bursts were then manually culled and verified by an epileptologist (KD). Examples of bursts at different time points are shown in Figure 56. To determine the effect of implantation on the number of bursts, a linear mixed model was used to model log burst counts in the first 100 days across all animals, where the dog was modeled as a random effect. Residuals were modeled with an autoregressive model to remove autocorrelation.

To determine how bursts dynamically change, we characterize each time point in a burst by their dynamic frequency content and compare between bursts using a similarity metric. First, time points in a burst are modeled as locally stationary autoregressive processes that change states over time according to a Markov switching model. In this model, event (burst and seizure) snippets are modeled together across all animals using a spatial autoregressive hidden Markov model (AR-HMM). This model was used to capture the relative spatial locations of the electrodes as well as capturing non-stationarity with a state-switching model. After statistical inference, each time point in each event is assigned a state, and we define a similarity metric as the probability that two events belong to the same state. Two identical events will have a similarity of 1, and two events with no time points in a common state will have a similarity of 0. This similarity is calculated by determining the number of time points in each burst that share the same state and provides a metric to compare dynamic similarities between one or more bursts.

Similarity matrices were created to show burst-burst similarity for each dog by visualizing the similarity of a given burst to all bursts. To determine stability across time, the similarity of bursts on each day was compared to all future bursts for each dog. Readers are referred

to our initial paper [28] as well as prior technical work for a more detailed description of the model [45, 163].

7.4 Results

7.4.1 Seizures

A total of 37, 14, 91, and 48 seizures were detected for dog 2, 4, 5 and 7, respectively. Seizures electrographically appeared qualitatively indistinguishable in onset and spread patterns compared to human seizures as determined by to two epileptologists (BL and KD). With the exception of the dog in status epilepticus (dog 5), most seizures in each dog occurred in clusters, where all consecutive seizures with an inter-seizure interval (ISI) less than or equal to 24 hours define a cluster (Figure 54). For Dogs 2, 4, 5, and 7, the mean cluster duration was 29 (sd=7.6), 39 (sd=0), 18 (sd=0), and 25.5 (sd=5.9) hours, respectively. The mean within-cluster ISI was 6.3 (sd=3.5), 3.5 (sd=2.5), 0.79 (sd=1.93), and 2.3 (sd = 3) hours, respectively. Importantly, each dog had multiple seizure types with onset zones arising from bilateral hemispheres independently. The seizure types fluctuated across time. Examples of two seizure subtypes from the same dog on day 14 and day 308 of recording are provided (Figure 55). Within the first 60 days, each dog displayed two seizure types. Across the entire recording there was more variability, as Dogs 2, 4, and 7 had three, two, and four different seizure subtypes, respectively. The first 14 days of recording, analogous to the human inpatient surgical evaluation period, did not capture the full extent of seizure types in any of the dogs. When Dog 5 died from status epilepticus, PHB was intermittently started for dog 2, 4, and 7 on days 54, 74, and 105, respectively. PHB therapy greatly lowered seizure frequency (Figure 54).
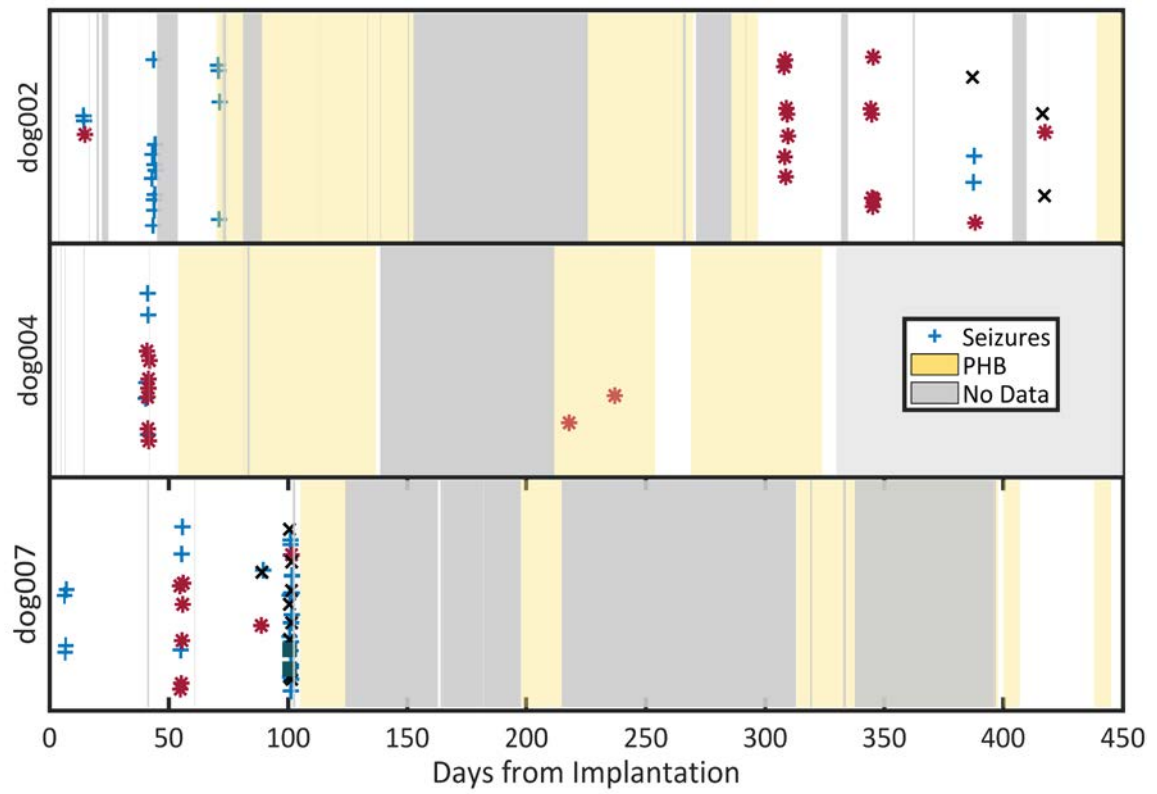
Figure 54: Seizures over the entire recording length across three dogs. Each marker represents a seizure, vertically jittered in time. Each color and symbol denote different seizure types as determined by a board certified epileptologist (KD). Gray represents periods of no data. Yellow represents periods of intermittent phenobarbital (PHB) administration.
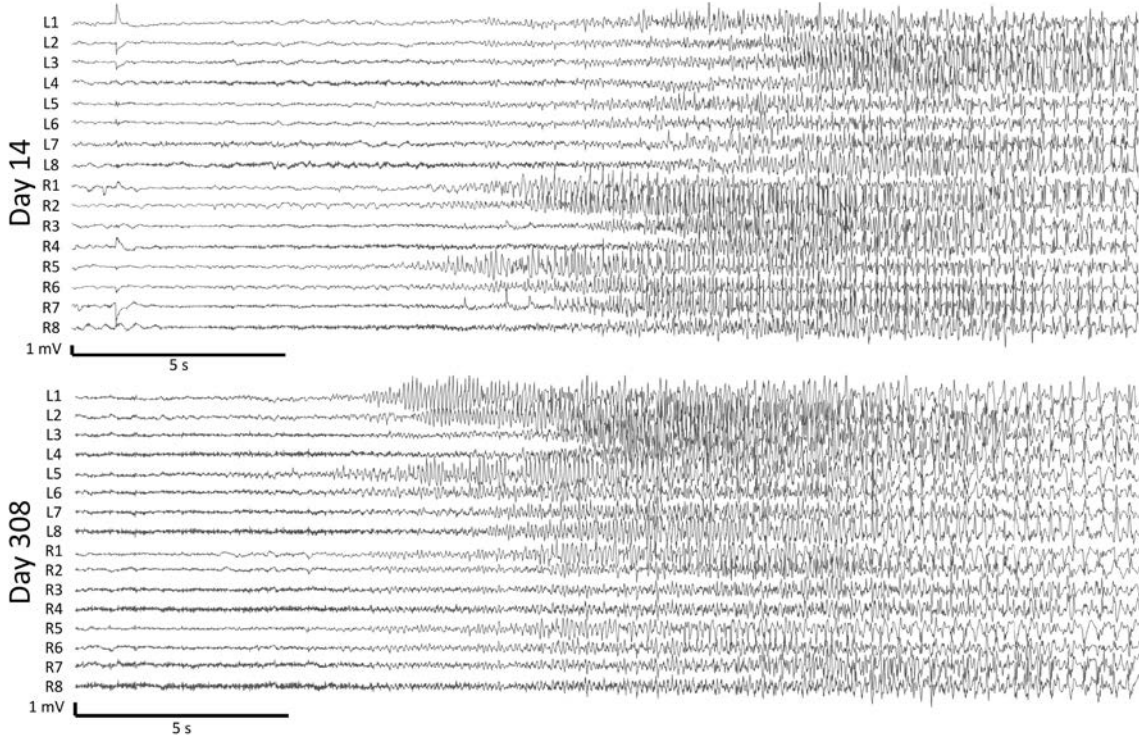
Figure 55: Two example seizure subtypes at Day 14 and Day 308 from dog 2. In panel A, seizure onset channels were determined to be in R5/R6 and propagating to R1. In panel B, seizure onset channels were on the left side, in channels L5/L6 and propagating to L1.

7.4.2 Interictal Bursts

Over 700 bursts were detected in each dog. Examples of bursts and the time of occurrence for one dog are given in Figure 56. In three dogs without status epilepticus, bursts showed temporal variation in similarity and in number. There were a significantly greater number of interictal bursts initially after implantation that decreased over time (P=0.03) (Figure 57). The similarity of bursts approaches that of those at steady state weeks after recording for each dog (Figure 58). A similarity matrix comparing bursts to all bursts show distinct clusters that indicate evolving event dynamics after implantation (Figure 59). It can be observed for dog 2 (6A), dog 4, (6B), and dog 7 (6C), that there are remarkably distinct

groups of bursts that are temporally restricted. For dogs 2 and 7, the largest and most stable group emerges in the first few weeks of recording, while dog 4's bursts undergo a more gradual, but still observable, transition. Interictal bursts were unaffected during PHB administration, both in count as well as in similarity.
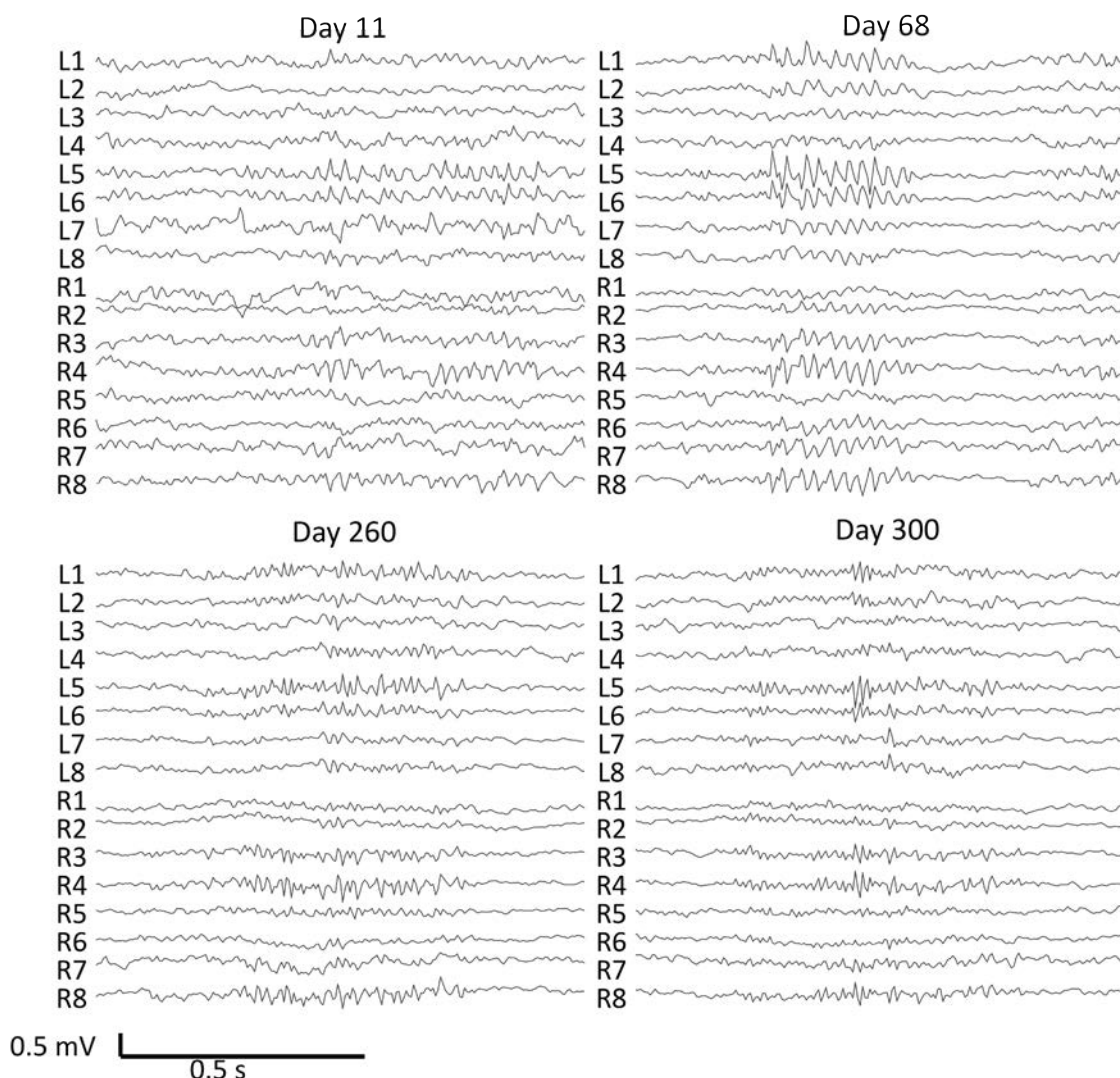
Figure 56: Examples of interictal bursts detected on the canine iEEG data and corresponding days after implantation from dog 2. There are 8 electrodes on each hemisphere, two parallel strips of four electrodes each. L1-8 are over the left hemisphere and R1-8 are over the right hemisphere. An average referential montage is displayed. (A) Burst of beta activity bilaterally most prominent in L5-6 and R3-4 on Day 11. (B) Burst of diffuse beta activity most marked at channels L5-L6 on Day 68. (C) Burst of rhythmic gamma activity most prominent in L5-6, R3-4,8 on Day 260. (D) Burst of gamma activity most prominent in L5 on Day 300.
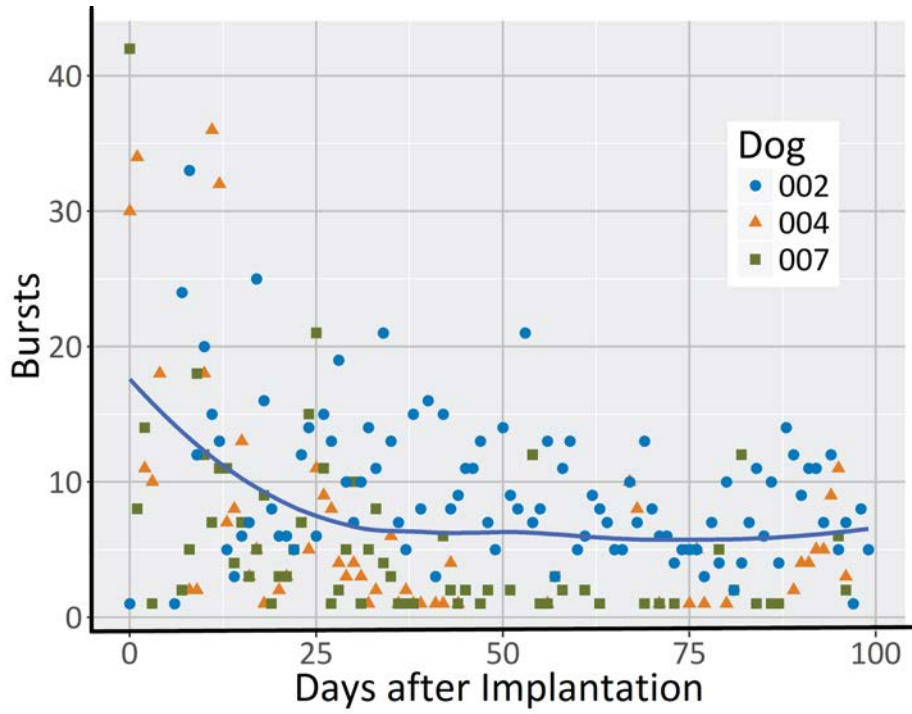
Figure 57: Average number of bursts per day for the first 100 days across three dogs (excluding dog with status epilepticus). The blue line represents the mean number of bursts across three dogs. A linear mixed model fit to log bursts show a significant decrease in burst count (p=0.03).
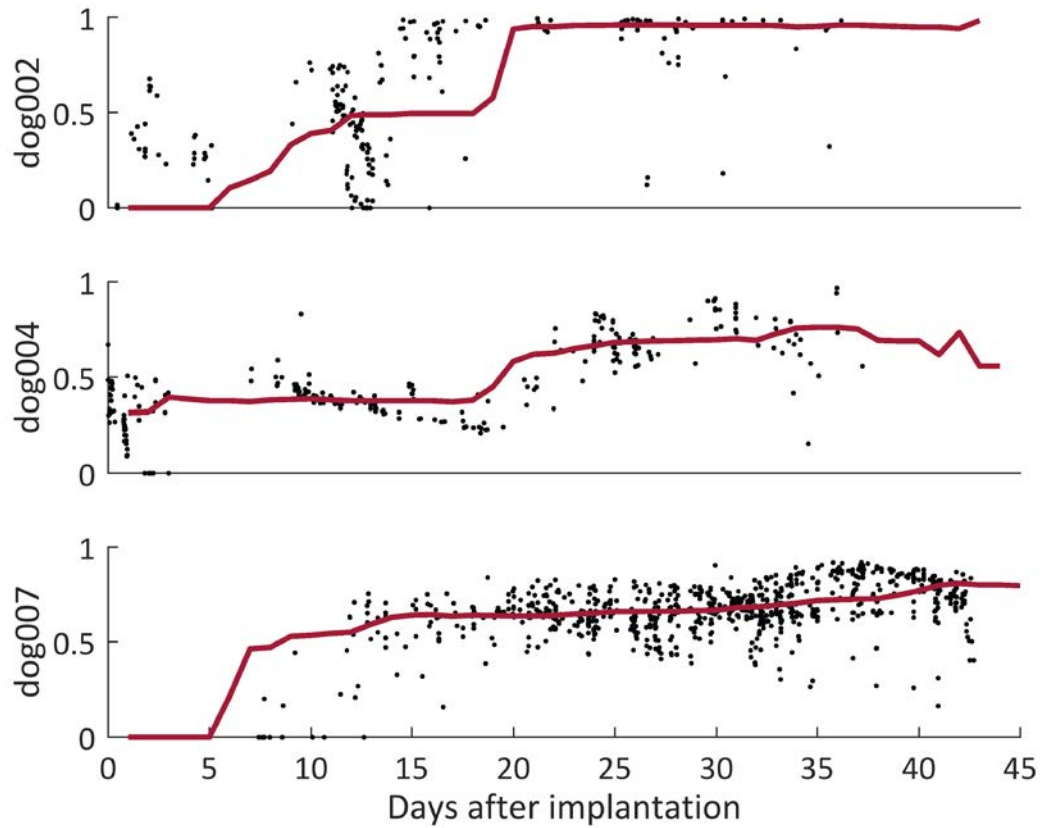
Figure 58: Normalized burst similarity in comparison with all future bursts in three dogs over the first 45 days of recording. Black points represent the similarity of the burst at that time point to future bursts. The red line denotes the median similarity within a 2-week moving window. High similarity represents a value of 1. Of note, early bursts are dissimilar to later bursts and that similarity levels off 20 days. Figure modified from [161].
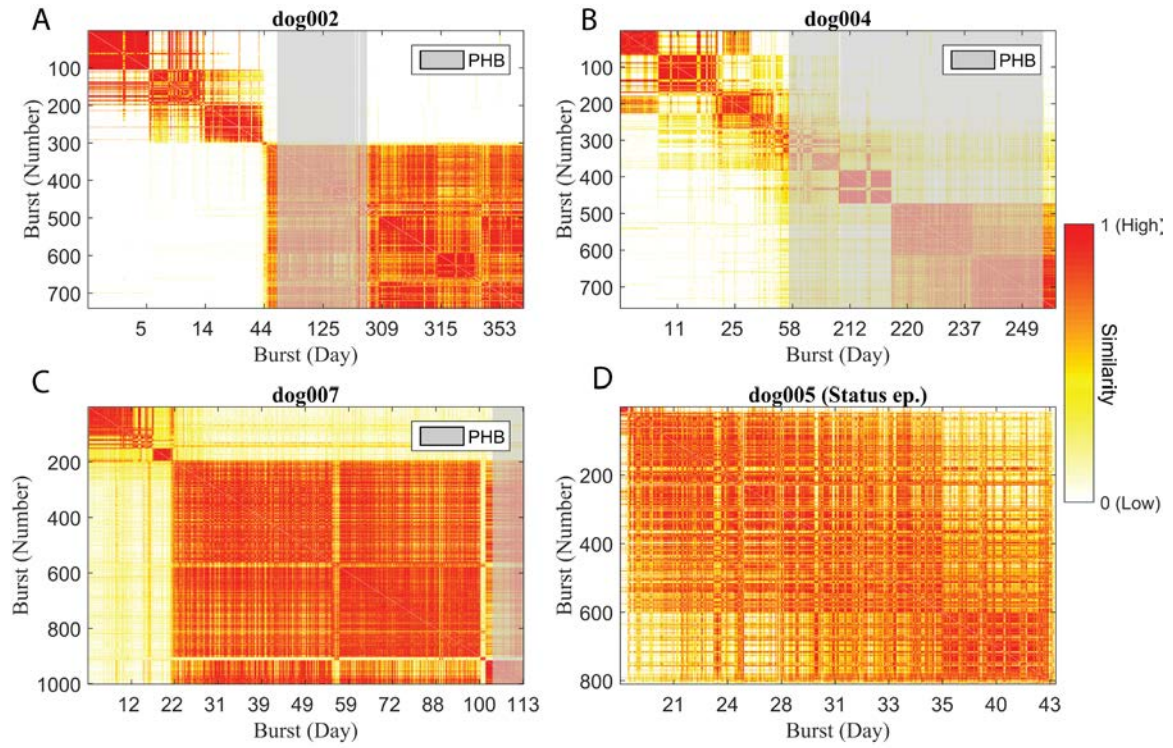
Figure 59: Similarity between bursts over time. Red indicates high similarity, white indicates low similarity. Vertical axes show bursts in rank order. Horizontal axes show bursts based on day of occurrence. Time periods when dogs received phenobarbital (PHB) are indicated in gray. Panels A, B, and C all show distinct clusters of bursts that are very similar to one another, indicated by well demarcated blocks of high similarity. Panel D displays similarities of all bursts during status epilepticus, showing that most bursts were dynamically similar. Figure modified from [161].

7.4.3 Status epilepticus

One dog died after developing status epilepticus one month following implantation. In this dog, all bursts showed remarkable similarity (Figure 59D), suggesting that a single network generated and sustained status epilepticus in this animal. Following the death of this dog, all other dogs were treated clinically with intermittent PHB.

7.5   Discussion

In this work, we investigated the temporal evolution of seizures and interictal bursts in long-term canine recordings and demonstrated that seizure onset location and burst dynamics fluctuate throughout the recording. These findings, while obtained in natural canine epilepsy, may have significant implications for current practice in the management of human epilepsy.

Intracranial EEG provides high resolution and fidelity recordings that allow interrogation of the epileptic network. However, most of these recordings are currently collected during clinical monitoring for resective surgery, lasting a few weeks at maximum due to the invasive nature of intracranial electrodes. Trauma to the brain during implantation may result in hemorrhage as well as an acute inflammatory response that activates surrounding glial cells as early as one day post-implantation [42]. A chronic foreign body reaction is often observed with the formation of a glial scar [116]. This reactive tissue at the electrode-tissue interface is presumed to be the cause of increased electrode impedance over time [134]. Acute implantation of electrodes also alters brain physiology, at least transiently, and even sometimes renders patients seizure free. Despite these findings, the gold standard for seizure onset localization is recorded while the brain is in an acute inflammatory state, and it is important to investigate the validity of inferences drawn from data collected in this period. Although impedance may lead to lower signal to noise ratios, we have shown here that seizure and burst patterns also change when studied over an extended period of time, an effect unlikely related to electrode impedance alone.

7.5.1   Seizures

We observed that seizures occur in clusters, a finding previously reported in human seizure diaries and short-term EEG monitoring. Confirmation of this finding in our rigorously

annotated data over many months further validates the relevance of naturally epileptic canines as a model of human epilepsy [60, 133]. It is interesting to note that across each dog there were relatively few clusters despite the relatively large number of seizures (Figure 54).

One interesting finding was the occurrence of multiple seizure types which were not all captured during the first two weeks of recording, a period analogous to inpatient presurgical monitoring. During this period, PHB had not yet been administered to the canines. It is important to note that many seizure clusters consisted primarily of one type of seizure, and that localizing all epileptogenic regions in these animals required recording not multiple seizures, but multiple clusters of seizures. This pattern may hold for humans as well.

Furthermore, while each seizure type included a different set of onset electrodes, there were similarities in each seizure type within individual dogs. The unequivocal electrographic change that localized the seizure onset zone alternates between a finite set of spatial locations, though in each type there were common channels. In other words, each seizure's onset channels formed an incomplete set of onset channels across all seizures. It is plausible that an underlying propagation pathway could have been kindled in these animals, and that these electrode locations are all part of a single epileptic network which can be ignited to begin from any of these locations. Thus, a patient with focal epilepsy may in fact involve multiple onset regions if enough observations are captured, suggesting that long-term monitoring to capture the full extent of a patient's network may be key to improving outcome from epilepsy surgery or implantable devices. This conclusion is supported by the work of DiLorenzo et al., who found that a group of patients who were poorly localized during acute implantation were well localized after chronic implantation of a neuromodulatory device and were seizure free following resection of their chronically localized network [31]. It is also possible that the emergence of other seizure patterns after months of chronic electrode

implantation could be due to secondary epileptogenesis, though data from King-Stephens, DiLorenzo, and significant relapse rates after resection of well localized unilateral temporal lobe seizure during acute intracranial recordings argue against this conclusion [31, 75]. The recurrence of early seizure types later in our canine recordings suggests that the initial seizure types are likely not a transient result of tissue reaction post-implantation. The variability observed in seizure types and the associated trend might be also be interpreted as a recovery phase from which a patient's true network emerges following resolution of the acute trauma, which itself or coupled to acute medication withdrawal might initiate atypical seizures [36].

Since our seizure subtyping was based on electrographic focal onset and spread, one may expect clinical semiology to vary with each type. Interestingly, each seizure's clinical semiology appeared grossly similar on continuous video recording, and no relationship between subtypes and generalization was observed. Our observations regarding shifting onset patterns may be a feature specific to canine epilepsy, but no detailed IEEG studies of human epilepsy currently exist to allow for adequate comparisons. Our group is actively trying to determine the extent of these findings to human epilepsy in an analogous human dataset.

7.5.2   Interictal Bursts

In addition we found significant variability in the dynamics of interictal bursts throughout the recording. In this study, we found that the number of bursts is significantly elevated in the weeks after implantation (Figure 57). This period of abnormal electrographic activity may represent the decline of the acute inflammatory stage and possibly stabilization through chronic inflammation and a foreign body reaction. Though this may result in increased electrode impedance and reduced voltage readings, we report also a decline in the number of interictal bursts. This is important because the former may necessitate measures to correct for impedance, but the latter suggests more cautious interpretation of traditional epilep-

tiform patterns that may be transiently distorted by electrode implantation. This effect is unlikely to be medication-driven because the decreasing trend of burst count stabilizes around day 25, before any PHB was administered.

For each dog it is clear that the dynamics of interictal bursts are in flux during the initial stages of a recording. By comparing the similarity of a burst to all future bursts, we observe that the event dynamics of the bursts begin to stabilize days to weeks post-implantation (Figure 58). Distinct groups of bursts are also seen in Figure 59 and it is plausible that they reflect the current state of an underlying seizure generating network. Observationally, the period of time where bursts are heterogeneous correspond to periods where multiple seizure types originate. For example, in the first 50 days dog 4's burst types are constantly changing, and the seizure cluster on day 45 consists of two different seizure types. In dog 7, different seizure types were observed before and after day 22. Furthermore, around day 100, many new seizure types are seen, and a break in similarity is also seen near day 100. PHB does not appear to have any effect on burst dynamics or frequency, though it did control seizures. In previous work we showed that these bursts are dynamically similar to seizure onsets. This suggests that bursts and seizures may share a similar underlying mechanism, and that the former represents seizures that fail to initiate. It is possible then that PHB preferentially inhibits seizures but not necessarily abnormal interictal patterns, a finding previously reported in children and rodents [26, 89].

The observations that seizure onset electrodes vary over an extended recording and that the initial weeks after implantation represents an unstable electrographic network may have important implications in the clinical management of human epilepsy. If present in humans, this suggests that chronic outpatient iEEG monitoring during presurgical evaluation may more accurately define the epileptic network and ultimately lead to improved seizure free-dom after surgery. In light of our findings, the reliability of potential biomarkers such as

high frequency oscillations extracted within the first several weeks after implantation must be interpreted with caution, as the variability of iEEG properties may be too great during the acute and subacute phases to use these features for clinical decision-making.

Dog 5 is an example of canine status epilepticus and provides an interesting case to analyze. The bursts before and during status epilepticus were very similar to each other, even though the first seizure occurred at day 25 (Figure 59D). It is plausible that the bursts were a result of implant injury, or otherwise coincidental during recording, and subsequently evolved into status epilepticus and resulted in death. An alternative explanation is that there was one particular region of the network that gave rise to status epilepticus, and that its particular neurophysiologic composition might have been predisposed to seizures that would not stop spontaneously. Although these observations were made in only one dog, comparison of results with the other three dogs suggests that bursts and seizures that occur during status epilepticus are different from more typical seizures and is supported by prior work in human and other animal models of status epilepticus [148]. It deserves further study to determine if there is high burst similarity in human status epilepticus and whether burst variability is mechanistically involved in seizure cessation.

7.5.3   Limitations and Future Directions

The observation that iEEG patterns do not stabilize until weeks after implantation could have significant implications for the interpretation of iEEG both in clinical and research realms. However, there are significant limitations that require further investigation and that must temper this conclusion. First, this study involves a limited number of canines, which may have different etiologies of epilepsy particularly as a result of inbreeding, though many studies demonstrate striking similarities between human and canine epilepsy such as in response rates, refractory rates to therapy, and clinical and electrographic presentations [118]. To ultimately determine both the generalizability and applicability of our conclusions,

current work in our lab is directed towards verifying and extending these findings to human long-term iEEG. Nevertheless, we believe that our findings on a novel long-term ambulatory EEG dataset will help evaluate canines as an experimental model and lend insights into the investigation of similar datasets in humans.

Phenobarbital was also administered intermittently to all dogs following the death of one animal from status epilepticus. While this likely reduced the occurrence of seizures, it did not have an effect on burst-burst similarities as indicated in Figure 59. In addition, although a large portion of time was recorded during PHB administration, this was started no earlier than 50 days post-implantation, which still allows for interpretation of the initial weeks of recording. This finding is interesting as humans undergoing presurgical evaluation are typically continued on anti-epileptic drugs, which are tapered during significant periods of iEEG recording.

Finally, the issue of whether the steady state of our recordings represents the true natural state of epileptic networks, or a state of recovery following traumatic electrode implantation, is difficult to answer. DiLorenzo's data demonstrating more accurate localization of typical seizures and seizure freedom after chronic localization suggest that the patients' long-term steady state is likely to represent their true baseline. Still, DiLorenzo's study contains only three patients. The much larger study by King-Stephens et al. is more supportive of our conjecture that our chronic recordings resolve to the patient's more natural steady state, but outcome data after some of these patients go to surgery will lend itself to useful insights into this issue. In the meantime, there is no alternative to chronically implanted electrodes for obtaining these kinds of recordings, and we believe that studying these types of chronic implants is warranted.

7.5.4   Conclusion

This study provides insight into the stability of iEEG recordings immediately after intracranial electrode implantation in canines, and there is growing evidence that the conclusions may be very relevant to human studies. The observation that seizure onset zones, interictal burst counts, and burst similarities do not stabilize until weeks after implantation of intracranial electrodes suggests that there is initial variability in iEEG recordings that may not accurately delineate an individual's epileptic network. Rather these recordings may be biased as a result of injury and inflammation from surgery. Though further work is necessary to determine generalizability of our findings to humans, they contribute to a growing literature suggesting that in at least some patients iEEG obtained during standard hospital evaluation of refractory epilepsy with intracranial EEG may not be sufficient to define the epileptic network for optimal therapy.

Chapter 8

Transient changes in Long Term ECoG

8.1 Overview

Implanting subdural and penetrating electrodes in brain causes acute trauma and inflammation, which alters intracranial electroencephalographic (iEEG) recordings. This behavior and its potential impact on clinical decision-making and algorithms for implanted devices have not been assessed in detail. In this study we characterize temporal and spatial variability in continuous, prolonged human iEEG recordings obtained from fifteen patients with drug-refractory epilepsy, each implanted with 16 subdural electrodes and continuously monitored for an average of 18 months. Time and spectral domain features were computed each day for each channel in five-minute non-overlapping windows for the duration of each patient recording's. A linear mixed model was used to characterize transient group-level changes in feature values post-implantation. A significant change in features important to seizure detection and prediction algorithms, mean line length, energy, and half-wave as well as mean power in the Berger and high gamma bands was observed in the majority of patients over 100 days following implantation. In addition there was spatial variability across electrodes post-implantation before stabilization. All selected features decreased by 14-50% in the initial 75 days of recording. Our findings demonstrate that iEEG signal features are unstable for over 2 months following implantation, most notably immediately post-implant, when patients are evaluated for surgery. These findings suggest that conclusions drawn

152

from iEEG, for research or clinical purposes, should account for this initial period of variability and that properly assessing the iEEG in patients, depending upon the region and application, may require extended monitoring.

8.2 Introduction

Intracranial electrodes are routinely used to sample and map cortical networks when patients with drug-resistant, localization-related epilepsy are evaluated for epilepsy surgery [110]. Emerging technologies of closed-loop stimulation and brain-machine interface (BMI) technologies are broadening applications for chronic intracranial electrodes to include therapeutic electrical stimulation, seizure monitoring and warning systems, responsive neurostimulation, and adaptive deep brain stimulation [23, 93, 102, 108, 159]. Each of these applications requires a thorough understanding of acute changes at the brain-electrode interface and how they affect recorded signals.

Electrode implantation causes acute trauma and an immunologic reaction that has been studied extensively [59, 141, 151, 119, 166, 116]. Greater than 50% of patients have histopathological changes from electrode implantation as soon as one day after surgery [42]. This reaction has been associated with changes in electrode impedance [12, 21, 90, 119, 160] and overall signal quality [94]. However, no studies have characterized the effect of such changes on signal features other than signal-to-noise ratios and impedance measurements. Furthermore, no analysis has been performed on long-term continuous recordings in humans, which has direct implications for algorithm design and clinical interpretation. For example, the Responsive Neurostimulator (RNS ®) System (NeuroPace; Mountain View, CA) currently requires physicians to manually tune algorithm parameters to maintain high sensitivity seizure detection over extended use [102]. Likewise, in the NeuroVista (Seattle, WA) seizure advisory system study, feature drift was observed and algorithm retraining was

necessary for months after implantation [23]. Characterizating changes in signal features (line length, area, energy, half-wave, power) used in these two devices for seizure detection would improve algorithm development, patient-specific customization, and clinical interpretation of recorded results [24, 29, 33, 38, 53, 92, 141, 159].

Similarly, short-term intracranial EEG (iEEG) is the gold standard for guiding surgical treatment of localization-related epilepsy, yet these therapies result in only 66% long-term seizure remission rates at best [145]. In an attempt to electrographically localize the seizure onset zone, iEEG recordings are obtained in an inpatient hospital setting, typically over 1-2 weeks. If reactions occurring at the brain-electrode interface affect recorded signals to the degree that extracted biomarkers become unreliable, then clinical decisions based on these features should be questioned. In addition, emergence of biomarkers such as high-frequency oscillations for surgical planning [56] adds importance to assessing time-dependent changes in spectral characteristics.

In this study, we evaluate continuous subdural iEEG recordings from 15 ambulatory human patients recorded for an average of 18 months. We aim to characterize the temporal variability of each feature as well as the spatial variability across electrodes, specifically focusing on time and spectral domain features that are of clinical and algorithmic interest.

8.3 Methods

8.3.1 Dataset

Fifteen patients with drug resistant, localization-related epilepsy were each implanted with 16 subdural platinum-iridium electrodes during a pilot trial of the NeuroVista seizure prediction device [23]. Electrodes were placed over the region containing the presumed seizure onset region as determined by standard clinical evaluation. In patients with bilateral tem-

poral lobe seizures, leads were placed over the hemisphere observed to generate the greatest number of seizures. Patient demographics and recording duration are given in Table 11. Further details about the human subjects are discussed in the original manuscript reporting this trial [23].

Table 11: Subject demographics at baseline and recording duration

Subject	Age	Sex	Diagnosis age	Duration (Days)	AEDs	Epileptigenic Zone
1 (23_002)	26	M	4	767.4	CLZ, LEV, LTG, VPA	PT
2 (23_003)	44	M	12	730.1	LCM, LTG, OXC , VPA	OP
3 (23_004)	22	F	16	557.5	CBZ, LTG, PHT	PT
4 (23_005)	61	M	48	233	CBZ, LCM, LTG, TPM, PHT	PT
5 (23_006)	20	F	1	272.9	CLZ , LTG, OXC, TPM	FT
6 (23_007)	62	M	37	441.3	None	T
7 (24_001)	52	M	26	184.9	CBZ, CLZ, LEV	FT
8 (24_002)	48	M	20	558.4	CBZ, LEV	FT
9 (24_004)	51	F	10	394.9	CBZ	OP
10 (24_005)	50	F	15	373.2	LEV, OXC, ZNS	FT
11 (25_001)	53	F	15	721.6	LCM, PHT, PRP	FT
12 (25_002)	43	M	20	729	LTG, LCM, PHT, RTG	T
13 (25_003)	50	M	20	746.9	CBZ, CLZ, LEV, LCM	T
14 (25_004)	49	F	4	627	CLZ, OXC	PT
15 (25_005)	36	M	5	465.6	CBZ, LCM, PRP, TPM	T

PT = Parietal-Temporal, OP = Occipital-parietal, FT = Frontal-temporal,T = Temporal
CLZ = clonazepam, LEV = levetiracetam, LTG = lamotrigine, VPA = Valproate, OXC = oxcarbazepine , CBZ = carbamazepine, PHT = phenytoin, LCM = lacosamide, TPM = topiramate, ZNS = zonisamide, PRP = perampanel

8.3.2   Recording device

The NeuroVista device consists of four electrode arrays each with four platinum-iridium contacts implanted subdurally on the cortical surface. The electrodes were connected to a hermetically sealed subclavicular implantable telemetry unit that sampled 16 channels each at 400 Hz. The telemetry unit was inductively recharged and collected data, which was wirelessly transmitted to an external belt-worn computing and warning device. Technical difficulties and patient-related factors (e.g. telemetry dropouts, flat batteries) occasionally interrupted data acquisition throughout the trial, resulting in occasional data gaps. The data were converted to the Multiscale Electrophysiology Format (MEF) [16], ported to ieeg.org, and accessed in Matlab using the IEEG-Portal toolbox for data analysis.

8.3.3   Feature Extraction

Each channel was initially low-pass filtered at 180 Hz with a third order Butterworth filter. Four time-domain features (line length [38], area [141], energy, and half-wave amplitude [54]) as well as average spectral power in delta [0.1-4 hz], theta [4-8], alpha [8-12], beta [12-30], gamma [30-100], and high-gamma [100-180] bands were computed. These features were selected to represent those commonly used in algorithms to detect epileptiform activity as well as common, interpretable spectral bands. Line length is the absolute derivative of signal amplitude, described by Esteller et al [38]. Area is defined as the absolute amplitude [33, 92]. The energy of a signal is calculated as the squared voltage amplitude. The half wave feature represents the amplitude and duration of a signal after segmented based on local minima and maxima [53, 142]. From the segmentation, the amplitude and duration can be extracted and reflects energy at various frequencies depending on tunable parameters. Here, the average amplitude is calculated. Spectral power was calculated using Welch's power spectral density estimate. Specific details of feature calculations are provided in the

appendix.

The mean value of each feature within each 5-minute window was subsequently averaged across 24-hour segments to reduce data dimensionality and account for changes due to circadian rhythm.

8.3.4   Preprocessing

Artifacts, which were relatively rare, were identified for the majority of patients through visualization of extracted features. Outliers were manually identified based on large spikes or large drops in each feature space and, if verified to arise from artifacts on raw EEG, were removed from corresponding channels across all features. Large increases in feature values were often correlated with short periods of line noise harmonics or transient epileptiform activity (seizures), particularly if these periods occurred in windows overlapping with data gaps as they would not be averaged out. Large decreases correlated most often with multiple electrode drop offs. In total, 396 out of 6565 days, or 6.1% of available days, were removed. Examples of artifact are shown in Figure 60.
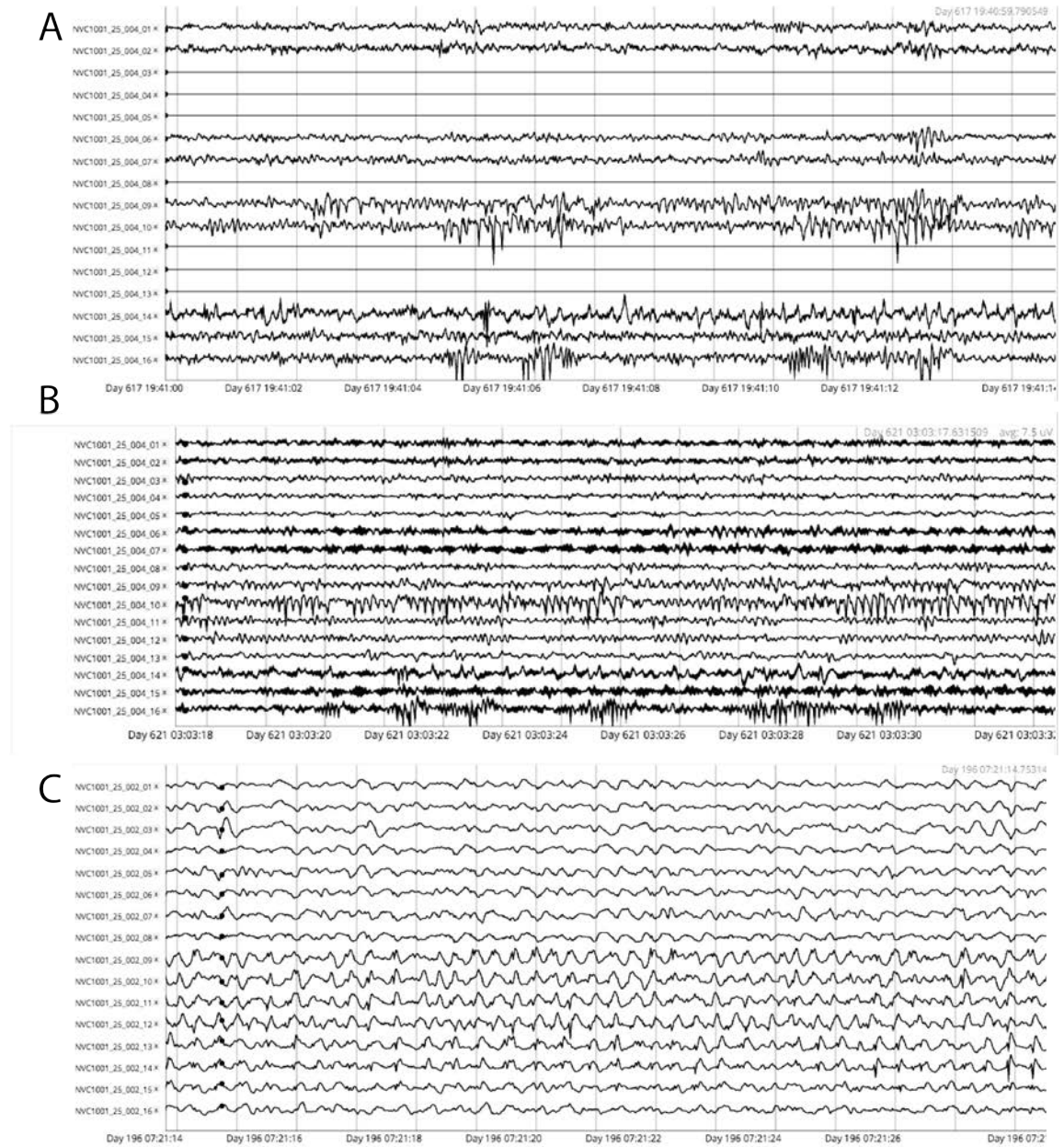
Figure 60: Examples of removed artifacts. Artifacts were identified based on features and subsequently verified on raw data. (A) Electrode dropouts in several channels resulting in abrupt decreases in feature values (B) High frequency noise, possibly a harmonic of line noise and (C) high frequency seizure activity causing sudden increases in feature values. Seizure activity in general was not artifactual when averaged over a given day, however, days with signal dropout artificially inflated feature values due to seizures and were removed.

8.3.5 Statistical Analysis

Statistical analyses were performed in R. For each subject and for each day, the mean and coefficient of variation (standard deviation/mean) across channels were calculated on each day. The coefficient of variation captured spatial variability normalized by the mean feature value. Before averaging across subjects for a group level analysis, feature values for each channel and coefficients of variation for each subject were independently normalized to [0-1] based on 95% of the values. Normalization enabled different channels and subjects to be combined into a group level analysis and allows us to focus on time dependent changes. Individuals were also analyzed independently to understand variability in mean feature values.

Individual statistics   Changes in feature values were observed to follow a linear trend before stabilizing. To determine the average rate of change in feature values, independent linear models were fit on the first 75 days post-implantation for each feature, for each subject with time in days as the covariate. The significant main effects of time are reported after adjusting for false discovery rate (FDR) of 0.05 (Benjamini-Hochberg). These main effects (betas) represent the rate of decay (or growth) of a feature over time and whether this rate is statistically different than 0 (indicating stability).

Group statistics   To determine times where mean feature values and coefficients of variation differed from a stable period, a null normal distribution was obtained from the mean and standard deviation of values from day 200 to day 500. As subjects dropped out due to variable recording durations, these times were selected to include at minimum the majority of subjects (8/15). Means corresponding to a critical value of a one-sided Z test with significance of $p=0.05$ ($z=1.645$) were selected as the threshold. Values greater than this threshold were significantly different than the distribution of values expected for a particular feature.

To model the group level change in feature values in the initial 75 days post-implantation, a linear mixed model (equation 8.1) was used with day as a covariate and feature value averaged over channels as a response variable. Linear mixed models allow modeling of patient specific trends and are also robust to missing at random data. Separate models were fit for each feature and group level fixed effects (β_1) and intercepts (β_0) are reported. As the feature value on day 1 and the rate of change across days 1-75 may vary with each subject, a random intercept (b_{0i}) and slope ($b_1 i$) was used. The Wald t-statistic was used to determine the significance of any trend across time.

$$Y_{ij} = \beta_0 + \beta_1 t_{ij} + b_{0i} + b_{1i} t_{ij} + \epsilon ij \tag{8.1}$$

where $b_{oi} \sim \mathcal{N}(0, \tau^2), b_{1i} \sim \mathcal{N}(0, \tau_{1i}^2), Y_{ij}$ denotes the feature value, t_{ij} indexes the day after implantation, b_{oi} and b_{1i} are random intercepts and slopes for each patient, for subject i and time j.

8.4 Results

8.4.1 Temporal stability

The day after implantation that each feature enters a steady state distribution is given in Table **??**. Time domain features show a prominent transient response in the first 100 days after implantation (Figure 61). Specifically, line length, capturing both voltage and frequency fluctuations, half-wave amplitude, and energy are increased at implantation, enter the steady state bound from day 27-48 and steadily decrease 36-42% until approximately day 75, where they stabilize (Table 13). Area follows the same initial decreasing trend, but fluctuates throughout the recording window and thus falls within our defined stable distribution.

Table 12: Days to stabilization

	Days to Stabilization	
Feature	**Temporal**	**Spatial**
Line Length	37.3	52.1
Area	*	*
Half-wave	8.9	37.5
Energy	21.6	*
Delta	17	52.5
Theta	23.5	41.6
Alpha	20.8	38.7
Beta	26.6	40.9
Gamma	42.9	*
High Gamma	42.4	*

For each feature, the time to stabilization is calculated as the first day when the mean value across subjects enters a stable range. This range is determined by the critical value of 1.645 (one sided Z-test) calculated from the null distribution across days 200 to 500. *within stable distribution at implantation

Table 13: Linear mixed model estimates

Feature	(/Day)	SE	t(812)	Adj. P		% Change from Day 1-75
Line Length	0.332	0.076	-4.346	<0.001	0.68	36.6
Area	0.118	0.075	-1.574	0.116	0.605	14.7
HW	0.307	0.072	-4.28	<0.001	0.615	37.4
Energy	0.34	0.075	-4.542	<0.001	0.599	42.6
Delta	0.434	0.094	-4.636	<0.001	0.634	51.3
Theta	0.43	0.102	-4.2	<0.001	0.651	49.6
Alpha	0.318	0.06	-5.255	<0.001	0.61	39.1
Beta	0.295	0.063	-4.7	<0.001	0.615	35.9
Gamma	0.35	0.082	-4.276	<0.001	0.668	39.2
High Gamma	0.232	0.092	-2.522	0.0119	0.615	28.3

The fixed effect of time is shown for each feature. P values are adjusted for FDR at 0.05. The estimated total percent change from Day 1 to Day 75 is calculated by as $\beta_0 - (\beta_2 * 75)$
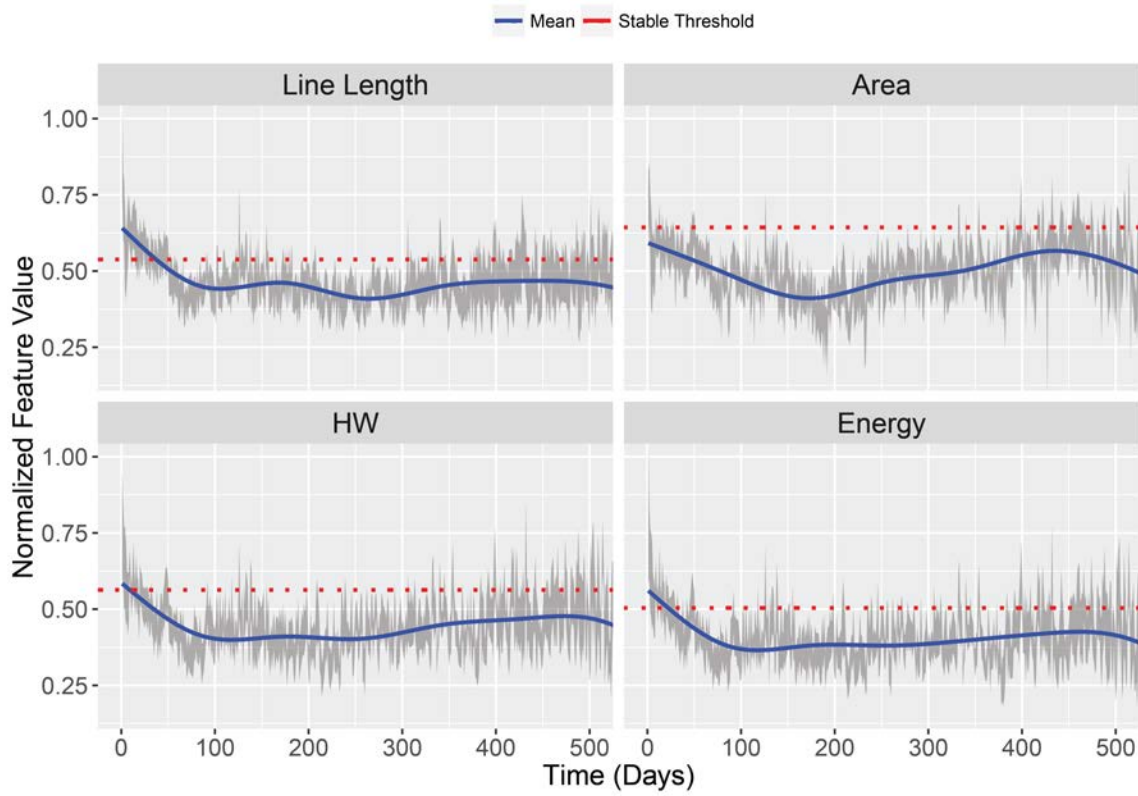
Figure 61: Time domain feature trends. Line length, area, half-wave, and energy are shown. The vertical axis represents a within-channel normalization to [0 1] based on 95% of each channel's values. For each feature, the smoothed mean (blue) and standard deviation (gray) across subjects are shown. The red dashed line indicates the feature value that corresponds to significance at p=0.05 (z=1.645) of a one-sided z test, with the null distribution generated from day 200 to 500.

All spectral bands show an initial period of decline that stabilizes by 100 days (Figure 62).

The decline in power was 40% on average from day 1 to day 75 (Table 13).
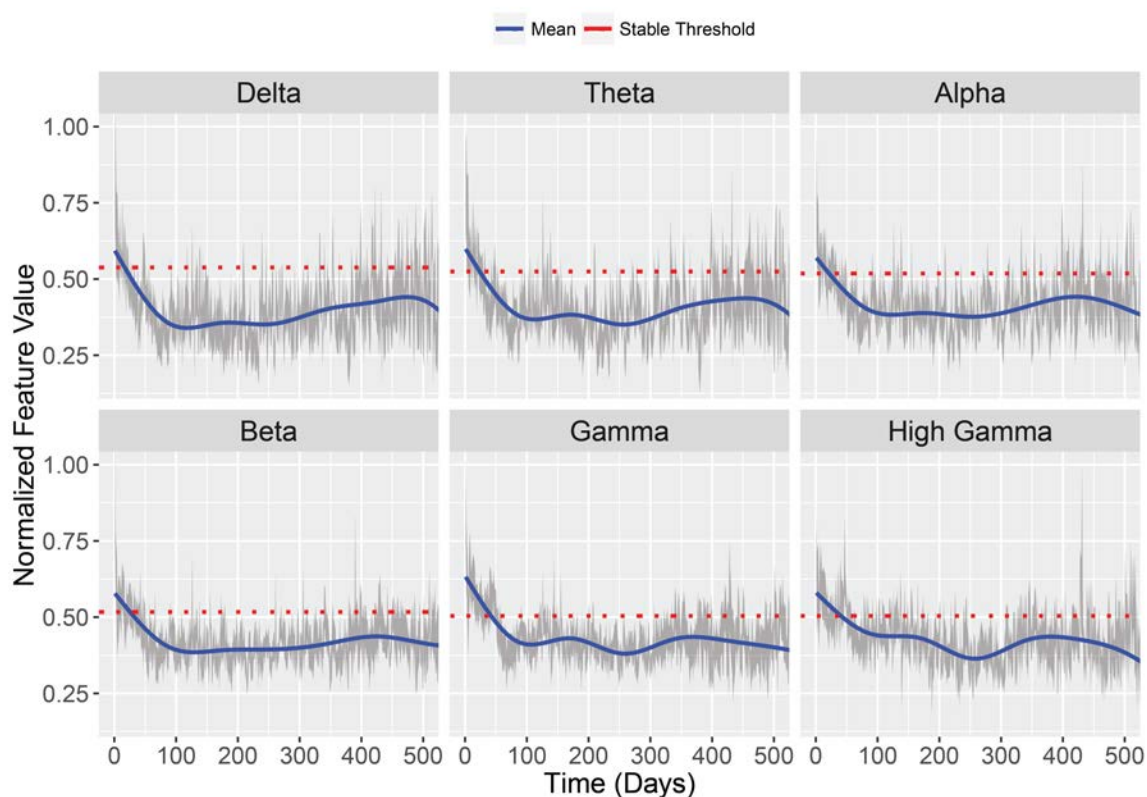
Figure 62: Spectral domain feature trends. Average power in delta (0-4 hz), theta (4-8), alpha (8-12), beta (12-30), gamma (30-100), and high-gamma (100-180) frequencies are shown. The vertical axis represents a within-channel normalization to [0 1] based on 95% of each channel's values. For each feature, the smoothed mean (blue) and standard deviation (gray) across subjects are shown. The red dashed line indicates the feature value that corresponds to significance at p=0.05 (z=1.645) of a one-sided z test, with the null distribution generated from day 200 to 500.

8.4.2   Spatial variability

The coefficient of variation for line length and half-wave declined in the first 100 days, whereas the coefficients of variation for area and energy fluctuated within a stable boundary (Figure 63). The coefficient of variation for spectral power in the delta, theta, alpha, and beta bands also declined in the initial stages of recording. Increasing frequency bands were

inversely related to the magnitude of post-implantation effect (Figure 64). These findings indicate that spatial variability of lower frequency power bands across channels decreases over time, entering our defined stable distribution between 37-52 days after implantation.
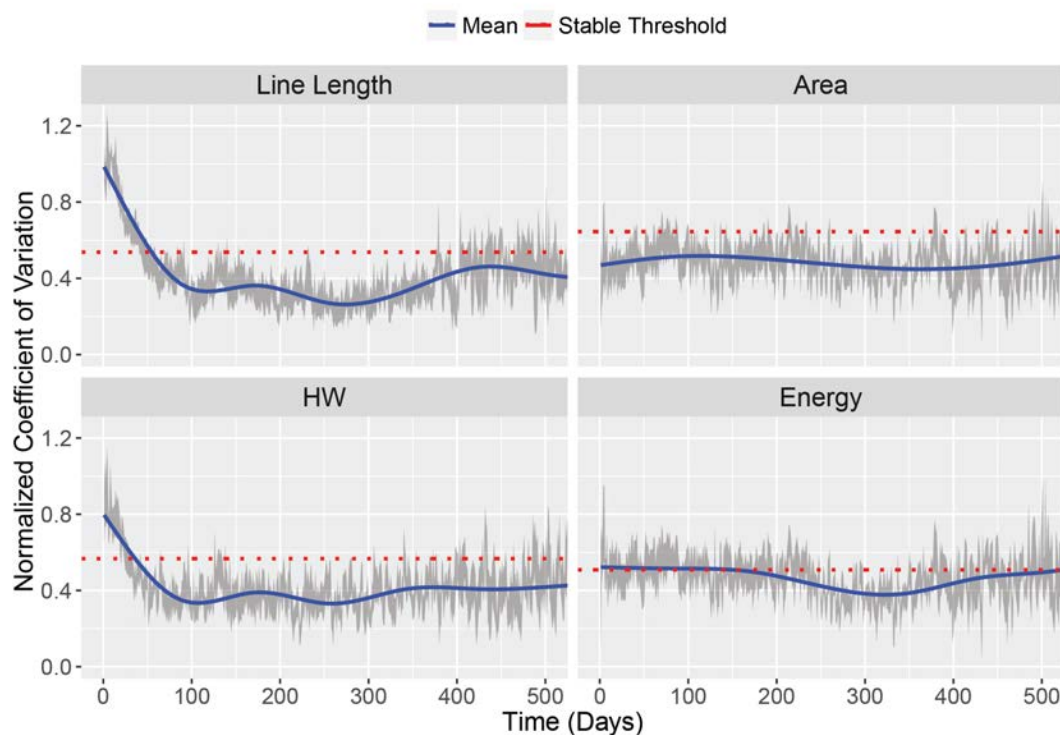

Figure 63: Spatial variation - Time features. The mean coefficient of variation is shown for each time domain feature. This is calculated on a subject level as the ratio of the standard deviation across channels to the mean. The smoothed mean (blue) and the standard deviation (gray) of the coefficient of variation across subjects are shown. The red line indicates the feature value that corresponds to significance at $p = 0.05 (z = 1.96)$, with the null distribution generated from day 200 to 500.
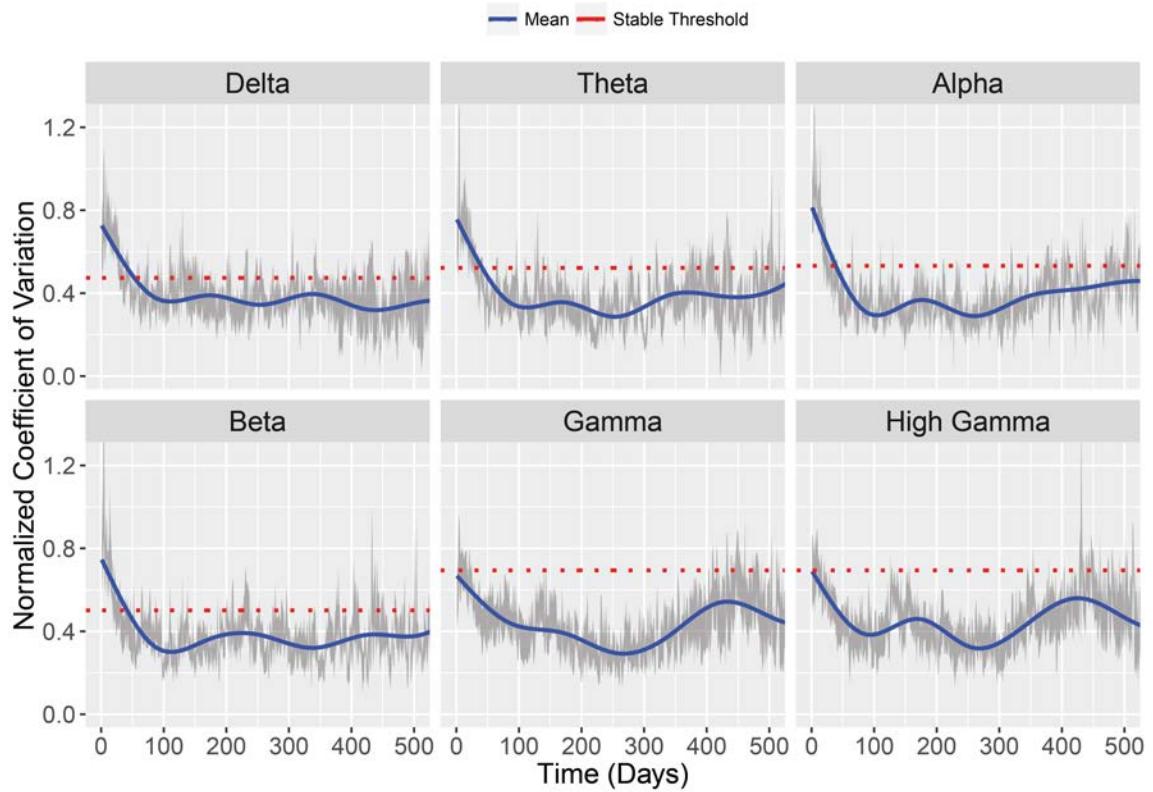
Figure 64: Spatial variation spectral features. The mean coefficient of variation is shown for each feature. This is calculated on a subject level as the ratio of the standard deviation across channels to the mean. The smoothed mean (blue) and the standard deviation (gray) of the coefficient of variation across subjects are shown. The red dashed line indicates the feature value that corresponds to significance at p=0.05 (z=1.645) of a one-sided z test, with the null distribution generated from day 200 to 500.

Table 14: Pearson Correlation between all features

	LL	Area	HW	Energy	Delta	Theta	Alpha	Beta	Gamma
Area	0.41								
HW	0.54	0.67							
Energy	0.56	0.73	0.90						
Delta	0.41	0.67	0.86	0.86					
Theta	0.56	0.64	0.85	0.83	0.80				
Alpha	0.64	0.54	0.74	0.71	0.60	0.81			
Beta	0.82	0.41	0.52	0.52	0.36	0.55	0.74		
Gamma	0.79	0.32	0.36	0.38	0.28	0.35	0.42	0.64	
High Gamma	0.41	0.21	0.21	0.22	0.20	0.22	0.22	0.27	0.58

8.4.3 Individual Fits

Beta estimates for each patient and each feature are shown in Figure 65. Of the 135 patient-feature combinations, 83 displayed a statistically significant linear trend after False Discovery Rate correction, 79 of which declined in the initial 75 days. Fourteen of the 15 subjects had significantly decreasing values in at least one feature. Subject 3 and 5's recordings were more stable in the spectral domain, resulting in insignificant beta estimates across all power bands.
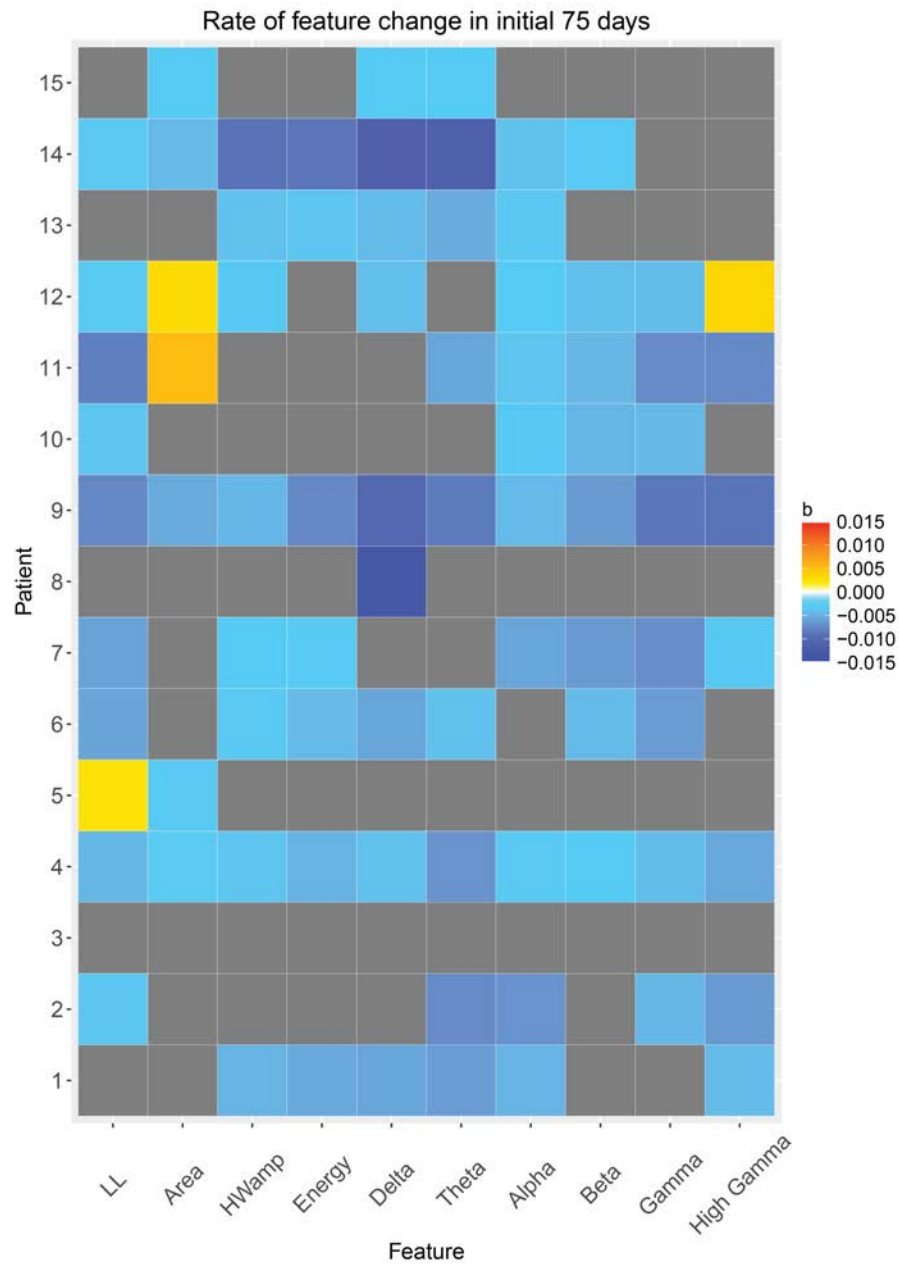
Figure 65: Individual variability. The beta estimates from a linear model was fit for each patient for each feature from day 1 to day 75. Color scale indicates beta values (% change/day), with red indicating an increase in feature values and blue indicating a decrease. Grey indicates betas that were not significant after FDR correction. LL = line length.
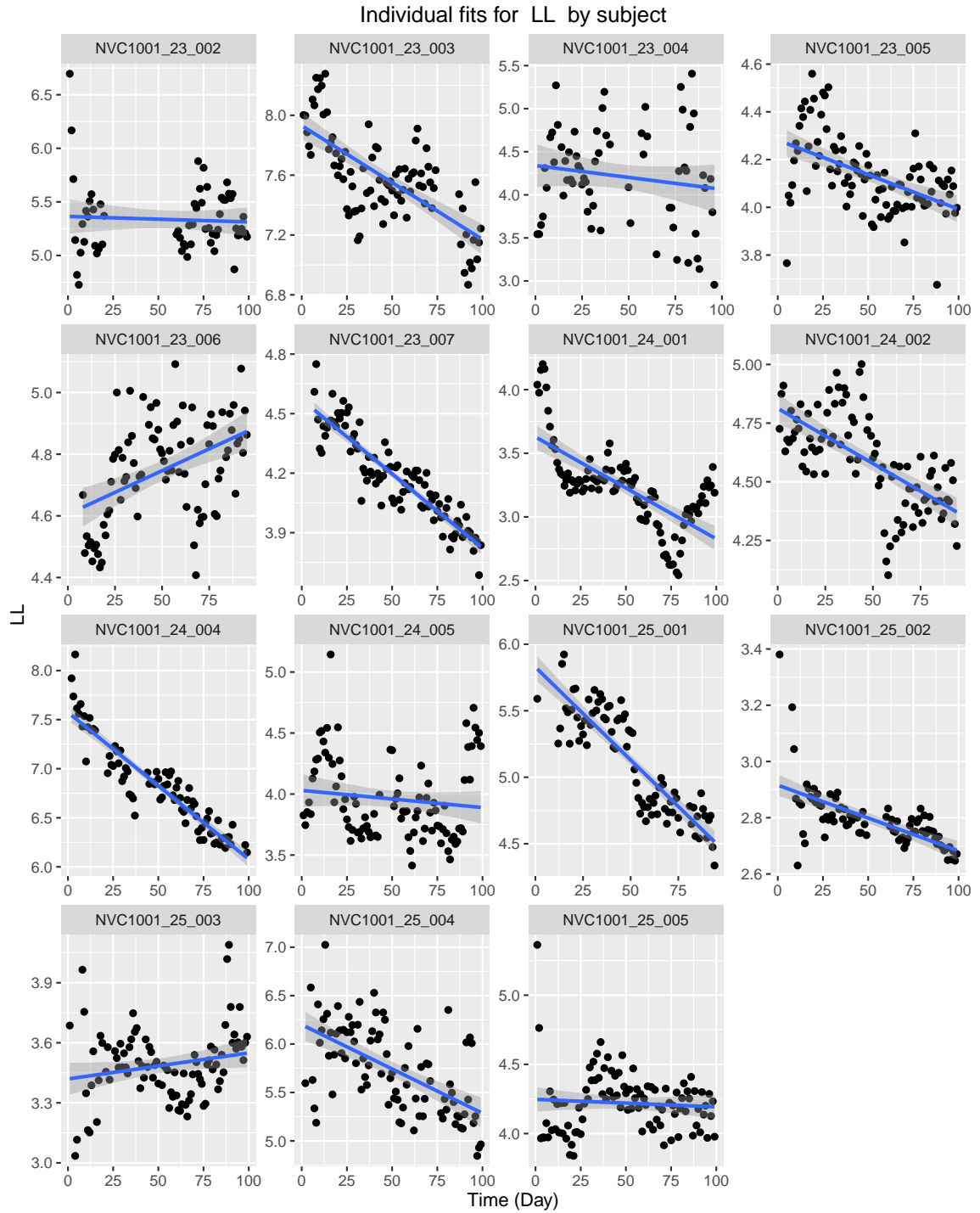
Figure 66: Individual plots of line length for the first 100 days. Each subject is included in a subplot, and each point represents the averaged feature value for the given day. A best smooth linear regression is shown. Additional plots are provided in A
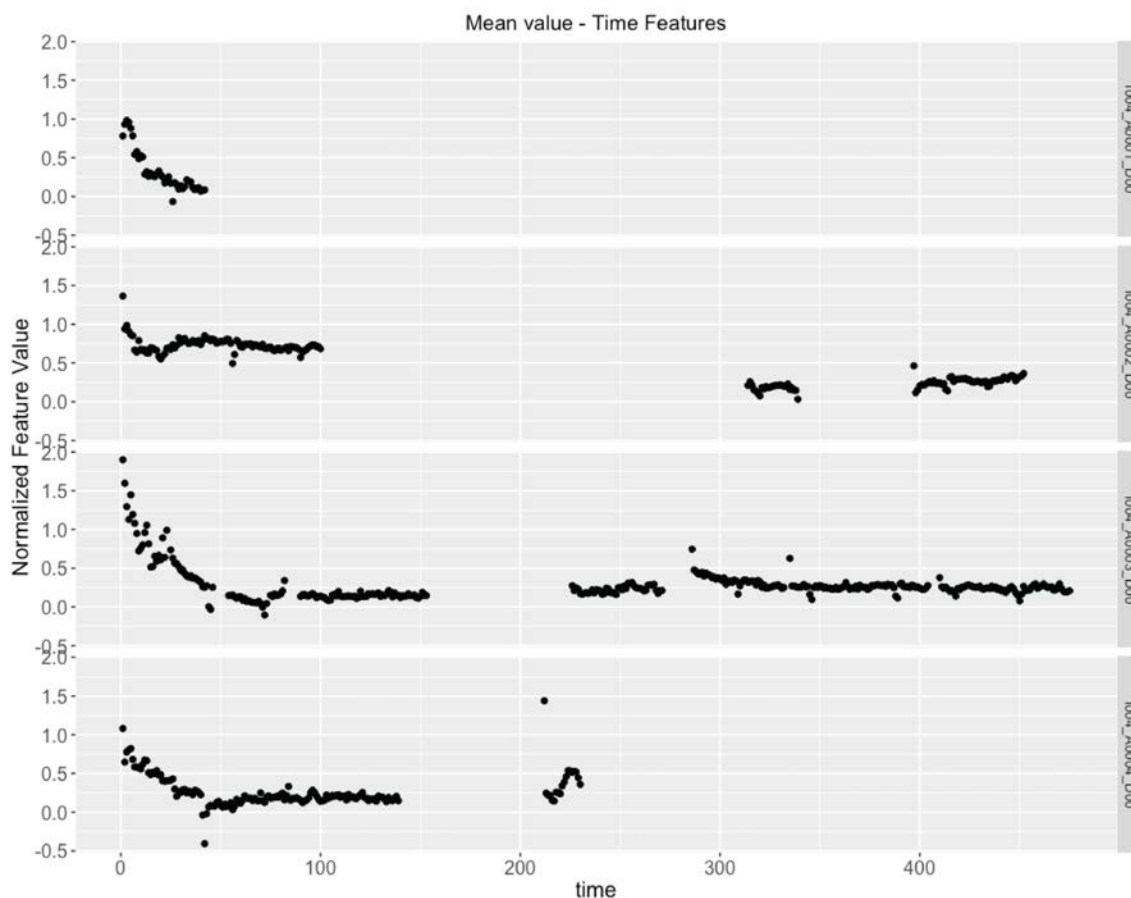
Figure 67: Individual trends for each dog across days. Normalized line length is shown

8.5 Discussion

In this study we analyze continuous long-term ambulatory recordings from subdural iEEG electrodes implanted in humans and characterize the temporal and spatial variability of time and spectral domain features frequently used in research and device algorithms. This study is unique, as it explores the only known dataset of long-term continuously recorded human iEEG spanning an average of 1.5 years, as opposed to episodic, brief recordings lasting up to a few weeks. Our findings may directly impact the clinical management of human

patients, since the selected features represent those used in current implantable devices. We show that in the majority of features, there is an initial temporal decline in the mean values that plateaus roughly 100 days after implantation (Figure 61, 62). This trend in feature values is consistent in 13/15 patients. Furthermore, for line length, half-wave, and a number of spectral bands (delta to beta), there is increased spatial variability between channels that stabilizes in a similar time frame. These observations demonstrate an initial period of spatial and temporal variability in iEEG recordings that requires several months to stabilize.

8.5.1   Temporal variability

Both mean line length and mean energy significantly decrease from day zero to day 21-37 (Table 13) and reach a plateau by day 100 (Figure 61). Since line length captures features of both frequency and voltage, there is an expected correlation between this feature and energy that is reflected in similar temporal trends. Half-wave amplitude, also an indirect measure of power, follows a similar trend. Area, however, fluctuates throughout the long-term recording and does not stabilize in the same manner as the other features. For the spectral domain features, each band is initially elevated before reaching a stable range 17-43 days after implantation, with a plateau by 100 days (Figure 62). As expected, there is a strong correlation between line length and power (e.g. Pearson $r = 0.82$ between beta power and line length), which, coupled with the dissimilarity in trends with area, suggests that line length in practice is more sensitive to recording changes in frequency than voltage amplitude.

These findings immediately demonstrate the temporal variability present in time and frequency domain features following implantation. Line length and half-wave, two features used in the NeuroPace [141] and NeuroVista [23] algorithms, exhibit high temporal instability, decreasing by over 30% in the first 75 days. Using these features for seizure detection

or prediction may lead to decreased sensitivity over time as feature values trend down. Furthermore, power features decrease dramatically by over 40% on average (Table 13). This drift must be accounted for in chronic neurodevices, either by directly modeling the change or waiting until after day 75 before optimizing algorithms. Additionally, changes in RNS detections observed in the first few months after a chronic implant should be interpreted with caution, so as not to falsely attribute perceived clinical response to early changes in stimulation parameters.

It is interesting to note that the canines' feature values all follow a similar trend as the humans, however, there is a much steeper decline in the mean values (Figure 67). This suggests that the tissue reaction occurs at a faster timescale, potentially a reflection of differences in immune reactivity or experimental procedure variability between humans and canines. These findings imply that there are species specific changes that also need to be taken into account (discussed further below).

8.5.2   Spatial variability

It is also important to capture the variability among electrodes to inform algorithms that utilize spatial features (measurements among channels). If the processes causing post-implantation changes affect all electrodes equally, the mean may decrease while the coefficient of variation, which is normalized by the mean, would remain stable. However, we observed that the spatial variation of line length, half-wave, and spectral power decreases over time (Figures 63, 64) and, similar to temporal variability, this effect is more significant in the lower frequencies. Notably, while the spatial variation enters the defined stable distribution later than the temporal variation, suggesting a different rate of decline, the coefficients of variation form plateaus roughly the same time (day 100) as their corresponding mean feature values. A decrease in the coefficient of variation suggests that the processes responsible for the trend in mean feature values affect each electrode differently, and the

magnitude of this difference decreases over time. As a result, we can expect any spatial measures of iEEG to be unstable in the initial periods after an implant.While we did not find an obvious association between electrode location in the brain, hospital of insertion (patients were implanted at 3 different hospitals at the University of Melbourne [23]), or specific operative technique to account for spatial variability, these were not investigated in detail and patient numbers were too small to adequate test these hypothesis.

8.5.3   Previous studies

Histological changes at the brain-electrode interface likely explain our observed feature variability following implantation, since both follow a similar time course. These interactions have been studied extensively in electrodes implanted into animals and human [94, 116, 141, 151] and involve an acute inflammatory response followed by chronic fibrosis that significantly diminishes by 6-8 weeks [128, 140, 141, 158]. Notably, many of these past studies analyzed the impact of intracortical electrodes, which penetrate the cortical surface and have an increased burden on the brain. Several studies in non-human primates and rats with subdural electrodes have shown minimal damage to the cortex but fibrous tissue encapsulation over time [30, 61, 125] that subsequently lead to greater changes in electrode impedance relative to intracortical electrodes [74, 134, 160]. Since electrode impedance directly impacts our calculated features, we relate our observations to previously reported changes in electrode impedance in studies of subdural iEEG. Specifically, subdural electrodes implanted in rats have shown an increase in impedance in the first 30 days after implantation that stabilizes after week 18 [61]. On histology, fibrous tissue encapsulation was observed surrounding the electrodes. Interestingly, a recent study in non-human primates recorded for over 600 days reported root-mean-square (RMS) voltage stability at 300 days, which is much later than the stability we observe in signal features [30] and possibly suggests different timescales between non-human primates and humans. This difference

might be related to differences in immune response in these animals, sterile conditions of the implants or perhaps mechanical or material factors. In humans, Sillay et al. recently showed that impedance in the NeuroPace RNS®subdural electrodes increases an estimated 30% from day 1 to day 84 after implantation and stabilizes by four months [134]. This is similar to the magnitude of change that we observed in our time and spectral features from day 0 to day 75 (Table 13), suggesting that our observed changes are similar to previously described changes in impedance. However, it should be noted that the RNS impedance recordings were collected intermittently with limited temporal resolution, whereas our recordings were continuous. Notably, while we observe high degree of similarity between the time courses of each of the power bands, the decrease in power was greatest in lower frequencies. These changes could be motivated by an increase in both the resistive and capacitive impedance due to tissue encapsulation, as previously reported in microelectrodes [124].

8.5.4   Clinical Implications

Our study is the first of its kind to extend these observations of RMS and impedance to signal features in continuous recordings, a next step towards translating these findings into clinically meaningful attributes. Variability in signal properties has ramifications for emerging closed loop systems for the treatment of drug-resistant epilepsy [102] with important implications for device development and clinical trial design. These systems must be cognizant of post-implant variability, suggesting a need for strategies to either algorithmically control for this instability or focus optimization only following stabilization. As an example, current common practice using the NeuroPace device includes a postoperative waiting period to capture seizures for algorithm training. Detection parameters optimized before stabilization may result in poor early performance.

Figure 65 shows that there is significant variability in the response of certain patients, with some subjects (3 and 5) displaying more stable features following implantation. These sub-

jects are relatively younger individuals who may have a more robust wound healing response [52], though we do not have enough data to draw any definitive conclusions. Additional insights may be found as chronic invasive recording becomes more widely available, though in our cohort, 99.5% of statistically significant feature trends decreased over time.

It is also important to determine the impact of these changes on clinical biomarkers that are used in the care of the drug resistant epilepsy population. Acute implantation can induce interictal epileptiform activity and seizures that do not accurately represent the patient's underlying disorder [7, 43]. This may be a result of direct effects, such as of trauma, electrode contact with the cortical tissue, or complications of electrode placement such as hemorrhage, fluid collections or cerebral edema [7]. Seizure onset localization relies on identifying subtle electrographic changes that are spatially distinct, so any changes in spatial variability may interfere with the localization procedure. Of interest, there is evidence that patients who appear to have multifocal onset seizures immediately after electrode implantation during standard clinical evaluation localize to one predominant area in the chronic steady state, eventually resulting in seizure-free outcome after surgery [31]. This provides at least circumstantial evidence that the chronic steady state may better reflect a patient's baseline than alterations of the network from implantation. In this dataset, clinical seizure semiology typically did not change in the chronic state from pre-implantation in most of our patients, giving some reassurance that these effects are limited in scope. However, it has been demonstrated in that seizures can have similar clinical appearance while arising from different parts of an epileptic networks, sometimes with different EEG signatures. A recent study by our group shows this phenomenon in a long-term canine model [149]. Classifying seizures and mapping their temporal trends is an ongoing project in our laboratory.

An interesting question to consider from our findings is whether the steady state observed

after stabilization of chronic intracranial recordings represents ground truth. This question is particularly important when considering epilepsy biomarkers, such as interictal epileptiform discharges and seizures, and interpreting what their temporal and spatial distributions mean with respect to the fundamental mechanisms underlying epileptic networks. Like the Heisenberg Uncertainty Principle, unfortunately, it is clear that our measurements of the iEEG, for which there is not currently a noninvasive alternative, perturb the system and may induce chronic change. At present, iEEG studies provide the best way of assessing an epileptic network's broad band activity on a clinical scale, even taking this limitation into consideration. It will be important in future studies from this unique data archive, to determine if localization of seizures and interictal epileptiform discharges change similarly over the first 100 days, which may have more important consequences for current epilepsy surgery and ablative therapies. Should spatial localizations change, as the paper by DiLorenzo et al suggests, either due to brain disruption or merely inadequate temporal sampling, this may require a paradigm shift in the duration of monitoring required to localize epileptic networks for intervention. This might require that we monitor patients in the ambulatory setting for months, rather than weeks in the hospital.

8.5.5 Conclusion

We have shown that human subdural recordings exhibit a temporal and spatial post-implantation response that requires 100 days for complete stabilization. These findings directly explain observed trends in human neurodevice implants and show that systems that use or interpret subdural electrode recordings must account for these changes for optimal performance. Implications for clinical care will require further evaluation of chronic iEEG recordings to see if seizure localization is affected by acute electrode implantation.

Chapter 9

Conclusions

Epilepsy is a chronic disorder that provides a wealth of EEG data that enables many opportunities for scientific discovery. This amount of data requires automated data mining, machine learning, and robust statistical analyses to draw meaningful conclusions about the underlying electrophysiological network. In this thesis, we've introduced an interactive framework for detecting and characterizing transient interictal patterns. Though this thesis focuses on spikes and bursts, the general framework can be applied to detect any marked pattern, with informative features easily added. We have applied this pipeline to animal and human datasets and studied their interaction in health and disease.

In Chapter 3, we showed that interictal spikes, the significance of which was unclear, are indeed not benign and impedes in human cognition in a spatially specific manner. This was made possible through an automated spike detection algorithm that mined 67 human ECoG patients to determine the effect of spikes on word recall. Interestingly, the effect of spikes was not seen in the seizure onset zone, which suggests potential utility in spike-aided identification of dysfunctional tissue.

Chapter 4 examined a rat model of epileptogenesis, and found that a subset of bursts may predict epileptogenesis post-TBI. This finding suggests that epileptiform bursts may be precursors to seizures, though experiments with continuous recordings and simultaneous video and electromyography are required for future improvements.

In a canine model, we showed in Chapters 5, 6, and 7 that bursts are similar to seizure onsets and display dynamics similar to the observed seizures. These findings suggest that bursts may represent seizures that fail to manifest. In addition, there is evidence that these bursts may localize to the seizure onset zone, though more work is necessary in humans with better-defined seizure onset zones. Finally, we also show that burst dynamics fluctuate over time in a manner that mimics seizures, suggesting that long-term recordings may be necessary to provide a more complete picture of a patient's epilepsy.

This was investigated further in Chapter 8, which focused on the analysis of year-long continuous human iEEG. We showed that long-term recordings require several months for stabilization. These were represented in features currently used in clinical devices and explain the anecdotal instability in the development of neurodevice algorithms. Our findings have significant implications for any scenario that incorporates invasive recordings, from brain machine interfaces to clinical invasive monitoring for seizure localization.

We believe automated analysis of EEG is necessary to answer important questions about brain electrophysiology. However, there are several steps that are imperative to achieving this aim. Gold standard annotated data are necessary to improve the generalizability of algorithms that we've developed. These data and algorithms should be publicly shared to expedite research progress and translation into clinical utility. In the meantime, our framework allows for an interactive pattern detection paradigm by which users can train and test their own models quickly, with annotations uploaded to a publicly accessible database. The hope is that patterns in this thesis as well as other patterns can be incorporated into robust biomarker detection scheme. Though we are still far from the ease of automatic EEG reading as predicted nearly half a century ago, we hope our efforts will help pave the way.

9.1   Future Directions

1. Technical Framework - The technical framework developed in this thesis will be packaged and made available for public use. In conjunction with an open, shared platform such as the IEEG.org portal, we can begin to develop a set of standardized EEG records with validated tools to analyze them, which will pave the way for more generalizable biomarker detection algorithms. This is much needed in the field of epilepsy, where no standardized datasets or algorithms currently exist.

2. Biomarkers of epileptogenesis - The work involving post-traumatic epilepsy is very promising but requires additional experiments to be performed for validation. Now that we've developed the technical pipeline for automated analysis, continuous rat datasets collected toward electrographic biomarker discovery can be quickly analyzed. Ideally, this recordings will also have simultaneous video and/or EMG to also learn about the origins of these patterns, which has not yet been well described in the field.

3. Cognitive spikes - In this particular project, we've shown that spikes affect cognition. However, the effect is relatively small, and it is unknown how spikes affect cognition outside of a short-term memory task. Improving the spike detections and more rigorously investigating associations with clinically important variables such as surgical resection volume may improve the clinical applicability of spikes.

4. Bursts and seizures in Human EEG - We have detected and characterized bursts in a canine model, showing that bursts as well as seizure onset changes over time. It is imperative to continue this work in humans in order to more directly guide clinical assessment of bursts and seizures in the context of long term iEEG. This work has the potential to introduce long term ambulatory monitoring as an alternative therapy for a sub-population of patients.

5. Seizure Prediction - Our long-term human iEEG dataset with clinically annotated seizures is the only dataset of its kind that will allow for assessment of seizure prediction. Previous datasets consisted of short term recordings aggregated over multiple patients, reducing the generalizability and validity of previously published algorithms. In this particular case, we have enough seizures to train a patient-specific algorithm to determine the predictability of seizures in a use-case scenario.

APPENDIX

A.1 Common time domain features

Line length: $\frac{1}{N}(\sum_{i=1}^{n-1}(|x_{i+1} - x_i|))$

Area: $\frac{1}{N}(\sum_{i=1}^{N-1}(|x[i]|))$

Energy: $\frac{1}{N}(\sum_{i=1}^{N-1}(x[i]^2))$

Halfwave: The halfwave procedure decomposes a given signal into defined half waves. These halfwaves are found by segmentation of signal based on local minima. Applied a duration threshold of half wave as well as an amplitude threshold essentially calculates power above/below a certain frequency. The duration threshold applied in this experiment was 10 samples (with a sample rate of 400) and average amplitude is reported.

A.2 Individual plots of feature values from Chapter 8
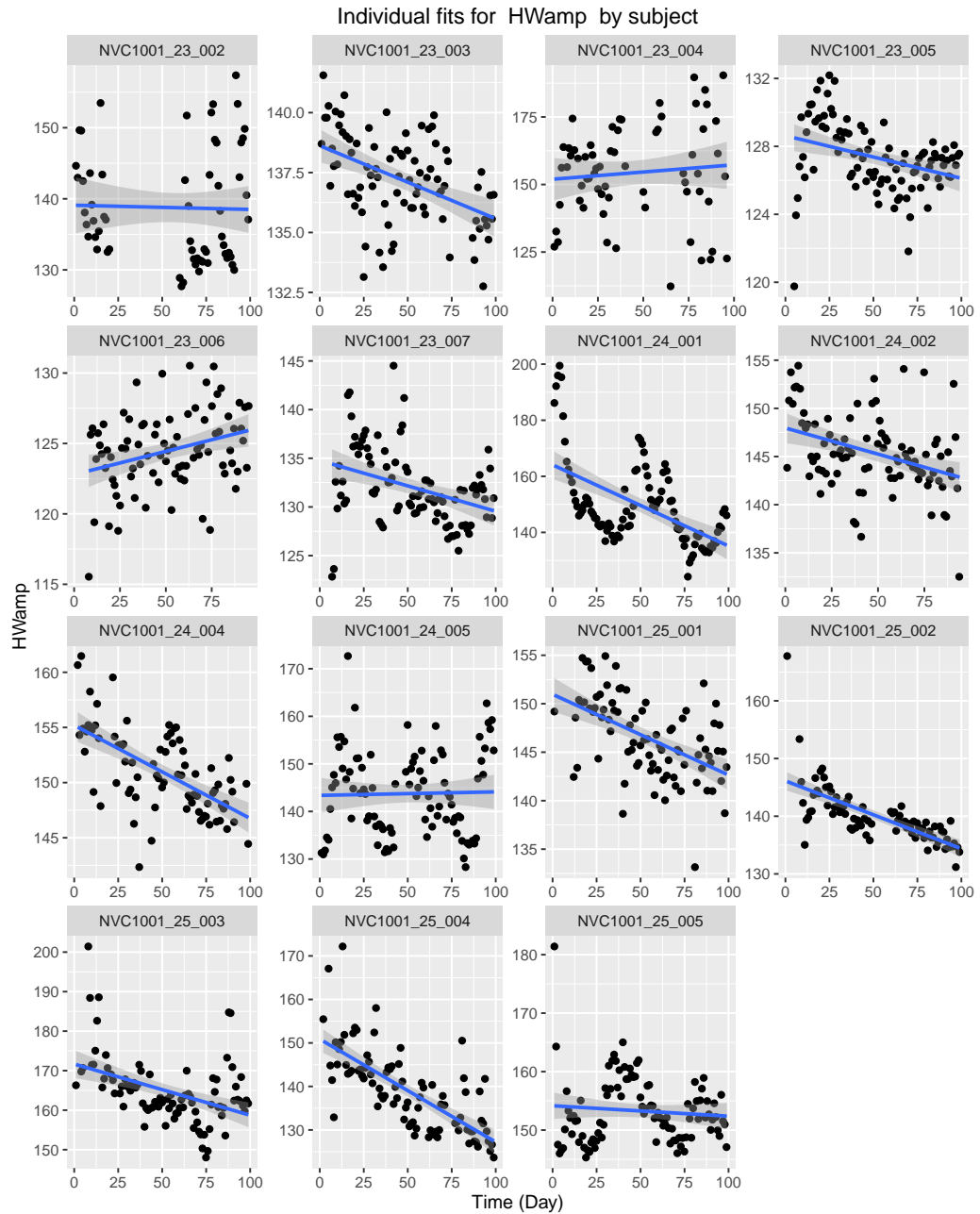
Figure 68: Individual plots of Halfwave amplitude for the first 100 days
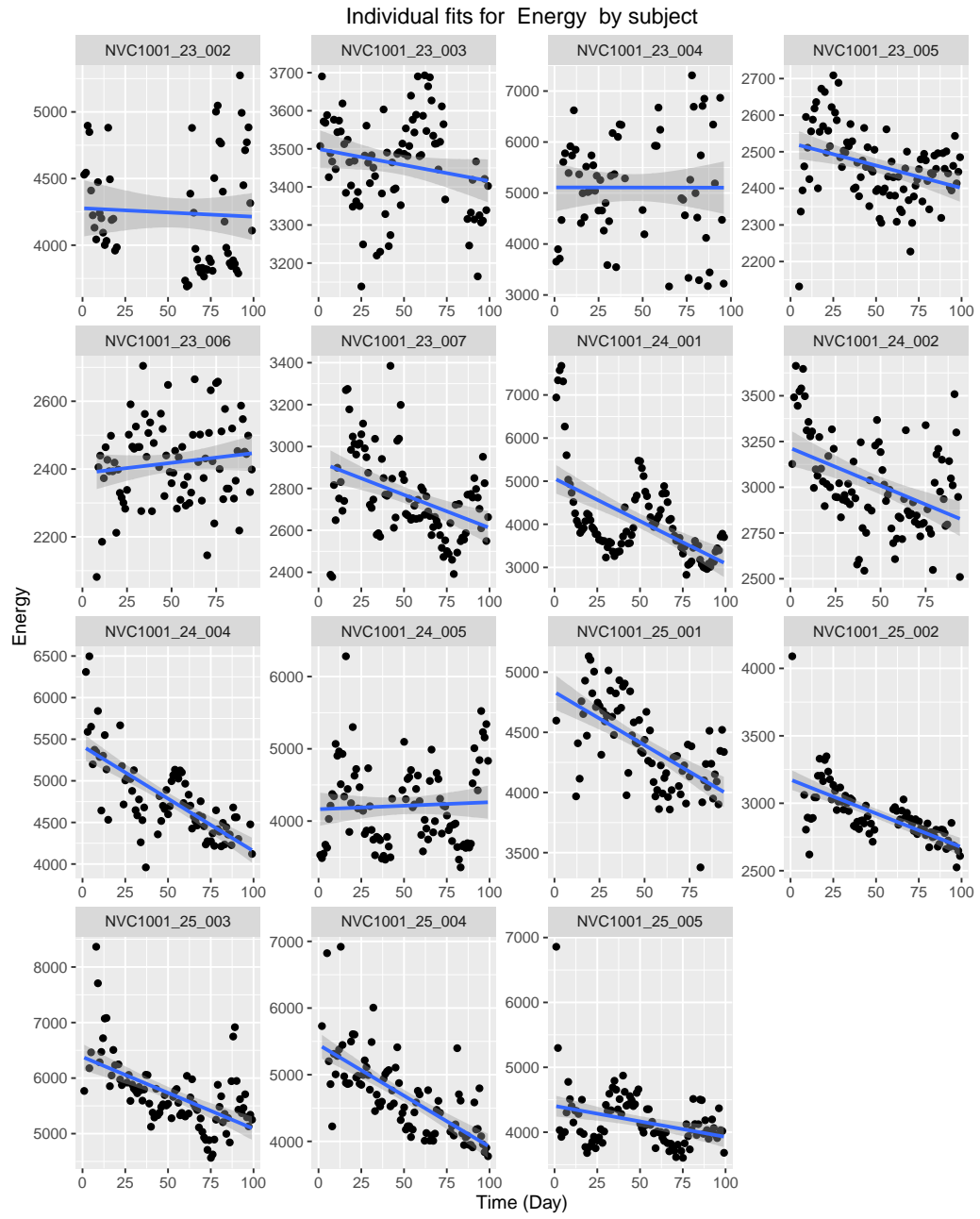
Figure 69: Individual plots of Energy power for the first 100 days
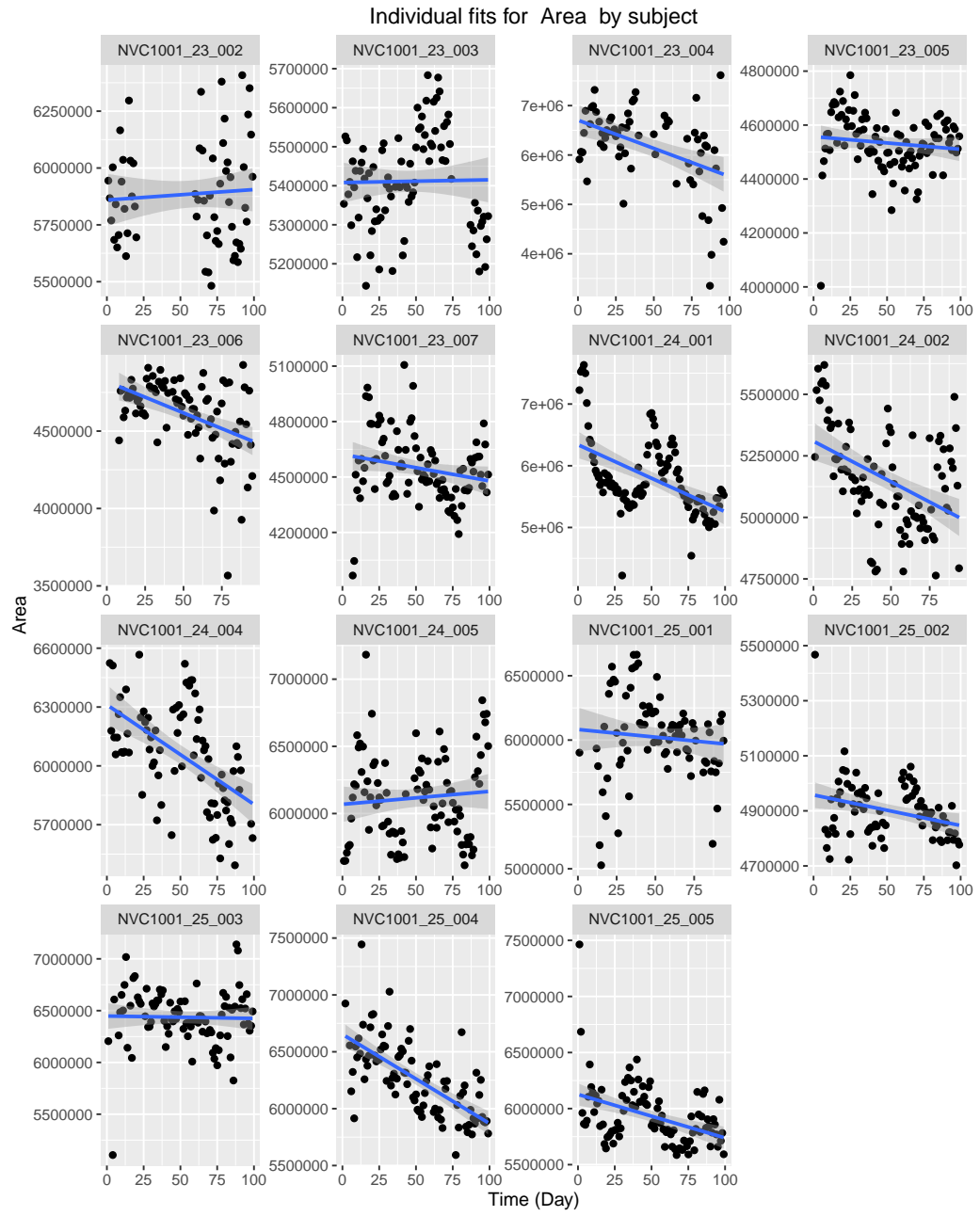
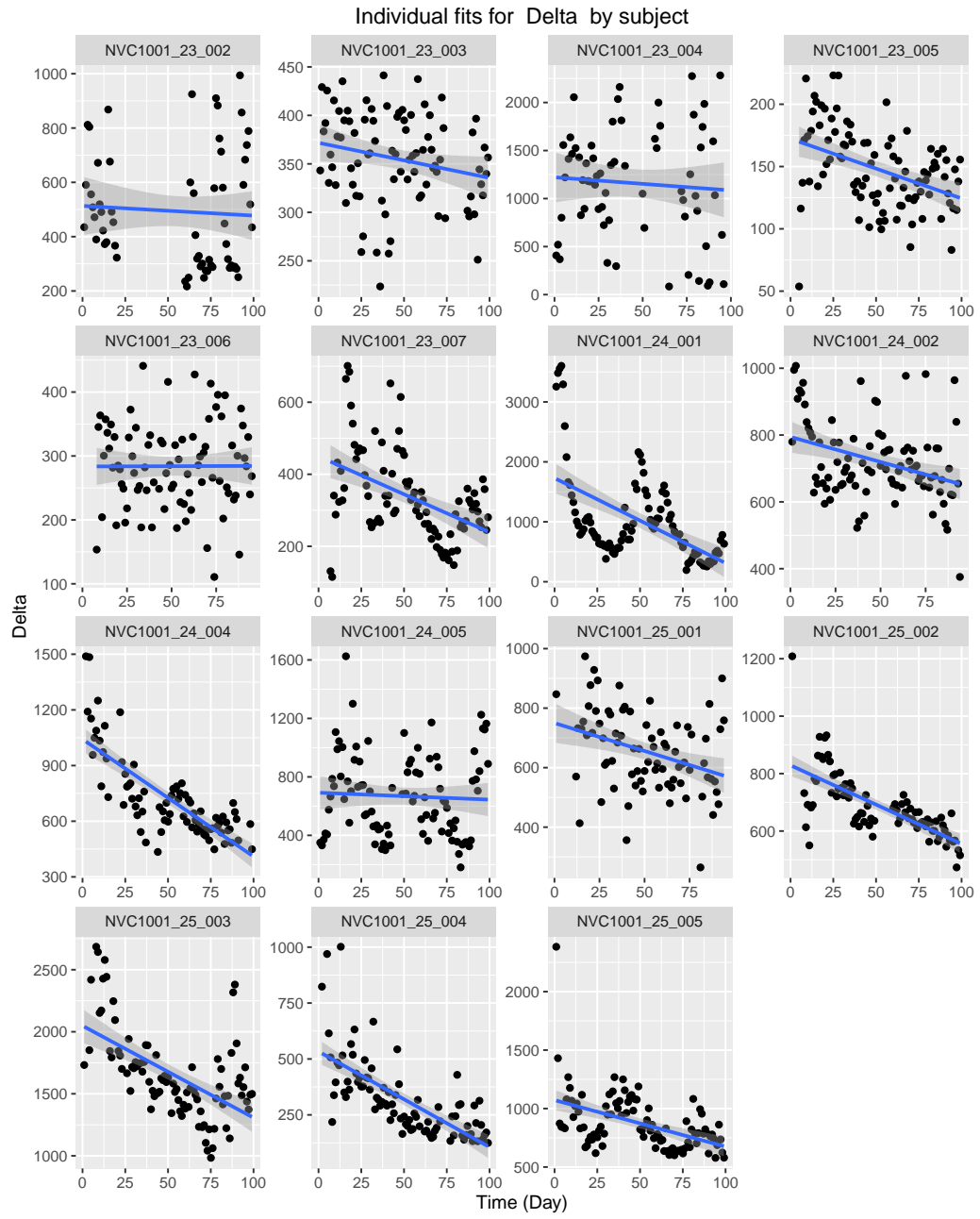Figure 70: Individual plots of Area power for the first 100 days

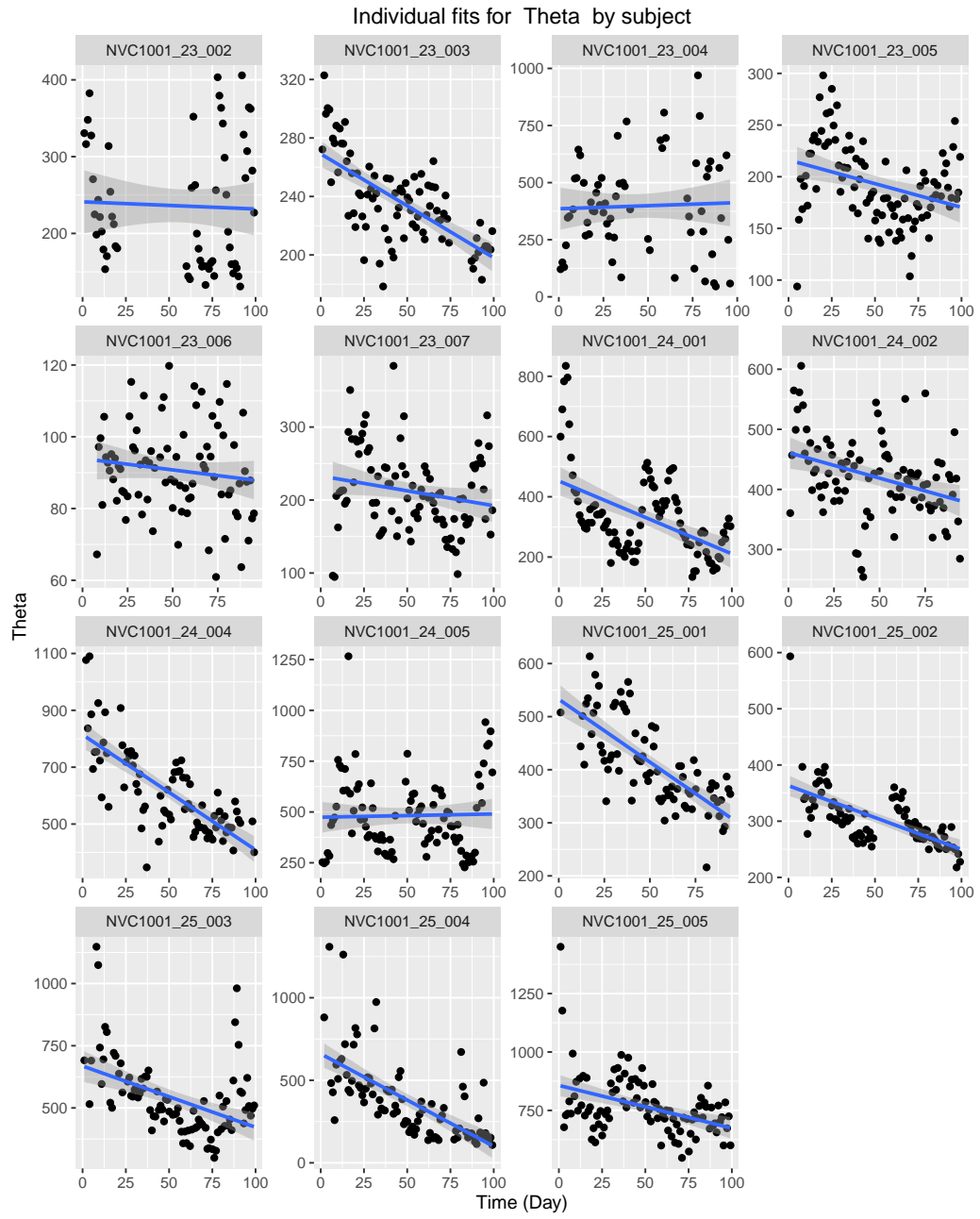Figure 71: Individual plots of delta power for the first 100 days

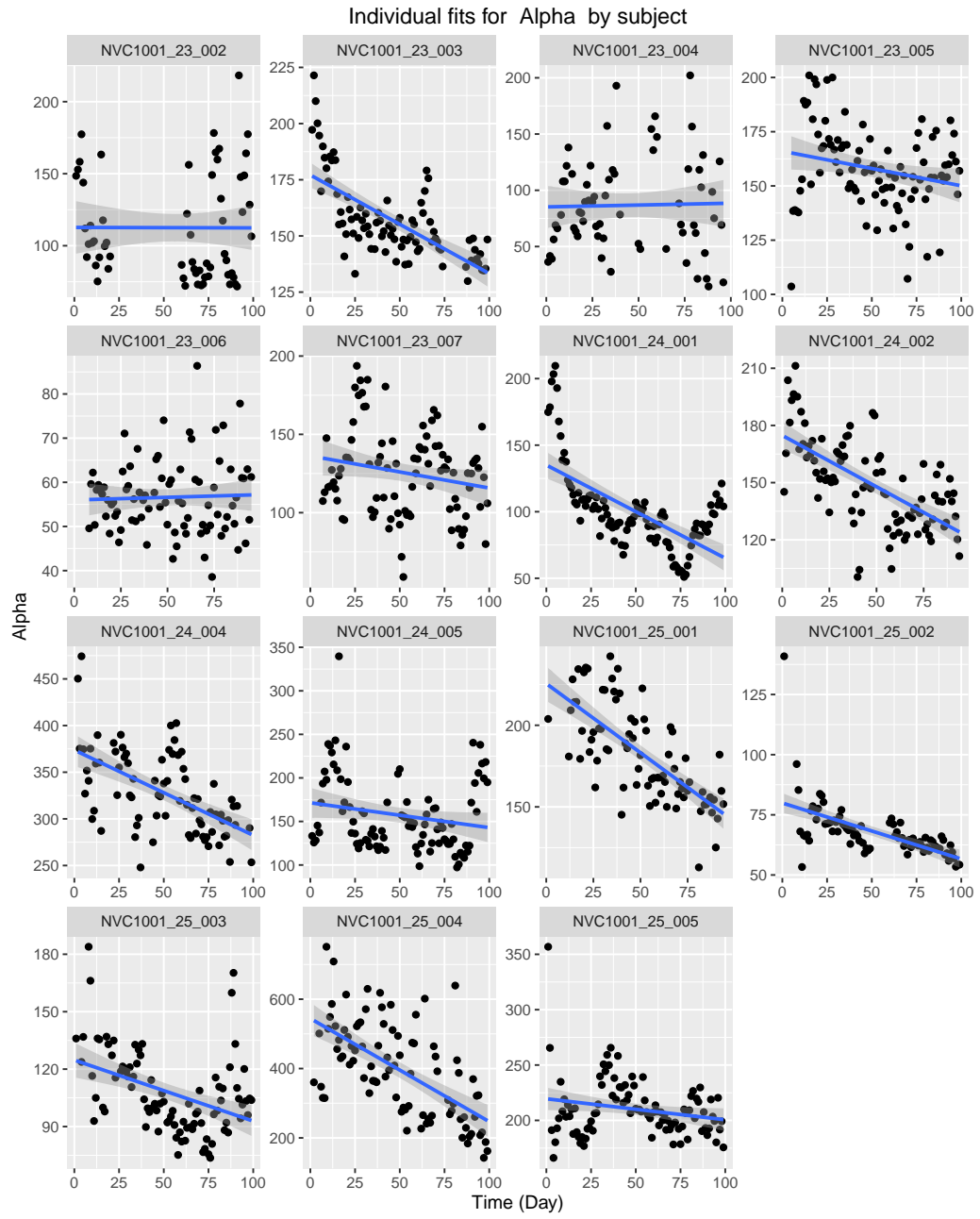Figure 72: Individual plots of theta power for the first 100 days

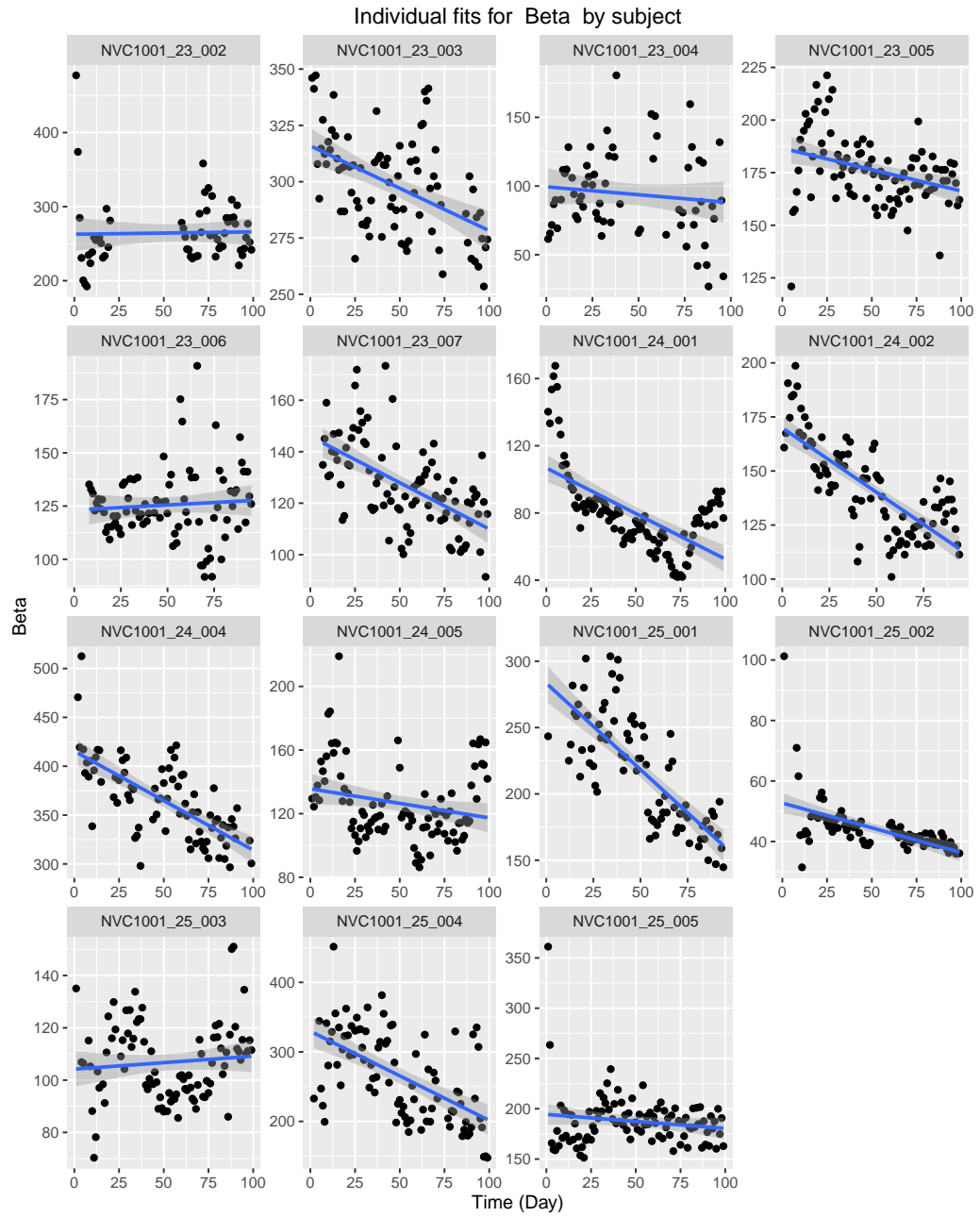Figure 73: Individual plots of alpha power for the first 100 days

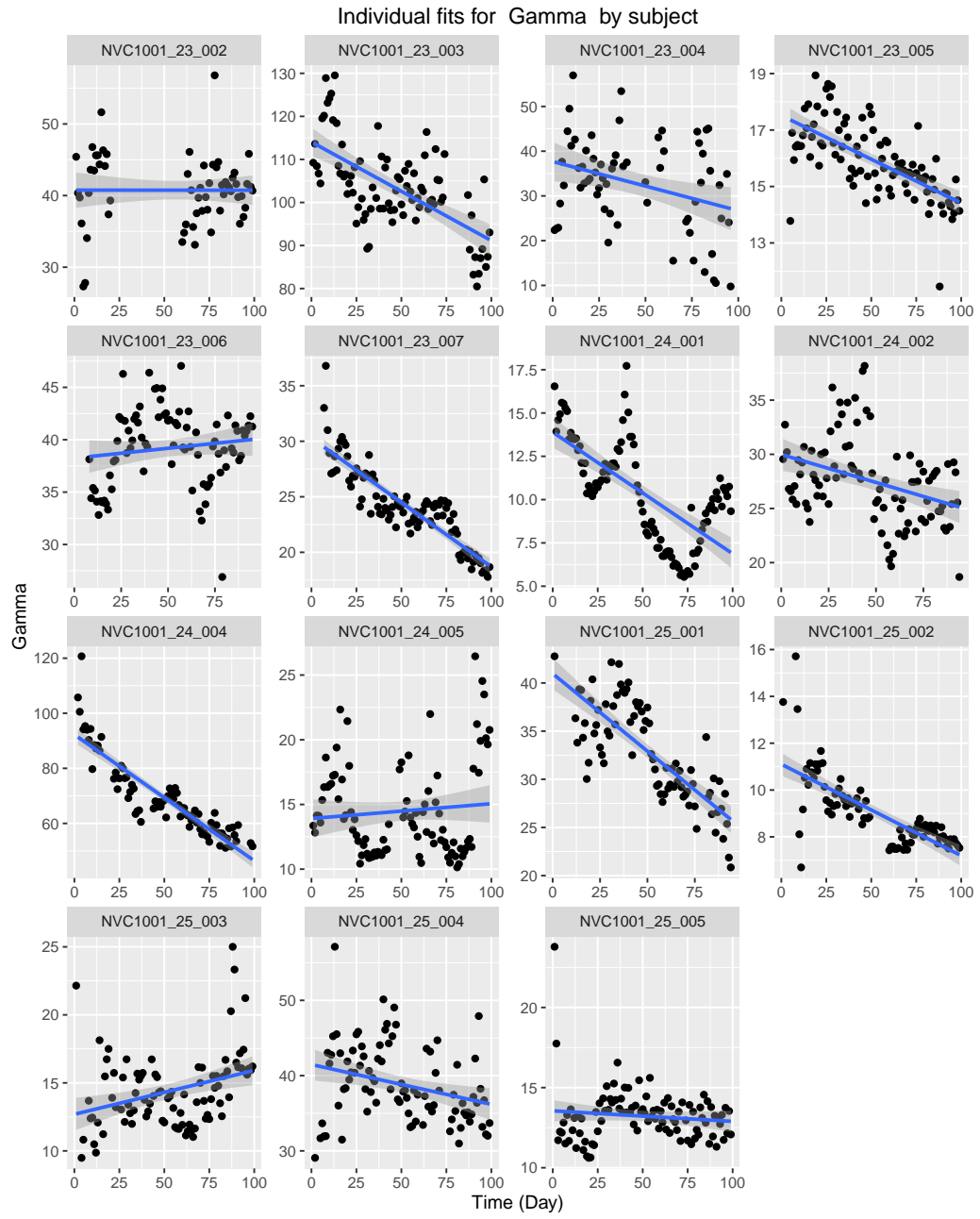Figure 74: Individual plots of beta power for the first 100 days

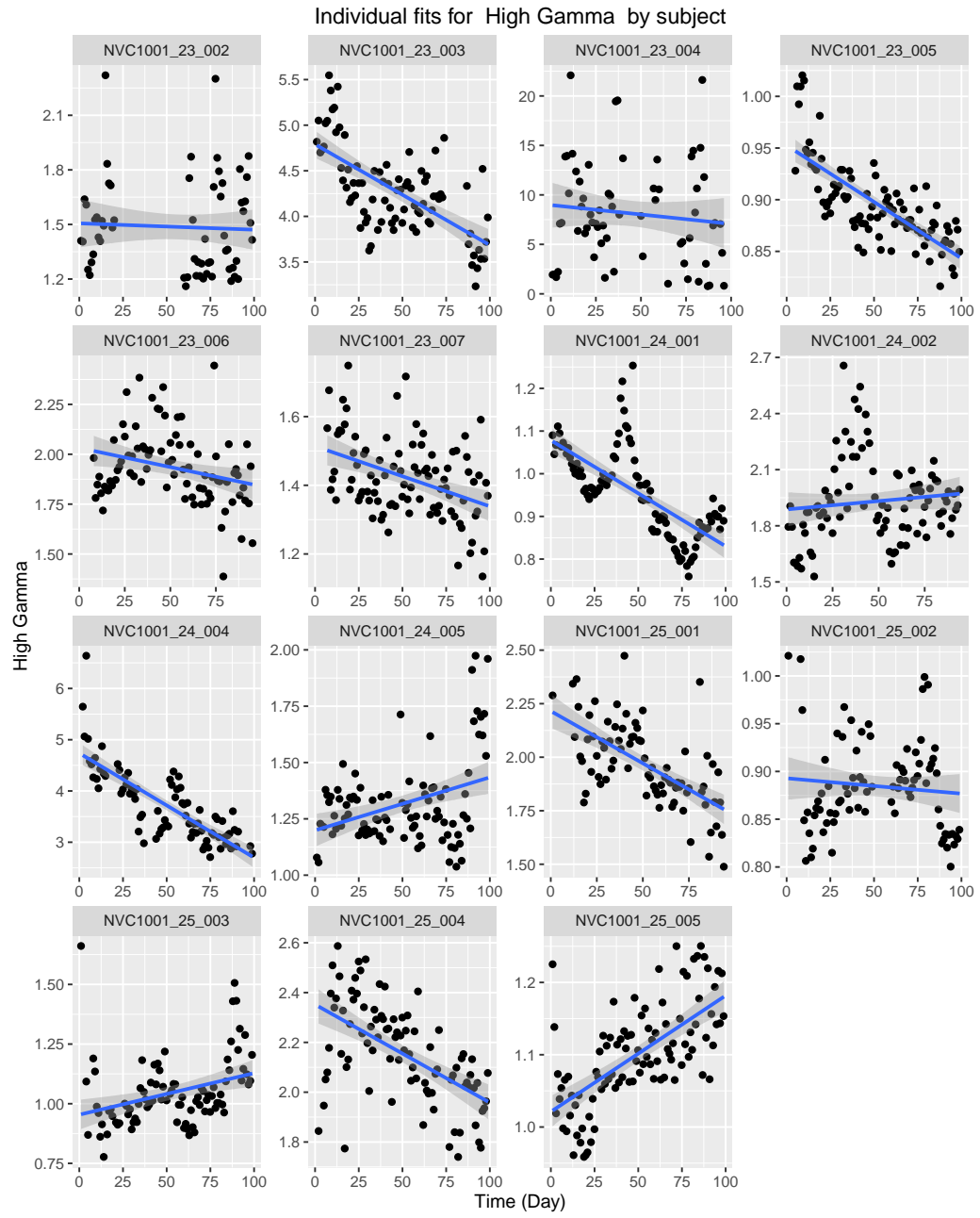Figure 75: Individual plots of gamma power for the first 100 days

Figure 76: Individual plots of High Gamma power for the first 100 days

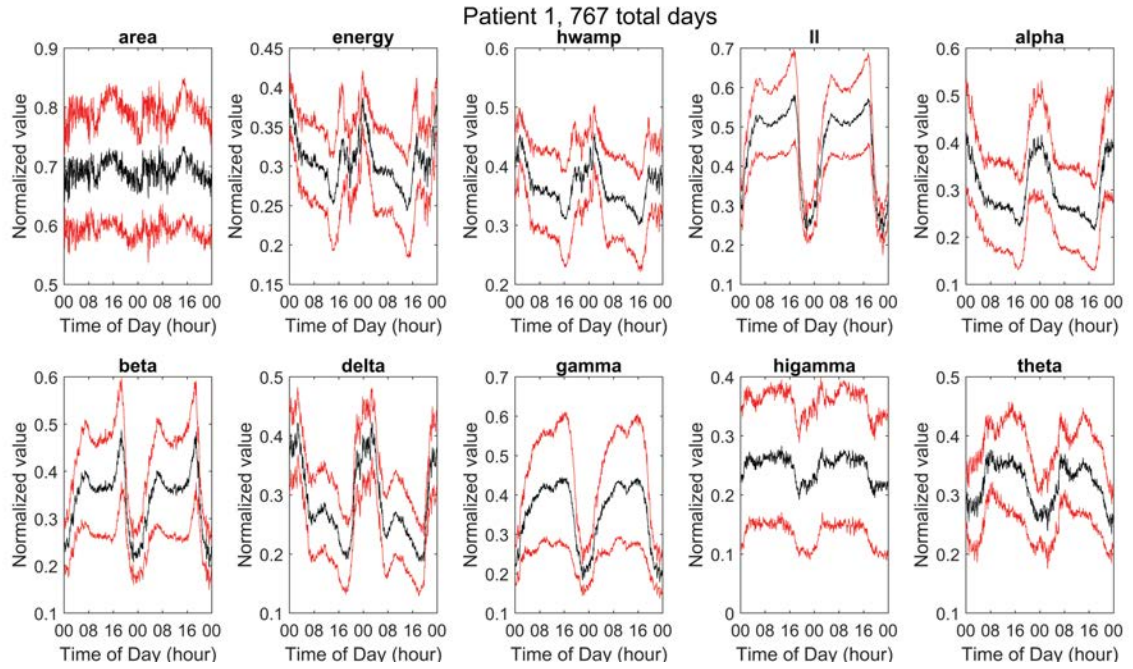## A.3 Circadian Rhythm of Time and Spectral domain features

Figure 77: Circadian rhythm for $NVC1001\_23\_002$, all features

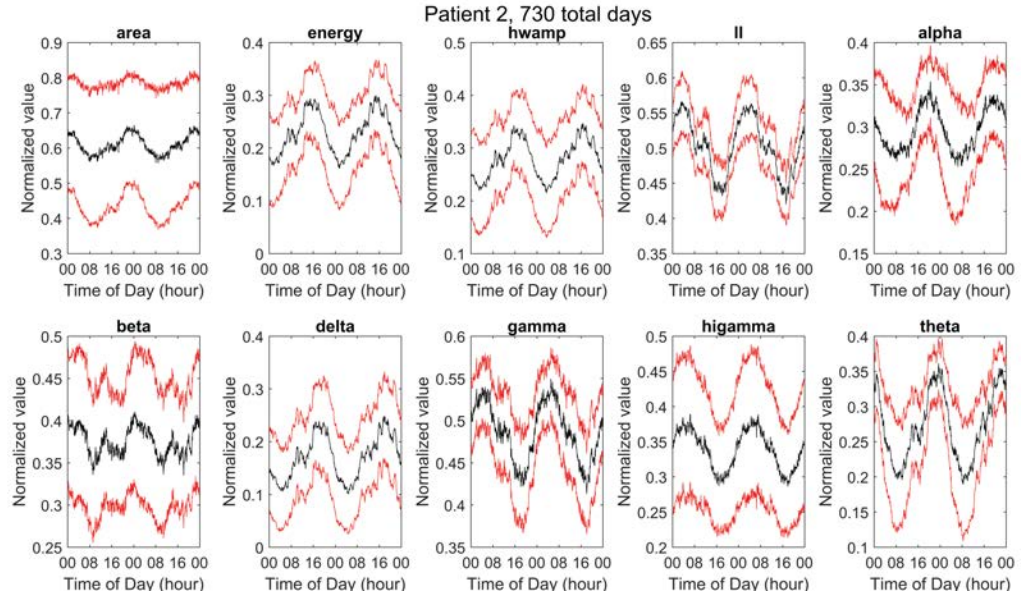Figure 78: Circadian rhythm for $NVC1001\_23\_003$, all features

Figure 79: Circadian rhythm for $NVC1001\_23\_004$, all features

Figure 80: Circadian rhythm for $NVC1001\_23\_005$, all features

Figure 81: Circadian rhythm for $NVC1001\_23\_006$, all features

Figure 82: Circadian rhythm for $NVC1001\_23\_007$, all features

Figure 83: Circadian rhythm for $NVC1001\_24\_001$, all features

Figure 84: Circadian rhythm for $NVC1001\_24\_002$, all features

Figure 85: Circadian rhythm for $NVC1001\_24\_004$, all features

197

Figure 86: Circadian rhythm for $NVC1001\_24\_005$, all features
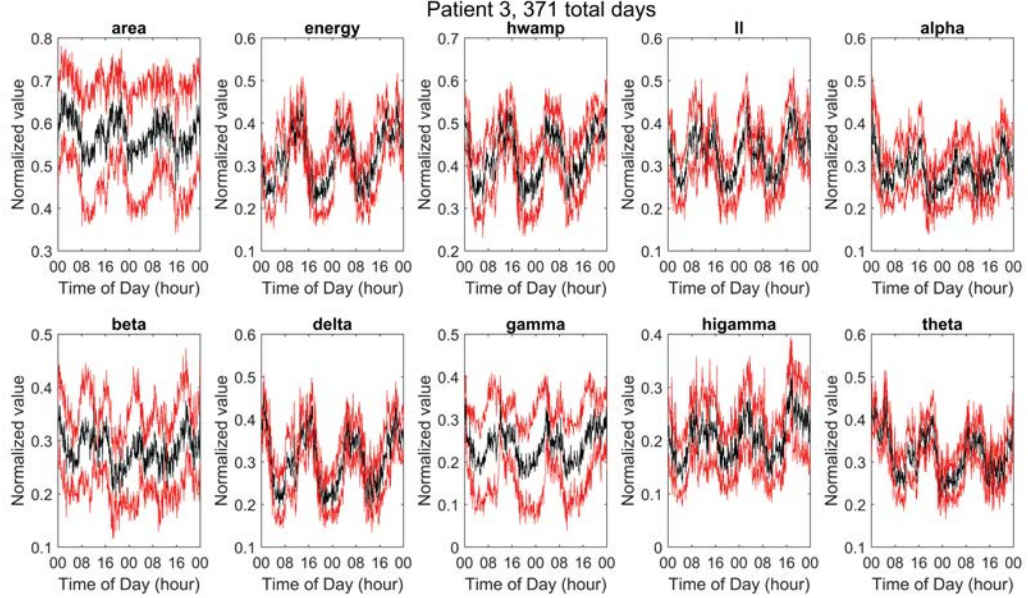

Figure 87: Circadian rhythm for $NVC1001\_25\_001$, all features

Figure 88: Circadian rhythm for $NVC1001\_25\_002$, all features

Figure 89: Circadian rhythm for $NVC1001\_25\_003$, all features

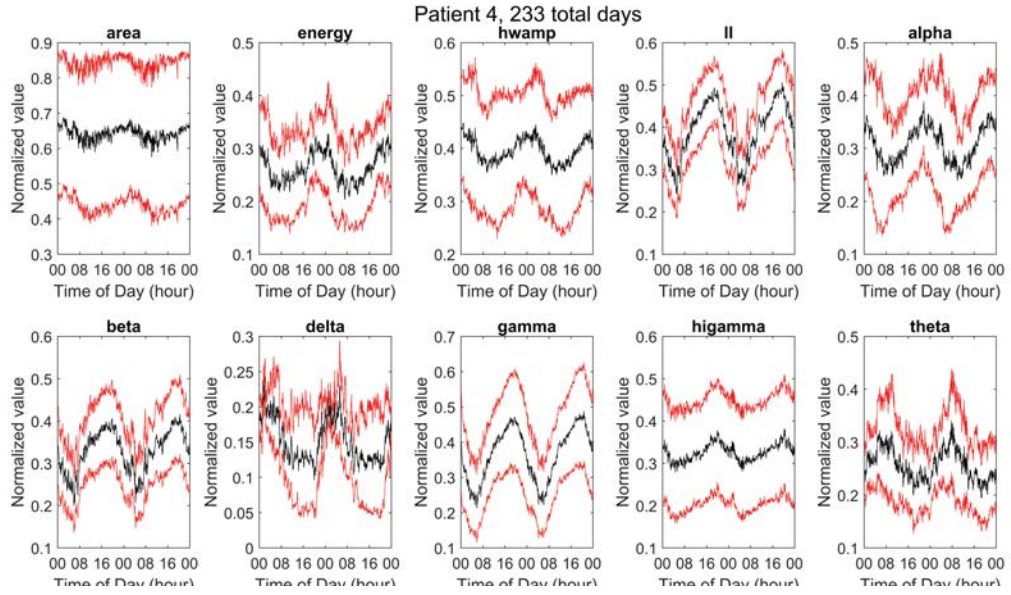Figure 90: Circadian rhythm for $NVC1001\_25\_004$, all features

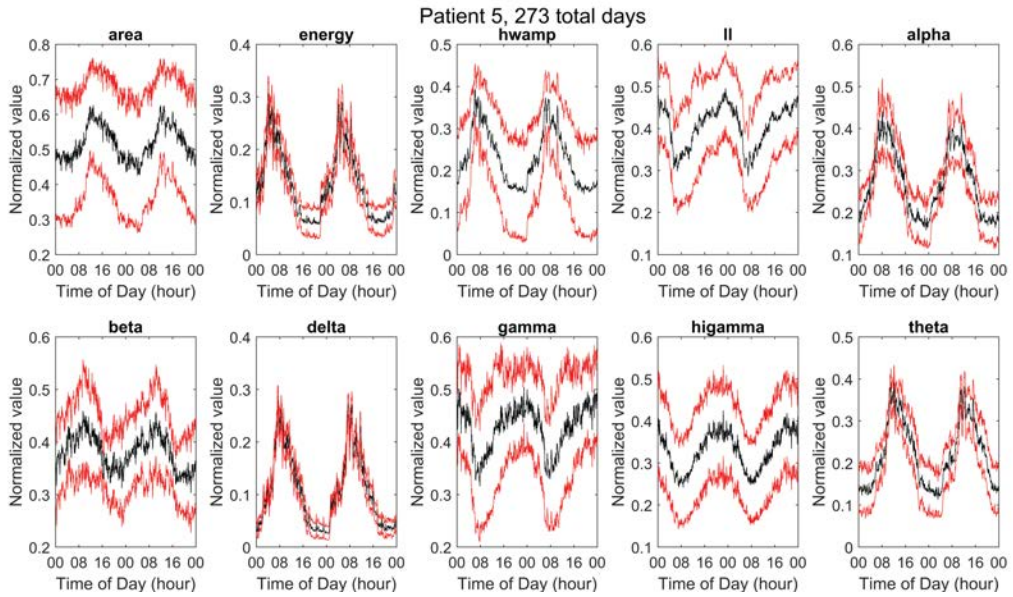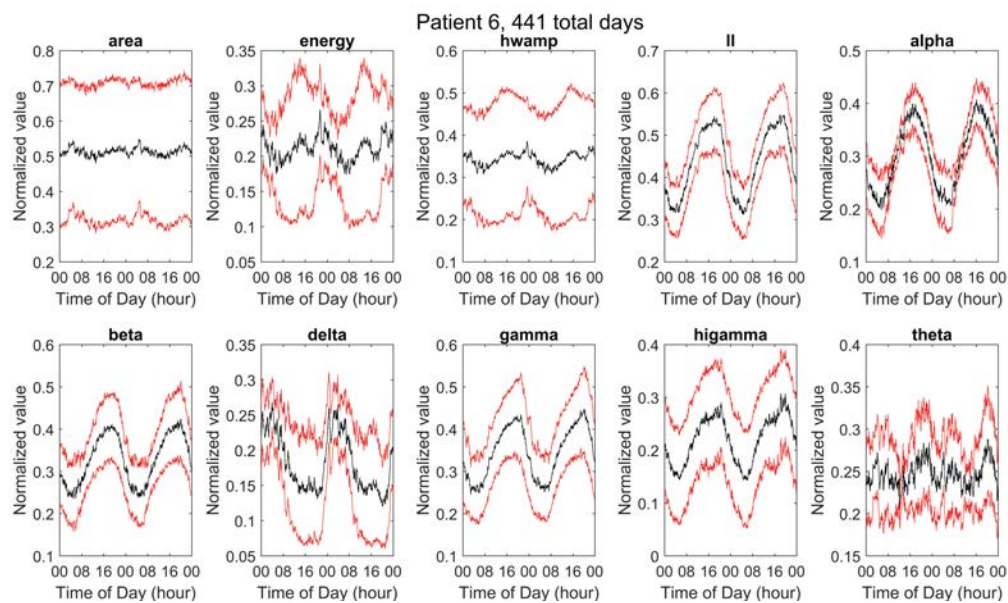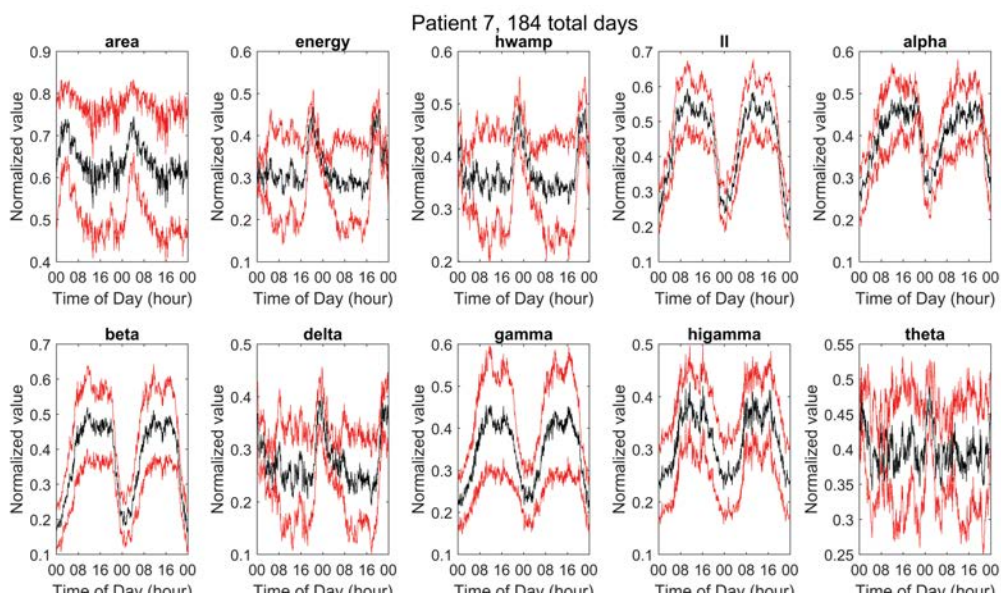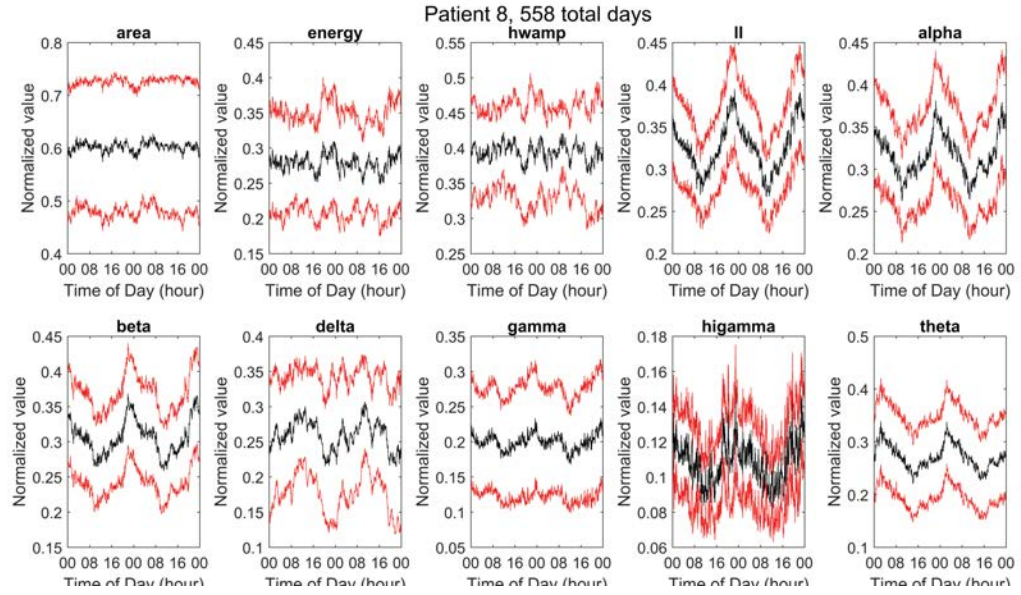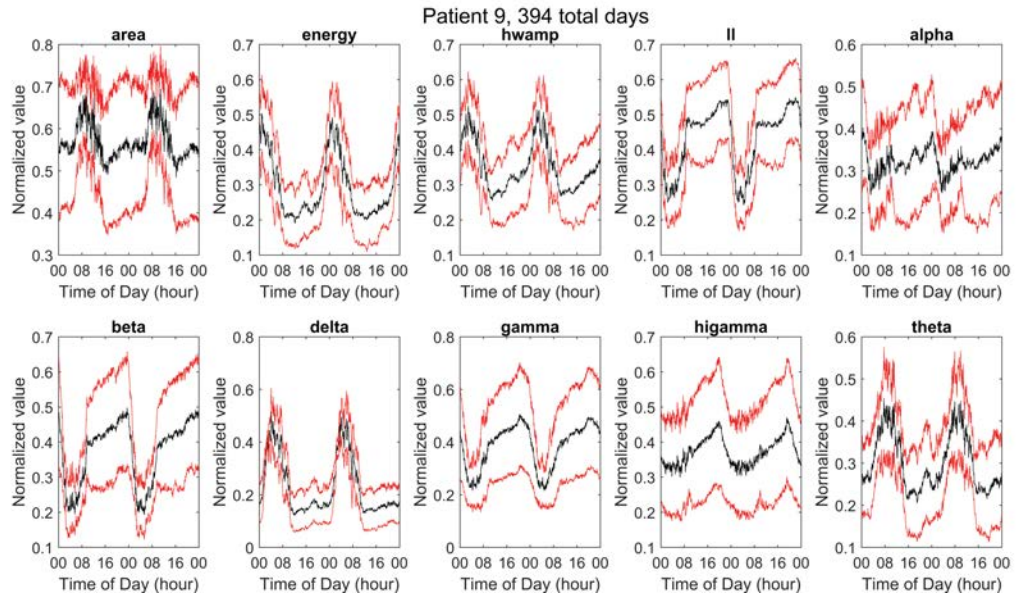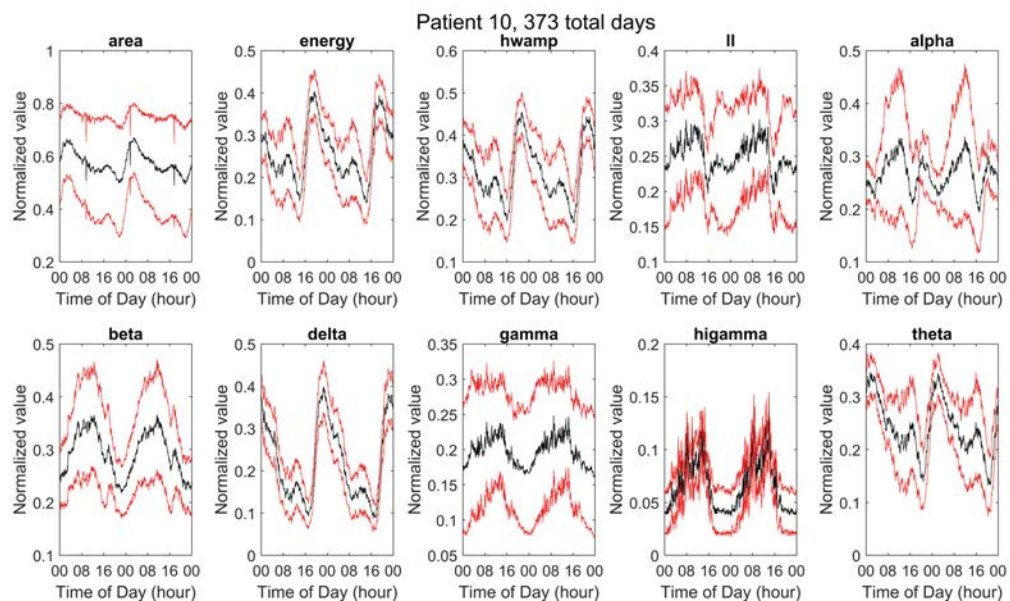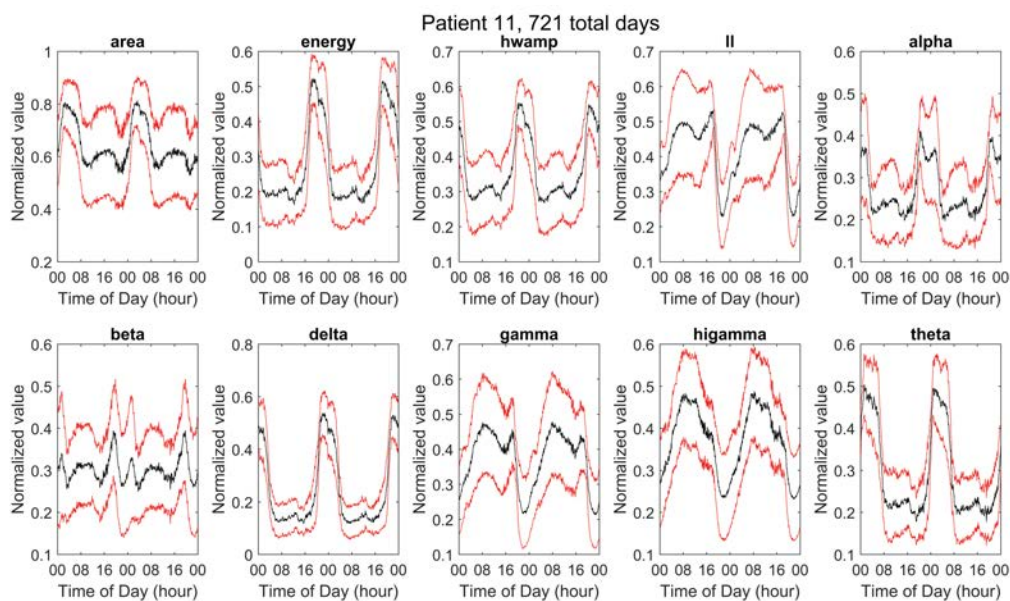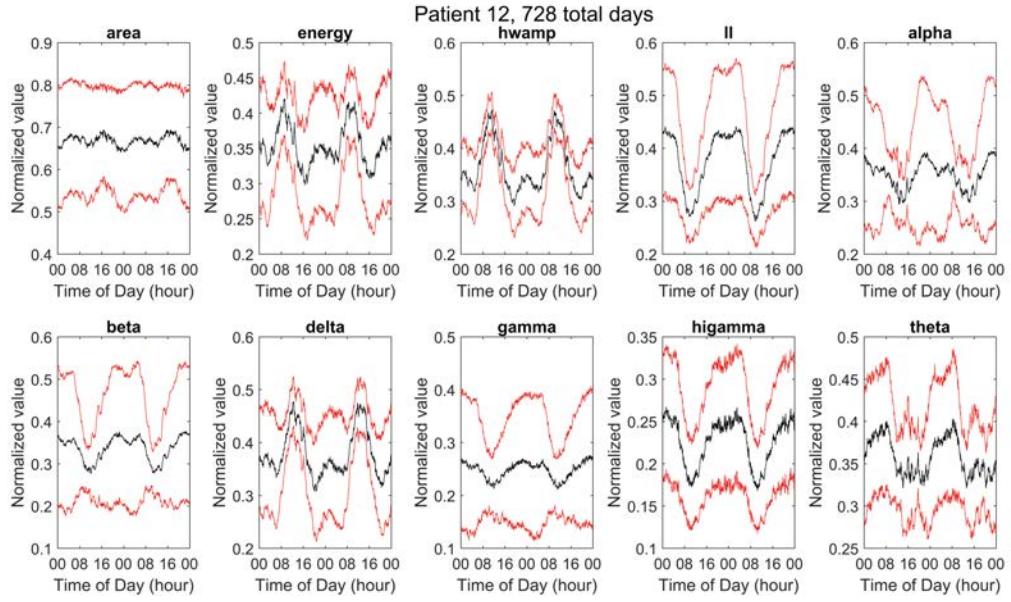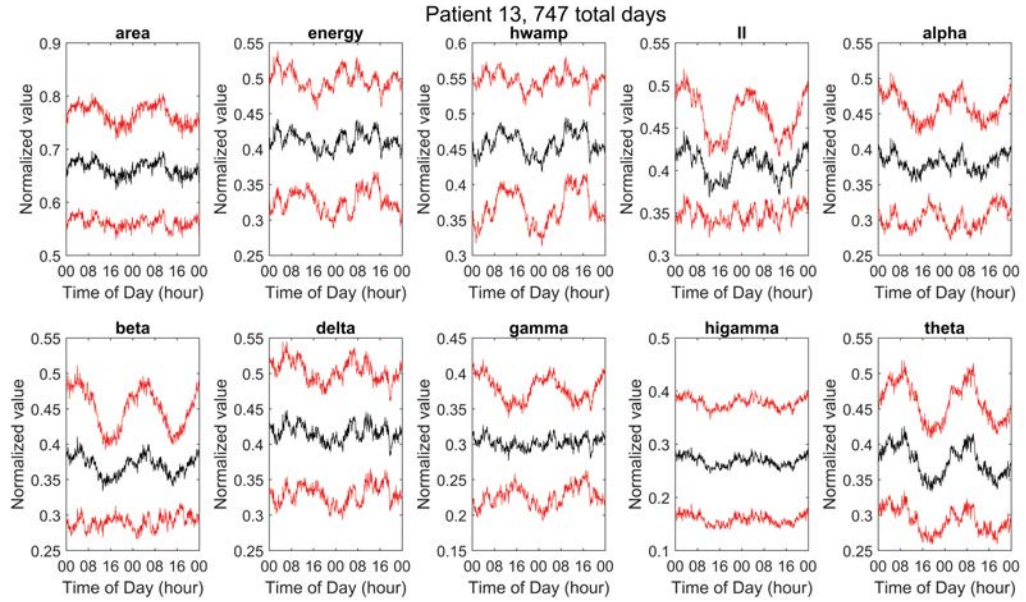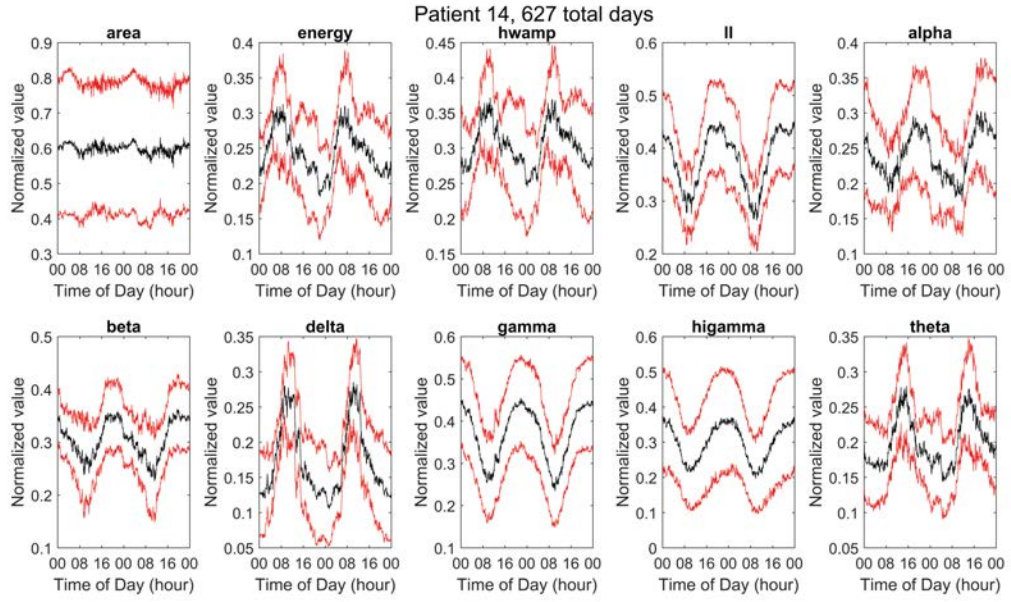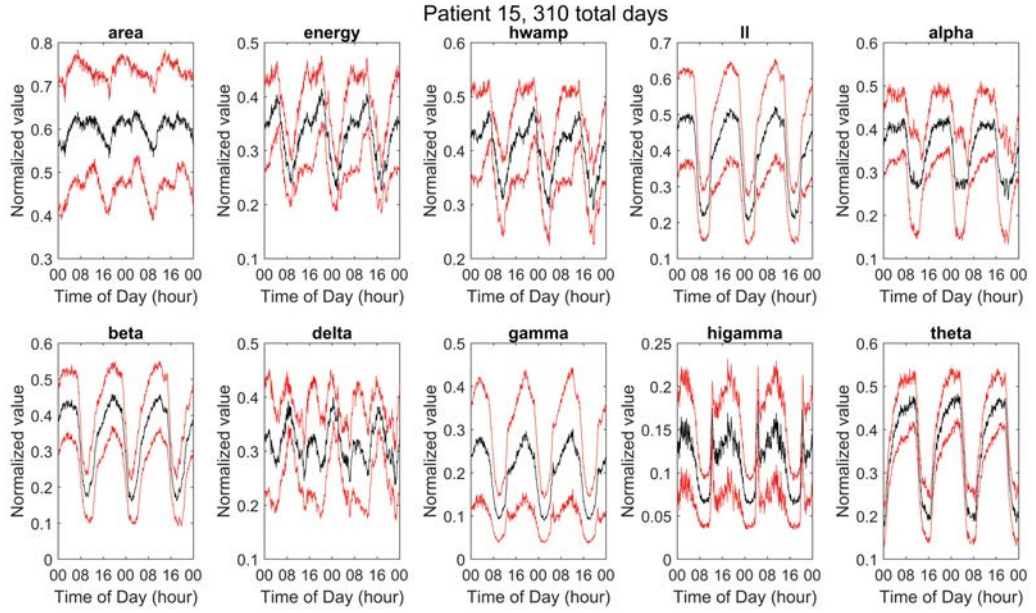Figure 91: Circadian rhythm for $NVC1001\_25\_005$, all features

BIBLIOGRAPHY

[1] J H Aarts et al. "Selective cognitive impairment during focal and generalized epileptiform EEG activity." In: *Brain* 107 (Pt 1 (1984), pp. 293–308. ISSN: 0006-8950.

[2] Nicholas S Abend and Courtney J Wusthoff. "Neonatal seizures and status epilepticus." In: *Journal of clinical neurophysiology : official publication of the American Electroencephalographic Society* 29.5 (2012), pp. 441–8. ISSN: 1537-1603. DOI: `10.1097/WNP.0b013e31826bd90d`.

[3] Amit Agrawal et al. *Post-traumatic epilepsy: An overview.* 2006. DOI: `10.1016/j.clineuro.2005.09.001`.

[4] Z Ahmad et al. "Auditory comprehension of language in young children: neural networks identified with fMRI". In: *Neurology* 60.10 (2003), pp. 1598–1605. ISSN: 1526-632X. DOI: `10.1212/01.WNL.0000059865.32155.86`.

[5] Frédérique Amor et al. "Cortical local and long-range synchronization interplay in human absence seizure initiation". In: *NeuroImage* 45.3 (2009), pp. 950–962. ISSN: 10538119. DOI: `10.1016/j.neuroimage.2008.12.011`.

[6] John F. Annegers and Sharon Pasternak Coan. "The risks of epilepsy after traumatic brain injury". In: *Seizure* 9.7 (2000), pp. 453–457. ISSN: 10591311. DOI: `10.1053/seiz.2000.0458`.

[7] Ravindra Arya et al. "Adverse events related to extraoperative invasive EEG monitoring with subdural grid electrodes: A systematic review and meta-analysis". In: *Epilepsia* 54.5 (2013), pp. 828–839. ISSN: 00139580. DOI: `10.1111/epi.12073`.

[8] Mark G. Baxter. *Involvement of Medial Temporal Lobe Structures in Memory and Perception.* 2009. DOI: `10.1016/j.neuron.2009.02.007`.

[9] Pedro Beleza et al. "Epidural and foramen-ovale electrodes in the diagnostic evaluation of patients considered for epilepsy surgery". In: *Epileptic Disorders* 12.1 (2010), pp. 48–53. ISSN: 12949361. DOI: `10.1684/epd.2010.0297`.

[10] Gregory K Bergey et al. "Long-term treatment with responsive brain stimulation in adults with refractory partial seizures". In: *Neurology* 84.8 (2015), pp. 810–7. ISSN: 1526-632X. DOI: `10.1212/WNL.0000000000001280`. URL: `http://www.pubmedcentral.nih.gov/articlerender.fcgi?artid=4339127{\&}tool=pmcentrez{\&}rendertype=abstract`.

[11] Colin D. Binnie. *Cognitive impairment during epileptiform discharges: Is it ever justifiable to treat the EEG?* 2003. DOI: `10.1016/S1474-4422(03)00584-2`.

[12] Roy Biran, David C. Martin, and Patrick A. Tresco. "Neuronal cell loss accompanies the brain tissue response to chronically implanted silicon microelectrode arrays". In: *Experimental Neurology* 195 (2005), pp. 115–126. ISSN: 00144886. DOI: `10.1016/j.expneurol.2005.04.020`.

[13] R V Blake et al. "Accelerated forgetting in patients with epilepsy: evidence for an impairment in memory consolidation". In: *Brain* 123.0006-8950 (2000), pp. 472–483. ISSN: 0006-8950. DOI: `10.1093/brain/123.3.472`.

[14] Leo Breiman. "Random forests". In: *Machine Learning* 45.1 (2001), pp. 5–32. ISSN: 08856125. DOI: 10.1023/A:1010933404324. arXiv: /dx.doi.org/10.1023{\%}2FA{\%}3A1010933404324 [http:]. URL: http://link.springer.com/10.1023/A:1010933404324.

[15] Leo Breiman. "Statistical Modeling: The Two Cultures". In: *Statistical Science* 16.3 (2001), pp. 199–231. ISSN: 08834237. DOI: 10.2307/2676681. arXiv: 0010. URL: http://projecteuclid.org/Dienst/getRecord?id=euclid.ss/1009213726/.

[16] Benjamin H. Brinkmann et al. "Multiscale electrophysiology format: An open-source electrophysiology format using data compression, encryption, and cyclic redundancy check". In: *Proceedings of the 31st Annual International Conference of the IEEE Engineering in Medicine and Biology Society: Engineering the Future of Biomedicine, EMBC 2009*. 2009, pp. 7083–7086. ISBN: 9781424432967. DOI: 10.1109/IEMBS.2009.5332915. arXiv: NIHMS150003.

[17] Samuel P Burns et al. "Network dynamics of the brain and influence of the epileptic seizure onset zone". In: *Proceedings of the National Academy of Sciences of the United States of America* 111.49 (2014), E5321–5330. ISSN: 1091-6490. DOI: 10.1073/pnas.1401752111. URL: http://www.pnas.org/content/111/49/E5321.abstract.

[18] György Buzsáki, Costas a Anastassiou, and Christof Koch. "The origin of extracellular fields and currents–EEG, ECoG, LFP and spikes." In: *Nature reviews. Neuroscience* 13.6 (2012), pp. 407–20. ISSN: 1471-0048. DOI: 10.1038/nrn3241. arXiv: NIHMS150003. URL: http://www.ncbi.nlm.nih.gov/pubmed/22595786.

[19] Laetitia Chauvière et al. "Changes in interictal spike features precede the onset of temporal lobe epilepsy". In: *Annals of Neurology* 71.6 (2012), pp. 805–814. ISSN: 03645134. DOI: 10.1002/ana.23549.

[20] Jakob Christensen et al. "Long-term risk of epilepsy after traumatic brain injury in children and young adults: a population-based cohort study." In: *Lancet* 373.9669 (2009), pp. 1105–1110. ISSN: 1474-547X. DOI: 10.1016/S0140-6736(09)60214-2.

[21] Stuart F Cogan. "Neural stimulation and recording electrodes." In: *Annual review of biomedical engineering* 10 (2008), pp. 275–309. DOI: 10.1146/annurev.bioeng.10.061807.160518.

[22] Laurent Cohen et al. "Language-specific tuning of visual cortex? Functional properties of the Visual Word Form Area." In: *Brain* 125.5 (2002), pp. 1054–1069. ISSN: 0006-8950. DOI: 10.1093/brain/awf094.

[23] Mark J. Cook et al. "Prediction of seizure likelihood with a long-term, implanted seizure advisory system in patients with drug-resistant epilepsy: A first-in-man study". In: *The Lancet Neurology* 12.6 (2013), pp. 563–571. ISSN: 14744422. DOI: 10.1016/S1474-4422(13)70075-9.

[24] Maryann D'Alessandro et al. "Epileptic seizure prediction using hybrid feature selection over multiple intracranial EEG electrode contacts: a report of four patients." In: *IEEE transactions on bio-medical engineering* 50.5 (2003), pp. 603–15. DOI: 10.1109/TBME.2003.815899.

[25] Raimondo D'Ambrosio et al. "Post-traumatic epilepsy following fluid percussion injury in the rat". In: *Brain* 127.2 (2004), pp. 304–314. ISSN: 00068950. DOI: `10.1093/brain/awh038`.

[26] Margherita D'Antuono et al. "Antiepileptic drugs abolish ictal but not interictal epileptiform discharges in vitro". In: *Epilepsia* 51.3 (2010), pp. 423–431. ISSN: 00139580. DOI: `10.1111/j.1528-1167.2009.02273.x`.

[27] Kathryn A Davis et al. "A novel implanted device to wirelessly record and analyze continuous intracranial canine EEG." In: *Epilepsy research* 96.1-2 (2011), pp. 116–22. ISSN: 1872-6844. DOI: `10.1016/j.eplepsyres.2011.05.011`.

[28] Kathryn A Davis et al. "Mining continuous intracranial EEG in focal canine epilepsy: Relating interictal bursts to seizure onsets." In: *Epilepsia* 57.1 (2016), pp. 89–98. ISSN: 1528-1167. DOI: `10.1111/epi.13249`. URL: `http://www.ncbi.nlm.nih.gov/pubmed/26608448`.

[29] Ross Davis and Sandra E Emmonds. "Cerebellar stimulation for seizure control: 17-year study". In: *Stereotactic and Functional Neurosurgery*. Vol. 58. 1-4. 1992, pp. 200–208. ISBN: 1011-6125 (Print)\r1011-6125 (Linking). DOI: `10.1159/000098996`.

[30] Alan D Degenhart et al. "Histological evaluation of a chronically-implanted electrocorticographic electrode grid in a non-human primate". In: *Journal of Neural Engineering* 13.4 (2016), p. 046019. ISSN: 1741-2560. DOI: `10.1088/1741-2560/13/4/046019`. URL: `http://stacks.iop.org/1741-2552/13/i=4/a=046019?key=crossref.fbb51d6754f6c5d84615ef40c9ba1b10`.

[31] Daniel J DiLorenzo et al. "Chronic unlimited recording electrocorticography-guided resective epilepsy surgery: technology-enabled enhanced fidelity in seizure focus localization with improved surgical efficacy." In: *Journal of neurosurgery* 120.June (2014), pp. 1402–14. ISSN: 1933-0693. DOI: `10.3171/2014.1.JNS131592`. URL: `http://www.ncbi.nlm.nih.gov/pubmed/24655096`.

[32] Daniel L. Drane et al. "Better object recognition and naming outcome with MRI-guided stereotactic laser amygdalohippocampotomy for temporal lobe epilepsy". In: *Epilepsia* 56.1 (2015), pp. 101–113. ISSN: 15281167. DOI: `10.1111/epi.12860`.

[33] J. Echauz et al. *Median-based filtering methods for EEG seizure detection.* 1999. DOI: `10.1109/IEMBS.1999.802517`. URL: `http://ieeexplore.ieee.org/lpdocs/epic03/wrapper.htm?arnumber=802517`.

[34] H Eichenbaum, A P Yonelinas, and C Ranganath. "The medial temporal lobe and recognition memory." In: *Annual review of neuroscience* 30 (2007), pp. 123–52. ISSN: 0147-006X. DOI: `10.1146/annurev.neuro.30.051606.094328`. arXiv: `NIHMS150003`. URL: `http://www.scopus.com/inward/record.url?eid=2-s2.0-34249055712{\&}partnerID=tZOtx3y1`.

[35] Jerome Engel. *Biomarkers in epilepsy: foreword.* 2011. DOI: `10.2217/bmm.11.63`.

[36] Jerome Engel and Paul H. Crandall. "Falsely Localizing Ictal Onsets with Depth EEG Telemetry During Anticonvulsant Withdrawal". In: *Epilepsia* 24.3 (1983), pp. 344–355. ISSN: 0013-9580. DOI: `10.1111/j.1528-1157.1983.tb04898.x`. URL: `http://doi.wiley.com/10.1111/j.1528-1157.1983.tb04898.x`.

[37] Jerome Engel et al. "Epilepsy biomarkers." In: *Epilepsia* 54 Suppl 4 (2013), pp. 61–9. ISSN: 1528-1167. DOI: 10.1111/epi.12299. URL: http://www.pubmedcentral.nih.gov/articlerender.fcgi?artid=4131763{\&}tool=pmcentrez{\&}rendertype=abstract.

[38] R. Esteller et al. "Line length: an efficient feature for seizure onset detection". In: *2001 Conference Proceedings of the 23rd Annual International Conference of the IEEE Engineering in Medicine and Biology Society* 2.3 (2001), pp. 1707–1710. ISSN: 1094-687X. DOI: 10.1109/IEMBS.2001.1020545.

[39] Simon Finnigan, Andrew Wong, and Stephen Read. "Defining abnormal slow EEG activity in acute ischaemic stroke: Delta/alpha ratio as an optimal QEEG index". In: *Clinical Neurophysiology* 127.2 (2016), pp. 1452–1459. ISSN: 13882457. DOI: 10.1016/j.clinph.2015.07.014.

[40] Robert S. Fisher et al. "ILAE Official Report: A practical clinical definition of epilepsy". In: *Epilepsia* 55.4 (2014), pp. 475–482. ISSN: 15281167. DOI: 10.1111/epi.12550. URL: http://doi.wiley.com/10.1111/epi.12550.

[41] Robert Fisher et al. "Electrical stimulation of the anterior nucleus of thalamus for treatment of refractory epilepsy". In: *Epilepsia* 51.5 (2010), pp. 899–908. ISSN: 00139580. DOI: 10.1111/j.1528-1167.2010.02536.x.

[42] Joanna S. Fong et al. "Pathologic findings associated with invasive EEG monitoring for medically intractable epilepsy". In: *American Journal of Clinical Pathology* 138.4 (2012), pp. 506–510. ISSN: 00029173. DOI: 10.1309/AJCPGSNL9VDVNJMX. URL: http://www.ncbi.nlm.nih.gov/pubmed/23010704.

[43] Kostas N. Fountas et al. "Nonhabitual seizures in patients with implanted subdural electrodes". In: *Stereotactic and Functional Neurosurgery* 82.4 (2004), pp. 165–168. ISSN: 10116125. DOI: 10.1159/000081881.

[44] Emily B. Fox et al. "Sharing Features among Dynamical Systems with Beta Processes". In: *Advances in Neural Information Processing Systems 23: 24th Annual Conference on Neural Information Processing Systems 2010.* 2009, pp. 388–396. ISBN: 9781615679119.

[45] Emily Fox et al. "Bayesian nonparametric methods for learning markov switching processes". In: *IEEE Signal Processing Magazine* 27.6 (2010), pp. 43–54. ISSN: 10535888. DOI: 10.1109/MSP.2010.937999.

[46] Lauren C Frey. "Epidemiology of posttraumatic epilepsy: a critical review." In: *Epilepsia* 44 Suppl 1 (2003), pp. 11–17. ISSN: 0013-9580. DOI: 10.1046/j.1528-1157.44.s10.4.x.

[47] Nicolas Gaspard and Lawrence J Hirsch. "Pitfalls in ictal EEG interpretation: critical care and intracranial recordings." In: *Neurology* 80.1 Suppl 1 (2013), S26–42. ISSN: 1526-632X. DOI: 10.1212/WNL.0b013e31827974f8.

[48] Nicolas Gaspard et al. "Automatic detection of prominent interictal spikes in intracranial EEG: Validation of an algorithm and relationsip to the seizure onset zone". In: *Clinical Neurophysiology* 125.6 (2014), pp. 1095–1103. ISSN: 13882457.

DOI: 10.1016/j.clinph.2013.10.021. URL: http://www.ncbi.nlm.nih.gov/pubmed/24269092.

[49] Jennifer N Gelinas et al. "Interictal epileptiform discharges induce hippocampalcortical coupling in temporal lobe epilepsy". In: *Nature Medicine* advance on (2016). ISSN: 1078-8956. DOI: 10.1038/nm.4084. URL: http://dx.doi.org/10.1038/nm.4084.

[50] Irina I. Goncharova et al. "Intracranially recorded interictal spikes: Relation to seizure onset area and effect of medication and time of day". In: *Clinical Neurophysiology* 124.11 (2013), pp. 2119–2128. ISSN: 13882457. DOI: 10.1016/j.clinph.2013.05.027.

[51] Jorge A. González-Martínez et al. "Long-term seizure outcome in reoperation after failure of epilepsy surgery". In: *Neurosurgery* 60.5 (2007), pp. 873–879. ISSN: 0148396X. DOI: 10.1227/01.NEU.0000255438.13871.FA.

[52] Ankush Gosain and Luisa A. DiPietro. *Aging and Wound Healing*. 2004. DOI: 10.1007/s00268-003-7397-6.

[53] J Gotman. "Automatic seizure detection: improvements and evaluation". In: *Electroencephalography and Clinical Neurophysiology* 76.4 (1990), pp. 317–324. ISSN: 00134694. DOI: 10.1016/0013-4694(90)90032-F.

[54] J. Gotman and P. Gloor. "Automatic recognition and quantification of interictal epileptic activity in the human scalp EEG". In: *Electroencephalography and Clinical Neurophysiology* 41.5 (1976), pp. 513–529. ISSN: 00134694. DOI: 10.1016/0013-4694(76)90063-8.

[55] Brian P Grone and Scott C Baraban. "Animal models in epilepsy research: legacies and new directions". In: *Nature Neuroscience* 18.3 (2015), pp. 339–343. ISSN: 1097-6256. DOI: 10.1038/nn.3934. URL: http://dx.doi.org/10.1038/nn.3934.

[56] Claire Haegelen et al. "High-frequency oscillations, extent of surgical resection, and surgical outcome in drug-resistant focal epilepsy". In: *Epilepsia* 54.5 (2013), pp. 848–857. ISSN: 00139580. DOI: 10.1111/epi.12075.

[57] C M Hamame et al. "Reading the mind's eye: online detection of visuo-spatial working memory and visual imagery in the inferior temporal lobe". In: *Neuroimage* 59.1 (2012), pp. 872–9. ISSN: 1095-9572. DOI: 10.1016/j.neuroimage.2011.07.087. URL: http://www.sciencedirect.com/science/article/pii/S1053811911008822http://www.ncbi.nlm.nih.gov/pubmed/21839843.

[58] A Handforth et al. *Vagus nerve stimulation therapy for partial-onset seizures: a randomized active-control trial.* Tech. rep. 1. 1998, pp. 48–55. DOI: 10.1212/WNL.51.1.48.

[59] Uwe-Karsten Hanisch. "Microglia as a source and target of cytokines." In: *Glia* 40.2 (2002), pp. 140–55. ISSN: 0894-1491. DOI: 10.1002/glia.10161.

[60] Sheryl R. Haut et al. "Seizure clustering during epilepsy monitoring". In: *Epilepsia* 43.7 (2002), pp. 711–715. ISSN: 00139580. DOI: 10.1046/j.1528-1157.2002.26401.x.

[61] C. Henle et al. "First long term in vivo study on subdurally implanted Micro-ECoG electrodes, manufactured with a novel laser technology". In: *Biomedical Microdevices* 13.1 (2011), pp. 59–68. ISSN: 13872176. DOI: 10.1007/s10544-010-9471-9.

[62] Arthur E. Hoerl and Robert W. Kennard. "Ridge Regression: Biased Problems Nonorthogonal Estimation for". In: *Technometrics* 42.1 (2000), pp. 80–86. ISSN: 0040-1706. DOI: 10.1080/00401706.1970.10488634. URL: http://www.tandfonline.com/doi/abs/10.1080/00401706.1970.10488634http://www.jstor.org/stable/1271436{\%}5Cnhttp://www.jstor.org/{\%}5Cnhttp://www.jstor.org/action/showPublisher?publisherCode=astata..

[63] Sture Holm. "A Simple Sequentially Rejective Multiple Test Procedure". In: *Scandinavian Journal of Statistics* 6.2 (1979), pp. 65–70. ISSN: 0303-6898. DOI: 10.2307/4615733.

[64] Gregory L. Holmes and Pierre Pascal Lenck-Santini. *Role of interictal epileptiform abnormalities in cognitive impairment*. 2006. DOI: 10.1016/j.yebeh.2005.11.014.

[65] Christian Hoppe, Christian E Elger, and Christoph Helmstaedter. "Long-term memory impairment in patients with focal epilepsy." In: *Epilepsia* 48 Suppl 9 (2007), pp. 26–9. ISSN: 0013-9580. DOI: 10.1111/j.1528-1167.2007.01397.x. URL: http://www.ncbi.nlm.nih.gov/pubmed/18047597.

[66] Peter Horak et al. "Interictal Epileptiform Discharges Impair Word recall in Multiple Brain Areas". In: *Epilepsia (Submitted)* (2016).

[67] A Hufnagel et al. "Clinical relevance of quantified intracranial interictal spike activity in presurgical evaluation of epilepsy." In: *Epilepsia* 41.4 (2000), pp. 467–478. ISSN: 0013-9580. DOI: 10.1111/j.1528-1157.2000.tb00191.x.

[68] Bahman Jabbari, Michael B. Russo, and Michelle L. Russo. "Electroencephalogram of asymptomatic adult subjects". In: *Clinical Neurophysiology* 111.1 (2000), pp. 102–105. ISSN: 13882457. DOI: 10.1016/S1388-2457(99)00189-3.

[69] Joshua Jacobs and Michael J. Kahana. *Direct brain recordings fuel advances in cognitive electrophysiology*. 2010. DOI: 10.1016/j.tics.2010.01.005.

[70] Ann Jacoby. "Epilepsy and the quality of everyday life. Findings from a study of people with well-controlled epilepsy". In: *Social Science and Medicine* 34.6 (1992), pp. 657–666. ISSN: 02779536. DOI: 10.1016/0277-9536(92)90193-T.

[71] Radek Janca et al. "Detection of Interictal Epileptiform Discharges Using Signal Envelope Distribution Modelling: Application to Epileptic and Non-Epileptic Intracranial Recordings". In: *Brain Topography* 28.1 (2014), pp. 172–183. ISSN: 15736792. DOI: 10.1007/s10548-014-0379-1.

[72] Ioannis Karakis et al. "Foramen ovale electrodes in the evaluation of epilepsy surgery: Conventional and unconventional uses". In: *Epilepsy and Behavior* 22.2 (2011), pp. 247–254. ISSN: 15255050. DOI: 10.1016/j.yebeh.2011.06.013.

[73] I Kharatishvili et al. "A model of posttraumatic epilepsy induced by lateral fluid-percussion brain injury in rats." In: *Neuroscience* 140.2 (2006), pp. 685–97. ISSN: 0306-4522. DOI: 10.1016/j.neuroscience.2006.03.012. URL: http://www.ncbi.nlm.nih.gov/pubmed/16650603.

[74] Young Tae Kim et al. "Chronic response of adult rat brain tissue to implants anchored to the skull". In: *Biomaterials* 25.12 (2004), pp. 2229–2237. ISSN: 01429612. DOI: 10.1016/j.biomaterials.2003.09.010.

[75] David King-Stephens et al. "Lateralization of mesial temporal lobe epilepsy with chronic ambulatory electrocorticography." In: *Epilepsia* 56.6 (2015), pp. 959–67. ISSN: 1528-1167. DOI: 10.1111/epi.13010. URL: http://www.pubmedcentral.nih.gov/articlerender.fcgi?artid=4676303{\&}tool=pmcentrez{\&}rendertype=abstract.

[76] Jonathan K Kleen et al. "Hippocampal interictal epileptiform activity disrupts cognition in humans." In: *Neurology* 81.1 (2013), pp. 18–24. ISSN: 1526-632X. DOI: 10.1212/WNL.0b013e318297ee50. URL: http://www.neurology.org/content/81/1/18.short.

[77] Jonathan K. Kleen et al. "Hippocampal interictal spikes disrupt cognition in rats". In: *Annals of Neurology* 67.2 (2010), pp. 250–257. ISSN: 03645134. DOI: 10.1002/ana.21896.

[78] Eliane Kobayashi et al. "Temporal and extratemporal BOLD responses to temporal lobe interictal spikes". In: *Epilepsia* 47.2 (2006), pp. 343–354. ISSN: 00139580. DOI: 10.1111/j.1528-1167.2006.00427.x.

[79] Ron Kohavi. "A Study of Cross-Validation and Bootstrap for Accuracy Estimation and Model Selection". In: *International Joint Conference on Artificial Intelligence* 14.12 (1995), pp. 1137–1143. ISSN: 10450823. DOI: 10.1067/mod.2000.109031.

[80] Yumiko Kondo et al. "Changes in brain activation associated with use of a memory strategy: A functional MRI study". In: *NeuroImage* 24.4 (2005), pp. 1154–1163. ISSN: 10538119. DOI: 10.1016/j.neuroimage.2004.10.033.

[81] Mark A Kramer et al. "Coalescence and fragmentation of cortical networks during focal seizures." In: *The Journal of neuroscience : the official journal of the Society for Neuroscience* 30.30 (2010), pp. 10076–85. ISSN: 1529-2401. DOI: 10.1523/JNEUROSCI.6309-09.2010.

[82] Mark A Kramer et al. "Emergence of persistent networks in long-term intracranial EEG recordings." In: *The Journal of neuroscience : the official journal of the Society for Neuroscience* 31.44 (2011), pp. 15757–67. ISSN: 1529-2401. DOI: 10.1523/JNEUROSCI.2287-11.2011.

[83] Patrick Kwan and Martin J Brodie. "Early identification of refractory epilepsy." In: *The New England journal of medicine* 342.5 (2000), pp. 314–9. ISSN: 0028-4793. DOI: 10.1056/NEJM200002033420503. URL: http://www.ncbi.nlm.nih.gov/pubmed/10660394.

[84] Patrick Kwan, SC Schachter, and MJ Brodie. "Drug-resistant epilepsy". In: *New England Journal of . . .* 365 (2011), pp. 919–926. URL: http://www.nejm.org/doi/full/10.1056/NEJMra1004418.

[85] Patrick Kwan et al. *Definition of drug resistant epilepsy: Consensus proposal by the ad hoc Task Force of the ILAE Commission on Therapeutic Strategies.* 2010. DOI: 10.1111/j.1528-1167.2009.02397.x. arXiv: arXiv:1011.1669v3.

[86] Jean-Philippe Lachaux et al. "High-frequency neural activity and human cognition: past, present and possible future of intracranial EEG research." In: *Progress in neurobiology* 98.3 (2012), pp. 279–301. ISSN: 1873-5118. DOI: 10.1016/j.pneurobio.2012.06.008. URL: http://www.sciencedirect.com/science/article/pii/S0301008212001062.

[87] Jack L. Lancaster et al. "Automated Talairach Atlas labels for functional brain mapping". In: *Human Brain Mapping* 10.3 (2000), pp. 120–131. ISSN: 10659471. DOI: 10.1002/1097-0193(200007)10:3<120::AID-HBM30>3.0.CO;2-8.

[88] S K Lee et al. "Surgical outcome and prognostic factors of cryptogenic neocortical epilepsy". In: *Ann Neurol* 58.4 (2005), pp. 525–532. DOI: 10.1002/ana.20569.

[89] M H Libenson and B Caravale. "Do antiepileptic drugs differ in suppressing interictal epileptiform activity in children?" In: *Pediatr Neurol* 24.3 (2001), 214–8 ST –Do antiepileptic drugs differ in suppr. ISSN: 0887-8994. DOI: S0887-8994(00)00271-X[pii]ET-2001/04/13. URL: http://www.ncbi.nlm.nih.gov/entrez/query.fcgi?cmd=Retrieve{\&}db=PubMed{\&}dopt=Citation{\&}list{_}uids=11301223LA-eng{\%}5Cnhttp://www.ncbi.nlm.nih.gov/entrez/query.fcgi?cmd=Retrieve{\&}db=PubMed{\&}dopt=Citation{\&}list{_}uids=11301223.

[90] Gustav Lind et al. "Multiple implants do not aggravate the tissue reaction in rat brain." In: *PloS one* 7.10 (2012), e47509. DOI: 10.1371/journal.pone.0047509.

[91] Brian Litt and Javier Echauz. *Prediction of epileptic seizures*. 2002. DOI: 10.1016/S1474-4422(02)00003-0.

[92] Brian Litt et al. "Epileptic Seizures May Begin Clinical Study Hours in Advance of Clinical Onset:A Report of Five Patients". In: *Neuron* 30.1 (2001), pp. 1–14.

[93] Simon Little et al. *Adaptive deep brain stimulation in advanced Parkinson disease*. 2013. DOI: 10.1002/ana.23951.

[94] X. Liu et al. "Stability of the interface between neural tissue and chronically implanted intracortical microelectrodes". In: *IEEE Transactions on Rehabilitation Engineering* 7.3 (1999), pp. 315–326. ISSN: 10636528. DOI: 10.1109/86.788468.

[95] Joan S. Lockard et al. "Cerebellar Stimulation in Alumina???Gel Monkey Model: Inverse Relationship Between Clinical Seizures and EEG Interictal Bursts". In: *Epilepsia* 20.3 (1979), pp. 223–234. ISSN: 15281167. DOI: 10.1111/j.1528-1157.1979.tb04799.x.

[96] W Löscher. "Animal models of intractable epilepsy." In: *Progress in neurobiology* 53.2 (1997), pp. 239–58. ISSN: 0301-0082.

[97] Hans O Lüders et al. "The epileptogenic zone: General principles". In: *Epileptic Disorders*. Vol. 8. SUPPL. 2. 2006. ISBN: 978 1 84184 576 0.

[98] Eric D. Marsh et al. "Interictal EEG spikes identify the region of electrographic seizure onset in some, but not all, pediatric epilepsy patients". In: *Epilepsia* 51.4 (2010), pp. 592–601. ISSN: 00139580. DOI: 10.1111/j.1528-1167.2009.02306.x. arXiv: NIHMS150003. URL: http://onlinelibrary.wiley.com/doi/10.1111/j.1528-1167.2009.02306.x/abstract.

[99] Bruce D. McCandliss, Laurent Cohen, and Stanislas Dehaene. *The visual word form area: Expertise for reading in the fusiform gyrus*. 2003. DOI: `10.1016/S1364-6613(03)00134-7`.

[100] Martin M Monti, Lawrence M Parsons, and Daniel N Osherson. "The boundaries of language and thought in deductive inference." In: *Proceedings of the National Academy of Sciences of the United States of America* 106.30 (2009), pp. 12554–9. ISSN: 1091-6490. DOI: `10.1073/pnas.0902422106`. URL: `http://www.pubmedcentral.nih.gov/articlerender.fcgi?artid=2718391{\&}tool=pmcentrez{\&}rendertype=abstract{\%}5Cnhttp://www.ncbi.nlm.nih.gov/pubmed/19617569`.

[101] Filipe Denaur De Moraes and Daniel Antonio Callegari. "Automated Detection of Interictal Spikes in EEG: A literature review". In: (2015), p. 29. URL: `http://www3.pucrs.br/pucrs/files/uni/poa/facin/pos/relatoriostec/TR081.pdf`.

[102] Martha J. Morrell. "Responsive cortical stimulation for the treatment of medically intractable partial epilepsy." In: *Neurology* 77.13 (2011), pp. 1295–304. ISSN: 00283878. DOI: `10.1212/WNL.0b013e3182302056`.

[103] G L Morris and W M Mueller. "Long-term treatment with vagus nerve stimulation in patients with refractory epilepsy. The Vagus Nerve Stimulation Study Group E01-E05." In: *Neurology* 53.8 (1999), pp. 1731–1735. ISSN: 0028-3878.

[104] Bennet B Murdock. "The serial position effect of free recall." In: *Journal of Experimental Psychology* 64.5 (1962), pp. 482–488. ISSN: 00221015. DOI: `10.1037/h0045106`. URL: `http://content.apa.org/journals/xge/64/5/482`.

[105] Lakshmi Nagarajan, Linda Palumbo, and Soumya Ghosh. "Brief electroencephalography rhythmic discharges (BERDs) in the neonate with seizures: their significance and prognostic implications." In: *Journal of child neurology* 26.12 (2011), pp. 1529–33. ISSN: 1708-8283. DOI: `10.1177/0883073811409750`.

[106] Theoden I. Netoff and Steven J. Schiff. "Decreased Neuronal Synchronization during Experimental Seizures". In: *J. Neurosci.* 22.16 (2002), pp. 7297–7307.

[107] Anthony K. Ngugi et al. "Estimation of the burden of active and life-time epilepsy: A meta-analytic approach". In: *Epilepsia* 51.5 (2010), pp. 883–890. ISSN: 00139580. DOI: `10.1111/j.1528-1167.2009.02481.x`.

[108] Luis Fernando Nicolas-Alonso and Jaime Gomez-Gil. *Brain computer interfaces, a review*. 2012. DOI: `10.3390/s120201211`.

[109] Soheyl Noachtar and Ingo Borggraefe. "Epilepsy surgery: a critical review." In: *Epilepsy & behavior : E&B* 15.1 (2009), pp. 66–72. ISSN: 1525-5069. DOI: `10.1016/j.yebeh.2009.02.028`.

[110] Soheyl Noachtar and Jan Rémi. *The role of EEG in epilepsy: A critical review*. 2009. DOI: `10.1016/j.yebeh.2009.02.035`.

[111] Anna C Nobre, Truett Allison, and Gregory McCarthy. "Word recognition in the human inferior temporal lobe". In: *Nature* 372 (1994), pp. 260–263. DOI: `10.1038/372260a0`.

[112] George Nune, Christopher DeGiorgio, and Christianne Heck. *Neuromodulation in the Treatment of Epilepsy*. 2015. DOI: 10.1007/s11940-015-0375-0. URL: http://link.springer.com/10.1007/s11940-015-0375-0.

[113] Ken A. Paller and Anthony D. Wagner. *Observing the transformation of experience into memory*. 2002. DOI: 10.1016/S1364-6613(00)01845-3.

[114] Adrien Peyrache et al. "Spatiotemporal dynamics of neocortical excitation and inhibition during human sleep." In: *Proceedings of the National Academy of Sciences of the United States of America* 109.5 (2012), pp. 1731–6. ISSN: 1091-6490. DOI: 10.1073/pnas.1109895109. URL: http://www.ncbi.nlm.nih.gov/pubmed/22307639http://www.pubmedcentral.nih.gov/articlerender.fcgi?artid=PMC3277175http://www.pubmedcentral.nih.gov/articlerender.fcgi?artid=3277175{\&}tool=pmcentrez{\&}rendertype=abstract.

[115] Jyoti Pillai and Michael R. Sperling. *Interictal EEG and the diagnosis of epilepsy*. 2006. DOI: 10.1111/j.1528-1167.2006.00654.x.

[116] Vadim S Polikov, Patrick A Tresco, and William M Reichert. "Response of brain tissue to chronically implanted neural electrodes." In: *Journal of neuroscience methods* 148.1 (2005), pp. 1–18. ISSN: 0165-0270. DOI: 10.1016/j.jneumeth.2005.08.015.

[117] M I Posner and B D McCandliss. "Brain circuitry during reading". In: *Converging Methods for Understanding Reading and Dyslexia*. 1992, pp. 305–337. ISBN: 0262112477. DOI: 10.1016/S1364-6613(00)01551-5.

[118] Heidrun Potschka et al. *Canine epilepsy as a translational model?* 2013. DOI: 10.1111/epi.12138.

[119] Abhishek Prasad and Justin C Sanchez. "Quantifying long-term microelectrode array functionality using chronic in vivo impedance testing." In: *Journal of neural engineering* 9.2 (2012), p. 026028. DOI: 10.1088/1741-2560/9/2/026028.

[120] F D Raslau et al. "Memory part 1: overview." In: *AJNR. American journal of neuroradiology* 35.11 (2014), pp. 2058–60. ISSN: 1936-959X. DOI: 10.3174/ajnr.A4059. URL: http://www.ajnr.org/content/35/11/2058.short.

[121] F D Raslau et al. "Memory part 2: the role of the medial temporal lobe." en. In: *AJNR. American journal of neuroradiology* 36.5 (2015), pp. 846–9. ISSN: 1936-959X. DOI: 10.3174/ajnr.A4169. URL: http://www.ajnr.org/content/36/5/846.full.

[122] F Rosenow and H Lüders. "Presurgical evaluation of epilepsy." In: *Brain* 124.Pt 9 (2001), pp. 1683–700. ISSN: 0006-8950. DOI: 10.4103/1817-1745.40593. URL: http://www.ncbi.nlm.nih.gov/pubmed/11522572.

[123] Vicenta Salanova et al. "Long-term efficacy and safety of thalamic stimulation for drug-resistant partial epilepsy." In: *Neurology* 84.10 (2015), pp. 1017–25. ISSN: 1526-632X. DOI: 10.1212/WNL.0000000000001334. URL: http://www.neurology.org/content/84/10/1017.short.

[124] Viswanath Sankar et al. "Electrode impedance analysis of chronic tungsten microwire neural implants: understanding abiotic vs. biotic contributions." In: *Frontiers in neuroengineering* 7 (2014), p. 13. ISSN: 1662-6443. DOI: 10.3389/fneng.2014.

00013. URL: http://www.pubmedcentral.nih.gov/articlerender.fcgi?artid=4021112{\&}tool=pmcentrez{\&}rendertype=abstract.

[125]   Amelia a Schendel et al. "The effect of micro-ECoG substrate footprint on the meningeal tissue response." In: *Journal of neural engineering* 11.4 (2014), p. 046011. ISSN: 1741-2552. DOI: 10.1088/1741-2560/11/4/046011. URL: http://www.ncbi.nlm.nih.gov/pubmed/24941335.

[126]   Mark S. Scher et al. "Ictal and Interictal Electrographic Seizure Durations in Preterm and Term Neonates". In: *Epilepsia* 34.2 (1993), pp. 284–288. ISSN: 0013-9580. DOI: 10.1111/j.1528-1157.1993.tb02412.x.

[127]   Kaspar A Schindler et al. "Evolving functional network properties and synchronizability during human epileptic seizures." In: *Chaos (Woodbury, N.Y.)* 18.3 (2008), p. 033119. ISSN: 1089-7682. DOI: 10.1063/1.2966112.

[128]   S Schmidt, K Horch, and R Normann. "Biocompatibility of silicon-based electrode arrays implanted in feline cortical tissue". In: *Journal of Biomedical Materials Research.* Vol. 27. 11. 1993, pp. 1393–1399. ISBN: 0021-9304 (Print). DOI: 10.1002/jbm.820271106.

[129]   D. L. Schomer and F. Lopes da Silva. *Niedermeyer's Electroencephalography: Basic Principles, Clinical Applications, and Related Fields.* Vol. 1. 2012, p. 1296. ISBN: 0781789427. URL: http://books.google.com/books?hl=fr{\&}lr={\&}id=xSKqZxXOlukC{\&}pgis=1.

[130]   Per B. Sederberg et al. "Hippocampal and neocortical gamma oscillations predict memory formation in humans". In: *Cerebral Cortex* 17.5 (2007), pp. 1190–1196. ISSN: 10473211. DOI: 10.1093/cercor/bhl030.

[131]   Per B Sederberg et al. "Theta and gamma oscillations during encoding predict subsequent recall." In: *The Journal of neuroscience : the official journal of the Society for Neuroscience* 23.34 (2003), pp. 10809–10814. ISSN: 1529-2401. DOI: 23/34/10809[pii].

[132]   D A Shewmon. "What is a neonatal seizure? Problems in definition and quantification for investigative and clinical purposes." In: *Journal of clinical neurophysiology : official publication of the American Electroencephalographic Society* 7.3 (1990), pp. 315–368. ISSN: 0736-0258. DOI: 10.1097/00004691-199007000-00003.

[133]   Matti Sillanpää and Dieter Schmidt. "Seizure clustering during drug treatment affects seizure outcome and mortality of childhood-onset epilepsy". In: *Brain* 131 (2008), pp. 938–944. ISSN: 00068950. DOI: 10.1093/brain/awn037.

[134]   Karl A Sillay et al. "Long-term measurement of impedance in chronically implanted depth and subdural electrodes during responsive neurostimulation in humans." In: *Brain stimulation* 6.5 (2013), pp. 718–26. ISSN: 1935-861X. DOI: 10.1016/j.brs.2013.02.001. URL: http://www.sciencedirect.com/science/article/pii/S1935861X13000752.

[135]   N So et al. "Depth electrode investigations in patients with bitemporal epileptiform abnormalities." In: *Annals of neurology* 25.5 (1989), pp. 423–31. ISSN: 0364-5134. DOI: 10.1002/ana.410250502.

[136] Susan Spencer and Linda Huh. *Outcomes of epilepsy surgery in adults and children.* 2008. DOI: 10.1016/S1474-4422(08)70109-1.

[137] L R Squire and S Zola-Morgan. "The medial temporal lobe memory system." In: *Science* 253.5026 (1991), pp. 1380–1386. ISSN: 0036-8075. DOI: 10.1126/science.1896849.

[138] Larry R Squire, Craig E L Stark, and Robert E Clark. "The medial temporal lobe." In: *Annual review of neuroscience* 27 (2004), pp. 279–306. ISSN: 0147-006X. DOI: 10.1146/annurev.neuro.27.070203.144130. URL: http://www.ncbi.nlm.nih.gov/pubmed/15217334.

[139] Kevin J Staley and F Edward Dudek. "Interictal Spikes and Epileptogenesis". In: *Epilepsy Currents* 6 (2006), pp. 199–202. ISSN: 1535-7597. DOI: 10.1111/j.1535-7511.2006.00145.x.

[140] Paula Stice et al. "Thin microelectrodes reduce GFAP expression in the implant site in rodent somatosensory cortex." In: *Journal of neural engineering* 4.2 (2007), pp. 42–53. ISSN: 1741-2560. DOI: 10.1088/1741-2560/4/2/005. URL: http://www.ncbi.nlm.nih.gov/pubmed/17409479.

[141] David a Sun et al. "Postmortem analysis following 71 months of deep brain stimulation of the subthalamic nucleus for Parkinson disease." In: *Journal of neurosurgery* 109.2 (2008), pp. 325–9. DOI: 10.3171/JNS/2008/109/8/0325.

[142] Felice T Sun, Martha J Morrell, and Robert E Wharen. "Responsive Cortical Stimulation for the Treatment of Epilepsy". In: *Neurotherapeutics* 5.1 (2008), pp. 68–74. ISSN: 19337213. DOI: 10.1016/j.nurt.2007.10.069.

[143] Rainer Surges and Josemir W Sander. "Sudden unexpected death in epilepsy: mechanisms, prevalence, and prevention." In: *Current opinion in neurology* 25.2 (2012), pp. 201–7. ISSN: 1473-6551. DOI: 10.1097/WCO.0b013e3283506714. URL: http://www.ncbi.nlm.nih.gov/pubmed/22274774.

[144] Thomas P Sutula, Joshua Hagen, and Asla Pitkänen. "Do epileptic seizures damage the brain?" In: *Current opinion in neurology* 16.2 (2003), pp. 189–95. ISSN: 1350-7540. DOI: 10.1097/01.wco.0000063770.15877.bc. URL: http://www.ncbi.nlm.nih.gov/pubmed/12644748.

[145] José F Téllez-Zenteno, Raj Dhar, and Samuel Wiebe. "Long-term seizure outcomes following epilepsy surgery: a systematic review and meta-analysis." In: *Brain : a journal of neurology* 128.Pt 5 (2005), pp. 1188–98. ISSN: 1460-2156. DOI: 10.1093/brain/awh449. URL: http://brain.oxfordjournals.org/content/128/5/1188.long.

[146] R Tibshirani, G Walther, and T Hastie. *Estimating the number of clusters in a data set via the gap statistic.* 2001. DOI: 10.1111/1467-9868.00293. URL: http://onlinelibrary.wiley.com/doi/10.1111/1467-9868.00293/abstract.

[147] Robert Tibshirani. *Regression Selection and Shrinkage via the Lasso.* 1994. DOI: 10.2307/2346178. URL: http://citeseer.ist.psu.edu/viewdoc/summary?doi=10.1.1.35.7574.

[148] D M Treiman, N Y Walton, and C Kendrick. "A progressive sequence of electroencephalographic changes during generalized convulsive status epilepticus." In: *Epilepsy research* 5 (1990), pp. 49–60. ISSN: 09201211. DOI: `10.1016/0920-1211(90)90065-4`.

[149] Hoameng Ung et al. "Temporal Behavior of Seizures and Interictal Bursts in Prolonged Intracranial Recordings from Epileptic Canines". In: *Epilepsia* ().

[150] A. Uriarte and I. Maestro Saiz. *Canine versus human epilepsy: are we up to date?* 2016. DOI: `10.1111/jsap.12437`.

[151] Kris Van Kuyck et al. "Histological alterations induced by electrode implantation and electrical stimulation in the human brain: a review." In: *Neuromodulation : journal of the International Neuromodulation Society* 10.3 (2007), pp. 244–61. ISSN: 1094-7159. DOI: `10.1111/j.1525-1403.2007.00114.x`.

[152] a D Wagner et al. "Building memories: remembering and forgetting of verbal experiences as predicted by brain activity." In: *Science (New York, N.Y.)* 281.5380 (1998), pp. 1188–1191. ISSN: 0036-8075. DOI: `10.1126/science.281.5380.1188`.

[153] Wei-Han Wang et al. "Neuropsychological performance and seizure-related risk factors in patients with temporal lobe epilepsy: A retrospective cross-sectional study". In: *Epilepsy & Behavior* 22.4 (2011), pp. 728–734. ISSN: 15255050. DOI: `10.1016/j.yebeh.2011.08.038`. URL: `http://dx.doi.org/10.1016/j.yebeh.2011.08.038`.

[154] Christopher P Warren et al. "Synchrony in normal and focal epileptic brain: the seizure onset zone is functionally disconnected." In: *Journal of neurophysiology* 104.6 (2010), pp. 3530–3539. ISSN: 0022-3077. DOI: `10.1152/jn.00368.2010`.

[155] C. Wilke et al. "Identification of epileptogenic foci from causal analysis of ECoG interictal spike activity". In: *Clinical Neurophysiology* 120.8 (2009), pp. 1449–1456. ISSN: 13882457. DOI: `10.1016/j.clinph.2009.04.024`.

[156] S. B. Wilson et al. "Spike detection. I. Correlation and reliability of human experts". In: *Electroencephalography and Clinical Neurophysiology* 98.3 (1996), pp. 186–198. ISSN: 00134694. DOI: `10.1016/0013-4694(95)00221-9`.

[157] Scott B. Wilson and Ronald Emerson. "Spike detection: a review and comparison of algorithms". In: *Clinical Neurophysiology* 113.12 (2002), pp. 1873–1881. ISSN: 13882457. DOI: `10.1016/S1388-2457(02)00297-3`. URL: `http://www.sciencedirect.com/science/article/pii/S1388245702002973`.

[158] Brent D Winslow et al. "A comparison of the tissue response to chronically implanted Parylene-C-coated and uncoated planar silicon microelectrode arrays in rat cortex". In: *Biomaterials* 31.35 (2010), pp. 9163–9172. ISSN: 01429612. DOI: `10.1016/j.biomaterials.2010.05.050`.

[159] Chengyuan Wu and Ashwini D. Sharan. *Neurostimulation for the treatment of epilepsy: A review of current surgical interventions.* 2013. DOI: `10.1111/j.1525-1403.2012.00501.x`.

[160] Chengyuan Wu et al. *Impedance variations over time for a closed-loop neurostimulation device: Early experience with chronically implanted electrodes.* 2013. DOI: `10.1111/j.1525-1403.2012.00529.x`.

[161] Drausin F. Wulsin. "Bayesian Nonparametric Modeling of Epileptic Events". PhD thesis. University of Pennsylvania, 2013.

[162] Drausin F. Wulsin, Emily B. Fox, and Brian Litt. "Modeling the complex dynamics and changing correlations of epileptic events". In: *Artificial Intelligence* 216 (2014), pp. 55–75. ISSN: 00043702. DOI: 10.1016/j.artint.2014.05.006.

[163] Drausin F. Wulsin et al. "Parsing Epileptic Events Using a Markov Switching Process for Correlated Time Series". In: *Proceedings of the 30th International Conference on Machine Learning (ICML-13)*. 2013, pp. 356–364.

[164] Ji Yeoun Yoo et al. "Brief potentially ictal rhythmic discharges in critically ill adults." In: *JAMA neurology* 71.4 (2014), pp. 454–62. ISSN: 2168-6157. DOI: 10.1001/jamaneurol.2013.6238. URL: http://www.ncbi.nlm.nih.gov/pubmed/24535702.

[165] G B Young, K G Jordan, and G S Doig. "An assessment of nonconvulsive seizures in the intensive care unit using continuous EEG monitoring: an investigation of variables associated with mortality." In: *Neurology* 47.1 (1996), pp. 83–9. ISSN: 0028-3878.

[166] G H Yuen and F Agnewandleok Bullara. "Tissue response to potential materials implanted neuroprosthetic subdurally". In: (1986).

[167] J. Zabara. "Inhibition of experimental seizures in canines by repetitive vagal stimulation". In: *Epilepsia* 33.6 (1992), pp. 1005–1012. ISSN: 00139580. DOI: 10.1111/j.1528-1157.1992.tb01751.x.

[168] R Zahn et al. "Hemispheric lateralization at different levels of human auditory word processing: a functional magnetic resonance imaging study." In: *Neuroscience letters* 287.3 (2000), pp. 195–198. ISSN: 0304-3940. DOI: S0304394000011605[pii].

[169] Hui Zou and Trevor Hastie. "Regularization and variable selection via the elastic net". In: *Journal of the Royal Statistical Society. Series B: Statistical Methodology* 67.2 (2005), pp. 301–320. ISSN: 13697412. DOI: 10.1111/j.1467-9868.2005.00503.x. URL: http://doi.wiley.com/10.1111/j.1467-9868.2005.00503.x.